Quarkonium Production at High-Energy Hadron Colliders

A Systematic Gauge-Invariant Approach to Relativistic Effects of J/ψ, ψ' and Υ Production

Thesis by

Jean-Philippe Lansberg

University of Liège – Fundamental Theoretical Physics

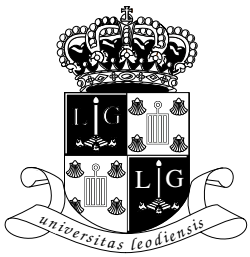

University of Liège
Liège, Belgium

Thesis presented in fulfilment of the requirements for the Degree of Doctor of Science

Academic year 2004-2005
–Defended on April 22, 2005–

Thesis Jury:

President:

Yves Lion	(Liège)

External Members:

François Le Diberder	(IN2P3 & LAL, Orsay)
James W. Stirling	(CPT & IPPP, Durham)

Internal Members:

Maxim V. Polyakov	(PTF, Liège)
Lech Szymanowski	(PTF, Liège & SINS, Warsaw)

Advisor:

Jean-René Cudell	(PTF, Liège)

A tout ces gens,
qui ne me doivent rien,
et à qui je dois énormément.

Αφιερώνω επίσης αυτήν την εργασία
στις Μούσες μου,
παρελθοντικές,
παρούσες
και μελλοντικές.

You see, in this world,
there's two kinds of people
... my friend:
Those with loaded guns,
and those who dig...you dig!

The man with no name (Clint Eastwood),
The Good, the Bad and the Ugly

Remerciements – Acknowledgments

Je voudrais tout d'abord remercier ma mère, ma marraine et mon parrain pour leur soutien constant, tant matériel que moral, depuis ces longues années. Inutile de préciser que cela aurait été singulièrement plus compliqué sans leur présence. Je tiens aussi à remercier les autres membres de ma famille qui m'ont tous, à un moment ou à un autre, donné le petit coup de pouce nécessaire quand il le fallait.

Ensuite, bien évidemment, je tiens à remercier Jean-René Cudell tant pour l'encadrement scientifique qui m'a permis de mener à bien ce travail de longue haleine, que pour l'aide, un peu moins scientifique, mais tout aussi précieuse, que furent ses innombrables relectures de mes écrits (lettres, e-mails, mémoires et cette thèse), ses conseils administratifs, ses suggestions et soutiens pour mes demandes de financements, etc. Cela fait maintenant plus de six ans que je suis rentré pour la première fois dans son bureau, où j'appris que "la Chromodynamique Quantique n'était qu'une matrice à la place d'un nombre dans le facteur de phase de la fonction d'onde" (sic); si ma motivation pour la recherche est intacte, c'est en grande partie grâce à lui.

Mes plus sincères remerciements vont également au chef de notre groupe, Joseph Cugnon, pour m'avoir accordé le poste de chercheur IISN qui m'a permis de mener à bien cette thèse, pour m'avoir autorisé à prendre part à de nombreux séjours scientifiques qui furent pour moi une source fondamentale de motivations et qui, maintenant, me permettent de jouir d'une certaine perspective sur mes recherches futures grâce aux contacts que j'ai pu nouer avec d'autres physiciens. Je le remercie aussi de m'avoir confié une partie de l'organisation de la conférence en Décembre dernier, l'édition des proceedings, ainsi que d'autres tâches dans le cadre de notre groupe. Cela m'a permis de découvrir pleinement des aspects de la vie scientifique auxquels normalement nous n'avons pas l'occasion de goûter en tant que doctorants.

J'aimerais en outre remercier Laurent et Voica – *la mia sorella* – pour la relecture attentive de ma thèse, mais bien au-delà de cette relecture, pour nos innombrables discussions électroniques, tout au long de ma thèse. J'espère les avoir aidés et divertis lors de moments moins agréables autant qu'eux ont pu le faire pour moi. Pour leur amitié, je voudrais aussi remercier Muriel, Frédéric, Philippe et Nicolas.

Next, I woud like to thank Yura Kalinovsky for his everlasting good mood but also for his scientific help concerning this work. Without his method to tackle this "bloody" (sic) integral appearing in the chapter 6, my task would have been certainly more awkward. I also thank him and Pedro Costa to have shared their results with me.

I would like also to express my sincere acknowledgments to the members of the jury for

having accepted to join it, in spite of their overbooked agenda. I am deeply grateful to them for that. I would like also to underline the constant kindness and attention of Lech Szymanowski.

I would like finally to thank all the physicists whom I met and who did their best to answer my questions.

Enfin, je réserve quelques mots de remerciements pour mes collègues de bureau, Michel et Aurore; pour Alice et Cédric qui remplacent avantageusement les ordinateurs du 4/03, les étudiants en physique que j'ai eu le plaisir de côtoyer, dont Christophe et Grégory, le groupe des "ingénieurs", Stéphane et François ("ce sont quand même de bons acteurs !"), Marie-Paule Biémont pour sa précieuse aide logistique, Michel Bawin pour nos discussions Linuxiennes ainsi que toutes les personnes qui se sont intéressées à un moment ou à un autre à mon travail.

Merci à tous !

Contents

Chapter 1

Introduction

1.1 History

1.1.1 J/ψ and the November revolution

Simultaneously discovered in November 1974 by Ting *et al.* [1] at the Brookhaven National Laboratory[1] and by Richter *et al.* [2] at the Stanford Linear Accelerator[2], the J/ψ directly stands out from the crowd of other particles by its peculiar name composed of two symbols: J by Ting in comparison[3] to the electric current $j_\mu(x)$, and ψ because of the typical pattern of its decay in $\pi^+\pi^-$ at SPEAR (see Fig. 1.1).

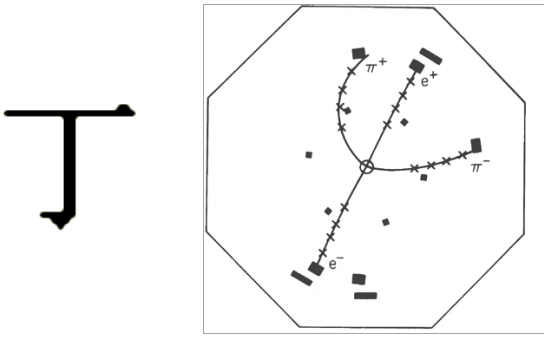

Figure 1.1: Left: the sound [dīng] in the Chinese alphabet; Right: typical Mark I (SPEAR) event display for J/ψ decay (from [3]).

Ting's experiment was based on the high-intensity proton beams of the Alternating Gradient Synchrotron (AGS) working at the energy of 30 GeV, which bombarded a fixed target with the consequence of producing showers of particles detectable by the appropriate apparatus. More precisely, they used a beryllium target and a beam with a momentum in

[1] BNL
[2] SLAC
[3] See however the left part of Fig. 1.1 ...

the laboratory frame of 19-20 GeV. Taking advantage of a double-arm spectrometer, they detected a strong peak in the energy distribution of the produced electron-positron pairs at a value of 3.1 GeV as can be seen on Fig. 1.2. On the other hand, Richter's experiment used the electron-positron storage ring SPEAR, whose center-of-momentum energy could be tuned at the desired value. With the Mark I detector, they discovered a sharp enhancement of the production cross section in different channels: e^+e^-, $\mu^+\mu^-$, $\pi^+\pi^-$,... The resulting cross sections are shown in Fig. 1.3.

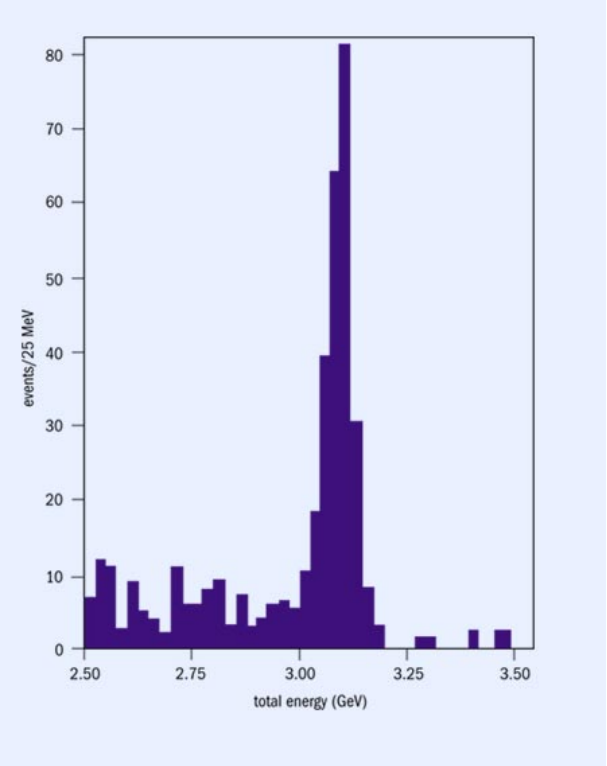

Figure 1.2: Energy distribution of the produced electron-positron pairs for Ting's experiment (from [4]).

In the following weeks, the Frascati group (Bacci *et al.* [5]) confirmed the presence of this new particle whose mass was approximately 3.1 GeV. The confirmation was so fast that it was actually published in the same issue of Physical Review Letters, *ie.* vol. 33, no. 23, issued the second of December 1974. In the meantime –ten days later according Richter's Nobel Lecture–, his group discovered another resonant state with a slightly higher mass which was called[4] ψ'.

In 1976, Ting and Richter were awarded the Nobel prize for this simultaneous discovery. Indeed, considering the state of comprehension of particle physics at that time, this discovery was a shock for many. During the two years between the discovery and the award of the

[4] We shall also make us of the name $\psi(2S)$.

Nobel prize, an intense research activity in this domain took place. Were these new states the sign of a new generation of quarks ? Was the quark model to be finally trusted?

An important fact to bear in mind here is that further studies based on the on- and off-peak production of muons and on forward/backward asymmetry in the observed angular distribution promptly established that the quantum numbers of the J/ψ were the same as those of the photon , *i.e.* 1^{--}. In a sense, this is not surprising at all since it is much more likely to produce a resonance with the same quantum number as the photon in e^+e^- colliding experiments than other resonances.

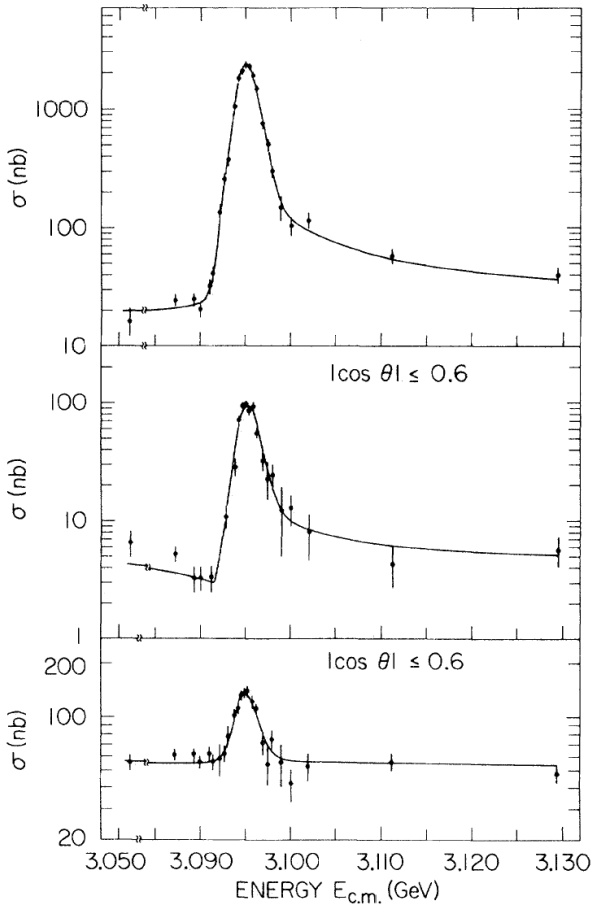

Figure 1.3: Various pair production cross sections as functions of the center-of-momentum energy (top: hadrons; middle: $\pi^+\pi^-$, $\mu^+\mu^-$ and K^+K^-; bottom: e^+e^-) [2].

Moreover, since the following ratio

$$R = \frac{\text{cross section for } e^+e^- \to \text{hadrons}}{\text{cross section for } e^+e^- \to \mu^+\mu^-} \tag{1.1}$$

was much larger on-resonance than off, it was then clear that the J/ψ did have direct hadronic decays. The same conclusion held for the ψ' as well. The study of multiplicity

in pion decays indicated that ψ decays were restricted by a specific selection rule, called G-parity conservation, known to hold only for hadrons. Consequently, J/ψ and ψ' entered the family of hadrons with isospin 0 and G-parity -1.

Particles with charge conjugation C different from -1, *i.e.* with quantum numbers different from those of the photon, were found later. Indeed, they were only produced by decay of ψ'' and the detection of the radiated photon during the (electromagnetic) decay was then required. The first to achieve this task and discover a new state was the DASP collaboration [6] based at DESY (Deutsches Elektronen-Synchrotron), Hamburg, working at an e^+e^- storage ring called DORIS. This new particle, named[5] P_c, had a mass of approximately 3.500 GeV. At SPEAR other resonances at 3.415, 3.450 and 3.550 GeV were discovered, the 3.500 GeV state was confirmed. Later, these states were shown to be $C = +1$.

Coming back to the ratio R, let us now analyse the implication in the framework of the quark model postulated by Gell-Mann[6] and Zweig in 1963. In 1974 at the London conference, Richter presented [7] the experimental situation as in Fig. 1.4.

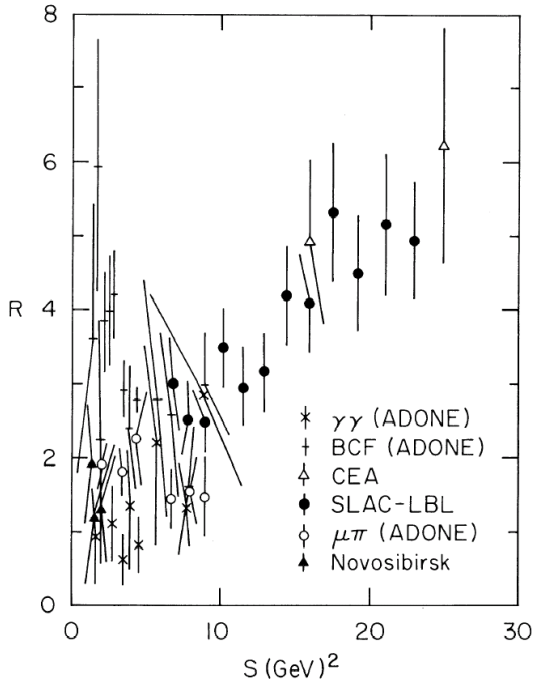

Figure 1.4: Experimental status of R as of July 1974 (from [7]).

In the framework of the Gell-Mann-Zweig quark model with three quarks, a plateau was

[5] The name chosen here reveals that physicists already had at this time an interpretation of this state as bound-state of quarks c. Indeed, the symbol P follows from the classical spectroscopic notation for a $\ell = 1$ state, where ℓ stands for the angular momentum quantum number.

[6] The name "quark" was chosen by Gell-Mann. He found this word in the James Joyce's novel *Finnegans Wake* where the following enigmatic sentence appears: 'Three quarks for Muster Mark'. This name comes from the standard English verb *quark*, meaning "to caw, to croak", and also from the dialectal verb *quawk*, meaning "to caw, to screech like a bird".

expected with a value of 2/3 or 2 if the quark were considered as "coloured" – a new concept introduced recently then –. The sign of a new quark – as the charm quark first proposed by Bjorken and Glashow in 1964 [8]– would have been another plateau from a certain energy (roughly its mass) with a height depending on its charge. Retrospectively, one cannot blame anyone for not having seen this "plateau" on this kind of plots. Quoting Richter, "the situation that prevailed in the Summer of 1974" was "vast confusion".

This charm quark was also theoretically needed following the work of Glashow, Iliopoulos and Maiani [9], which suggested that a symmetry between leptons and quarks should exist in order to cancel the anomaly in weak decays. And following this symmetry proposal, the charm quark was expected to exist and to have an electric charge 2/3. R was therefore to be 10/3 in the coloured quark model, still not obvious in Fig. 1.4. This explains why the discovery of such sharp and easily interpreted resonances in November 1974 was a revolution in particle physics.

It became quite rapidly obvious that the J/ψ was the lowest-mass $c\bar{c}$ system with the same quantum numbers as photons – explaining why it was so much produced compared to some other members of its system. These $c\bar{c}$ bound states were named "charmonium", firstly by Appelquist, De Rújula, Politzer and Glashow [10][7], in analogy with positronium, which has a similar bound-state level structure.

At that time, the charm had nevertheless always been found hidden, that is in charm-anti-charm bound states. On the other hand, it became quickly clear that the mass of the lightest possible state constituted of a charm quark and a light quark, thus an explicit charmed meson, named D, was to lie around 1900 MeV. A more precise lower bound, 1843 MeV, was inferred from the fact that the ψ' ($m_{\psi'} = 3684$ MeV) was too narrow or, in other words, had too long a lifetime to be above the threshold to produce a pair of D's, that is $2m_D$. The upper bound was, on the other hand, deduced from the point where R started to rise before reaching the plateau with 4 active quark flavours.

In order to study these D mesons, the investigations were based on the assumption that the D was to decay weakly and preferentially into strange quarks. The weak character of the decay motivated physicists to search for parity-violation signals. The first resonance attributed to D^0 meson was found in $K^+\pi^+$ decay by Goldhaber *et al.* [11] in 1976. A little later, D^+ and D^- were also discovered as well as an excited state, D^*, with a mass compatible with the decay $\psi''' \to D^0 D^*$. And, finally, the most conclusive evidence for the discovery of charmed meson was the observation of parity violation in D decays [12]. To complete the picture of the charm family, the first charmed baryon was discovered during the same year [13]. The quarks were not anymore just a way to interpret symmetry in masses and spins of particles, they had acquired an existence.

[7] To be complete, the initial title of the preprint "Charmonium spectroscopy" was immediately refused by the senior editor Pasternak of Physical Review Letters because of "frivolous new terminology". A consensus eventually emerged thanks to Glashow: the term was accepted in the text but not in the title!

1.1.2 The truth: a third generation

In 1975, another brand new particle was unmasked at SLAC by Perl *et al.* [14], for which he was awarded the Nobel prize twenty years later. This was the first particle of a third generation of quarks and leptons, the τ, a *lepton*[8]. Following the standard model, which was more and more a reference trusted by most, two other quarks were expected to exist. Their discovery would then be the very proof of the theory that was developed since the sixties. Two names for the fifth quark were already chosen: "beauty" and "bottom", and in both cases represented by the letter b; the sixth quark was as well already christened with the letter t for the suggested names[9] "true" or "top".

The wait was not long: two years. After a false discovery[10] of a resonance at 6.0 GeV, a new dimuon resonance similar to J/ψ and called Υ was brought to light at Fermilab, thanks to the FNAL proton synchrotron accelerator, by Herb *et al.* [16], with a mass of 9.0 GeV; as for charmonia, the first radial excited state ($\Upsilon(2S)$) was directly found [17] thereafter. Various confirmations of these discoveries were not long to come. The $3S$ state was then found [18] at Fermilab as well as evidence that the $4S$ state was lying above the threshold for the production of B mesons. The latter was confirmed at the Cornell e^+e^- storage ring with the CLEO detector. The first evidence for B meson and, thus, for unhidden b quark, was also brought by the CLEO collaboration [19] in 1980. One year later, "the first evidence for baryons with naked beauty"(*sic*) was reported by CERN physicists [20][11].

Another decade was needed for the discovery of the sixth quark which was definitely christened "top". Indeed, in 1994, the CDF Collaboration observed it at the Tevatron collider in Fermilab [21]. This accelerator – which reaches now a c.m. energy of 1960 GeV – and this collaboration will accompany us throughout this thesis, but for a different signal. Unfortunately, due to its very short lifetime, this quark cannot bind with its antiquark to form the toponium. To conclude this historical prelude, we give the spectra of the $c\bar{c}$ and $b\bar{b}$ systems as well as two tables summing up the characteristics of the observed states as of today.

Meson	$n^{2S+1}L_J$	J^{PC}	Mass (GeV)	$\Gamma_{\mu\mu}$ (keV)
η_c	$1\ ^1S_0$	0^{-+}	2.980	N/A
J/ψ	$1\ ^3S_1$	1^{--}	3.097	5.40
χ_{c0}, χ_{c1}, χ_{c2}	$1\ ^3P_{0,1,2}$	0^{++},1^{++},2^{++}	3.415,3.511,3.556	N/A
h_c	$1\ ^1P_0$	1^{+-}	3.523	N/A
$\eta_c(2S)$	$2\ ^1S_0$	0^{-+}	3.594	N/A
ψ'	$2\ ^3S_1$	1^{--}	3.686	2.12

Table 1.1: Properties of charmonia (cf. [57]).

[8] in contradiction with the etymology because it was *heavier* than most of known *baryons* at that time.

[9] The name "truth" was given as a reference to the fact that its discovery should be the proof of the truth of the standard model.

[10] Nonetheless, this paper [15] first suggested the notation Υ for any "onset of high-mass dilepton physics".

[11] Here is an unambiguous sign that European editors had a much softer editorial approach concerning titles of articles...

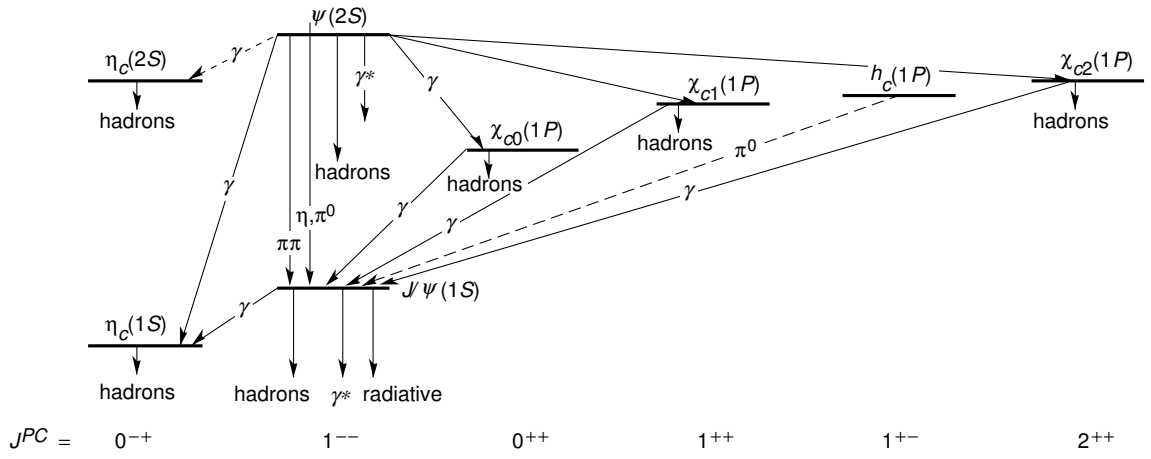

Figure 1.5: Spectrum and transitions of the charmonium family (from [57]).

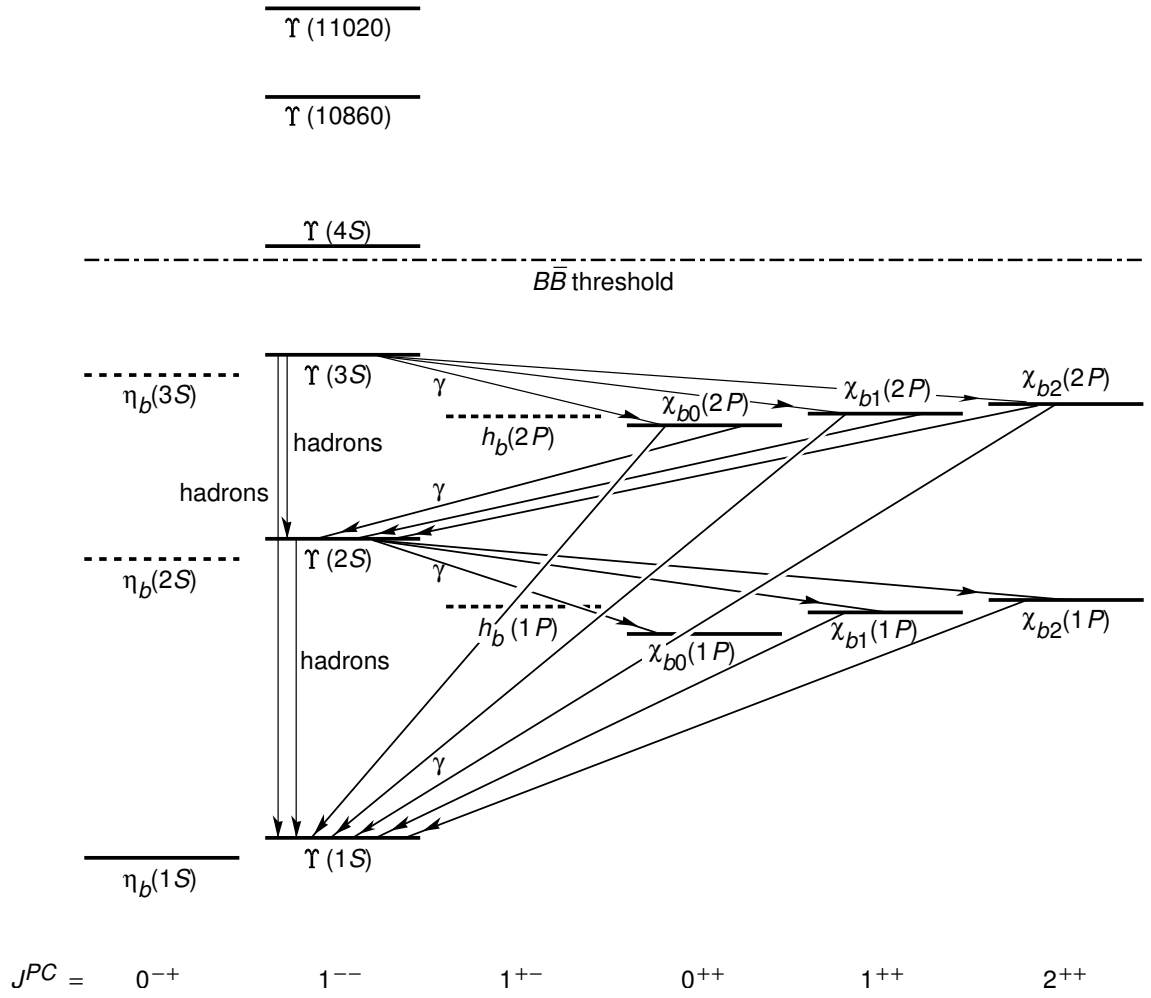

Figure 1.6: Spectrum and transitions of the bottomonium family (from [57]).

Meson	$n^{2S+1}L_J$	J^{PC}	Mass (GeV)	$\Gamma_{\mu\mu}$ (keV)
$\Upsilon(1S)$	1^3S_1	1^{--}	9.460	1.26
χ_{b0}, χ_{b1} , $\chi_{b2}(1P)$	$1\ ^3P_{0,1,2}$	0^{++},1^{++},2^{++}	9.860,9.893,9.913	N/A
$\Upsilon(2S)$	$2\ ^3S_1$	1^{--}	10.023	0.32
χ_{b0}, χ_{b1}, χ_{b2} (2P)	$1\ ^3P_{0,1,2}$	0^{++},1^{++},2^{++}	10.232,10.255,10.269	N/A
$\Upsilon(3S)$	$3\ ^3S_1$	1^{--}	10.355	0.48

Table 1.2: Properties of bottomonia (cf. [57]) .

1.2 Motivations

1.2.1 Why study quarkonium physics in the high-energy regime ?

The fact that J/ψ was the first particle with a c quark to be discovered is not an accident: it is in fact of fundamental importance in particle physics. Let us go back to its discovery: as we have said, two totally different experiments were involved in it. The first was a fixed-target experiment, whose main advantage was to scan all the energy range below the c.m. energy of the collision. Its main disadvantage was to produce many other particles than the resonance which it looked for. The second experiment was taking place at an e^+e^- collider with totally opposite characteristics, one given energy and a clean environment surrounding the expected resonance. In a sense, the J/ψ discovery is as if the Higgs boson had been discovered simultaneously at LEP and at the Tevatron...

The discovery in a fixed-target experiment shows that the J/ψ leptonic decay is significant, making it highly detectable compared to particles only detected through their hadronic decays. J/ψ is in fact so highly detectable that it was not a major problem to have bunches of other hadrons produced during the same collision.

Let us explain why this leptonic decay is significant. Firstly, the open charm channel (decay to D-mesons) is kinematically blocked since $m_{J/\psi} \leq 2m_D$; secondly, colour prevents decays in a single gluon; thirdly, the Landau-Yang theorem [22] or the G-parity conservation forbids its decay into two gluons. Therefore, three gluon emissions are required and, as the gluon emission rate from heavy quarks is reduced[12], one is not too surprised to get a total width of 91 ± 3 keV, much smaller than that of usual hadronic decays. Moreover, this value also includes leptonic channels. On the other hand, leptonic decays are not subject to all these restrictions: a single photon decay is allowed, making them competitive with hadronic decays. More precisely, they account for one third of the total width.

This significant branching ratio into leptons, especially into muons, is an incredible chance, like a metal detector to find a needle in a haystack. In high-energy hadron colliders, the number of background hadrons becomes annoyingly large and complicates the detection of particles with constrained kinematical characteristics. However, for muons, this is a completely different story, as they can go through the calorimeters without interaction and be seen in dedicated detectors. These can measure precisely their charge, momentum

[12] This comes from the fact that the scale of the process is of the order of m_Q and makes α_s relatively low. In fact, this results in the Zweig rules.

and direction, determining therefore their track. It is in turn possible to discriminate precisely which dimuon, out of the complete set of the detected muons and anti-muons, results from the decay of a J/ψ. The latter being a significant source of dimuons, it is therefore an ideal probe to understand high-energy hadron collisions where many other studies are prevented due to a high background.

Concerning its discovery with an e^+e^- collider, it results partly from the fact that the rather low J/ψ mass was accessible to the available experiments whereas had it been lower, say 1.5-2 GeV, J/ψ would perhaps have been lost among excited states of strange baryons.

The reasonably low mass of the J/ψ makes it highly producible, with an easily reachable threshold in energy. This explains why it is abundantly produced at the Tevatron, even at relatively large transverse momentum. This qualifies it, once more, as a good probe to study mechanisms associated with its production. Furthermore, its production at large transverse momentum, *i.e.* in a range where perturbative Quantum Chromodynamics (pQCD) is likely to be applicable, offers us a way to test the application of QCD. This statement that we have a sufficiently high scale to use pQCD will follow us all along this thesis.

To complete the picture, the Υ's, which are heavier, will be a useful benchmark; even though they are less produced due to their higher mass, they set a higher scale, for which pQCD should apply better, even under unfavourable kinematical conditions. Their quarks being heavier, their velocity inside the meson is expected to be much smaller and, consequently, relativistic effects to be less important. This lowers theoretical uncertainties and constrains more the quantities to be tested.

To be more definite, quarkonium production was thought, till the middle of the nineties, to be a good way to extract the gluon distribution function, both in electron-proton collisions where the modelisations are more reliable, and in proton-proton collisions where two gluon pdf's enter the calculation. As we shall see, the mechanisms of production of these quarkonia are not yet understood and do not provide us with a powerful tool to achieve the extraction of these pdf's.

1.2.2 The eighties: the time for predictions

The Colour-Singlet Model

This model is[13] the most natural application of QCD to heavy quarkonium production in the high-energy regime. It takes its inspiration in the factorisation theorem of QCD [23][14] where the hard part is calculated by the strict application pQCD and the soft part is factorised in a universal wave function. This model is meant to describe the production not only of J/ψ, $\psi(2S)$, $\Upsilon(1S)$, $\Upsilon(2S)$ and $\Upsilon(3S)$, *i.e.* the ${}^3S_1$ states, but also the singlet S states η_c and η_b as well as the P (χ) and D states.

Its greatest quality resides in its predictive power as the only input, apart form the pdf, namely the wave function, can be determined from data on decay processes or by application of potential models. Nothing more is required. It was first applied to hadron colliders [24],

[13] before the inclusion of fragmentation contributions.

[14] proven for some definite cases, *e.g.* Drell-Yan process.

then to electron-proton colliders [25]. The cross sections for ${}^3S_1$ states were then calculated, as well as also for η and χ, for charmonium and for bottomonium. These calculations were compared to ISR and FNAL data from $\sqrt{s} = 27$ GeV to $\sqrt{s} = 63$ GeV for which the data extended to 6 GeV for the transverse momentum. Updates [26, 27] of the model to describe collisions at the CERN $p\bar{p}$ collider ($\sqrt{s} = 630$ GeV) were then presented. At that energy, the possibility that the charmonium be produced from the decay of a beauty hadron was becoming competitive. Predictions for Tevatron energies were also made [27].

In order to introduce the reader to several concepts and quantities that will be useful throughout this work, let us proceed with a detailed description of this model.

The Model as of early 90's

It was then based on several approximations or postulates:

- If we decompose the quarkonium production in two steps, first the creation of two *on-shell* heavy quarks (Q and $\bar{Q}$) and then their binding to make the meson, one *postulates the factorisation* of these two processes.
- As the scale of the first process is approximately $M^2 + p_T^2$, one considers it as a *perturbative* one. One supposes that its cross section be computable with Feynman-diagram methods.
- As we consider only bound states of heavy quarks (charm and bottom quarks), their velocity in the meson must be small. One therefore supposes that the meson be created with its 2 constituent quarks *at rest* in the meson frame. This is *the static approximation.*
- One finally assumes that the colour and the spin of the $Q\bar{Q}$ pair do not change during the binding. Besides, as physical states are colourless, one requires the pair be produced in a *colour-singlet state*. This explains the name Colour-Singlet Model (CSM).

In high-energy hadronic collisions, the leading contribution comes from a gluon fusion process; as the energy of the collider increases, the initial parton momentum fraction x_i needed to produce the quarkonium decreases to reach the region in x where the number of gluons becomes much larger than the number of quarks. One has then only six Feynman diagrams for the ${}^3S_1$ states production associated with a gluon[15] (see Fig. 1.7).

One usually starts with $\mathcal{M}(p)$, the perturbative amplitude to produce the heavy quark pair on-shell with relative momentum p and in a configuration similar to the one of the meson. To realize the latter constraint, one introduces a projection operator[16]; the amplitude $\mathcal{M}(p)$ is then simply calculated with the usual Feynman rules.

The amplitude to produce the meson is thence given by

$$\mathcal{A} = \int \Phi(\vec{p})\mathcal{M}(p)\delta(2p^0)dp, \tag{1.2}$$

[15] This is the dominant process when the transverse momentum of the meson is non-vanishing.

[16] In fact, this amounts to associate a γ^5 matrix to pseudoscalars, γ^μ to vectors, etc.

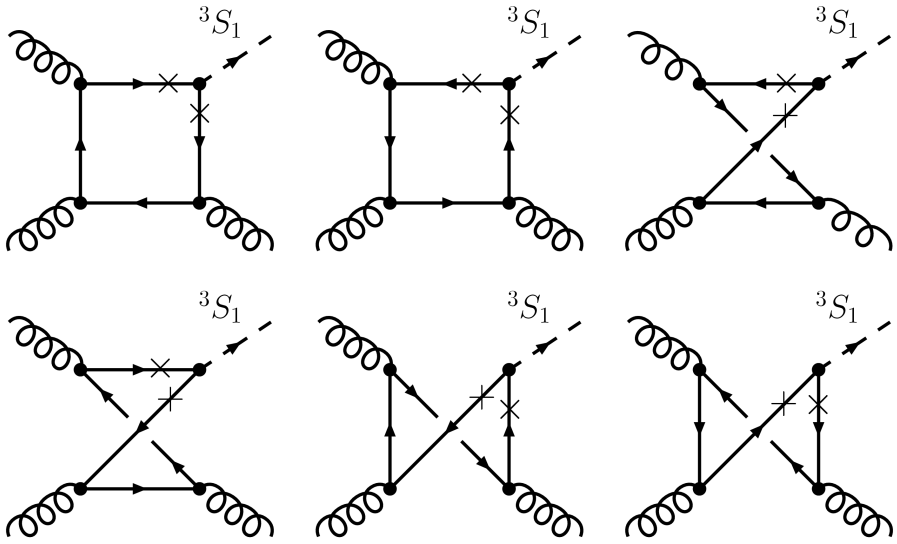

Figure 1.7: The 6 diagrams for $gg \to {}^3S_1 g$ at LO within the CSM.

where $\Phi(\vec{p})$ is the usual Schrödinger wave-function.

Fortunately, one does not have to carry out the integration thanks to the *the static approximation* which amounts to considering the first non-vanishing term of $\mathcal{A}$ when the perturbative part $\mathcal{M}$ is expanded in p. For S-wave, this gives

$$\int \Phi(\vec{p})\mathcal{M}(p)\delta(2p^0)dp \simeq \mathcal{M}|_{p=0}\, \Psi|_{\vec{x}=0}\,, \tag{1.3}$$

where Ψ is the wave-function in coordinate space, and $\Psi|_{\vec{x}=0}$ or $\Psi(0)$ is its value at the origin. For P-waves, $\Psi(0)$ is zero, and the second term in the Taylor serie must be considered; this makes appear $\Psi'(0)$. $\Psi(0)$ (or $\Psi'(0)$) is the non-perturbative input, which is also present in the leptonic decay width from which it can be extracted.

If the perturbative part $\mathcal{M}(p)$ is calculated at the leading order in α_s, this will be referred to as the Leading Order CSM (LO CSM) [24, 25].

The Colour Evaporation Model

This model was initially introduced in 1977 [29, 30] and was revived in 1996 by Halzen *et al.* [31], following a prescription by Buchmüller and Hebecker [32] to explain rapidity gap production in deep-inelastic scattering.

The main characteristic of this model is the total rejection of the role of colour. Contrarily to the CSM, the heavy quark pair produced by the perturbative interaction is not assumed to be in a colour-singlet state. One simply considers that the colour and the spin of the asymptotic $Q\bar{Q}$ state is randomised by numerous soft interactions occurring after its production, and that, as a consequence, it is not correlated with the quantum numbers of the pair right after its production.

A first consequence of this statement is that the production of a ${}^3S_1$ state by one gluon is possible, whereas in the CSM it was forbidden solely by colour conservation. In addition, the probability that the $Q\bar{Q}$ pair eventually be in a colour-singlet state is therefore $\frac{1}{9}$, which gives the total cross section to produce a quarkonium:

$$\sigma_{onium} = \frac{1}{9} \int_{2m_Q}^{2m_{\bar{q}Q}} dm \frac{d\sigma_{Q\bar{Q}}}{dm}. \tag{1.4}$$

This amounts to integrating the cross sections of production of $Q\bar{Q}$ from the threshold $2m_Q$ up to the threshold to produce two charm or beauty mesons (designated here by $\bar{q}Q$) and one divides by 9 to get the probability of having a colour-singlet state.

The procedure to get the cross section for a definite state, for instance a J/ψ, is tantamount to "distributing" the cross sections among all states:

$$\sigma_{J/\psi} = \rho_{J/\psi} \sigma_{onium}. \tag{1.5}$$

The natural value for $\rho_{J/\psi}$, as well as for the other states in that approximation, is the inverse of the number of quarkonium lying between $2m_c$ and $2m_D$. This can be refined by factors arising from spin multiplicity arguments or by the consideration of the mass difference between the produced and the final states. These are included in the Soft-Colour-Interactions approach (SCI) [33].

By construction, this model is unable to give information about the polarisation of the quarkonium produced, which is a key test for the other models [34]. Furthermore, nothing but fits can determine the values to input for ρ, except perhaps the SCI approach which relies on Monte-Carlo simulation, but this does not help to understand the underlying mechanisms. Considering production ratios for charmonium states within the simplest approach for spin, we should have for instance $\sigma[\eta_c] : \sigma[J/\psi] = 1 : 3$ and $\sigma[\chi_{c0}] : \sigma[\chi_{c1}] : \sigma[\chi_{c2}] = 1 : 3 : 5$, whereas deviations from the predicted ratio for χ_{c1} and χ_{c2} have been observed. Moreover, it is unable to describe the observed variation – from one process to another – of the production ratios for charmonium states. For example, the ratio of the cross sections for χ_c and J/ψ differs significantly in photoproduction and hadroproduction, whereas for the CEM these number are strictly constant.

All these arguments make us think that despite its simplicity and its phenomenological reasonable grounds, this model is less reliable than the CSM. It is also instructive to point out that the invocation of reinteractions after the $Q\bar{Q}$ pair production contradicts factorisation, which is albeit required when the pdf are used. However, as we shall see now, the CSM has undergone in the nineties a lashing denial from the data.

1.2.3 The nineties: the time for disillusions

ψ' anomaly

In 1984, Halzen *et al.* [26] noticed that charmonium production from a weak B decay could be significant at high energy – their prediction were made for $\sqrt{s} = 540$ GeV – and could

even dominate at high enough p_T. This can be easily understood having in mind that the B meson is produced by fragmentation of a b quark – the latter dresses with a light quark –. And to produce only one b quark at high p_T is not so burdensome; the price to pay is only to put one quark propagator off-shell, instead of two for $gg \to \psi g$.

This idea was confirmed by the calculations of Glover *et al.* [27], which were used as a benchmark by the UA1 Collaboration [28]. After the introduction of a K factor of 2, the measurements agreed with the predictions; however the p_T slope was not compatible with b-quark fragmentation simulations.

From 1993, the CDF collaboration undertook an analysis of ψ[17] production. They managed to extract unambiguously the *prompt* component of the signal (not from B decay) using a Silicon Vertex Detector (SVX) [35][18].

The preliminary results showed an unexpectedly large *prompt* component. For the ψ', the *prompt* cross section was orders of magnitude above the predictions of the LO CSM (compare the data to the dashed curve on Fig. 1.8 (b)) . This problem was then referred to as the ψ' anomaly. For J/ψ, the discrepancy was smaller (Fig. 1.8 (a)), but it was conceivably blurred by the fact that a significant part of the production was believed to come from χ_c radiative feed-down, but no experimental results were there to confirm this hypothesis.

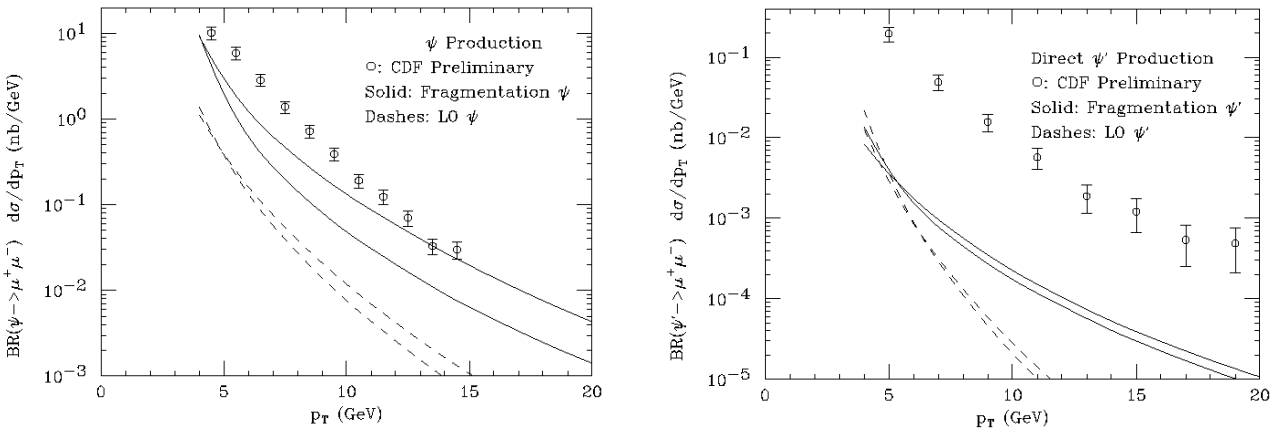

(a) J/ψ (b) ψ'

Figure 1.8: Cross sections obtained by Braaten *et al.* for LO CSM (dashed curves) of J/ψ (a) and ψ' (b), as well as for CSM fragmentation contribution (solid curves). In each case, the two curves depict the extremum values obtained by varying parameters such as m_c and the different scales: μ_R, μ_F, μ_{frag} (from [40]).

[17] In the following, ψ stands for both J/ψ and ψ'.

[18] The details of the analysis are given in the following chapter.

Fragmentation within the CSM

The prediction from the LO CSM for *prompt* ψ being significantly below these preliminary measurements by CDF, Braaten and Yuan [36] pointed out in 1993 that gluon fragmentation processes, even though of higher order in α_s, were to prevail over the LO CSM for S-wave mesons at large p_T, in same spirit as the production from B was dominant as it came from a fragmentation process. Following this paper, with Cheung and Fleming [37], they considered the fragmentation of c quark into a ψ in Z_0 decay. From this calculation, they extracted the corresponding fragmentation function. In another paper [38], they considered gluon fragmentation into P-wave mesons. All the tools were then at hand for a full prediction of the prompt component of the J/ψ and ψ' at the Tevatron. This was realised simultaneously by Cacciari and Greco [39] and by Braaten *et al.* [40]. We shall discuss their results after a digression about the formalism.

To understand how the fragmentation process is factorised from the hard interaction and how it can be so enhanced that it becomes larger than the LO terms, let us consider the η_c production as was done in [36]. Since its charge conjugation is +1, it can be produced in association with two gluons. The LO CSM diagram is depicted in Fig. 1.9 (a), whereas one of the NLO CSM diagram is on depicted in Fig. 1.9 (b).

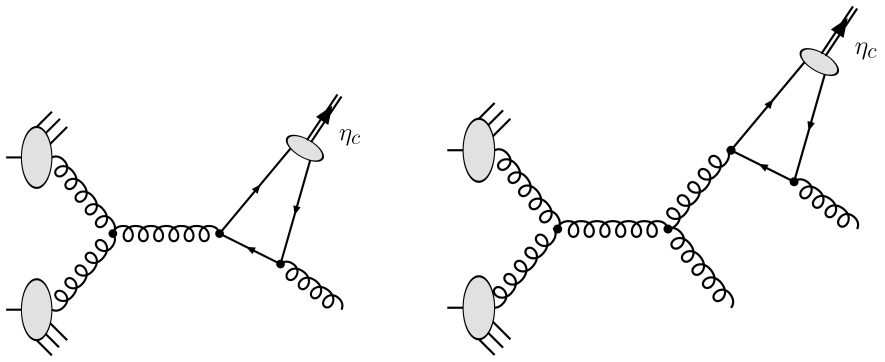

(a) J/ψ (b) $\psi(2S)$

Figure 1.9: The LO CSM diagram for η_c production in gluon fusion process (a), one of the NLO CSM diagram for the same process (b) .

Normally, the two virtual gluons of the NLO process (Fig. 1.9 (b)) are off their mass shell by $\sim p_T$, as well as the virtual gluon and the virtual quark in the LO process (Fig. 1.9 (a)). The NLO diagram is then solely suppressed by one power of α_s at the chosen scale, which can be p_T. However, in some regions of phase space, namely when the off-shell gluon attached to the $c\bar{c}$ is soft – with an off-shellness of the order of m_c –, this diagram is enhanced by a factor of $\frac{p_T^2}{m_c^2}$ compared to the LO one. At sufficiently large values of p_T, this enhancement can overcome the α_s suppression. This behaviour can in fact be traced back to the impossibility of large relative momentum configurations for the constituents of the bound state.

In this region, this NLO contribution can factorised: the first factor is the amplitude $gg \to gg^*$ where the off-shell and the on-shell gluons in the final state have a high p_T and where the same off-shell gluon has a small off-shellness $q^2 \ll p_T^2$; the second factor is the propagator of the gluon, $1/q^2$, and the third corresponds to the fragmentation function $g^* \to \eta_c g$. Taking into consideration the restriction on the relative momentum within the bound state, we can therefore express the differential cross section to produce the η_c with a momentum P as:

$$d\sigma_{\eta_c}(P) \simeq \int_0^1 dz d\sigma_g\left(\frac{P}{z}\right) D_{g\to\eta_c}(z), \tag{1.6}$$

$d\sigma_g\left(\frac{P}{z}\right)$ being the differential cross section for $gg \to gg^*$ where the momentum of g^* is $\frac{P}{z}$ and $D_{g\to\eta_c}(z)$ is the gluon fragmentation function.

It is now possible to generalise this to all quarkonia. To take into account collinear production of fragmenting gluons from a higher energy parton, a fragmentation scale μ_{frag} is introduced which is meant to include logarithms of p_T/m_Q appearing in these collinear emissions ($\ln(p_T/m_Q) = \ln(p_T/\mu_{frag}) + \ln(\mu_{frag}/m_Q)$). Hence, to all orders in α_s, we have the following fragmentation cross section for a quarkonium $\mathcal{Q}$:

$$\sigma_{\mathcal{Q}}(P) \simeq \sum_i \int_0^1 dz d\sigma_i(\frac{P}{z}, \mu_{frag}) D_{i\to\mathcal{Q}}(z, \mu_{frag}). \tag{1.7}$$

The scale is as usual chosen to avoid large logarithms of p_T/μ_{frag} in $\sigma_i(\frac{P}{z}, \mu_{frag})$, that is $\mu_{frag} \simeq p_T$. The summation of the corresponding large logarithms of μ_{frag}/m_Q appearing in the fragmentation function is realised via an evolution equation [41, 42].

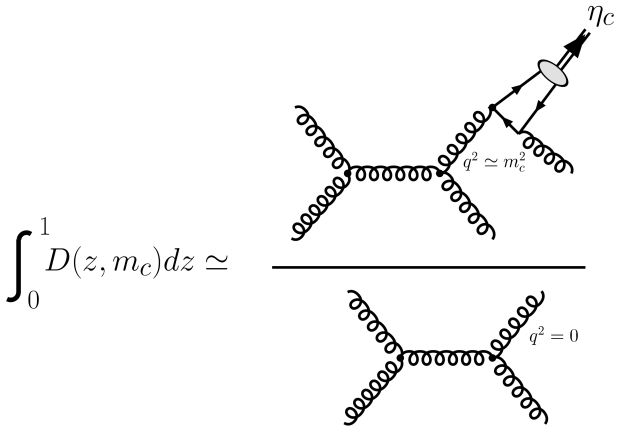

Figure 1.10: Illustration of how to obtain $\int_0^1 D(z, m_c)$.

The interesting point raised by Braaten and Yuan is that the fragmentation functions can be calculated perturbatively in α_s at the scale $\mu_{frag} = 2m_Q$. For instance, in the case of gluon fragmentation into an η_c, the trick is to note that $\int_0^1 dz D_z(z, m_c)$ is the ratio to the rates for

the well-known $gg \to gg$ process and $gg \to \eta_c gg$ (Fig. 1.10). After some manipulations, the fragmentation function can be obtained from this ratio by identifying the integrand in the z integral. This gives :

$$D_{g\to\eta_c}(z, 2m_c) = \frac{1}{6}\alpha_s^2(2m_c)\frac{|\psi(0)|^2}{m_c^3}[3z - 2z^2 + 2(1-z)\ln(1-z)]. \tag{1.8}$$

The other fragmentation functions of a given parton i into a given quarkonium $\mathcal{Q}$, $D_{i\to\mathcal{Q}}(z, \mu_{frag})$, were obtained in the same spirit. For the Tevatron, the differential cross section versus p_T of various CSM fragmentation processes are plotted in Fig. 1.11.

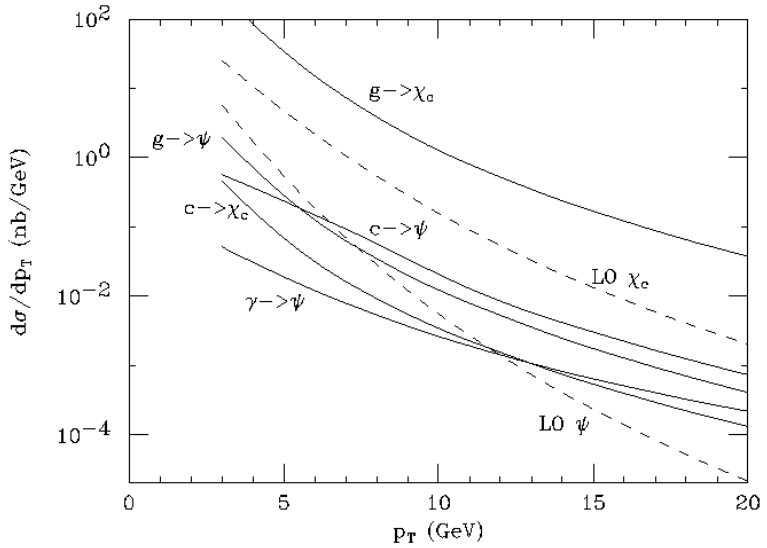

Figure 1.11: Differential cross section versus p_T of various CSM fragmentation processes for J/ψ to be compared with the LO contributions (from [40]).

The *prompt* component of the J/ψ and the direct component of the ψ' could in turn be obtained and compared with the preliminary data of CDF (see the solid curves in plots in Fig. 1.8 above). For the J/ψ, the previous disagreement was reduced and could be accounted for by the theoretical and experimental uncertainties; on the other hand, for the ψ', the disagreement continued to be dramatic. The situation would be clarified by the extraction of the direct component for J/ψ, for which theoretical uncertainties are reduced and are similar to those for the ψ'.

The CDF collaboration undertook the disentanglement of the direct J/ψ signal [43]. They searched for J/ψ associated with the photon emitted during this radiative decay: the result was a direct cross section 30 times above expectations from LO CSM plus fragmentation. This was the confirmation that the CSM was not the suitable model for heavy quarkonium production in high-energy hadron collisions.

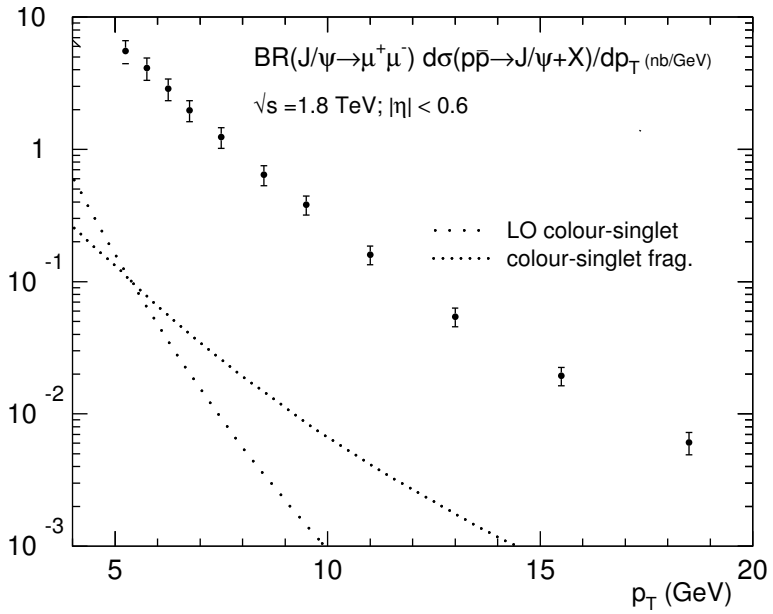

Figure 1.12: Differential cross section versus p_T of the CSM (fragmentation and LO) production to be compared with the direct production of J/ψ from CDF (Adapted from [44]).

NRQCD: successes and doubts...

In 1992, Bodwin *et al.* considered new Fock state contributions in order to cancel exactly the IR divergence in the light hadron decays of χ_{c1} at LO. This decay proceeds via two gluons, one real and one off-shell, which gives the light-quark pair forming the hadron. When the first gluon becomes soft, the decay width diverges. The conventional treatment [45], which amounts to regulating the divergence by an infrared cut-off identified with the binding energy of the bound state, was not satisfactory: it supposed a logarithmic dependence of $\Psi'(0)$ upon the binding energy. They looked at this divergence as being a clear sign that the factorisation was violated in the CSM.

Their new Fock states for χ_c were *e.g.* a gluon plus a $c\bar{c}$ pair, in a ${}^3S_1$ configuration and in a *colour-octet* state. The decay of this Fock state occurred through the transition of the coloured pair into a gluon (plus the other gluon already present in the Fock state as a spectator). This involves a new phenomenological parameter, H_8, which is related to the probability that the $c\bar{c}$ pair of the χ_c be in a colour-octet S-wave state. The key point of this procedure is that a logarithmic dependence on a new scale Λ – a typical momentum scale for the light quark – appears naturally within the effective field theory Non-Relativistic Quantum Chromodynamic (NRQCD) [46, 47].

This effective theory is based on a systematic expansion in both α_s and v, which is the quark velocity within the bound state. For charmonium, $v_c^2 \simeq 0.23$ and for bottomonium $v_b^2 \simeq 0.08$. One of the main novel features of this theory is the introduction of dynamical gluons in the Fock state decomposition of the physical quarkonium states. In the case of

S-wave orthoquarkonia ($^3S_1$), we schematically have, in the Coulomb gauge:

$$\begin{aligned}|\mathcal{Q}_Q\rangle =&\mathcal{O}(1)|Q\bar{Q}[\,^3S_1^{(1)}]\rangle + \mathcal{O}(v)|Q\bar{Q}[\,^3P_J^{(8)}g]\rangle + \mathcal{O}(v^2)|Q\bar{Q}[\,^1S_0^{(8)}g]\rangle \\ &+ \mathcal{O}(v^2)|Q\bar{Q}[\,^3S_1^{(1,8)}gg]\rangle + \mathcal{O}(v^2)|Q\bar{Q}[\,^3D_J^{(1,8)}gg]\rangle + \dots\end{aligned} \tag{1.9}$$

whereas for P-wave orthoquarkonia (^3P_J), the decomposition is as follows

$$|\mathcal{Q}_{Q_J}\rangle =\mathcal{O}(1)|Q\bar{Q}[\,^3P_J^{(1)}]\rangle + \mathcal{O}(v)|Q\bar{Q}[\,^3S_1^{(8)}g]\rangle + \dots \tag{1.10}$$

In these two formulae, the superscripts (1) and (8) indicate the colour state of the $Q\bar{Q}$ pair. The $\mathcal{O}(v^n)$ factors indicate the order in the velocity expansion at which the corresponding Fock state participates to the creation or the annihilation of quarkonia. This follows from the *velocity scaling rules* of NRQCD (see *e.g.* [47]).

In this formalism, it is thus possible to demonstrate, in the limit of large quark mass, the factorisation between the short-distance – and perturbative – contributions and the hadronisation of the $Q\bar{Q}$, described by non-perturbative matrix elements defined within NRQCD. For instance, the differential cross section for the production of a quarkonium $\mathcal{Q}$ associated with some other hadron X reads

$$d\sigma(\mathcal{Q}+X) = \sum d\hat{\sigma}(Q\bar{Q}[^{2S+1}L_J^{(1,8)}]+X)\langle\mathcal{O}^{\mathcal{Q}}[^{2S+1}L_J^{(1,8)}]\rangle, \tag{1.11}$$

where the sum stands for S, L, J and the colour.

The long-distance matrix element (LDME) $\langle\mathcal{O}^{\mathcal{Q}}[^{2S+1}L_J^{(1,8)}]\rangle$ takes account of the transition between the $Q\bar{Q}$ pair and the final physical state $\mathcal{Q}$. Its power scaling rule comes both from the suppression in v of the Fock state component $[^{2S+1}L_J^{(1,8)}]$ in the wave function of $\mathcal{Q}$ and from the scaling of the NRQCD interaction responsible for the transition.

Usually, one defines $\mathcal{O}^{\mathcal{Q}}[^{2S+1}L_J^{(1,8)}]$ as the production operator that creates and annihilates a point-like $Q\bar{Q}$ pair in the specified state. This has the following general expression

$$\begin{aligned}\mathcal{O}^{\mathcal{Q}}[^{2S+1}L_J^{(1,8)}] &= \chi^\dagger K\psi\left(\sum_X\sum_{J_z}|\mathcal{Q}+X\rangle\langle\mathcal{Q}+X|\right)\psi^\dagger K\chi \\ &= \chi^\dagger K\psi(a_{\mathcal{Q}}^\dagger a_{\mathcal{Q}})\psi^\dagger K\chi,\end{aligned} \tag{1.12}$$

where[19] ψ and χ are Pauli spinors and the matrix K is a product of colour, spin and covariant derivative factors. These factors can be obtained from the NRQCD lagrangian [47]. For instance, $\mathcal{O}^{\mathcal{Q}}[\,^3S_1^{(1)}] = \chi^\dagger\vec{\sigma}\psi(a_{\mathcal{Q}}^\dagger a_{\mathcal{Q}})\psi^\dagger\vec{\sigma}\chi$. However some transitions require the presence of chromomagnetic ($\Delta L = 0$ and $\Delta S = \pm 1$) and chromoelectric ($\Delta L = \pm 1$ and $\Delta S = 0$) terms for which the expressions of K are more complicated.

On the other hand, the general scaling rules relative to the LDME's [44] give:

$$\langle\mathcal{O}^{\mathcal{Q}}[^{2S+1}L_J^{(1,8)}]\rangle = v^{3+2L+2E+4M}, \tag{1.13}$$

[19] The second line of Eq. (1.12) is nothing but a short way of expressing this operator.

where E and M are the minimum number of chromoelectric and chromomagnetic transitions for the $Q\bar{Q}$ to go from the state $[^{2S+1}L_J^{(1,8)}]$ to the dominant quarkonium $\mathcal{Q}$ Fock state.

The idea of combining fragmentation as the main source of production with allowed transitions between a χ_c to a $^3S_1$ in a colour-octet state, had already been applied by Braaten and Yuan in the above mentioned paper [38]. Indeed, similar formulae can be written for fragmentation functions [48]:

$$D_{g\to\mathcal{Q}}(z,\mu) = \sum d_{[^{2S+1}L_J^{(1,8)}]}(z,\mu)\langle\mathcal{O}^{\mathcal{Q}}[^{2S+1}L_J^{(1,8)}]\rangle, \tag{1.14}$$

where $d_{[.]}(z,\mu)$ accounts for short-distance contributions and does not depend on which $\mathcal{Q}$ is involved. But since the theoretical predictions for prompt J/ψ production did not disagree dramatically with data and since there was no possible χ_c decay to ψ', a possible enhancement of the χ_c cross section by colour-octet mechanism (COM) was not seen as a key-point both for J/ψ and ψ' production.

However, in the case of J/ψ and ψ' production, COM could still matter in a different manner: fragmentation of a gluon into a $^3P_J^{(8)}$ is possible with solely one gluon emission and fragmentation into a $^3S_1^{(8)}$ requires no further gluon emission (at least in the hard process described by $d_{[.]}(z,\mu)$). Concerning the latter process, as two chromoelectric transitions are required for the transition $|c\bar{c}gg\rangle$ to $|c\bar{c}\rangle$, the associated LDME $\langle\mathcal{O}^{\psi}[^3S_1^{(8)}]\rangle$ was expected to scale as $m_c^3v^7$. In fact, $d_{[^3S_1^{(8)}]}$, the contribution to the fragmentation function of the short-distance process $g\to{}^3S_1^{(8)}$ was already known since the paper of Braaten and Yuan [38] and could be used here, as the hard part $d_{[.]}(z,\mu)$ of the fragmentation process is independent of the quarkonium.

In a key paper, Braaten and Fleming [38] combined everything together to calculate, for the Tevatron, the fragmentation rate of a gluon into an octet $^3S_1$ that subsequently evolves into a ψ'. They obtained, with[20] $\langle\mathcal{O}^{\psi(2S)}[^3S_1^{(8)}]\rangle = 4.2\times10^{-3}$ GeV^3, a perfect agreement with the CDF preliminary data: compare these predictions in Fig. 1.13 with the previous ones in Fig. 1.8 (b).

A straightforward and unavoidable consequence of this solution to the ψ' anomaly was raised by Cho and Wise [49]: the ψ', produced in the latter way, was 100% transversally polarised. A suggested test of this prediction was also given, *i.e.* the measurement of the lepton angular distribution in $\psi'\to\ell^+\ell^-$, which should behave as

$$\frac{d\Gamma}{d\cos\theta}(\psi'\to\ell^+\ell^-) \propto (1+\alpha\cos^2\theta), \tag{1.15}$$

with α=1 for 100% transversally polarised particles. Further details are given in section 2.5.

Following these studies, a complete survey on the colour-octet mechanism was made in two papers by Cho and Leibovich [50, 51]. The main achievements of these papers were the calculation of colour-octet P-state contributions to ψ, the first prediction for direct colour-octet J/ψ production through *e.g.* the χ_c feed-down calculation, the first predictions for Υ

[20] This corresponds to a suppression of 25 compared to the "colour-singlet matrix element" $\langle\mathcal{O}^{\psi(2S)}[^3S_1^{(1)}]\rangle$, which scales as $m_c^3v^3$. This is thus in reasonnable agreement with a v^4 suppression.

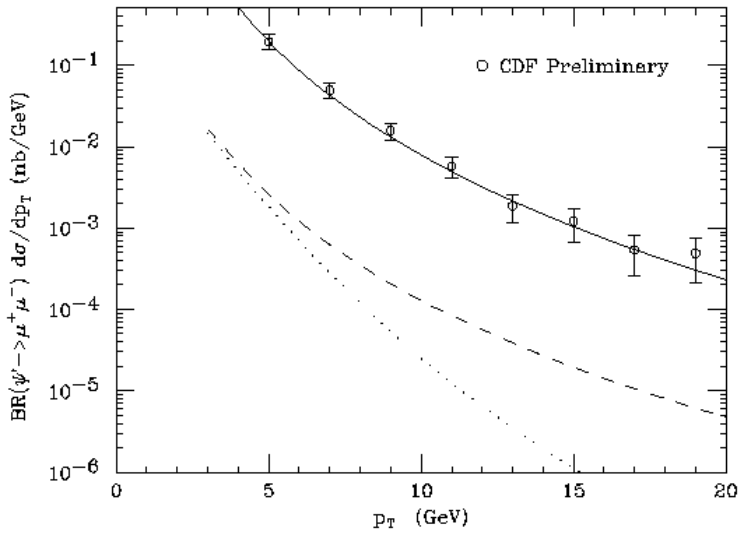

Figure 1.13: Differential cross section versus p_T of the CSM (dotted: LO; dashed: fragmentation and LO) production and of the COM fragmentation (solid curve) to be compared with CDF preliminary direct production of ψ' (from [38]).

and the complete set of $2 \to 3$ parton processes like $ij \to c\bar{c} + k$, all this in agreement with the data.

A few year later, however, the CDF collaboration carried out the study of polarisation of prompt ψ [52]. The outcome was $\alpha = 0$ for ψ', or even $\alpha < 0$ when p_T becomes large. For J/ψ, the same behaviour showed up, whereas comparison with theory is still difficult because of the χ_c feed-down. In any case, no sign of strong transverse polarisation was seen, in total contradiction with all predictions of the COM.

Summary

To sum up, we have seen that the LO CSM gives smaller contributions than the fragmentation processes for the CSM, where the heavy quark pair produced in the hard part of the process has strictly the same quantum numbers as the final physical state. On the other hand, in order to solve problems connected with the factorisation for χ_c decay, one is driven to introduce new contributions from higher Fock states.

In the context of production, this allows a given physical state to come from a heavy quark pair with different quantum numbers, *e.g.* in a colour-octet state. For the case of fragmentation, even though these higher Fock-state contributions are suppressed, they involve lower-order contributions in α_s and are shown to dominate for intermediate and large momentum transfer.

All these statements can be easily understood by analysing the large P_T behaviour of the differential cross section, $\frac{d\sigma}{dP_T^2}$, from typical diagrams relevant for the considered processes. For the LO CSM, at large P_T, the two internal lines not linked with the bound state are

off-shell by $\sim P_T^2$ and make the partonic differential cross section behave like $\frac{d\sigma}{dP_T^2} \sim \frac{1}{P_T^8}$, as depicted in Fig. 1.14 (a).

To what concerns fragmentation, it behaves like a single particle production process, thus like $\frac{d\sigma}{dP_T^2} \sim \frac{1}{P_T^4}$, if we consider that, at large P_T, the effects of the quarkonium mass become negligible. Even though fragmentation processes (Fig. 1.14 (b)) are of higher order in α_s (α_s^5 instead of α_s^3), they scale like $\frac{P_T^4}{(2m_c)^4}$ compared to LO CSM and dominate over the latter for $P_T \gg 2m_c$.

The inclusion of colour-octet channels can be analysed with similar arguments. For the ${}^3S_1^{(8)}$ channel, the only difference comes from the powers of α_s and v. No similar estimation for power counting of the P_T dependence can be done for the other $\mathcal{O}(v^4)$ channels [51], however the gluon t-channel dominance argument [44] provides us with the scaling $\frac{1}{P_T^6}$. Indeed these channels are significant at moderate P_T of the order of $2m_c$, as one can conclude from the complete analysis made in [51].

On the other hand, the statement that the polarisation of ψ produced at large P_T be entirely transverse – at variance with experimental data – follows simply and only from the on-shellness of the fragmenting gluon and from the approximate spin symmetry of NRQCD.

Considering that no solution of the polarisation issue has been proposed so far, we have decided to undertake an analysis of the non-static effect of the LO CSM, with the first hope to state that the static approximation was not viable for previously unknown reasons, but also with the goal to attain new insights about some other unknown effects linked with quarkonium production. As we shall see, it seems that the static approximation is not problematic. However, we have realised than unconstrained contributions could be introduced in the description of the production of the quarkonium in association with a gluon – as it should be at non vanishing transverse momentum. This introduction can bring the theoretical predictions in agreement with experimental measurements, for the cross section and for the polarisation.

(a) leading-order colour-singlet: $g + g \to c\bar{c}[^3S_1^{(1)}] + g$

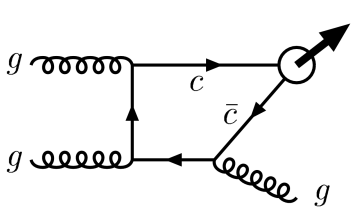

$+ \ldots \qquad \sim \alpha_s^3 \frac{(2m_c)^4}{p_t^8}$

(b) colour-singlet fragmentation: $g + g \to [c\bar{c}[^3S_1^{(1)}] + gg] + g$

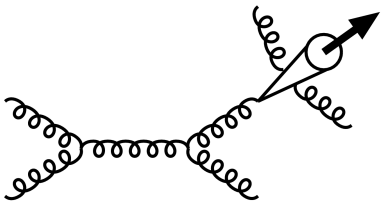

$+ \ldots \qquad \sim \alpha_s^5 \frac{1}{p_t^4}$

(c) colour-octet fragmentation: $g + g \to c\bar{c}[^3S_1^{(8)}] + g$

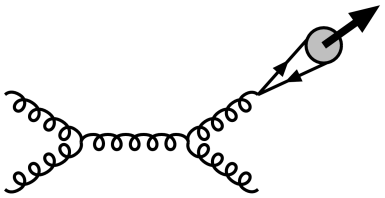

$+ \ldots \qquad \sim \alpha_s^3 \frac{1}{p_t^4} v^4$

(d) colour-octet t-channel gluon exchange: $g + g \to c\bar{c}[^1S_0^{(8)}, ^3P_J^{(8)}] + g$

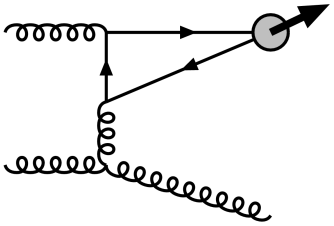

$+ \ldots \qquad \sim \alpha_s^3 \frac{(2m_c)^2}{p_t^6} v^4$

Figure 1.14: Summary of the different processes arising in the direct production of ψ within the CSM and the COM and their p_T dependence (from Krämer [44]).

Chapter 2

Experimental results

2.1 Foreword

Before broaching a review of the most recent results on high-energy hadroproduction of J/ψ, ψ' and Υ's, let us remind the reader of the various kinds of collisions and colliders in which these particles can be created.

For most of the following discussion, we shall limit ourselves to high-energy collider experiments, because most of the models that we shall consider in this thesis are valid in the perturbative regime of QCD, *i.e.* when the coupling constant α_s is clearly less than 1; this is likely to be the case for reactions with c.m. energy larger than, say, 5 GeV. Furthermore, the factorisation hypothesis relies on the assumption of having a sufficiently inclusive reaction, although the quarkonium is actually detected. This is another reason to impose a large energy. Concerning fixed target experiments, for which factorisation is uncertain, we shall not include them in our survey, even though heavy quarkonium production in that regime is certainly of great interest.

Limiting ourselves to high-energy collisions, the most recent published results for quarkonium hadroproduction come from two accelerators:

1. **The Tevatron** at Fermilab which – as stated by its name – runs at TeV energy with proton-antiproton collisions. For Run I ("Run IA" 1993-94 and "Run IB" 1995-96), the energy in c.m. was 1.8 TeV. For Run II, it has been increased to 1.96 TeV. The experimental analyses for this Run are still being carried out.

2. **RHIC** at BNL running at 200 GeV for the J/ψ study with proton-proton collisions.

There exist also data from electron-proton collision from **HERA** at DESY running with electron-proton beams with proton energy of 820 GeV and electrons energy of 27.6 GeV.

Results for e-p collisions come for the most part from two collaborations, namely ZEUS and H1. Two classes of processes can be distinguished depending on the off-shellness of the photon emitted by the scattering electron. If the photon is on-shell, we are dealing with photoproduction, otherwise, we deal with electroproduction. Results on photoproduction

are compatible with NLO calculations within CSM [53]. Occasionally, we shall mention these in the following discussion.

Finally, three e^+e^- collider are yielding data on quarkonium at present time:

1. **LEP** at CERN running from around Z_0 mass up to around 210 GeV with electron-positron collisions.

2. B factories, **PEP II** at SLAC and **KEK B** at KEK running mainly at the $\Upsilon(4S)$ (10.58 GeV) resonance with electron-positron collisions.

However, quarkonium physics at LEP is very different from that at B factories. Due to its large c.m. energy, LEP can significantly produce ψ through $\gamma\gamma$ collisions which can be selected via kinematical constraints. From a theoretical point of view, this is rather interesting since this way of producing ψ is similar to those at work in hadroproduction, although potentially better understood. On the other hand, to what concerns B factories results, we think that the energy is such that the reactions are not sufficiently inclusive to be straightforwardly compared to reactions that take place at HERA, RHIC or the Tevatron. However, it is very important to keep in mind that there exist serious disagreements between measurements and theoretical predictions of both CSM and COM. Sometimes they are thought to come from missing contributions at end-point which arise when re-summation techniques are applied; this is indeed the sign that some kinds of "exclusive" effects become important at these low energies. For further information, the interested reader may have a look at [34].

Concerning hadroproduction, the above-mentioned deviations between theoretical predictions and measurements of the CDF collaboration could be actually considered as a confirmation of the prior UA1 analysis [28]. The deviations were confirmed by D$\emptyset$ later on [54]. For the Tevatron, only CDF analysis will be presented in the following. Concerning RHIC, we shall expose the analysis for J/ψ in 200 GeV pp collisions from the PHENIX collaboration [55].

It is worth pointing out here that high-energy p-$\bar{p}$ and p-p collisions give similar results for the same kinematics, due to the small contribution of valence quarks.

2.2 Different type of heavy quarkonium production

As we have already explained, the detection of quarkonia proceeds via the identification of their leptonic decay products. We give in Tab. (2.1) the relative decay widths into muons.

Meson	$\Gamma(\mu^+\mu^-)/\Gamma(total)$
J/ψ	0.0588 ± 0.0010
$\psi(2S)$	0.0073 ± 0.0008
$\Upsilon(1S)$	0.0248 ± 0.0006
$\Upsilon(2S)$	0.0131 ± 0.0021
$\Upsilon(3S)$	0.0181 ± 0.0017

Table 2.1: Table of branching ratios in dimuons [57].

It is interesting to note that the CDF analysis that lead to the problem of quarkonium hadroproduction was in fact not devoted to ψ production but to b-quark production through its (weak) decay into ψ [35]. The value of this decay was already quite well known [56] at that time and a measurement of the proportion of ψ's produced through this decay was expected to give the total number of b quarks produced.

Their study succeeded and they extracted the percentage of ψ's produced through b decays and of ψ's *promptly* produced. The latter was unexpectedly large. Indeed, the production through b decays was expected to behave like a fragmentation process and to dominate at moderate and large p_T. This was not the case and the slight disagreement between total production predictions [27] and UA1 measurements [28] was blown away by a striking incompatibility between prompt ψ production predictions and CDF data. A factor 60 of discrepancy was for instance found for ψ' (see Fig. 1.8 (b)).

In this case, no higher excited states was expected to contribute to its production (see Fig. 1.5), contrarily to the case of the J/ψ which can be the product of a χ_c (P-state) electromagnetic decay. In order to get a complete picture of the problem, the CDF collaboration decided to proceed to a study of the direct production of this meson [43]. This involved the detection of the photon emitted during the radiative decay,

$$\chi_c \to J/\psi + \gamma. \tag{2.1}$$

They then found a direct production 30 times above theoretical predictions.

Briefly, the problem of direct J/ψ production separation comprises three steps:

- muon detection;
- elimination of J/ψ produced by hadrons containing b quarks ;
- elimination of χ_c radiative-decay production;

The following table summarises the different processes to be discussed and the quantities linked.

1^{st} step	2^{nd} step	3^{rd} step	Type	Associated quantity
$p\bar{p} \to c\bar{c} + X$	$c\bar{c} \to J/\psi$	–	Direct prod.	$F(\not{b}, \not{\chi}, \not{\psi}(2S))^{J/\psi}$
	$c\bar{c} \to \chi_c$	$\chi_c \to J/\psi + \gamma$	Prompt prod. by decay of χ_c	$F(\not{b})^{J/\psi}_{\chi}$
	$c\bar{c} \to \psi(2S)$	$\psi(2S) \to J/\psi + X$	Prompt prod. by decay of $\psi(2S)$	$F(\not{b})^{J/\psi}_{\psi(2S)}$
$p\bar{p} \to \bar{b}c + X$	$c\bar{c} \to J/\psi$	–	–	$f_b (or F_b)$
$\bar{b}c \to \bar{c}c + \ell^- + \bar{\nu}_\ell$	$c\bar{c} \to \chi_c$	$\chi_c \to J/\psi + \gamma$	–	
etc ...				

Table 2.2: Different processes involved in J/ψ production accompanied by quantities used in the following discussion.

Let us explain the different fractions that appear in the latter table:

- $F(\not{b}, \not{\chi}, \not{\psi}(2S))^{J/\psi}$ is the *prompt* fraction of J/ψ that do not come χ, neither from $\psi(2S)$, *i.e.* the direct fraction.

- $F(\not{b})^{J/\psi}_{\psi(2S)}$ is the *prompt* fraction of J/ψ that come from $\psi(2S)$.

- $F(\not{b})^{J/\psi}_{\chi}$ is the *prompt* fraction of J/ψ that come from χ.

- F_b (or f_b) is the *non-prompt* fraction or equally the fraction that come for b quarks.

Concerning $\psi(2S)$, due to the absence of stable higher excited states likely to decay into it, we have the following summary for the different processes to be discussed and the quantities linked:

1^{st} step	2^{nd} step	3^{rd} step	Type	Associated quantity
$p\bar{p} \to c\bar{c} + X$	$c\bar{c} \to \psi(2S)$	–	Direct/Prompt prod.	$F(\not{b})^{\psi(2S)}$
$p\bar{p} \to b\bar{c} + X$ $\bar{b}c \to \bar{c}c + \ell^- + \bar{\nu}_\ell$ etc ...	$c\bar{c} \to \psi(2S)$	–	–	$f_b (or F_b)$

Table 2.3: Different processes involved in ψ' production accompanied by quantities used in the following discussion.

Let us explain the different fractions that appear in the latter table:

- $F(\not{b})^{\psi(2S)}$ is the *prompt* fraction of $\psi(2S)$, *i.e.* the direct production.

- F_b (or f_b) is the *non-prompt* fraction or equally the fraction that come for b quarks.

Considering the similarities between the charmonium and bottomonium systems (see Fig. 1.6 for the spectrum), a substantive part of the discussion will be also devoted to it. As can be seen in Tab. (2.1), the leptonic branching ratio are also relatively high. The detection and the analysis of the bottomonia are therefore carried out in the same fashion. For the extraction of the direct production, the b-quark feed-down is obviously not relevant, only the decays from stable higher resonances of the family are to be considered.

All the quantities useful for the bottomonium discussion are summarised in the following table:

1^{st} step	2^{nd} step	3^{rd} step	Type	Associated quantity
$p\bar{p} \to b\bar{b} + X$	$b\bar{b} \to \Upsilon(nS)$	–	Direct prod.	$F^{\Upsilon(nS)}_{direct}$
	$b\bar{b} \to \chi_b$	$\chi_b \to \Upsilon(nS) + \gamma$	Prod. by decay of χ_b	$F^{\Upsilon(nS)}_{\chi_b}$
	$b\bar{b} \to \Upsilon(n'S)$	$\Upsilon(nS) \to \Upsilon(n'S) + X$	Prod. by decay of $\Upsilon(n'S)$	$F^{\Upsilon(nS)}_{\Upsilon(n'S)}$

Table 2.4: Different processes involved in $\Upsilon(nS)$ $(n = 1, 2, 3)$ production accompanied by quantities used in the following discussion.

Let us explain the different fractions that appear in the latter table:

- $F^{\Upsilon(nS)}_{direct}$ is the direct fraction of $\Upsilon(nS)$.
- $F^{\Upsilon(nS)}_{\chi_b}$ is the fraction of $\Upsilon(nS)$ that come from χ_b.
- $F^{\Upsilon(nS)}_{\Upsilon(n'S)}$ is the fraction of $\Upsilon(nS)$ that come from a higher $\Upsilon(n'S)$.

2.3 CDF analysis for ψ production cross sections[1,2]

2.3.1 Succinct description of the parts of the detector used in this analysis

Without entering too much into the details, let us recall the main elements of the detector used for this analysis.

- A superconducting solenoid;
- A central muon detector (CMU: central muon system (or central muon chambers)). It covers the region[3] $|\eta| < 0.6$;
- The silicon vertex detector (SVX) which among other purposes enables to detect a second vertex resulting from the decay of a beauty hadron in a ψ. This detector directly surrounds the beam;
- Two calorimeters: an electromagnetic one and a hadronic one. They cover the whole azimuthal angle ϕ (cf. Fig. 2.1) and spread till pseudorapidity η of 4.2 in absolute value;

[1] Some plots shown in the following are preliminary. These are displayed only for an illustrative purpose. The discussion would have been the same if the corresponding final plots had been available. The plots relative to final observables are however all published ones.

[2] In the following, ψ stands for both J/ψ and ψ'.

[3] $\eta \equiv -\ln(\tan(\theta/2))$ where θ is the polar angle of the particle in the c.m. frame.

- A central tracking chamber (CTC) lying in the induction of the magnet. It enables the determination of the transverse momenta of the particles. It covers a pseudorapidity range of $|\eta| < 1.1$.

2.3.2 ψ total production

Muons are selected by a three-level trigger:

- The **level 1** requires two track segments in the CMU, separated by at least 5° in azimuth (cf. Fig. 2.1);
- The **level 2** requires that at least one of the muon track segments is matched in ϕ to a track found in the CTC by the central fast tracker, a hardware track-finding processor. These two tracks are then considered to come from a single particle;
- The **level 3** requires a pair of oppositely charged muons after full track reconstruction.

Besides this selection, muons are to satisfy other criteria:

- The CTC track is extrapolated to the CMU chambers and is required to lie within 3 σ of the CMU hits, where σ is the uncertainty in the extrapolated position due to multiple scatterings;
- A nonzero energy deposit is required in the calorimeter tower situated in front of the muon-chamber segment;
- To remain in the region of good trigger efficiency, both muons are required to have $p_T > 2.0$ GeV and one muon $p_T > 2.8$ GeV. The two muon tracks are fitted with the requirement that they originate from a common point;
- To remain in a region of good acceptance to ψ decays, the ψ candidate is required to satisfy $|\eta| < 0.6$ and $p_T > 5$ GeV.
- The invariant mass of the pair must lie within the region 3057 MeV $< M(pair) <$ 3137 MeV in order to be considered as coming from a J/ψ and 3646 MeV $< M(pair) <$ 3726 MeV to be considered as coming from a ψ'.

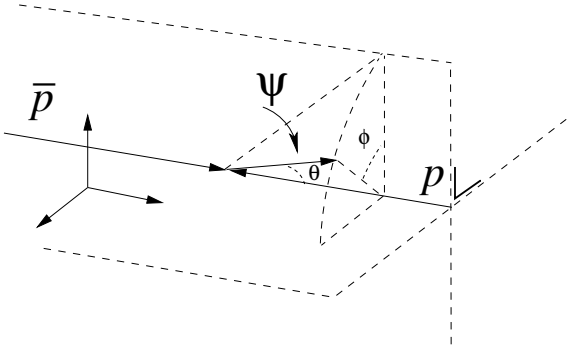

Figure 2.1: General drawing defining the angles.

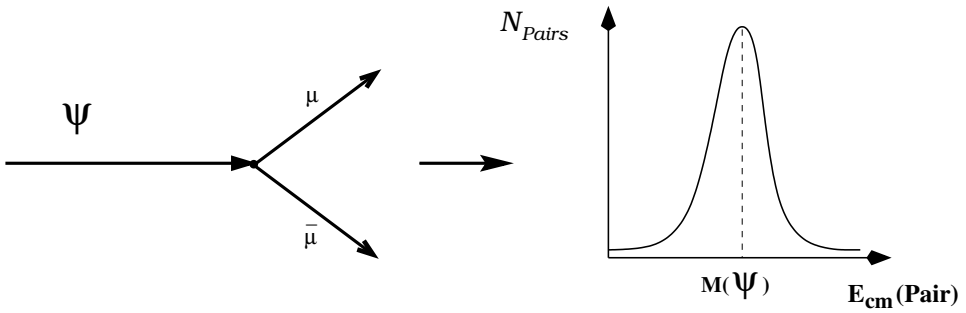

Figure 2.2: Invariant mass distribution of the muon pair in which the ψ decays. The c.m. energy amounts to ψ mass.

On the other hand, 60% of the muon tracks also have hits in the SVX which measures only r and ϕ and the resolution of their track impact parameter is $(13 + 40/p_T)\mu$m, where p_T (expressed in GeV) is the track momentum transverse to the beam line.

The sample of $p\bar{p}$ collisions amounts to 17.8 ± 0.6 pb^{-1} at $\sqrt{s} = 1.8$ TeV. For J/ψ, the considered sample consists however of 15.4 ± 0.6 pb^{-1} of integrated luminosity[4].

The number of ψ candidate is therefore determined by fitting the mass distribution of the muons in the c.m. frame (cf. Fig. 2.2 and Fig. 2.3 (a) and (b)) after subtraction of the noise, which is evaluated as follows.

Various corrections are evaluated by Monte-Carlo simulation. They incorporate deviations due to processes as $\psi \to \mu^+\mu^-\gamma$. Muon momenta are smeared in order to simulate the finite detector resolution. As the measurement of the muon energy is a function of p_T, data are fitted in separate p_T bins.

Concerning the trigger efficiency $\epsilon_{\text{trigger}}$, it is accounted for by weighting the event with $1/\epsilon_{\text{trigger}}$, which depends on p_T.

The mass distribution is then fitted to the signal shape fixed by simulation and to a linear background. The fit yields the mass of the particle and a background estimate; from this, it is easy to find back the number of particles which has decayed and from the branching ratio, the number of produced particles.

For the present study, the fits were reasonably good for each p_T-bin, the χ^2 per degree of freedom ranging from 0.5 to 1.5. The measured width of the mass peak was from 17 MeV to 35 MeV for p_T from 5 to 20 GeV.

Approximatively, 22100 J/ψ candidates and 800 ψ' candidates above a background of 1000 events were observed.

The acceptance was also determined by Monte-Carlo simulation. ψ's were generated with uniform distribution in p_T, η and ϕ. A simulated detector was used and the kinematic cuts already discussed were applied to the generated events. This leads to an acceptance of 9% at $p_T = 5$ GeV which rises to a plateau of 28 % for $p_T > 14$ GeV. It is important to note that the acceptance depends on the ψ polarisation. By simulation, the uncertainty on this

[4] This difference is due to the subtraction of data taken during a period of reduced level 3 tracking efficiency. These data have however been taken into account for $\psi(2S)$ after a correction derived from the J/ψ sample.

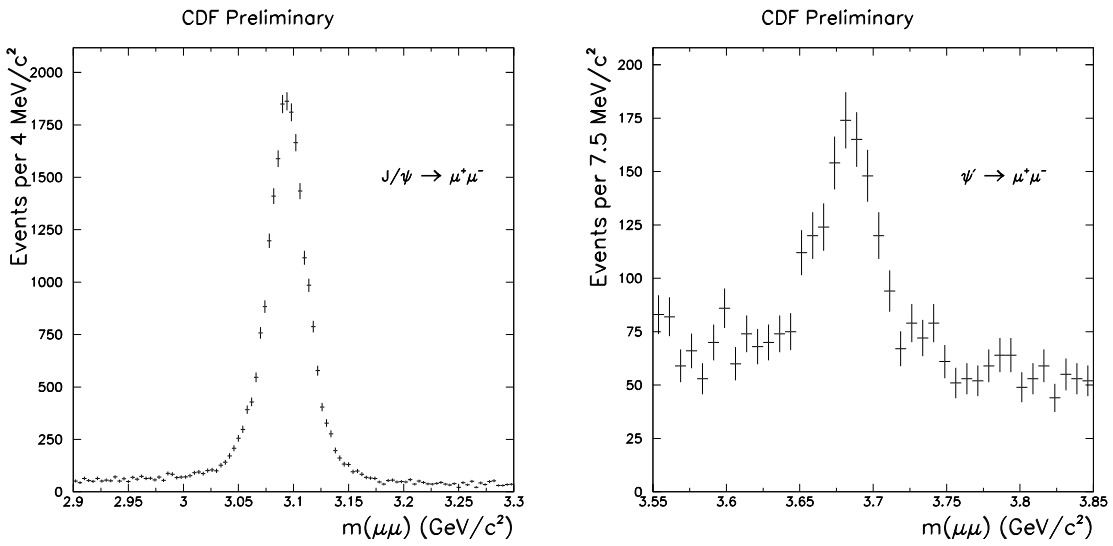

(a) J/ψ (b) ψ'

Figure 2.3: Resonance peak of J/ψ (a) and ψ' (b).

polarisation is shown to produce a 15% variation of the acceptance at $p_T = 5$ GeV and 5% at 20 GeV for prompt production, whereas the non-prompt production variation is from 6% to 3% for the same transverse momenta.

The efficiency of the CMU segment reconstruction is measured to be $97.2 \pm 1.2\%$ using dimuon events recorded with a single muon trigger. For CTC efficiency reconstruction, it is determined by a Monte-Carlo technique and is $96.4 \pm 2.8\%$ for both CTC tracks. The efficiency of the CMU-CTC matching requirements is estimated from the number of J/ψ before and after the matching requirements, to be $90.5 \pm 1.0\%$.

Systematics on the efficiency of the three triggers are evaluated by varying the functional form of the trigger efficiency. The J/ψ efficiency is then $97.0 \pm 0.2\%$ and the ψ' one is $92.3 \pm 0.2\%$.

The ψ differential cross section is experimentally defined as

$$\frac{d\sigma(\psi)}{dp_T} \cdot \mathcal{B}(\psi \to \mu^+\mu^-) = \frac{N(\psi)}{\epsilon \cdot \int \mathcal{L}dt \cdot \Delta p_T}, \tag{2.2}$$

where $N(\psi)$ is the number of ψ candidates in the Δp_T bin with efficiency corrections applied, and ϵ ($\neq \epsilon_{trigger}$) is the product of the acceptances (kinematic and detector-related), of the reconstruction efficiencies and of the corrections due to selection cuts.

The integrated cross sections were then measured to be

$$\sigma(J/\psi) \cdot \mathcal{B}(J/\psi \to \mu^+\mu^-) = 17.4 \pm 0.1(stat.)^{+2.6}_{-2.8}(syst.) \text{ nb} \tag{2.3}$$

$$\sigma(\psi(2S)) \cdot \mathcal{B}(\psi(2S) \to \mu^+\mu^-) = 0.57 \pm 0.04(stat.)^{+0.08}_{-0.09}(syst.) \text{ nb}. \tag{2.4}$$

where $\sigma(\psi) \equiv \sigma(p\bar{p} \to \psi X, p_T(\psi) > 5 \text{ GeV}, |\eta(\psi)| < 0.6)$. The evolution of $d\sigma \times \mathcal{B}$ as a function of p_T is shown in Fig. 2.4.

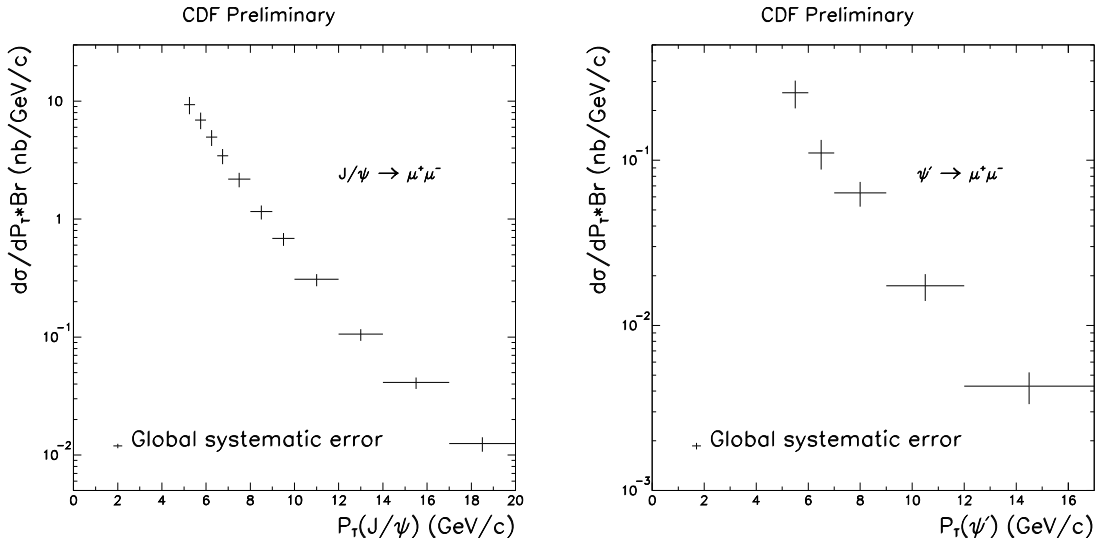

(a) J/ψ (b) ψ'

Figure 2.4: $\frac{d\sigma}{dp_T}\mathcal{B}$ (nb/GeV) as a function of p_T for J/ψ (a) and for ψ' (b).

2.3.3 Disentangling prompt charmonia

As already seen, prompt ψ's are the one that do not come from the decay of B mesons. Their production pattern has the distinctive feature compared to non-prompt one that there exists a measurable distance between the B production vertex and its decay into charmonium.

To proceed, it is necessary to use the SVX, whose resolution is 40μm, whereas B lifetime is $c\tau_B \approx 450\mu$m. Muons are constrained to come from the same point which is called the secondary vertex, as opposed to the primary vertex , which is the collision point of protons. Then the projection of the distance between these two vertices on the ψ momentum, L_{xy}, can be evaluated. It is converted into a proper time equivalent quantity using the formula, $c\tau = \frac{L_{xy}}{\frac{p_T(\psi)}{m(\psi)} \cdot F_{corr}}$, where F_{corr} is a correction factor, estimated by Monte-Carlo simulations, which links the ψ boost factor $\beta_T\gamma$ to this of the B [58].

The prompt component of the signal is parametrised by $c\tau = 0$ (a single vertex), the component coming from B decay is represented by an exponential whose lifetime is τ_b and is convoluted with the resolution function.

The $c\tau$ distribution (cf. Fig. 2.5) is fitted in each p_T-bin with an unbinned log-likelihood function. The noise is allowed to vary within the normalisation uncertainty extracted from the sidebands. The fraction of ψ coming from b, $f_b(p_T)$, is displayed as a function of p_T in Fig. 2.6 (a).

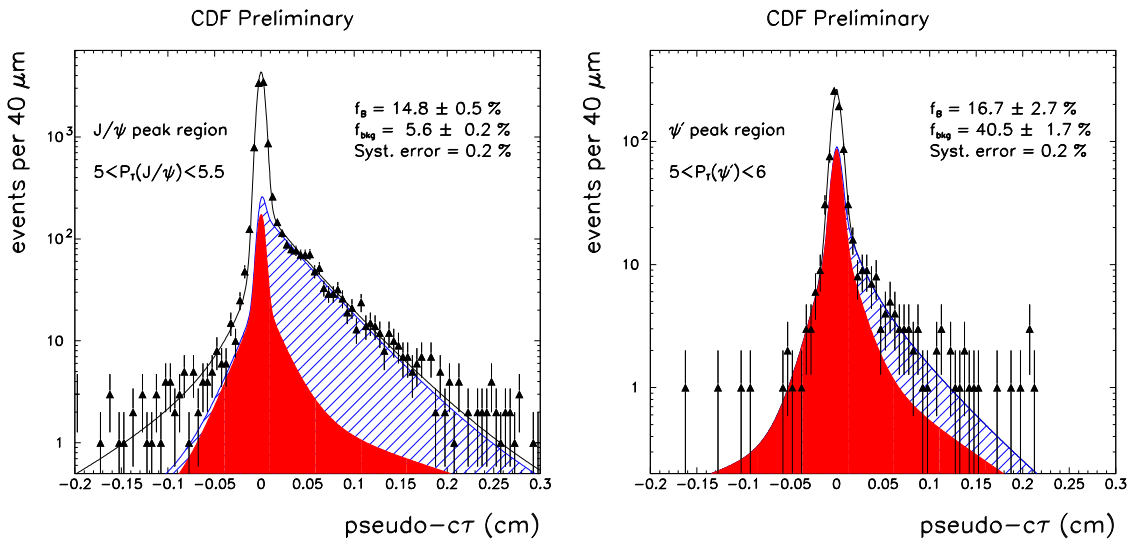

(a) J/ψ (b) ψ'

Figure 2.5: $c\tau$ distribution for J/ψ (a) and for ψ' (b). The solid region is the noise contribution (of null lifetime), the white region (just below the peak) give the null-lifetime signal: the prompt production, and finally the hashed region (mainly on the right side) is due to B component over background.

Uncertainties are evaluated as follows: a different choice of the fitting procedure implies a mean relative variation of $\pm 0.9\%$, this is included in the systematics on f_b. In the same fashion, a variation of the lifetime of B's of 1 σ modifies f_b by 0.7%.

The ψ production cross section from B decays is thus extracted by multiplying[5] $f_b^{fit}(p_T)$ by the inclusive ψ cross section. Multiplying the latter by $(1 - f_b^{fit}(p_T))$, we obviously get the prompt-production cross section (cf. Fig. 2.6 (b)).

2.3.4 Disentangling the direct production of J/ψ

The problem here is to subtract the J/ψ coming from χ_c decay, assuming that this is the only source of prompt J/ψ besides the direct production after subtraction of $F(\not{p})^{J/\psi}_{\psi(2S)}$, the *prompt* fraction of J/ψ that come from $\psi(2S)$. The latter is obtained from the $\psi(2S)$ cross section from the previous section and from Monte-Carlo simulation of the decays $\psi(2S) \rightarrow J/\psi X$ where $X = \pi\pi$, η and π^0. The delicate point here is the detection of the photon emitted during the radiative decay of the χ_c.

The events used in the analysis are collected by a dimuon trigger with same requirements as prior except than the lower bound on p_T is 4 GeV instead of 5 GeV.

[5] In order to reduce statistical fluctuations, f_b is fitted by a parabola weighted by the observed shape of the cross section [58].

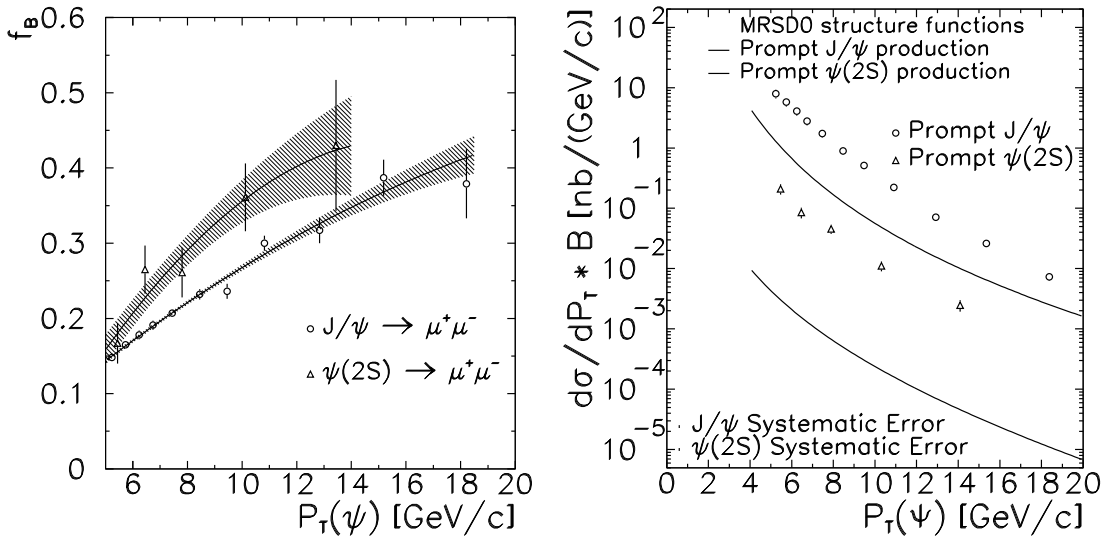

(a) $f_b(p_T)$ (b) $\frac{d\sigma}{dp_T}\mathcal{B}$

Figure 2.6: (a) Fraction of ψ from B decay as a function of p_T; (b) $\frac{d\sigma}{dp_T}\mathcal{B}$ from the prompt component of ψ [35]. The lines are the theoretical expectations based on the CSM (LO + fragment.)[40, 39].

With this selection, a sample of 34367 J/ψ is then obtained from which 32642 ± 185 is the number of real J/ψ when the estimated background is removed.

The requirements are as follow:

- an energy deposition of at least 1 GeV in a cell of the central electromagnetic calorimeter;
- a signal in the fiducial volume of the strip chambers (CES);
- the absence of charged particles pointing to the photon candidate cell (the no-track cut).

The direction of the photon is determined from the location of the signal in the strip chambers and from the event interaction point. All combinations of the J/ψ with all photon candidates that have passed these tests are made and the invariant-mass difference defined as $\Delta M = M(\mu^+\mu^-\gamma) - M(\mu^+\mu^-)$ can then be evaluated and plotted (see Fig. 2.7).

As expected, a clear peak from χ_c decays is visible near $\Delta M = 400$ MeV. Yet, distinct signals for $\chi_{c,1}$ and $\chi_{c,2}$ are not resolved as the two states are separated by 45.6 MeV and as the mass resolution of the detector is predicted to be respectively 50 and 55 MeV.

With regard to the background, its shape is simulated by replacing all charged particles (different from muons) by π^0, η and K^0_S with probabilities proportional to $4:2:1$. The detector response which results from the decay of these π^0, η and K^0_S is obtained using

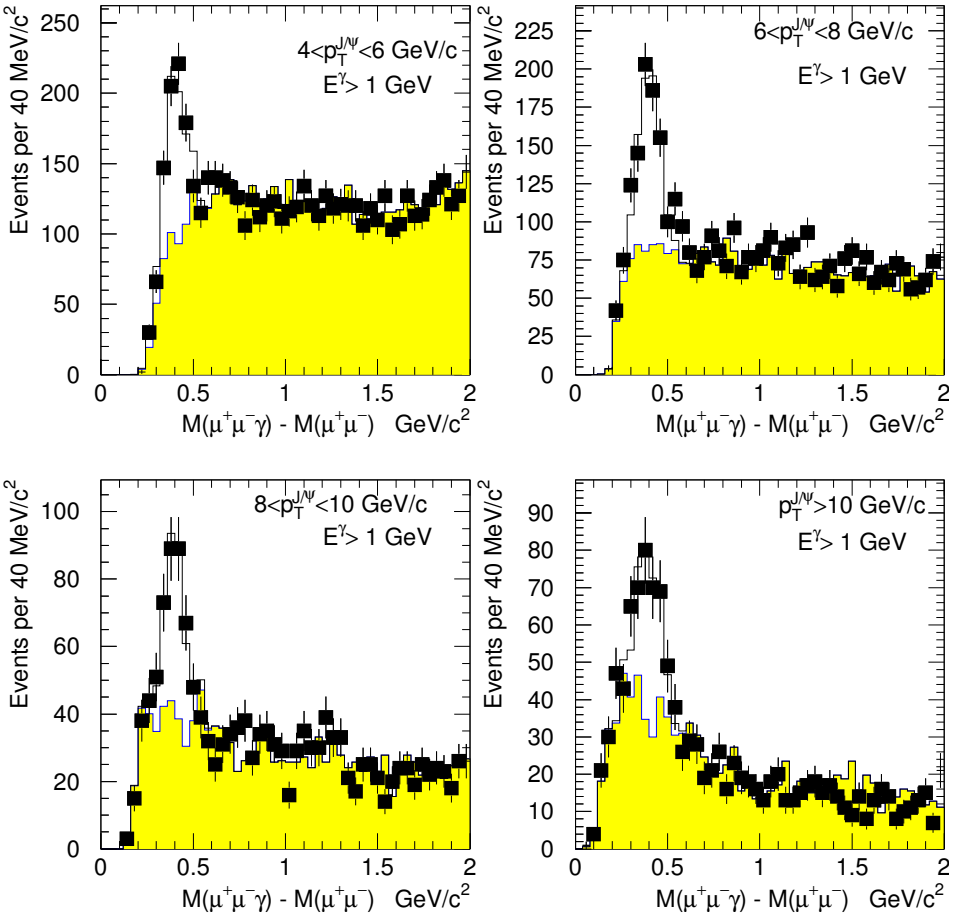

Figure 2.7: Number of events as a function of the mass difference after the selection procedure for the different p_T-bins. The points are the data; the solid region is Monte-Carlo simulation of the background. The solid line is a fit resulting from the background added to the contribution expected from a gaussian distribution [43].

a Monte-Carlo simulation. The ΔM distribution for the background is consequently obtained by applying on these simulated events the above-mentioned procedure as for real χ_c reconstruction. A simple test, which consists in trying to reproduce with this Monte-Carlo simulation the sideband signal, where there should not be any χ_c signal, was carried out successfully. Indeed imposing an equal number of events, the shape of the two distribution agree quite well (see Fig. 2.8).

Eventually, the ΔM distribution obtained from the data is fitted with a gaussian and with the background fixed by the procedure explained above but with a free normalisation. The parameter of the gaussian then lead to the number of signal events: 1230 ± 72 χ_c.

The analysis of the direct J/ψ signal is done within four p_T-bins: $4 < p_T^{J/\psi} < 6$, $6 < p_T^{J/\psi} < 8$, $8 < p_T^{J/\psi} < 10$ and $p_T^{J/\psi} > 10$ GeV. The proportion of J/ψ produced by χ_c

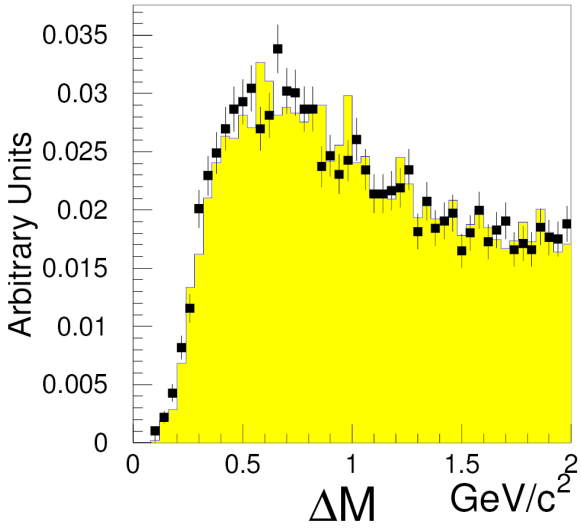

Figure 2.8: Comparison between the ΔM distribution for dimuons in the J/ψ sidebands, and the corresponding one predicted by the Monte-Carlo calculation; the two distributions are normalised to equal area and the vertical scale is arbitrary [43].

decay is given by:

$$F_{\chi}^{J/\psi} = \frac{N^{\chi}}{N^{J/\psi} \cdot A_{J/\psi}^{\gamma} \cdot \epsilon_{trk}^{\gamma} \cdot \epsilon_{env}^{\gamma}} \tag{2.5}$$

where $A_{J/\psi}^{\gamma}$ is the probability to reconstruct the photon once the J/ψ is found (or the photon acceptance), ϵ_{trk}^{γ} is the efficiency of the no-track-cut and ϵ_{env}^{γ} the efficiency to reconstruct the photon in the presence of additional energy deposited in the calorimeter. The latter quantities as well as the acceptance of the photon are evaluated with the help of a Monte-Carlo simulation in the spirit of the previous section. For instance, this acceptance is $0.146 \pm 0.002(stat.)$ for $p_T^{J/\psi} > 4.0$ GeV, whereas ϵ_{trk}^{γ} amounts to $97.9^{+2}_{-5}\%$ and ϵ_{env}^{γ} to $96.5^{+3.5}_{-4.5}\%$.

The total systematic uncertainty is estimated to be $\pm 18.9\%$ and is correlated in the four bins [43].

For $p_T^{J/\psi} > 4.0$ GeV and $|\eta^{J/\psi}| < 0.6$, the fraction of J/ψ from χ_c is then

$$F_{\chi}^{J/\psi} = 27.4\% \pm 1.6\%(stat.) \pm 5.2\%(syst.) \tag{2.6}$$

The last step now is the disentanglement of the prompt χ_c production, that is the determination of $F(\not{b})_{\chi}^{J/\psi}$. Let us here draw the reader's attention to the fact that by selecting prompt J/ψ (cf. section 2.3.3), J/ψ produced by *non-prompt* χ_c have also been eliminated; it is thus necessary to remove only the prompt production by χ_c decay, and nothing else. This necessitates the knowledge of $F(\not{b})_{\chi}^{J/\psi}$, the *prompt* fraction of J/ψ that come from χ.

The latter is calculated as follows:

$$F(\not{b})_{\chi}^{J/\psi} = \frac{N^{\chi} - N_b^{\chi}}{(N^{J/\psi} - N_b^{J/\psi}) \cdot A_{J/\psi}^{\gamma} \cdot \epsilon_{trk}^{\gamma} \cdot \epsilon_{env}^{\gamma}} = F_{\chi}^{J/\psi} \frac{1 - F_b^{\chi}}{1 - F_b^{J/\psi}}, \tag{2.7}$$

where N_b^{χ}, $N_b^{J/\psi}$ are the number of reconstructed χ_c and J/ψ from b's, F_b^{χ}, $F_b^{J/\psi}$ are the corresponding fractions.

$F_b^{J/\psi}$ (or f_b) has been extracted in the section 2.3.3; F_b^{χ} is obtained in same way and is $17.8\% \pm 0.45\%$ for $p_T > 4.0$ GeV. Consequently,

$$F(\not{b})_{\chi}^{J/\psi} = 29.7\% \pm 1.7\%(stat.) \pm 5.7\%(syst.) \tag{2.8}$$

and its evolution as a function of p_T is shown in Fig. 2.9. It is also found that the fraction of directly produced J/ψ is

$$F_{direct}^{J/\psi} = 64\% \pm 6\%, \tag{2.9}$$

and is almost constant from 5 to 18 GeV in p_T. We therefore conclude that direct production is the principal contribution to J/ψ (see Fig. 2.10).

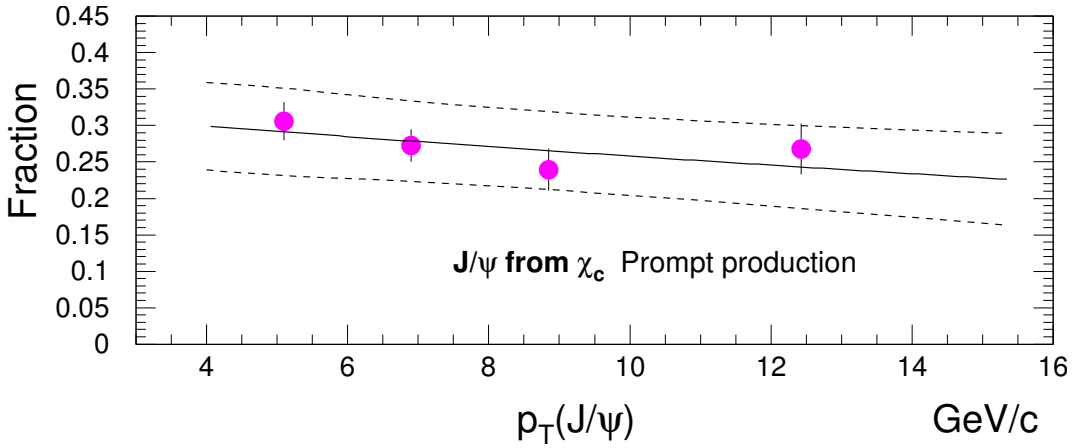

Figure 2.9: The fraction of J/ψ from χ_c as a function of p_T with the contribution of b's removed. The error bars correspond to statistical uncertainty.The solid line is the parametrisation of the fraction. The dashed lines show the upper and lower bounds corresponding to the statistical and systematic uncertainties combined [43].

In order to get the cross section of direct J/ψ production, it sufficient now to extract the contribution of ψ' obtained by Monte-Carlo simulation and of χ_c obtained by multiplying the cross section of prompt production by the factor $F(\not{b})_{\chi}^{J/\psi}$, which is a function of $p_T^{J/\psi}$. The different cross sections are displayed in Fig. 2.11.

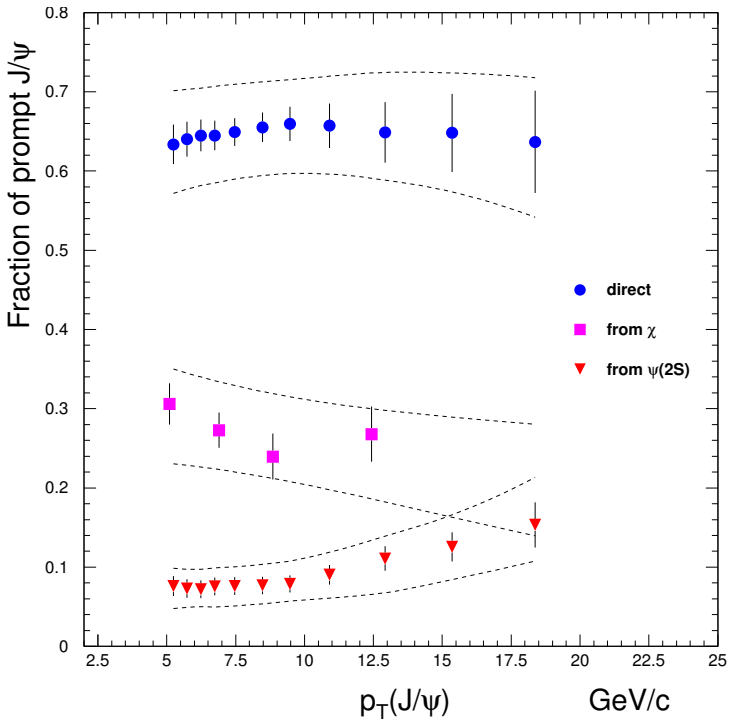

Figure 2.10: Fractions of J/ψ with the contribution of b's removed [43].

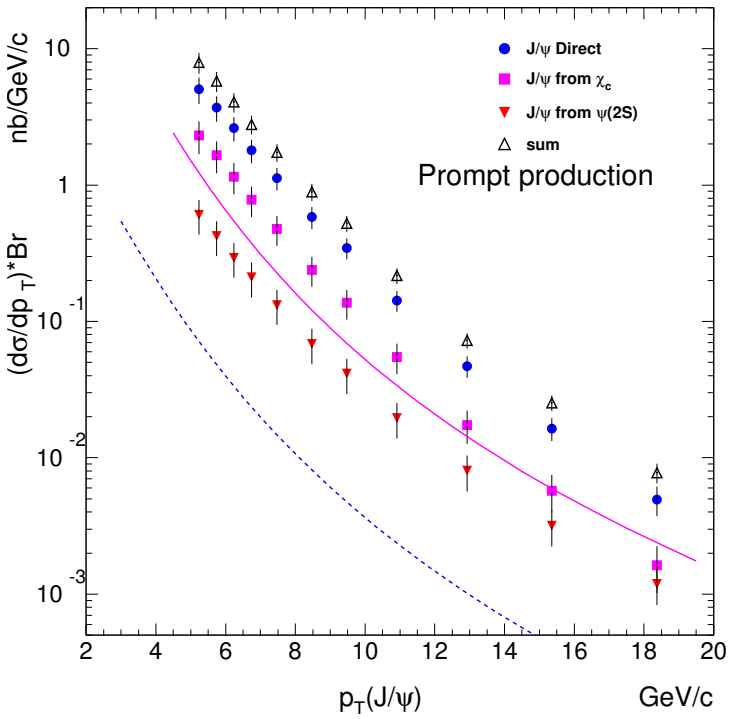

Figure 2.11: Differential cross section for prompt production of $J/\psi \to \mu^-\mu^+$ as a function of p_T. The dashed line gives the prediction of the CSM (LO+Fragmentation) [40, 39] and the solid lines that of the CSM + preliminary COM calculations for J/ψ from χ_c (see [43]), to be compared respectively with • and ■.

2.4 CDF measurement of the Υ production cross sections

As Υ states are similar to ψ states for which data are numerous and in contradiction with predictions, their study is just as good a point of comparison. Furthermore, many approximations performed in the models are better for $b\bar{b}$ states. Firstly, there is no expected decay from t quarks; secondly, the scale set by the quark mass is higher and therefore perturbation methods should be more suitable; thirdly, fragmentation would be significant only for large p_T. Classical production mechanisms based on LO pQCD can thus be considered as the only source of production; finally, the velocity of the heavy quarks within the meson being smaller, relativistic effects should be smaller, rendering the predictions of non-relativistic models more reliable.

In this section, we shall sum up the procedure and the results on Υ production in $p\bar{p}$ at $\sqrt{s} = 1.8$ TeV. These results were exposed in two letters [59, 60], and we shall mainly focus on the second one, which considered data collected in 1993-95 and corresponding to an integrated luminosity of 77 ± 3 pb^{-1}.

The parts of the detector used are the same as for the ψ's, with an additional muon detector, called central muon upgrade (CMP) outside the CMU. It covers the same rapidity range, *i.e.* $|\eta| < 0.6$, but it is located behind an additional steel shielding of ~ 2.4 interaction lengths. This increases its signal purity, although some muons from the CMU could have too few energy to reach it.

2.4.1 Υ total production

To what concerns muons, they are selected by a three level trigger:

- The **level 1** requires two track segments in the CMU (with efficiencies $\epsilon_1(p_T = 1.5 \text{ GeV}) = 40\%$ – $\epsilon_1(p_T > 3.0 \text{ GeV}) = 93\%$);
- The **level 2** requires that at least one of the muon-track segments be matched in ϕ (within 5°) to a track found in the CTC by the central fast tracker. These two tracks are then considered to come from a single particle (the efficiency is here $\langle \epsilon_1(p_T > 2.5 \text{ GeV}) \rangle = 95\%$);
- The **level 3** performs a 3D reconstruction and requires that muons pairs have an invariant mass in the region from 8.5 to 11.5 GeV.

Besides the selection, muons are to satisfy other criteria to isolate Υ resonances:

- Identification by CMU of both muons is required as well as at least one identification by the CMP;
- The momentum of each muons is determined using the CTC information combined with the constraint that they come from the beam line (no secondary vertex possible here);
- Only muons with $p_T > 2.2$ GeV were selected;

- Each muon-chamber track is required to match the extrapolation of a CTC to within 3 σ in $r-\phi$ and 3.5 σ in z (σ is the calculated uncertainty due to multiple scatterings and detection uncertainties, exactly as for the ψ's.);
- Muons are required to have opposite charge and the rapidity of the reconstructed pair is to be in the CMU fiducial rapidity region $|y| < 0.4$.
- The transverse momentum of the pair is finally restricted to be between 0 and 20 GeV.

The mass distribution obtained by CDF is shown in Fig. 2.12.

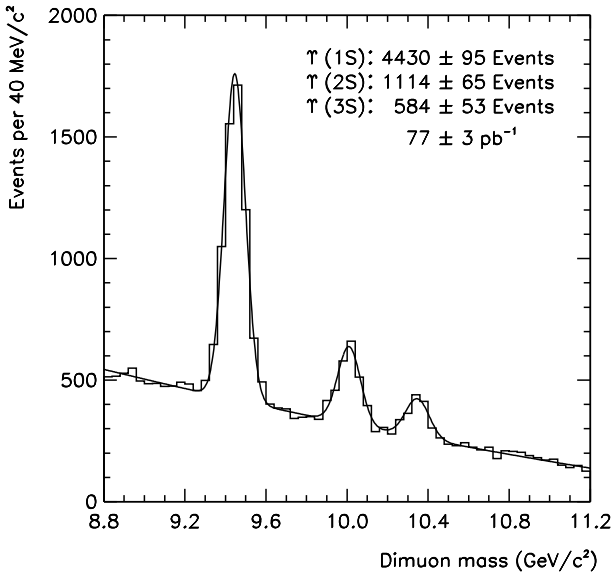

Figure 2.12: Resonance peaks of $\Upsilon(1S)$, $\Upsilon(2S)$, $\Upsilon(3S)$. The histogram represents the data and the solid curve a gaussian fit to each resonance plus a quadratic background [60].

The differential cross section times the branching ratio in dimuon is experimentally obtained as follow:

$$\left\langle \frac{d^2\sigma(\Upsilon)}{dp_T dy} \right\rangle_{|y|<0.4} \mathcal{B}(\Upsilon \to \mu^+\mu^-) = \frac{N_{fit}}{A(\int \mathcal{L}dt)\Delta p_T \Delta y \epsilon} \tag{2.10}$$

where N_{fit} is the number of Υ extracted from the gaussian fit on the signal for each p_T-bins similar to Fig. 2.12, A is the geometric and kinematic acceptance determined by Monte-Carlo simulation, ϵ represents the various efficiency corrections detailed in [60]. A is comparable for the three states and varies from 17% to 24% as a function of p_T.

Systematic uncertainties on $\frac{d^2\sigma}{dp_T dy}$ arise from $\mathcal{L}$ (4.1%), the level 1 and 2 trigger-efficiency correction ϵ_{trig} (4%) and from the remaining efficiency corrections (6%). Uncertainties are also due to the fact that the $\Upsilon(2S)$ and $\Upsilon(3S)$ polarisations are unknown. They were evaluated by running the simulation with extreme value of polarisation for these states (longitudinal or transverse). For the $\Upsilon(1S)$, as the polarisation is measured (cf. section 2.5),

the limits obtained are used as extrema for this variation and it is seen that the uncertainties are then negligible and no systematic error from this source is then to be added.

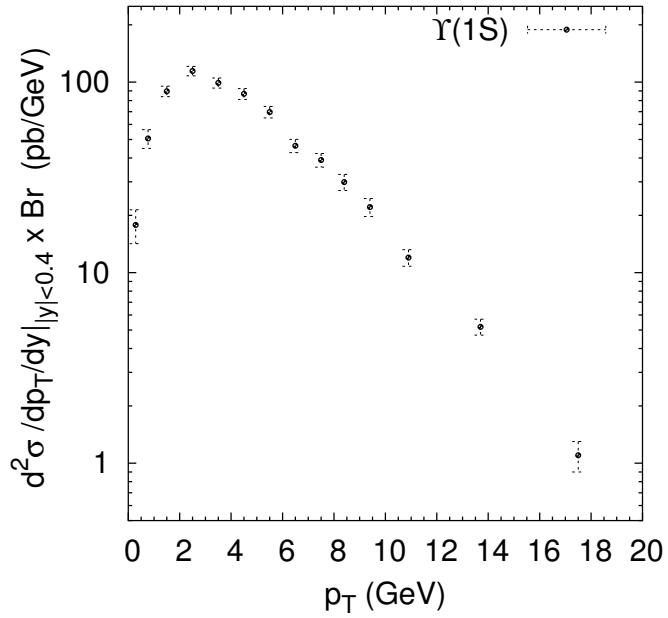

Figure 2.13: Differential cross section of $\Upsilon(1S) \to \mu^-\mu^+$ as a function of p_T for $|y| < 0.4$.

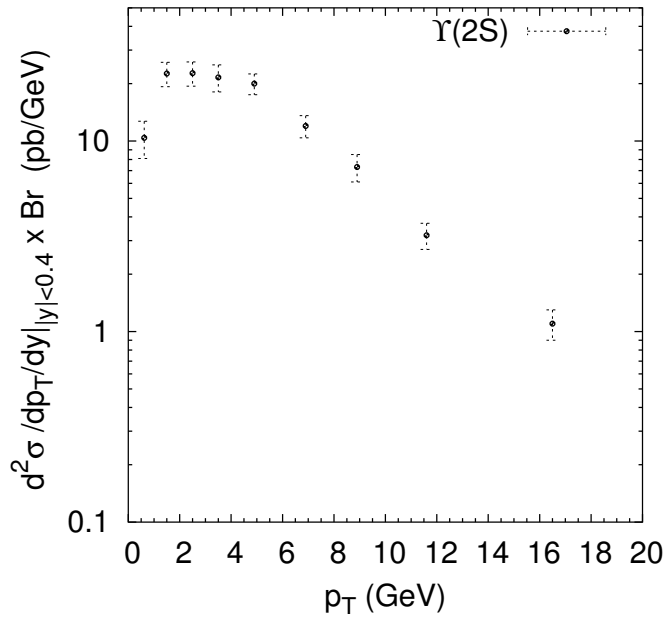

Figure 2.14: Differential cross section of $\Upsilon(1S) \to \mu^-\mu^+$ as a function of p_T for $|y| < 0.4$.

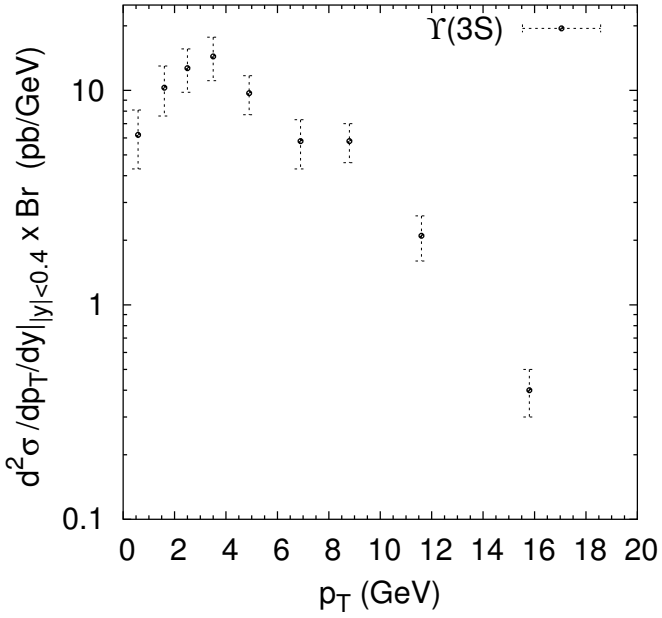

Figure 2.15: Differential cross section of $\Upsilon(1S) \to \mu^-\mu^+$ as a function of p_T for $|y| < 0.4$.

2.4.2 Disentangling direct production of $\Upsilon(1S)$

The analysis [61] presented here is for the most part the same as described in section 2.3.4. It is based on 90 pb^{-1} of data collected during the 1994-1995 run. The measurement has been constrained to the range $p_T > 8.0$ GeV because the energy of the photon emitted during the decay of χ_b decreases with p_T and ends up to be too small for the photon to be detected properly. In the same spirit, analysis relative to $\Upsilon(2S)$ has not been carried out, once again because of the lower energy of the radiative decay. Concerning $\Upsilon(3S)$, except for the unobserved $\chi_b(3P)$ (which is nevertheless supposed to be below the $B\bar{B}$ threshold), no P-states are supposed to be parents.

The event used are collected by a dimuon trigger (details are given in [61]) with the following requirements, which slightly differ from section 2.4.1:

- Two oppositely charged muons candidates observed in the muon chambers,
- Both with $p_T > 2.0$ GeV,
- The pair must have $p_T > 8.0$ GeV and $|\eta| < 0.7$,
- In order to be considered as coming from a $\Upsilon(1S)$, the invariant mass of the pair must lie within the region:

$$9300 \text{ MeV} < M(pair) < 9600 \text{ MeV}. \tag{2.11}$$

With this selection, a sample of 2186 $\Upsilon(1S)$ candidates is then obtained from which 1462 ± 55 is the estimated number of $\Upsilon(1S)$ after subtraction of the background. The resulting mass distribution is plotted in Fig. 2.16.

In this sample, photons likely to come from χ_b decay are selected as for the J/ψ case, except for the energy deposition in the central electromagnetic calorimeter, which is lowered to 0.7 GeV.

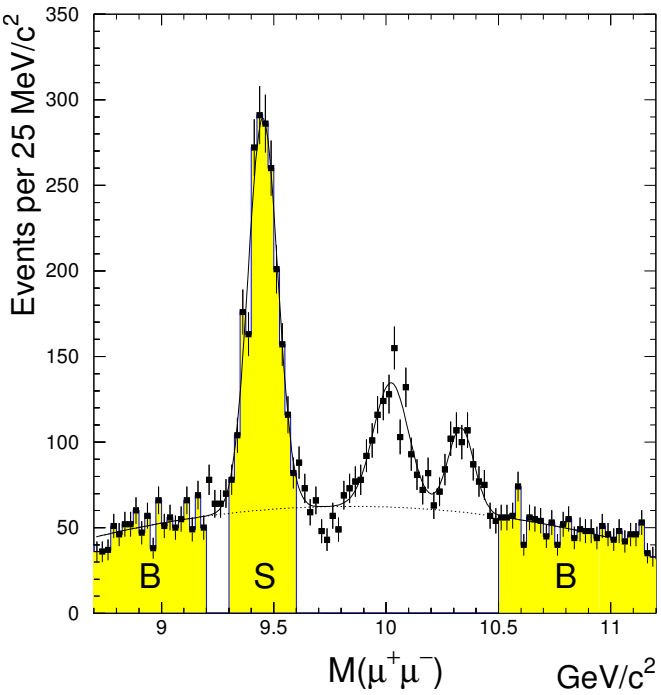

Figure 2.16: Muon pairs invariant mass distribution after the selection for $p_T > 8.0$ GeV. The dotted line is the fit to the background, the solid line is the fit to the data; the region S is the signal region and the region B is the sideband region.

The direction of the photon is determined from the location of the signal in the strip chambers and from the event-interaction point. All combinations of the $\Upsilon(1S)$ with all photon candidates that have passed these tests are made and the invariant-mass difference still defined by $\Delta M = M(\mu^+\mu^-\gamma) - M(\mu^+\mu^-)$ can then be evaluated. It is plotted in Fig. 2.17.

The background is evaluated as in the J/ψ analysis. A fit to the data then yields the number of signal events: 35.3 ± 9.0 for $\chi_b(1P)$ and 28.5 ± 12.0 for $\chi_b(2P)$. The analysis of the direct $\Upsilon(1S)$ signal is done within one single p_T-bin, as opposed to J/ψ case. The proportion of $\Upsilon(1S)$ produced by χ_b decay is given by:

$$F_\chi^{J/\psi} = \frac{N^{\chi_b}}{N^\Upsilon \cdot A_\Upsilon^\gamma \cdot \epsilon^\gamma}, \tag{2.12}$$

where N^{χ_b} and N^Υ are the numbers of reconstructed χ_b and $\Upsilon(1S)$ respectively, A_Υ^γ is the probability to reconstruct the photon once the Υ is found, ϵ^γ is the efficiency of the

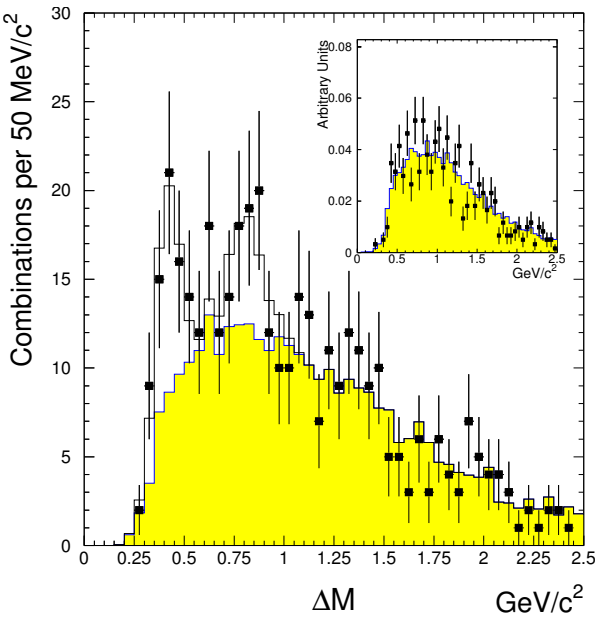

Figure 2.17: Number of events as a function of the mass difference after the selection procedure. The points are the data; the solid region is a Monte-Carlo simulation of the background. The solid line is a fit resulting from the background added to the contribution expected from two gaussian distributions [61]. The inset shows the comparison between the background of ΔM extracted from the sidebands and with the Monte-Carlo simulation.

isolation cuts. The latter quantities, as well as the acceptance of the photon, are evaluated with the help of simulations in the same spirit as that described in the previous section. For instance, this acceptance is $0.142 \pm 0.004(stat.)$ for $\chi_b(1P)$ and $0.284 \pm 0.006(stat.)$ for $\chi_b(2P)$, the difference between the two coming mainly from the lower energy of the photon for $\chi_b(2P)$ decays. The efficiencies ϵ^γ obtained are $0.627 \pm 0.013(stat.)$ for $\chi_b(1P)$ and $0.651 \pm 0.0013(stat.)$ for $\chi_b(2P)$. The efficiency for inclusive $\Upsilon(1S)$ is supposed to be the same as for the sub-sample considered.

The systematic uncertainties on $F_{\chi_b}^{\Upsilon(1S)}$ associated with the variation of the shape of the p_T spectrum and of the decay angular distribution is $\pm 13\%$ for $\chi_b(1P)$ and $\pm 9\%$ for $\chi_b(2P)$. The uncertainty from N^{χ_b} is $\pm 7\%$ for $\chi_b(1P)$ and $\pm 9\%$ for $\chi_b(2P)$, this comes from the background of the ΔM distribution and, from the uncertainty on the resolution of the gaussian signals in this same distribution. Other uncertainties are also considered, see [61] for more details. Assuming the independence of all these uncertainties, they are combined in a total systematic uncertainty: $\pm 16.4\%$ for $\chi_b(1P)$ and $\pm 13.7\%$ for $\chi_b(2P)$.

For $p_T^{\Upsilon(1S)} > 8.0$ GeV and $|\eta^{\Upsilon(1S)}| < 0.7$, the fractions of $\Upsilon(1S)$ from $\chi_b(1P)$ and from $\chi_b(2P)$ are

$$\begin{aligned} F_{\chi_b(1P)}^{\Upsilon(1S)} &= 27.1\% \pm 6.9\%(stat.) \pm 4.4\%(syst.), \\ F_{\chi_b(2P)}^{\Upsilon(1S)} &= 10.5\% \pm 4.4\%(stat.) \pm 1.4\%(syst.). \end{aligned} \tag{2.13}$$

In order to get the direct production of $\Upsilon(1S)$, one must still evaluate the feed-down from the S-waves $\Upsilon(2S)$ and $\Upsilon(3S)$. This is done using Monte-Carlo simulations of these decays normalised to the production cross sections discussed in section 2.4. It is found that for $p_T^{\Upsilon(1S)} > 8.0$ GeV the fraction of $\Upsilon(1S)$ from $\Upsilon(2S)$ and $\Upsilon(3S)$ are respectively

$$\begin{aligned} F^{\Upsilon(1S)}_{\Upsilon(2S)} &= 10.1\%^{+7.7}_{-4.8}\%, \\ F^{\Upsilon(1S)}_{\Upsilon(3S)} &= 0.8\%^{+0.6}_{-0.4}\%. \end{aligned} \tag{2.14}$$

Concerning the unobserved $\chi_b(3P)$, a maximal additional contribution is taken into account by supposing than all the $\Upsilon(3S)$ are due to $\chi_b(3P)$ and from theoretical expectation for the decay of this state, a relative rate of $\Upsilon(1S)$ from $\chi_b(3P)$ can obtained. This rate is less than 6%.

In conclusion, the fraction of directly produced $\Upsilon(1S)$ is obtained from

$$F^{\Upsilon(1S)}_{direct} = 1 - F^{\Upsilon(1S)}_{\chi_b(1P)} - F^{\Upsilon(1S)}_{\chi_b(2P)} - F^{\Upsilon(1S)}_{\Upsilon(2S)} - F^{\Upsilon(1S)}_{\Upsilon(3S)}, \tag{2.15}$$

for which the uncertainties come from that of cross sections and of branching ratio. It is eventually found that

$$F^{\Upsilon(1S)}_{direct} = 50.9\% \pm 8.2\%(stat.) \pm 9.0\%(syst.). \tag{2.16}$$

2.5 Polarisation at the Tevatron

As the considered bound states, ψ and Υ are massive spin-1 particles, they have three polarisations. In addition to measurements of their momentum after their production, the experimental set-up is sufficiently refined to provide us with a measurement of their spin alignment through an analysis of the angular distribution of the dimuon pairs from the decay.

The CDF collaboration has carried out two analyses, one for the ψ states [52] – for which the feed-down from b decay has been subtracted, but not the indirect component in the case of the J/ψ – and another for $\Upsilon(nS)$ [60].

In the following, we shall proceed to a brief outline of the analysis and give its main results.

2.5.1 Polarisation parameters

The polarisation state of the quarkonium can be deduced from the angular dependence of its decay into $\mu^+\mu^-$. Taking the spin quantisation axis along the quarkonium momentum direction in the $p\bar{p}$ c.m. frame, we define θ as the angle between the μ^+ direction in the

quarkonium rest frame and the quarkonium direction in the lab frame (see Fig. 2.18). Then the normalised angular distribution $I(\cos\theta)$ is given[6] by

$$I(\cos\theta) = \frac{3}{2(\alpha+3)}(1+\alpha\ \cos^2\theta) \tag{2.17}$$

where the interesting quantity is

$$\alpha = \frac{\frac{1}{2}\sigma_T - \sigma_L}{\frac{1}{2}\sigma_T + \sigma_L}. \tag{2.18}$$

$\alpha = 0$ means that the mesons are unpolarised, $\alpha = +1$ corresponds to a full transverse polarisation and $\alpha = -1$ to a longitudinal one.

As the expected behaviour is biased by muons cuts – for instance there exists a severe reduction of the acceptance as θ approaches 0 and 180 degrees, due to the p_T cuts on the muons –, the method followed by CDF was to compare measurements, not with a possible $(1+\alpha\ \cos^2\theta)$ distribution, but with distributions obtained after simulations of quarkonium decays taking account the geometric and kinematic acceptance of the detector as well as the reconstruction efficiency.

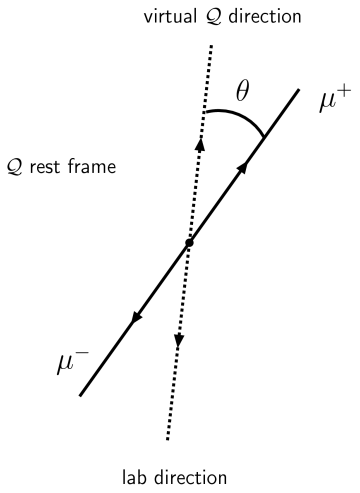

Figure 2.18: Definition of the angle θ used in the polarisation analysis of a quarkonium $\mathcal{Q}$.

The parts of the detector used are the same as before, with the additional central muon upgrade (CMP) outside the CMU.

2.5.2 Study of the ψ's

We give here the results relative to the CDF analysis published in 2000 [52]. The data used correspond to an integrated luminosity of 110 pb^{-1} collected between 1992 and 1995. The three-level trigger is similar as before. Beside this on-line selection, muons are to satisfy other criteria to isolate ψ resonances:

[6] For a derivation, see the Appendix A of [62].

- Identification by CMU of both muons is required as well as a matching of the corresponding tracks within the CMU with one of the CTC tracks. This reduces the rate from sources such as π/K meson decay-in-flight;
- These matches are required to pass a maximum χ^2 cut of 9 and 12 (for 1 degree of freedom) in the ϕ and z views respectively [52];
- Only muons with $p_T > 2$ GeV were selected;

Disentangling prompt production

The method followed here is on many aspects similar to the one exposed in section 2.3.3. As before, prompt events have $c\tau$ consistent with zero whereas b-quark decays have an exponential $c\tau$ distribution, all this with a smearing due to the detector resolution. The $c\tau$ distribution is fitted to obtain the relative fractions of prompt and b-decay production. Results are that the measured fraction of J/ψ mesons which come from b-hadron decay, $F_b^{J/\psi}$, increases from $(13.0 \pm 0.3)\%$ at $p_T = 4$ GeV to $(40 \pm 2)\%$ at 20 GeV and for ψ' mesons, $F_b^{\psi'}$ is $(21 \pm 2)\%$ at 5.5 GeV and $(35 \pm 4)\%$ at 20 GeV.

The following study is then based on two samples a short-lived one dominated by prompt production, and a long-lived one dominated by b-decays. The definitions used to separate the samples are the following $-0.1 \leq c\tau \leq 0.013[0.01]$ cm for the short-lived sample, and for the long-lived sample $0.013[0.01] \leq c\tau \leq 0.3$ cm, for the J/ψ [ψ'] analyses respectively[7].

Within a 3-standard-deviation mass window around the J/ψ peak, the data sample is of 180 000 J/ψ events. In order to study the effect of p_T, the data are divided into seven p_T-bins from 4 to 20 GeV. Because the number of ψ' events is lower, data for ψ' are divided into three p_T-bins from 5.5 to 20 GeV.

The J/ψ sample is divided into three sub-samples where the analysis is executed independently: the short-lived and long-lived SVX samples described above, and a third sample (the CTC sample) in which neither muon has SVX information and no $c\tau$ measurement is made.

For ψ', both muons are required to be reconstructed in the SVX and the number of signal events is found to 1855 ± 65 in a 3-standard-deviation mass window around the ψ' mass. The sample is further divided into two sub-samples based on the $c\tau$ distribution instead of 3 for J/ψ. Once again, because the number of events is lower than in the J/ψ case, 10 bins are used in $|\cos\theta|$ instead of 20 in $\cos\theta$ for J/ψ. Similarly to the latter, the number of events in each bin is obtained by fitting the mass distribution each time.

J/ψ polarisation measurement

The J/ψ polarisation is determined through a fit of the measured muonic $\cos\theta$ distributions to a set of Monte-Carlo templates. Implementing the experimental constraints with detector

[7] The boundary between the two $c\tau$ regions has been determined separately for the J/ψ and for the ψ'. Depending on p_T^{ψ}, the prompt fraction in the short-lived sample ranges from 85%[86%] to 96%[95%],and the B-decay fraction in the long-lived sample ranges from 83%[86%] to 98%[91%], for J/ψ [ψ'] respectively.

and trigger simulations, these templates are generated by processing simulated samples of $J/\psi \to \mu^+\mu^-$ decays.

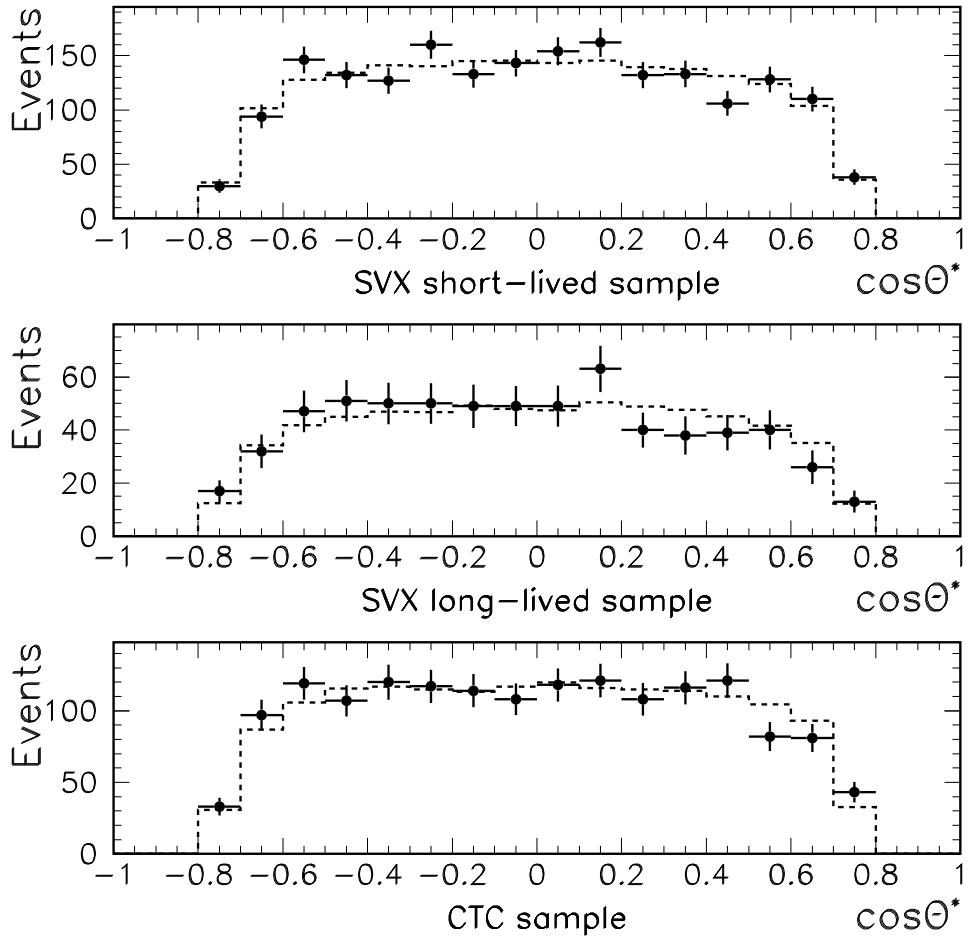

Figure 2.19: The points represent the data (with sideband signal subtracted); the dashed lines is the fit of the $\cos\theta$ distributions in the 12-15 GeV bin. The three plots correspond to the three samples defined in the text.

The polarisation is obtained using a χ^2 fit of the data to a weighted sum of transversely polarised and longitudinally polarised templates. The weight obtained with the fit provides us with the polarisation. Explanations relative to procedure used can be found in [52] and [62].

Note however that the polarisation is measured in each p_T bin and that separate polarisation measurements for direct J/ψ production and for production via χ_c and ψ' decays was found to be unfeasible. Let us recall here that χ_c and ψ' were shown to account for $36\pm6\%$ of the prompt production (cf. Eq. (2.9)) and to be mostly constant in the considered p_T range.

For J/ψ, the fit is performed simultaneously on the SVX short-lived, SVX long-lived and CTC samples, with two fit parameters: α_{Prompt} and α_{fromB}. As observed above, the long-lived and short-lived samples are not pure, this is of course taken into account. The B-decay fraction in the CTC sample is assumed to be the same as in the SVX sample. This seems reasonable as the main difference between the two samples resides primarily in the z position of the primary vertex. The fit in the p_T range 12-15 GeV is shown in Fig. 2.19.

Except in the lowest p_T bins, the systematic uncertainties are much smaller than the statistical one. The values obtained for α_{Prompt} and α_{fromB} are given in Tab. (2.5) and plotted with a comparison to NRQCD predictions in Fig. 2.20.

p_T bin (GeV)	Mean P_T (GeV)	α_{Prompt}	α_{fromB}
$4-5$	4.5	$0.30 \pm 0.12 \pm 0.12$	$-0.49 \pm 0.41 \pm 0.13$
$5-6$	5.5	$0.01 \pm 0.10 \pm 0.07$	$-0.18 \pm 0.33 \pm 0.07$
$6-8$	6.9	$0.178 \pm 0.072 \pm 0.036$	$0.10 \pm 0.20 \pm 0.04$
$8-10$	8.8	$0.323 \pm 0.094 \pm 0.019$	$-0.06 \pm 0.20 \pm 0.02$
$10-12$	10.8	$0.26 \pm 0.14 \pm 0.02$	$-0.19 \pm 0.23 \pm 0.02$
$12-15$	13.2	$0.11 \pm 0.17 \pm 0.01$	$0.11 \pm^{0.31}_{0.28} \pm 0.02$
$15-20$	16.7	$-0.29 \pm 0.23 \pm 0.03$	$-0.16 \pm^{0.38}_{0.33} \pm 0.05$

Table 2.5: Fit results for J/ψ polarisation, with statistical and systematic uncertainties.

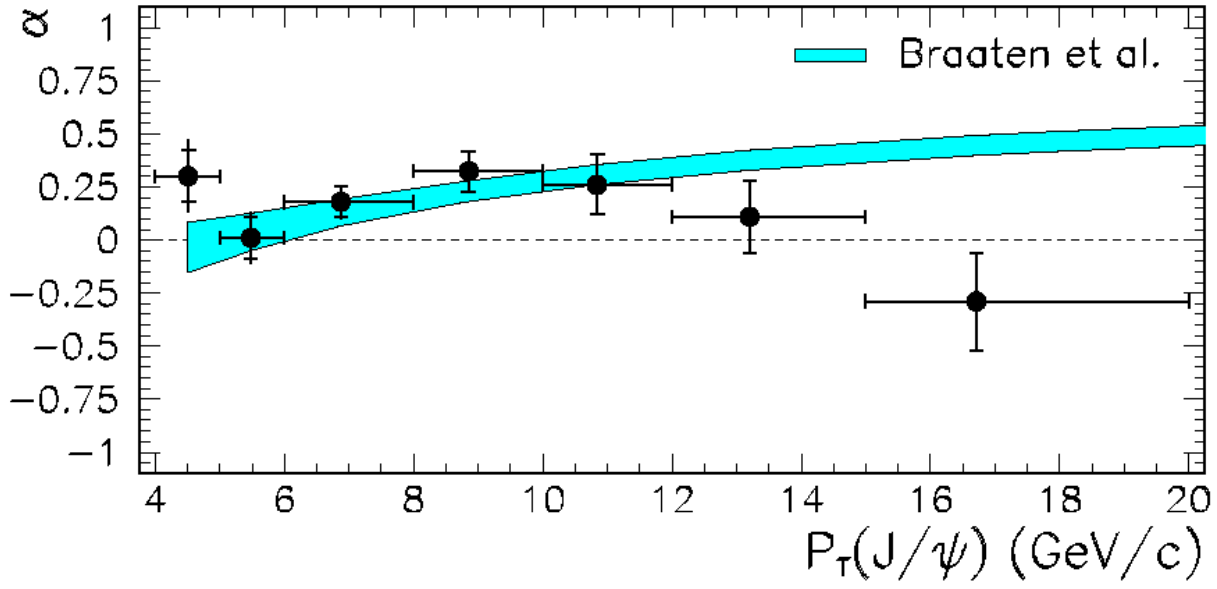

Figure 2.20: α_{Prompt} for J/ψ fitted for $|y^{J/\psi}| < 0.6$. Full error bars denote statistical and systematic uncertainties added in quadrature; ticks denote statistical errors alone. The shaded band shows a NRQCD-factorisation prediction [64] which includes the contribution from χ_c and ψ' decays.

ψ' polarisation measurement

The procedure to obtain α_{Prompt} and α_{fromB} is similar. Weighted simulations of the angular distribution are fitted to the data and the weight obtained gives the polarisation. The $|\cos\theta|$ distributions in the two $c\tau$ sub-samples are fitted simultaneously. As there is no expected radiative decay from higher excited charmonia, we are in fact dealing with direct production. The fit of the angular distribution in the three p_T-bins is shown on Fig. 2.21.

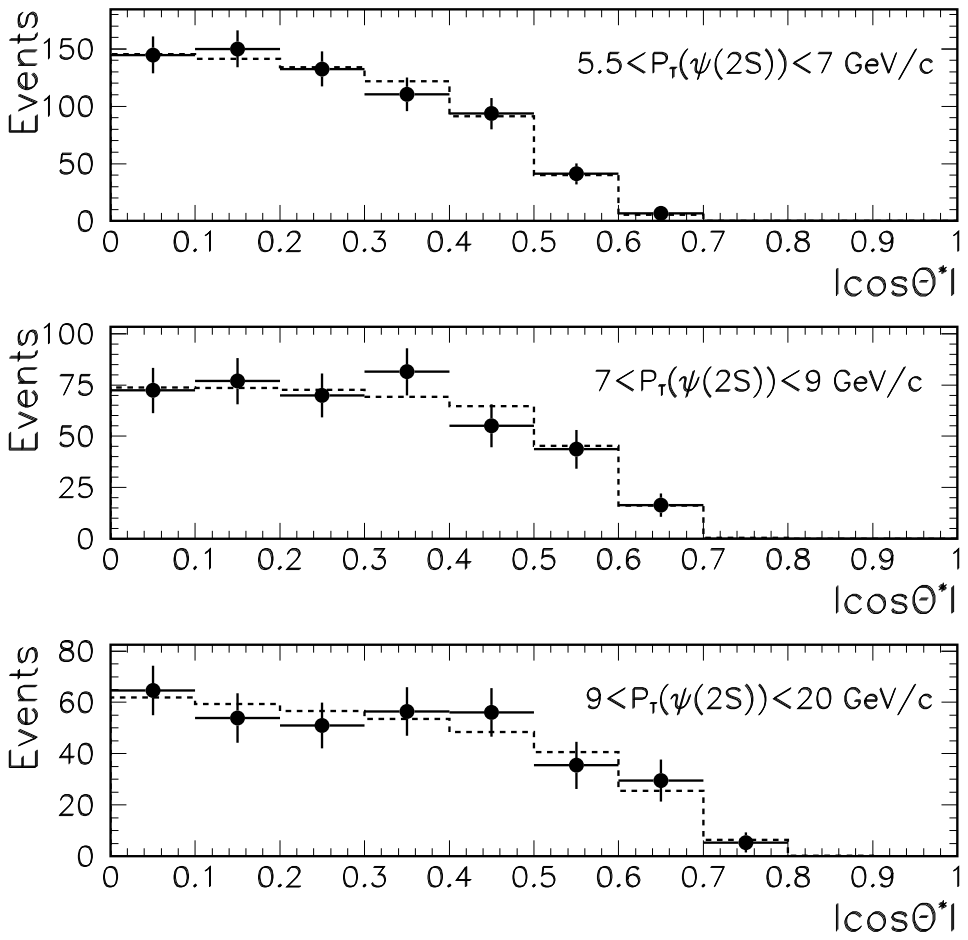

Figure 2.21: The points represent the ψ' data for the short-lived sample only; the dashed lines is the fit to the $|\cos\theta|$ distributions. The three plots correspond to the three samples in p_T defined in the text. Note the extension of the acceptance range in $|\cos\theta|$ as p_T increases.

Anew, the systematic uncertainties [52] are much smaller than the statistical uncertainties. The values obtained for α_{Prompt} and α_{fromB} are given in Tab. (2.6) and plotted with a

comparison to NRQCD predictions in Fig. 2.22.

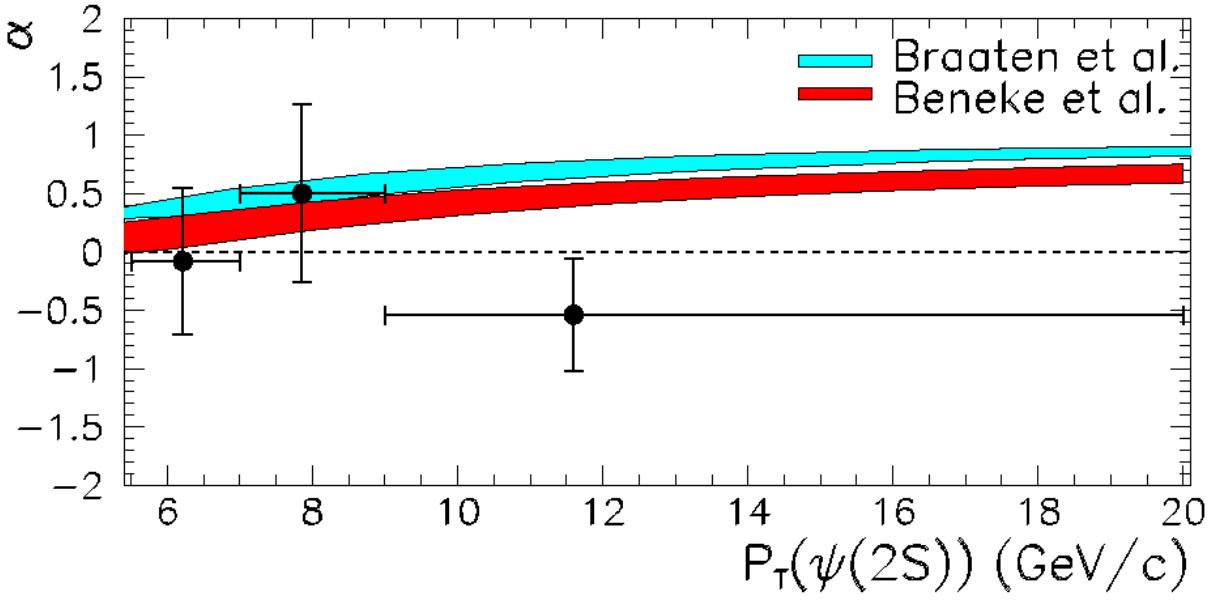

Figure 2.22: α_{Prompt} for ψ' fitted for $|y^{\psi'}| < 0.6$. Error bars denote statistical and systematic uncertainties added in quadrature. Shaded bands show two NRQCD-factorisation predictions [63, 64].

p_T bin (GeV)	Mean p_T (GeV)	α_{Prompt}	α_{fromB}
$5.5 - 7.0$	6.2	$-0.08 \pm 0.63 \pm 0.02$	$-0.26 \pm 1.26 \pm 0.04$
$7.0 - 9.0$	7.9	$0.50 \pm 0.76 \pm 0.04$	$-1.68 \pm 0.55 \pm 0.12$
$9.0 - 20.0$	11.6	$-0.54 \pm 0.48 \pm 0.04$	$0.27 \pm 0.81 \pm 0.06$

Table 2.6: Fit results for $\psi(2S)$ polarisation, with statistical and systematic uncertainties.

2.5.3 Study of the $\Upsilon(1S)$

As the procedure is quite similar as of the ψ study, we just present here the results. The measurements are made in the region of p_T from 0 to 20 GeV and with $|y| < 0.4$ and the data are separated in four p_T-bins [60].

Using the same technique as before, the longitudinal polarised fraction is obtained. Fig. 2.23 shows the $\cos\theta$ distribution with the two templates used, and the resulting fit.

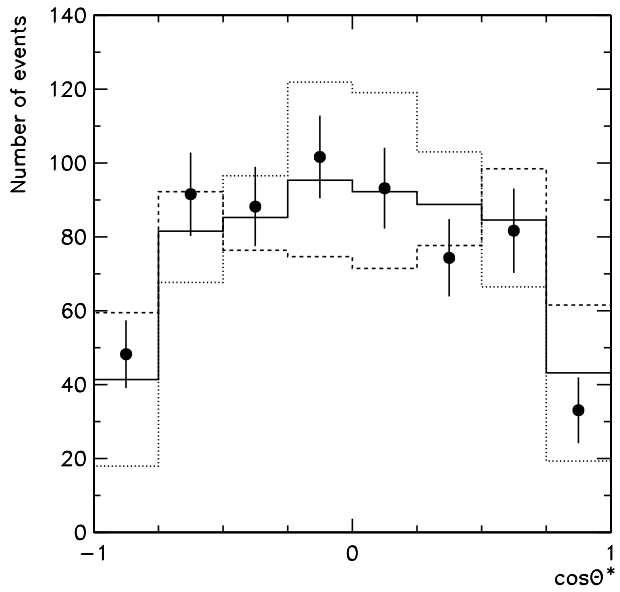

Figure 2.23: Uncorrected $\cos\theta$ distribution for $|y^{\Upsilon(1S)}| < 0.4$ and for the highest p_T-bin. The points are the data; the solid line, the result giving the weight of the transversal template (dashed line) and the longitudinal template (dotted line) [60].

In Tab. (2.7) are given the results for α and the same values are plotted in Fig. 2.24 in comparison with a theoretical prediction from NRQCD [65]. In conclusion, $\Upsilon(1S)$ are shown to be mostly unpolarised.

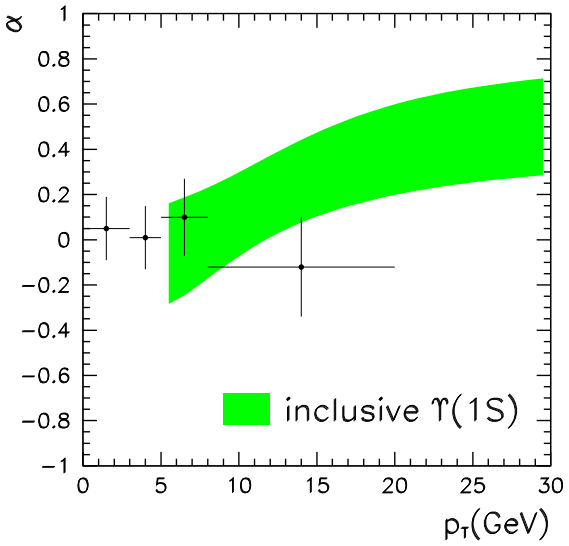

Figure 2.24: α for $\Upsilon(1S)$ fitted for $|y^{\Upsilon(1S)}| < 0.4$. The theoretical band represents the NRQCD prediction [65].

p_T bin (GeV)	α
$0.0 - 3.0$	$+0.05 \pm 0.14$
$3.0 - 5.0$	$+0.01 \pm 0.14$
$5.0 - 8.0$	$+0.10 \pm 0.17$
$8.0 - 20.0$	-0.12 ± 0.22

Table 2.7: Fit results for $\Upsilon(1S)$ polarisation.

2.6 PHENIX analysis for J/ψ production cross sections

In this section, we present the first measurements of $pp \to J/\psi + X$ at RHIC obtained by the PHENIX experiment [55] at a c.m. energy of $\sqrt{s} = 200$ GeV. The analysis was carried out by detecting either dielectron or dimuon pairs. The data were taken during the run at the end of 2001 and at the beginning of 2002. The data amounted to 67 nb^{-1} for $\mu^+\mu^-$ and[8] 82 nb^{-1} for e^+e^-. The B-decay feed-down is estimated to contribute less than 4% at $\sqrt{s} = 200$ GeV and is not studied separately.

Concerning the dielectron study, it relied on:

- Two central spectrometer arms covering $|\eta| \leq 0.35$ and $\Delta\phi = 90°$;
- An electromagnetic calorimeter (EMC);
- A ring imaging Čerenkov detector (RICH) with a rejection threshold for pions of 4.7 GeV.

whereas for muons, were used:

- Two muon-spectrometer arms covering $\Delta\phi = 360°$, of which only one was used ($1.2 \leq \eta \leq 2.2$);
- A muon-identifier system (MuID);
- A muon-tracker system (MuTr).

Concerning dielectrons, the trigger requirement was either a deposition of 0.75 GeV in a 2×2 pile of EMC towers or 2.1 GeV in a 4×4 pile. Electron candidates had to be associated with a RICH ring (with at least 2 photo-tubes hit) and with an EMC hit (within $\pm 4\sigma$ for the position). Furthermore, a correlation between the energy deposition in the EMC, E, and the momentum of the reconstructed track, p, was required through the condition $0.5 \leq E/p \leq 1.5$. Finally, to avoid pion signals from the RICH, a 5 GeV cut-off for the electrons was imposed.

On the other hand, the muon trigger required two deeply penetrating track seeds ("roads") in two distinct azimuthal quadrants of the MuID [66]. Then these seeds were matched to the

[8] The difference results from different cuts on the extrapolated vertex position.

cluster hits in the MuTr stations. A fit with energy-loss correction of the MuID and MuTr hit positions and of the collision vertex finally gave the momentum.

The net yield of J/ψ within the region 2.80 GeV $< M(pair) <$ 3.40 GeV was found to be 46.0 ± 7.4 for electrons, whereas for muons, it was 65.0 ± 9.5 J/ψ within the region 2.71 GeV $< M(pair) <$ 3.67 GeV. The mass distributions obtained are shown in Fig. 2.25 for both dimuon and dielectron selections. As an indication of the background, a like-sign pair distribution is shown by dashed lines.

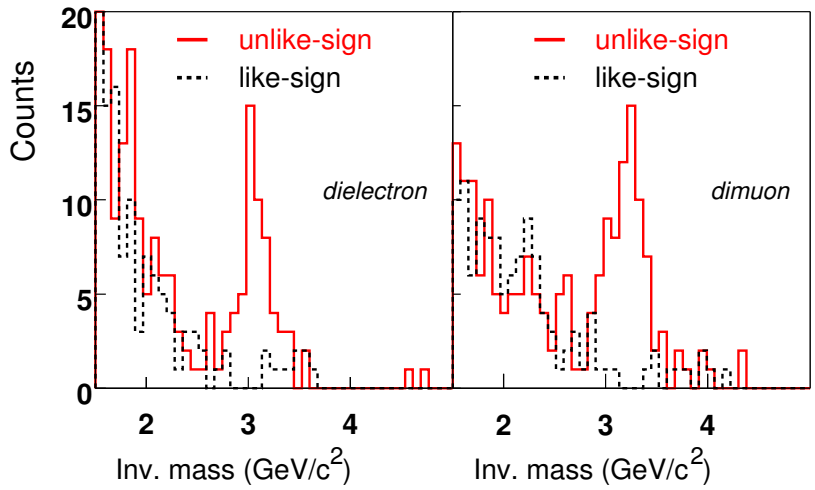

Figure 2.25: The invariant mass distribution for dielectron (left) and dimuon (right) pairs. The solid lines are for unlike-sign pairs and the dashed lines for like-sign pairs (from [55]).

The cross sections were in turn extracted using

$$\mathcal{B}\frac{d^2\sigma}{dydp_T} = \frac{N_{J/\psi}}{(\int \mathcal{L}dt)\Delta y \Delta p_T}\frac{1}{\epsilon_{bias}\epsilon_{trig}}\frac{1}{A\epsilon_{rec}}, \tag{2.19}$$

where $N_{J/\psi}$ is the measured J/ψ yield, $\int \mathcal{L}dt$ the integrated luminosity, ϵ_{bias} is the minimum bias trigger which is used to measure the luminosity, ϵ_{trig} is the trigger efficiency, A the acceptance for J/ψ reconstruction and finally ϵ_{rec} its efficiency.

We shall not describe here the method to evaluate the systematics, we simply reproduce *verbatim* the table given in [55]. Note however that the analysis of errors did not take into account possible polarisation effects.

Quantity	e^+e^-	$\mu^+\mu^-$
Yield	$\pm$ 5%	$\pm$ 5%
$A\epsilon_{rec}$	0.026-0.010 $\pm$ 13%	0.038 - 0.017 $\pm$ 13%
ϵ_{trig}	(2×2) 0.87-0.90 $\pm$ 5%	
	(4×4) 0.30-0.74 $\pm$ 36%	
ϵ_{bias}	0.75 $\pm$ 3%	0.75 $\pm$ 3%
$\int \mathcal{L}dt$	82 nb^{-1} $\pm$ 9.6%	67 nb^{-1} $\pm$ 9.6%
Total	$\pm$ 15%(sys) $\pm$ 10%(abs)	$\pm$ 14%(sys) $\pm$10%(abs)

Table 2.8: Table of quantities and their systematic-error estimates. Ranges are given for p_T dependent quantities. For the $\mu^+\mu^-$ case, the values of $A\epsilon_{rec}$ and ϵ_{trig} are combined. The absolute cross-section normalisation uncertainty from ϵ_{bias} and $\int \mathcal{L}dt$ is kept separate and is labeled "(abs)" (taken from [55]).

From Eq. (2.19), the cross section as a function of p_T is obtained for the two analyses. For p_T larger than two 2 GeV, it is compared in Fig. 2.26 with LO CSM and COM without fragmentation but with χ_c feed-down. These theoretical predictions are from Nayak *et al.* [67].

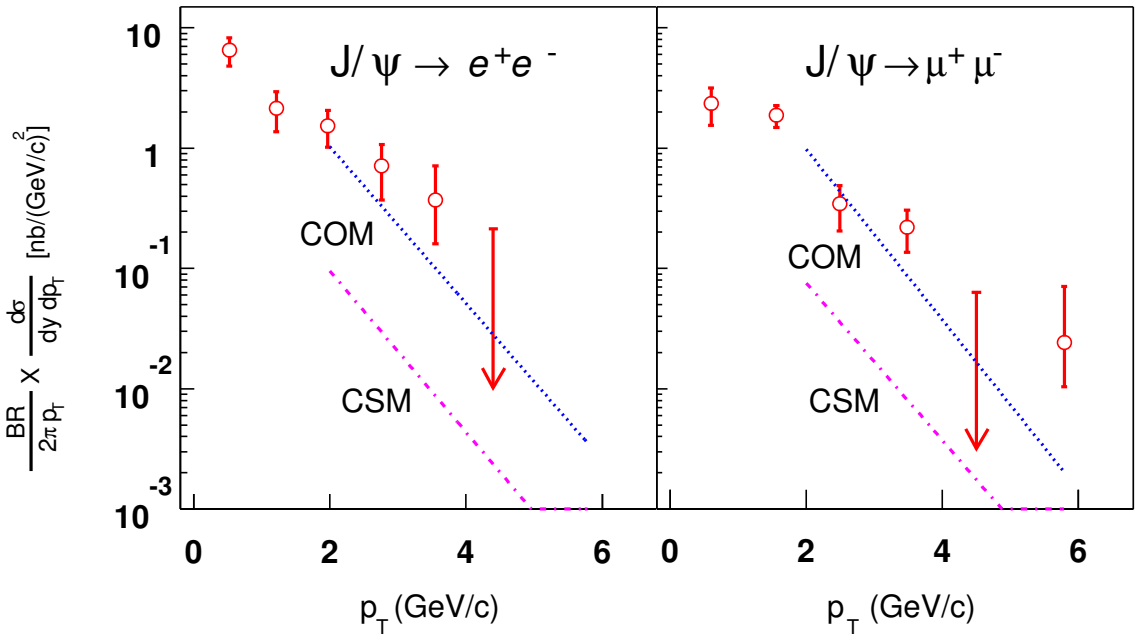

Figure 2.26: The differential cross section measured to be compared with theoretical predictions from CSM and COM (without fragmentation but with χ_c feed-down) of [67] (adapted from [55]).

Chapter 3

Building a new model

3.1 Foreword

We first present a study [68] of the theoretical uncertainties of the LO CSM as an indication of the uncertainties of all theoretical model. As we shall see, these are far from being sufficient to explain the discrepancies with experimental measurements.

These theoretical uncertainties can arise from errors on the leptonic decay width determination. The latter is used to determine the wave function at the origin, which is the non-perturbative input of the model. Similar inputs exist for the COM and they are associated with the probability for the $Q\bar{Q}$ pair to eventually evolve into a given physical state. These probabilities are obtained from fits and are subject to similar uncertainties.

Another main source of uncertainty is the parton distribution function. In the case at hand, only gluons are actually involved, as the energy of the colliding hadrons is very large, and the required momentum fraction of partons consequently low.

After the presentation of this study, we shall expose the guidelines that we shall follow in order to build a new model; in a sense, the model serves as a *non-static extension* of the CSM, but it could also be seen as a generalisation of the COM for $Q\bar{Q}g$ states with the gluon having a large momentum, whereas, in NRQCD, the momentum of the gluon associated with the heavy quark pair in the considered Fock state is necessarily lower than Mv where v is the typical velocity of the quarks within the bound state of mass M.

3.2 Theoretical uncertainties of the LO CSM

3.2.1 Wave function

At LO in α_s, the leptonic decay width reads:

$$\Gamma(^3S_1 \to \ell\bar{\ell}) = \frac{64\pi}{9}\frac{\alpha^2 e_q^2 |\Psi(0)|^2}{M^2}, \tag{3.1}$$

where α is the fine structure constant and e_q the quark charge in units of e. This is one of the consequences of the factorisation postulate.

We thus find that the error on $\Gamma_{^3S_1\to\mu\mu}$ introduces an error of at least 10% on the cross section.

Meson	$\lvert\Psi(0)\rvert^2 \pm \sigma_{\lvert\Psi(0)\rvert^2}$	Relative error
J/ψ	0.041 ± 0.0042 GeV^3	10%
$\psi(2S)$	0.024 ± 0.0025 GeV^3	10%
$\Upsilon(1S)$	0.397 ± 0.015 GeV^3	4%
$\Upsilon(2S)$	0.192 ± 0.030 GeV^3	16%
$\Upsilon(3S)$	0.173 ± 0.032 GeV^3	18%

Besides, one may consider the Colour Singlet Model as a level of approximation of the Non Relativistic Quantum Chromodynamics (NRQCD) (already exposed in the first chapter). Indeed this formalism describes the production of quarkonia by two main classes of processes, the first when the quark pair is perturbatively produced within a colour-singlet configuration – it can then have exactly the same quantum number as the meson, as in the CSM, or be in a different spin configuration–, the second class is when the quark pair is perturbatively produced within a colour-octet configuration.

In fact, as already mentioned, NRQCD predicts that there is an infinite number of Fock-state contributions to the production of a quarkonium $\mathcal{Q}$. Practically, one is driven to truncate the series; this is quite natural in fact since most of the contributions are known to be suppressed by factor of $\mathcal{O}(\frac{v^2}{c^2})$, where v is the quark velocity in the bound state.

For definiteness, the latest studies accommodating the production rate of $^3S_1$ states retain only the colour singlet state with the same quantum numbers as the bound state and colour octet P-wave states and singlet S-wave. In this context, the CSM can be thought as a further approximation to the NRQCD formalism.

However, in this formalism, factorisation tells us that each contribution is the product of a perturbative part and a non-perturbative matrix element, giving, roughly speaking, the probability that the quark pair perturbatively produced will evolve into the considered physical bound state. If one transposes this to the CSM, this means the wave function at the origin corresponds to this non-perturbative element. This seems reasonable since the wave function squared is also a probability.

Yet, one has to be cautious because one actually links production processes with decay processes. In NRQCD, two different matrix elements are defined for the "colour singlet" production and decay, and they are likely to be different and independent.

The only path left to recover the CSM is the use of a further approximation, the vacuum saturation approximation. The latter tells us that the matrix element for the decay is linked to the one for the production. This enables us to relate the wave function at the origin appearing in Eq. (3.1) to the colour-singlet NRQCD matrix element for production. This gives:

$$\left\langle \mathcal{O}_1^{\psi}(^3S_1) \right\rangle = 18\,|\psi(0)|^2 + \mathcal{O}(v^4). \tag{3.2}$$

The conclusion that could be drawn within NRQCD is that the extraction of non-perturbative input for production from the one for decay is polluted by factors of $\mathcal{O}(v^4)$.

3.2.2 Parton distribution functions

Let us now analyse the uncertainties due to the parton distribution functions (pdf). As there are two gluons coming from the initial hadronic state, these can induce non-negligible uncertainties on the cross section, either directly or via the associated $\alpha_s(Q^2)$.

For coherence, we have limited ourselves to LO pdf's. As a consequence, we have not felt the necessity to refine the study to the point of using the very last pdf on the market. This choice is further justified because we want to have an estimate of the effects due to extreme-case choices. Here are different plots obtained for a set of 12 pdf's (see the legend of Fig. 3.1) coded in PDFLIB [69] which illustrate these effects:

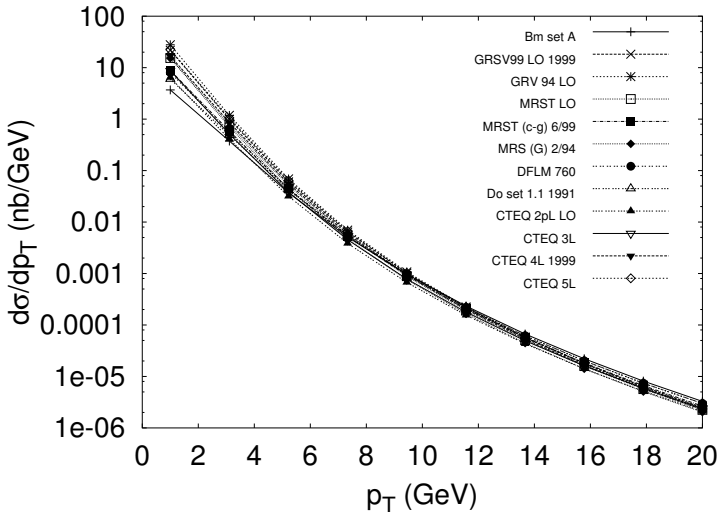

Figure 3.1: Variation of the cross sections obtained with various pdf's [69] due to the pdf's only.

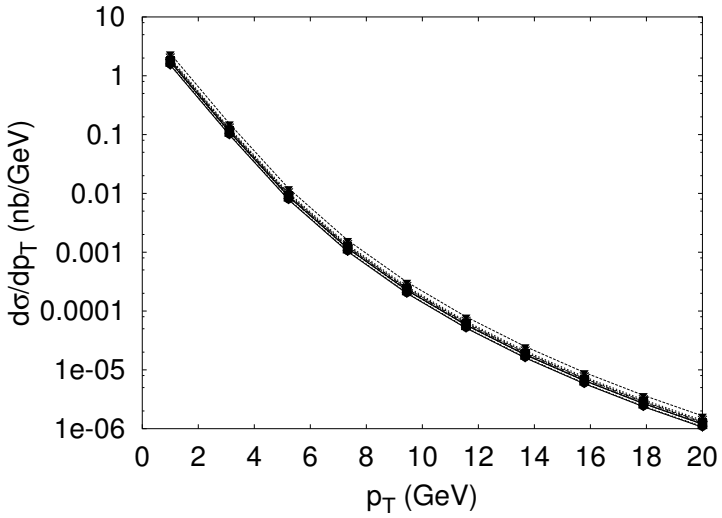

Figure 3.2: Variation of the cross sections due to α_s only.

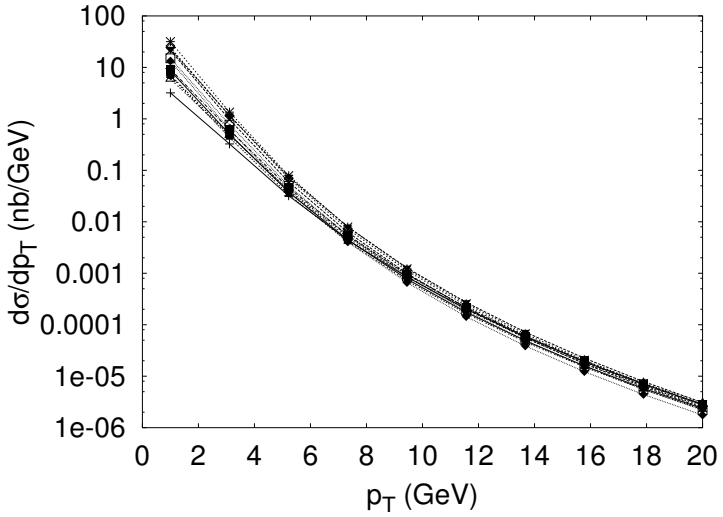

Figure 3.3: Variation of the cross sections obtained with various pdf's [69] due to α_s and the pdf's.

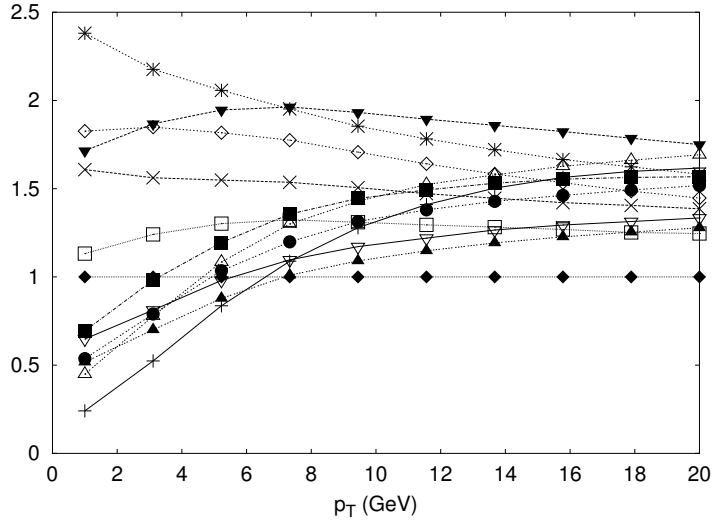

Figure 3.4: Ratio of the cross sections obtained with various pdf's [69] to the cross section obtained with MRS(G) 2-94.

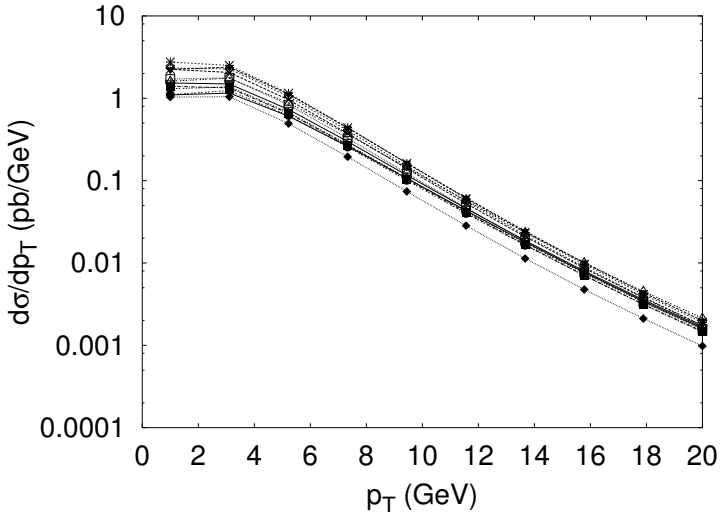

Figure 3.5: Variation of the cross sections obtained with various pdf's [69] for $\Upsilon(3S)$.

We thus found that the overall factor resulting from these 3 sources of uncertainties is at most 2-3 and roughly constant for different values of p_T. Hence, the discrepancy of the CSM with data is not due to conventional theoretical errors. Furthermore, these could not change polarisation results either, for which data seem to contradict NRQCD.

3.3 Assumptions for a new model

As we have already stated, no solution of the polarisation issue has been proposed so far, while we just have seen that conventional theoretical uncertainties are under control. We therefore propose to go beyond the traditional treatment which is to consider the heavy quarkonia as purely non-relativistic states with the consequence of neglecting *a priori* any effects that may come from the internal dynamics of quarks in the bound state. This approximation is sensible and supported by arguments such as the success of potential models, with instantaneous interactions. Nevertheless, it has never been demonstrated that non-static effects are systematically negligible and that the internal dynamics as well as the quark off-shellness in the meson do not provide any sizable modification of their description.

In order to tackle internal dynamics, we shall describe the heavy quarkonia with a phenomenological 3-particle vertex, made of a Dirac structure inferred from the quantum numbers of the considered quarkonium and a vertex function inspired by the Bethe-Salpeter formalism. The description and the justification of the different steps leading to this 3-particle vertex is made in the next chapter.

Nevertheless, as we shall see in chapter 5, the introduction of vertex functions breaks gauge invariance in production processes associated with a photon or a gluon. Our solution to this problem is the introduction of new 4-particles vertices restoring the invariance. A complete derivation of their characteristics will be undertaken. Gauge-invariance restoration leaves some freedom to add autonomous 4-particle vertices, which are gauge invariant alone.

In chapter 6, we shall then apply our approach to the determination of the imaginary part of the amplitude for $gg \to {}^3S_1 g$. This amplitude is the expected main contribution for ψ and Υ production at the Tevatron and RHIC at low P_T. This will enable us to calculate the various cross sections for these. In turn, we shall introduce the above-mentioned autonomous contributions that will allow us to fit the data rather well. A further and complete agreement with the data, namely with polarisation, will then be accomplished by a combination of our prediction with the colour octet ${}^3S_1$ fragmentation. Indeed, we eventually obtain a polarisation parameter roughly constant and compatible with an unpolarised production.

Chapter 4

Two-particle description of heavy quarkonia

In this chapter, we shall introduce the quantities required to study processes involving heavy quarkonia, such as decay and production mechanisms. In field theory, all the information needed can be parameterised by a vertex function, which describes the coupling of the bound state to the quarks and contains the information about the size of the bound state, the amplitude of probability for given quark configurations and the normalisation of the bound-state wave functions.

The vertex function has close links with the classical non-perturbative wave function introduced in quantum mechanics. We shall first consider those, and give their characteristics if one thinks that the quarkonia are purely non-relativistic bound-states. This will show us also that the mass of the quark is actually a poorly constrained parameter, which can be chosen with some freedom.

Then, we shall start the description of our approach to build the quarkonia vertex functions. Along the way, we shall explain why we do not rely on the Bethe-Salpeter Equation [70] (BSE), usually used to constrain the properties of vertex functions, for example, to relate the mass of the bound state to the mass of its constituent quarks. Beside problems with gauge invariance, all predictions coming from BSE are realised within Euclidean space (see *e.g.* [71, 72, 73]) and we shall show that the continuation to Minkowsky space is in general problematic. We shall make the choice to remain in Minkowsky space, at variance with other phenomenological models (see *e.g.* [74, 75]). The price to pay for not using BSE will be additional uncertainties due to the functional dependence of the vertex. Fortunately, most of these can be cancelled if one fixes the normalisation from the study of the leptonic decay width.

We shall thus explain only in few words how in principle from a given choice for the vertex functions, we may be able to fix some of the parameters by the use of the BSE.

4.1 The charmonium model

As soon as the J/ψ and the ψ' were discovered and the community of particle physicists started to convince itself that they were composed of a c and a $\bar{c}$ quark, Applequist and Politzer [76] proposed that these states should share some properties with positronium states made of e^+ and e^-. Their statement was mainly motivated by the discovery of asymptotic freedom in QCD [77, 78, 79, 80].

The identification of the J/ψ and ψ' as "ortho-charmonium" [1] was then straightforward. Concerning the decay, as the c-quark mass sets a sufficiently high scale compared to Λ_{QCD}, a formula similar to that for positronium – derived from the QED perturbative expansion – was therefore believed to be sufficient, with the natural replacements of α by α_s and m_e by m_c. In the latter formula, the use of a coulombic wave function gave the right order of magnitude for the leptonic decay width $\Gamma_{\ell\ell}$ [81].

As the Bohr radius ($(\frac{2}{3}\alpha_s m_c)^{-1}$) of these states was of the order of 1 fm (a typical hadron size), they could not be purely coulombic. A strong binding force operating at large distance was then added. It resulted in a coulombic potential with a linear rising term preventing the freedom of quarks.

This gave birth to what is referred to as the charmonium model [82] whose potential was initially of the form:

$$V(r) = -\frac{4}{3}\frac{\alpha_s}{r} + kr, \tag{4.1}$$

where k is the string tension.

From the Schrödinger equation

$$\left[-\frac{1}{m_c}\Delta + V(r)\right]\Psi_{n\ell m}(r) = E_{n\ell}\Psi_{n\ell m}(r), \tag{4.2}$$

the wave functions $\Psi_{n\ell m}(r)$ and the binding energies $E_{n\ell}$ were then calculated, the corresponding mass spectrum being then built using $M_{n\ell}(c\bar{c}) = 2m_c + E_{n\ell}$.

4.1.1 Refinements

Later on, in order to solve the entire spectroscopy of the charmonium and bottomonium family, other forms for the potential were proposed:

- The "Cornell" (COR) potential [84]

$$V(r) = -\frac{k}{r} + \frac{r}{a^2}, \tag{4.3}$$

with[2] $k = 0.52$, $a = 2.34$ GeV^{-1} [3] and $m_c = 1.84$ GeV or $m_b = 5.18$ GeV.

[1] S-wave ($n = 0, \ell = 0$), J=1.

[2] Comparing this form to the one of Eq. (4.1), we see that $\alpha_s = 0.38$ makes $k = \frac{4\alpha_s}{3}$ be 0.52.

[3] $\frac{1}{a^2}$ here plays the role of the string tension k of Eq. (4.1).

- The "Buchmüller & Tye" (BT) potential [85] such that

$$\begin{aligned} V(r) &\sim kr \quad (r_{crit} \leq r), \\ V(r) &\sim \frac{1}{r \ln(1/\Lambda^2_{QCD} r^2)} \left[1 + \mathcal{O}\left(\frac{1}{\ln(1/\Lambda^2_{QCD} r^2)} \right) \right], \end{aligned} \tag{4.4}$$

  where k is again the string tension, Λ_{QCD} is the QCD running scale, r_{crit} is fixed by $\frac{1}{r^2_{crit}\Lambda^2_{QCD,\overline{MS}}} = 100$ (see [85]) and $m_c = 1.48$ GeV or $m_b = 4.88$ GeV.

- The "Logarithmic" (LOG) potential [86] such that

$$V(r) = -0.6635 \text{ GeV } + (0.733 \text{ GeV}) \log(r \cdot 1 \text{ GeV }), \tag{4.5}$$

  with $m_c = 1.5$ GeV or $m_b = 4.906$ GeV.

- the "Power-law" (POW) potential [87]

$$V(r) = -8.064 \text{ GeV } + (6.898 \text{ GeV})(r \cdot 1 \text{ GeV })^{0.1}, \tag{4.6}$$

  with $m_c = 1.8$ GeV or $m_b = 5.174$ GeV.

For illustrative purpose, we show in Fig. 4.1 some wave functions obtained by Kopeliovich *et al.* [83] from Eqs.(4.2–4.6). As one may see, even though the values of the charm quark mass, m_c, differ substantially from one potential to another, the wave functions do not differ much for large r. On the other hand, they differ by 30 % at the origin, value which is a key input in the static approximation. Usually, it is extracted from the leptonic decay width but one is free to rely on these determinations from the resolution of the Schrödinger equation.

Please note also the presence of a node in the wave function for the first radial excitation (ψ') as should be from general theorems of quantum mechanics. This node at around 0.4 fm produces the suppression of photoproduction of ψ' compared to J/ψ [88].

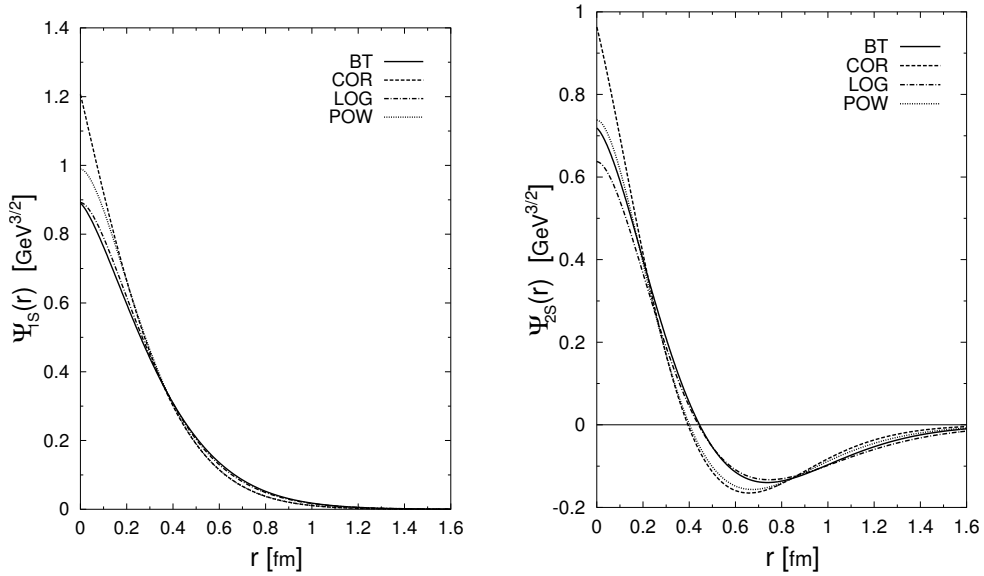

(a) J/ψ (b) $\psi(2S)$

Figure 4.1: The radial wave function $\Psi_{n\ell}(r)$ for the J/ψ $(1S)$ and ψ' $(2S)$ states obtained by Kopeliovich *et al.* [83] for four potential: BT, COR, LOG and POW.

4.2 Phenomenological approach to the vertex function

4.2.1 Wave function vs. vertex function

We have seen in the previous section how one can calculate the wave function for the quarkonia. One thing is however lacking, that is how to include this information in a calculation involving Feynman diagrams. The usual procedure can be summarised as follows:

- the quarks are to be on-shell within the quarkonia and therefore have to be produced on-shell;
- the Schrödinger wave function provides with the binding-probability amplitude ;
- the quantum numbers of the bound state come uniquely from the quarks configuration. The parity P and charge conjugation C are therefore given by $P = (-)^{L+1}$ and $C = (-)^{L+S}$ where L and S are given by the corresponding eigenvalues of the Schrödinger equation.

From this, it follows that the amplitude for producing a bound state of quantum numbers J, L, S is

$$\mathcal{M}_{tot} = \sum_{L_z,S_z} \langle LL_z; SS_z|JJ_z\rangle \sum_{\lambda,\bar{\lambda}} \int \frac{d^3\vec{p}}{(2\pi)^3} \mathcal{M}_{\lambda,\bar{\lambda}}(\vec{p}) \Psi^{L_z S_z}_{\lambda,\bar{\lambda}}(\vec{p})^*, \tag{4.7}$$

with $\vec{p}$, the relative momentum between the two quarks, $\lambda, \bar{\lambda}$, the spin projections of the quarks along the z-axis (quarkonium direction), $\mathcal{M}_{\lambda,\bar{\lambda}}(\vec{p})$, the amplitude for producing the heavy-quark pair and $\Psi^{L_z S_z}_{\lambda,\bar{\lambda}}(\vec{p})$, the wave function of the bound state.

The important point here is that the latter reads:

$$\Psi^{L_z S_z}_{\sigma\bar{\sigma}}(\vec{p})^* = \Psi^*_{LL_z}(\vec{p}) \frac{1}{2m} \bar{v}(-\vec{p}, \bar{\sigma}) \bar{\mathcal{P}}_{SS_z}(\vec{p}, -\vec{p}) u(\vec{p}, \sigma), \tag{4.8}$$

where $\Psi_{LL_z}(\vec{p})$ is the non-relativistic wave function, $\bar{v}$ and u are the spinors for the two on-shell heavy quarks – as stated in the assumptions – and $\bar{\mathcal{P}}_{SS_z}$ is *a spin-projection operator* whose explicit expression is [89]

$$\begin{aligned} \bar{\mathcal{P}}_{SS_z}(\vec{p}_1, \vec{p}_2) &= \frac{1}{2m} \sum_{\lambda_1,\lambda_2} \langle \frac{1}{2}\lambda_1, \frac{1}{2}\lambda_2 | S S_z \rangle v(\vec{p}_2, \lambda_2) \bar{u}(\vec{p}_1, \lambda_1) \\ &= \frac{1}{2m} \frac{\not{p}_2 - m}{\sqrt{p_{2,0} + m}} \bar{\Pi}_{SS_z} \frac{\gamma^0 + 1}{2\sqrt{2}} \frac{\not{p}_1 + m}{\sqrt{p_{1,0} + m}} \qquad (4.9) \\ \text{where} \quad \bar{\Pi}_{SS_z} &= \begin{bmatrix} -\gamma_5 & (S=0) \\ \gamma^\mu \varepsilon^*_\mu(S_z) & (S=1) \end{bmatrix} \qquad (4.10) \end{aligned}$$

The expressions in Eq. (4.10) are what we shall use for our vertex, for respectively a pseudoscalar particle and a vector particle. But we are going further by lifting the constraint that the quark be on their mass shell. *This generalises structureless vertices of the usual pQCD to bound states.*

4.2.2 Our choice for the vertex function

It has been shown elsewhere (see *e.g.* [72]) that other structures than γ^μ Dirac matrix for vector bound state are suppressed by one order of magnitude in the case of light mesons, and that this suppression is increasing for the meson ϕ ($s\bar{s}$). We have therefore reasons to believe that their effect are even more negligible in heavy quarkonia.

As a consequence, the following phenomenological Ansatz for the vector-meson vertex, inspired by Eq. (4.10), is likely to be sufficient for our purposes. It reads:

$$V_\mu(p, P) = \Gamma(p, P) \gamma_\mu, \tag{4.11}$$

with P the total momentum of the bound state, $P = p_1 - p_2$, and p the relative one, $p = (p_1 + p_2)/2$ as drawn in Fig. 4.2. This Ansatz amounts to multiplying the *point* vertex (corresponding to a structureless particle) by a function, $\Gamma(p, P)$.

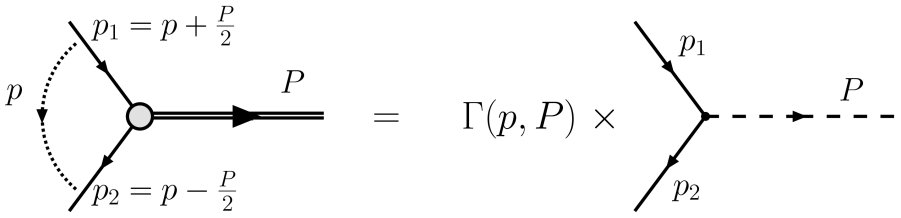

Figure 4.2: Phenomenological vertex obtained by multiplying a *point* vertex, representing a structureless particle, by a vertex function (or form factor).

The function Γ, which we shall call vertex function, can be chosen in different ways. Two simple Ansätze are commonly used in the context of Bethe-Salpeter Equation. We shall consider both. They correspond to two extreme choices at large distances: a dipolar form which decreases gently with its argument, and a gaussian form:

$$\Gamma_0(p, P) = \frac{N}{(1 - \frac{p^2}{\Lambda^2})^2}, \tag{4.12}$$

and

$$\Gamma_0(p, P) = N e^{\frac{p^2}{\Lambda^2}}, \tag{4.13}$$

both with a free size parameter Λ. As $\Gamma(p, P)$ in principle depends on p and P, we may shift the variable and use $p^2 - \frac{(p.P)^2}{M^2}$ instead of p^2 which has the advantage of reducing to $-|\vec{p}|^2$ in the rest frame of the bound state. We shall refer to it as the *vertex function with shifted argument*. In the latter cases, we have – in the rest frame –,

$$\Gamma(p, P) = \frac{N}{(1 + \frac{|\vec{p}|^2}{\Lambda^2})^2} \tag{4.14}$$

and

$$\Gamma(p, P) = N e^{\frac{-|\vec{p}|^2}{\Lambda^2}}. \tag{4.15}$$

Excited states

As one knows, the number of nodes in the wave function, in whatever space, increases with the principal quantum number n. This simple feature can be used to differentiate between $1S$ and $2S$ states.

We thus simply have to determine the position of the node of the wave function in momentum space. To what concerns the vertex function, working in the meson rest frame, the node comes through a prefactor, $1 - \frac{|\vec{p}|}{a_{node}}$, which multiplies the vertex function for the $1S$ state. Explicitly, this gives,

$$\Gamma_{2S}(p, P) = N' \left(1 - \frac{|\vec{p}|}{a_{node}}\right) \frac{1}{(1 + \frac{|\vec{p}|^2}{\Lambda^2})^2} \tag{4.16}$$

and

$$\Gamma_{2S}(p,P) = N' \left(1 - \frac{|\vec{p}|}{a_{node}}\right) e^{\frac{-|\vec{p}|^2}{\Lambda^2}}. \tag{4.17}$$

In order to determine the node position in momentum space, we can use two methods. The first is to fix a_{node} from its known value in position space, *e.g.* from potential studies, and to Fourier-transform the vertex function. In the case of a gaussian form, this can be carried out analytically.

The second method is to impose the following relation[4] between the $1S$ and $2S$ vertex functions:

$$\int |\vec{p}|^2 d|\vec{p}| e^{\frac{-|\vec{p}|^2}{\Lambda^2}} \left(1 - \frac{|\vec{p}|}{a_{node}}\right) e^{\frac{-|\vec{p}|^2}{\Lambda^2}} = 0. \tag{4.18}$$

The two methods give compatible results. The introduction of a second node to describe the $3S$ states is similar.

4.3 Normalising: the leptonic decay width

To fix the normalisation parameter N, we shall use the leptonic decay width. Besides, as the calculation is similar to the one for the production processes, we shall give a detailed explanation of this calculation as a pedagogical introduction to the production calculations which are the core of this work (see chapter 6).

The width in term of the decay amplitude $\mathcal{M}$, is given by

$$\Gamma_{\ell\ell} = \frac{1}{2M} \frac{1}{(4\pi^2)} \int \left|\bar{\mathcal{M}}\right|^2 d_2(PS), \tag{4.19}$$

where $d_2(PS)$ is the two-particle phase space [90].

The amplitude is obtained as usual via Feynman rules, for which we shall use our vertex function at the meson-quark-antiquark vertex. At leading order, the square of the amplitude is obtained from the cut-diagram drawn in Fig. 4.3.

In terms of the sub-amplitudes $A^{\mu\nu}$, $B^{\mu\nu}$ and $C^{\mu\nu}$ defined in Fig. 4.3, we have[5] :

$$\int \left|\bar{\mathcal{M}}\right|^2 d_2(PS) = \frac{1}{3} \Delta_{\mu\mu'} A^{\mu\nu} \left(\frac{-ig_{\nu\rho}}{M^2}\right) B^{\rho\rho'} \left(\frac{-ig_{\rho'\nu'}}{M^2}\right) C^{\nu'\mu'}, \tag{4.20}$$

where the factor $\Delta_{\mu\nu} = (g_{\mu\nu} - \frac{P_\mu P_{\nu'}}{M^2}) = \sum_i \varepsilon_{i,\mu} \varepsilon^\star_{i,\mu'}$ results from the sum over polarisations of the meson and the factor $\frac{1}{3}$ accounts for the averaging on these initial polarisations.

[4] inspired from the orthogonality between the $1S$ and $2S$ wave functions.

[5] In the Feynman gauge. The calculation can be shown to be gauge-invariant, though.

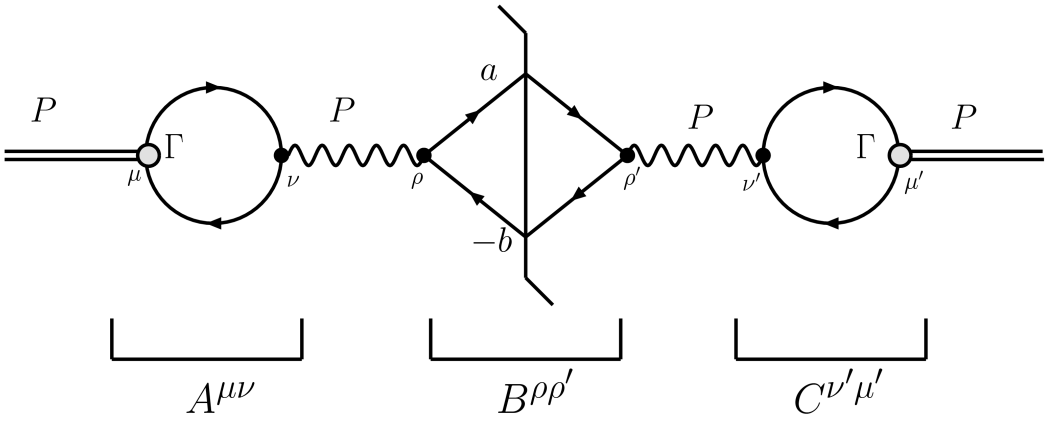

Figure 4.3: Feynman diagram for ${}^3S_1 \to \ell\bar{\ell}$.

.

4.3.1 First sub-amplitude

From the Feynman rules and using the vertex functions discussed above, we have (see Fig. 4.4)

$$\begin{aligned} iA^{\mu\nu} &= -3e_Q \int \frac{d^4k}{(2\pi)^4} \mathrm{Tr}\left((i\Gamma(p,P)\gamma^\mu) \frac{i(\not{k} - \frac{1}{2}\not{P} + m)}{(k-\frac{P}{2})^2 - m^2 + i\varepsilon} (ie\gamma^\nu) \frac{i(\not{k} + \frac{1}{2}\not{P} + m)}{(k+\frac{P}{2})^2 - m^2 + i\varepsilon} \right) \\ &= -3e_Q \int \frac{d^4k}{(2\pi)^4} \Gamma(p,P) \frac{g^{\mu\nu}(M^2 + 4m^2 - 4k^2) + 8k^\mu k^\nu - 2P^\mu P^\nu}{((k-\frac{P}{2})^2 - m^2 + i\varepsilon))((k+\frac{P}{2})^2 - m^2 + i\varepsilon))}, \end{aligned} \tag{4.21}$$

e_Q is the heavy-quark charge, -1 comes for the fermionic loop, 3 is the colour factor.

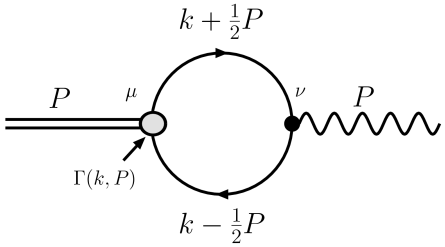

Figure 4.4: Feynman diagram for ${}^3S_1 \to \gamma$.

Since the relative momentum is k, we shall have in the bound-state rest frame, for the dipolar form of the vertex function as a function of k ,

$$\Gamma(p,P) = \frac{N}{(1 + \frac{|\vec{k}|^2}{\Lambda^2})^2}, \tag{4.22}$$

and for the gaussian form,

$$\Gamma(p,P) = Ne^{\frac{-|\vec{k}|^2}{\Lambda^2}}. \tag{4.23}$$

The expressions for the vertex functions of excited states immediately follow from the above discussion and are not written down.

We can easily motivate our choice of the argument of the vertex function, beside its simple relation with that of wave functions. Its main virtue is to regularise the integration in all spatial directions. In the meson-rest frame, the k^0 integral can be done by standard residue techniques, and the remaining $\vec{k}$ integral is guaranteed to converge. If one uses k^2 instead of $|\vec{k}|^2$ as an argument, it is possible to show that along the light cone, one obtains logarithmic divergences, which would presumably need to be renormalised. Besides, the k^0 integral then also becomes dependent on the singularity structure of the vertex function. These two reasons make us prefer the shifted vertex in our calculation.

A notable simplification can be obtained by guessing the tensorial form of $A^{\mu\nu}$. Indeed, current conservation (gauge invariance) for the photon can be expressed as:

$$A^{\mu\nu}P_\nu = 0. \tag{4.24}$$

It is equivalent to

$$iA^{\mu\nu} = iF(g^{\mu\nu} - \frac{P^\mu P^\nu}{M^2}) = iF\Delta^{\mu\nu}, \tag{4.25}$$

the coefficient F being $\frac{A^\mu{}_\mu}{3}$ since $A^\mu{}_\mu = A^{\mu\nu}g_{\nu\mu} = 3F$. This assumption can be easily verified in the bound-state rest frame $P = (M, 0, 0, 0)$ for which Eq. (4.24) reduces to $A^{\mu 0}M = 0 \Rightarrow A^{\mu 0} = 0$. We shall check this at the end of this calculation.

It is therefore sufficient to compute the following quantity, where we set $|\vec{k}|^2 \equiv K^2$:

$$\begin{aligned} iA^\mu{}_\mu = -3e_Q \int_0^\infty 4\pi K^2 dK \Gamma(-K^2)\times \\ \int_{-\infty}^\infty \frac{dk_0}{(2\pi)^4} \frac{4(-2(k^2 - \frac{M^2}{4}) + 4m^2)}{((k-\frac{P}{2})^2 - m^2 + i\varepsilon)((k+\frac{P}{2})^2 - m^2 + i\varepsilon))}. \end{aligned} \tag{4.26}$$

Integration on k_0

Let us first integrate on k_0 by residues. Defining $E = \sqrt{K^2 + m^2}$, we determine easily the position of the pole in k_0 (still in the bound-state rest frame)

$$\begin{aligned} &(k + \frac{P}{2})^2 - m^2 + i\varepsilon = k_0^2 + k_0 M + \frac{M^2}{4} - K^2 - m^2 + i\varepsilon = \\ &(k_0 + \frac{M}{2})^2 - E^2 + i\varepsilon = ((k_0 + \frac{M}{2}) + E - i\varepsilon')((k_0 + \frac{M}{2}) - E + i\varepsilon') = \\ &(k_0 - (\frac{-M}{2} + E + i\varepsilon'))(k_0 - (\frac{-M}{2} + E - i\varepsilon')), \end{aligned} \tag{4.27}$$

and

$$
\begin{aligned}
&(k-\frac{P}{2})^2-m^2+i\varepsilon = k_0^2-k_0M+\frac{M^2}{4}-K^2-m^2+i\varepsilon = \\
&(k_0-\frac{M}{2})^2-E^2+i\varepsilon = ((k_0-\frac{M}{2})+E-i\varepsilon')((k_0-\frac{M}{2})-E+i\varepsilon') = \\
&(k_0-(\frac{M}{2}-E+i\varepsilon'))(k_0-(\frac{M}{2}+E-i\varepsilon')).
\end{aligned}
\tag{4.28}
$$

To calculate the integral on k_0, we choose the contour as drawn in Fig. 4.5. Two poles $-E-\frac{M}{2}$ and $-E+\frac{M}{2}$ are located in the upper half-plane and the two others in the lower half-plane. We shall therefore have two residues to consider. The contribution of the contour $\mathcal{C}_R$ vanishes as R tends to ∞.

$$
\begin{aligned}
&iA^{\mu}_{\ \mu} = \frac{-3e_Q}{\pi^3}\int_0^\infty K^2dK\Gamma(-K^2)\times \\
&\int_{-\infty}^{\infty}\frac{dk_0(-2k_0^2+2K^2+\frac{M^2}{4}+4m^2)}{(k_0-(\frac{-M}{2}-E+i\varepsilon))(k_0-(\frac{-M}{2}-E-i\varepsilon))(k_0-(\frac{M}{2}-E+i\varepsilon))(k_0-(\frac{M}{2}+E-i\varepsilon))} \\
&=\frac{-3e_Q}{\pi^3}\int_0^\infty K^2dK\Gamma(-K^2)\times \\
&2i\pi\left[\frac{-2(-E-\frac{M}{2})^2+\frac{M^2}{2}+2E^2+2m^2}{(-2E)(-M)(-2(E+\frac{M}{2}))}+\frac{-2(-E+\frac{M}{2})^2+\frac{M^2}{2}+2E^2+2m^2}{M(-2(E-\frac{M}{2}))(-2E)}\right] \\
&=\frac{-3e_Q}{\pi^3}\int_0^\infty K^2dK\Gamma(-K^2)\frac{2i\pi}{4ME}\underbrace{\left[-\frac{2EM+2m^2}{E+\frac{M}{2}}+\frac{2EM+2m^2}{E-\frac{M}{2}}\right]}_{\frac{M(4E^2+2m^2)}{E^2-\frac{M^2}{4}}}.
\end{aligned}
\tag{4.29}
$$

Setting the constituent quark mass

This way of proceeding is correct only if the poles of the upper-plane are on the left and those of the lower-plane are on the right[6].

This crossing would first occur between the points $-E+\frac{M}{2}$ and $E-\frac{M}{2}$. Solving for E, we have:

$$
\begin{aligned}
-E+\frac{M}{2} = E-\frac{M}{2} &\Rightarrow E=\frac{M}{2}=\sqrt{K^2+m^2} \\
&\Rightarrow \frac{M^2}{4}=K^2+m^2 \\
&\Rightarrow \frac{M^2}{4}-m^2=K^2>0.
\end{aligned}
\tag{4.30}
$$

[6] If they cross, the integral acquires a discontinuity from the pinch and becomes complex.

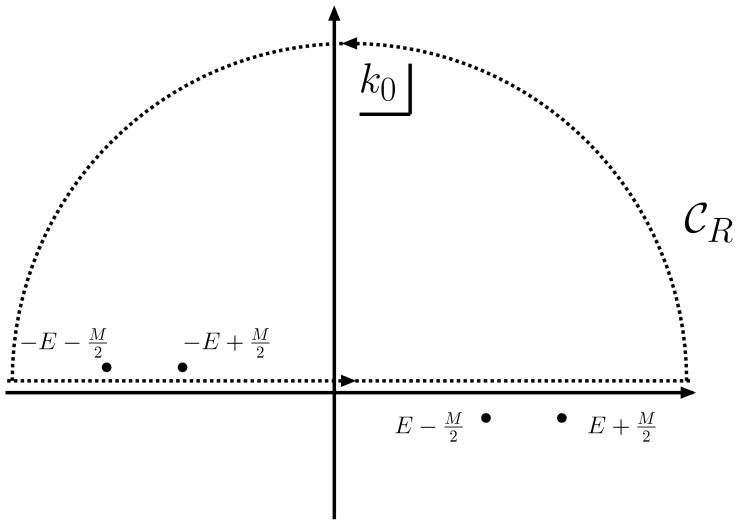

Figure 4.5: Illustration of the contour chosen to integrate on k_0.

.

The crossing is therefore impossible when $M < 2m$. Therefore, to get a coherent description of all charmonia (resp. bottomonia) below the open charm (resp. beauty) threshold, we shall set the quark mass high enough to avoid crossing for all of these. This sets m_c to 1.87 GeV (m_D) and m_b to 5.28 GeV (m_B). Considering the variety of results obtained from potential model, this seems to be a sensible choice.

Integration on K

Putting it all together, we get

$$A^{\mu}{}_{\mu} = \frac{-3e_Q}{\pi^2}\int_0^{\infty} dK \frac{K^2\Gamma(-K^2)}{\sqrt{K^2+m^2}} \frac{(2K^2+3m^2)}{(K^2+m^2-\frac{M^2}{4})}. \tag{4.31}$$

One is left with the integration on K for which we define the integral I depending on the vertex function whose normalisation is pulled off,

$$I(\Lambda, M, m) \equiv \int_0^{\infty} \frac{dKK^2}{\sqrt{K^2+m^2}} \frac{\Gamma(-K^2)}{N} \frac{(2K^2+3m^2)}{(K^2+m^2-\frac{M^2}{4})}, \tag{4.32}$$

I is a function of Λ through the vertex function $\Gamma(-K^2)$ and is not in general computable analytically. In the following we shall leave it as is and express $A^{\mu\nu}$ as:

$$A^{\mu}{}_{\mu} = \frac{-3e_Q}{\pi^2} NI(\Lambda, M, m) \Rightarrow A^{\mu\nu} = \frac{-e_Q}{\pi^2} NI(\Lambda, M, m)\Delta^{\mu\nu}. \tag{4.33}$$

Check of the assumption on $A^{\mu\nu}$

As said before, we can test our assumption of gauge invariance by checking that $A^{\mu 0} = 0$. For A^{i0}, this is straightforward as the integrand is odd. This is a bit less trivial for A^{00}.

Let us go back to Eq. (4.21) and write down $A^{00}(K)$ omitting the integration on K and neglecting the constant factors:

$$\begin{aligned}
A^{00}(K) &\propto \int_{-\infty}^{\infty} dk_0 \frac{(M^2+4m^2-4k^2)+8k_0k_0-2M^2}{((k-\frac{P}{2})^2-m^2+i\varepsilon)((k+\frac{P}{2})^2-m^2+i\varepsilon)} \\
&\propto \int_{-\infty}^{\infty} \frac{dk_0(k_0^2+E^2-\frac{M^2}{4})}{(k_0-(\frac{-M}{2}-E+i\varepsilon))(k_0-(\frac{-M}{2}-E-i\varepsilon))(k_0-(\frac{M}{2}-E+i\varepsilon))(k_0-(\frac{M}{2}+E-i\varepsilon))} \\
&\propto \left[\frac{E^2+\frac{M^2}{4}+EM-\frac{M^2}{4}+E^2}{(-2E)(-M)(-2(E+\frac{M}{2}))}+\frac{E^2+\frac{M^2}{4}-EM-\frac{M^2}{4}+E^2}{M(-2(E-\frac{M}{2}))(-2E)}\right] \propto \left[\frac{-1}{M}+\frac{1}{M}\right]=0.
\end{aligned} \tag{4.34}$$

4.3.2 Second sub-amplitude

From the Feynman rules, we have

$$\begin{aligned}
B^{\rho\rho'} &= (ie)^2 \int d_2(PS)\mathrm{Tr}(\gamma^\rho(-\not{a}+m_\ell)\gamma^{\rho'}(\not{b}+m_\ell)) \\
&= (ie)^2 \int d_2(PS)4(a.bg^{\rho\rho'}-a^\rho b^{\rho'}-a^{\rho'}b^\rho+g^{\rho\rho'}m_\ell^2).
\end{aligned} \tag{4.35}$$

where a and b are the momenta of the lepton and antilepton ($a+b=P$), and m_ℓ their mass. As m_ℓ is much smaller than M and m, we shall neglect it.

To perform the integration on the two-particle phase space, we shall use the following well-known relations [90]

$$\begin{aligned}
\int d_2(PS)a^\alpha b^\beta =& \frac{\pi M^2}{24}\sqrt{\lambda}\left(g^{\alpha\beta}\lambda+2\frac{P^\alpha P^\beta}{M^2}\left[1+\frac{a^2}{M^2}+\frac{b^2}{M^2}-2\frac{(a^2-b^2)^2}{M^4}\right]\right) \\
\simeq& \frac{\pi M^2}{24}\left(g^{\alpha\beta}+2\frac{P^\alpha P^\beta}{M^2}\right), \\
\int d_2(PS)a.b = \int d_2(PS)a^\alpha b^\beta g_{\alpha\beta} &= \frac{\pi M^2}{24}(4+2)=\frac{\pi M^2}{4}.
\end{aligned} \tag{4.36}$$

where $\lambda=\lambda(1,a^2/M^2,b^2/M^2)=\lambda(1,m_\ell^2/M^2,m_\ell^2/M^2)=1-2m_\ell^2/M^2\simeq 1$ if we neglect the lepton mass.

Therefore, we have

$$B^{\rho\rho'} = (ie)^2\left[\pi M^2 g^{\rho\rho'}-8\frac{\pi M^2}{24}\left(g^{\rho\rho'}+2\frac{P^\rho P^{\rho'}}{M^2}\right)\right] = (ie)^2\frac{2\pi}{3}M^2\underbrace{\left[g^{\rho\rho'}-\frac{P^\rho P^{\rho'}}{M^2}\right]}_{\Delta^{\rho\rho'}}. \tag{4.37}$$

4.3.3 Third sub-amplitude

We simply have

$$C^{\nu'\mu'} = (A^{\nu'\mu'})^\dagger = A^{\nu'\mu'}. \tag{4.38}$$

4.3.4 Results

Now that all quantities in Eq. (4.20) are determined, we can combine them. Thence, we obtain[7]:

$$\int \left|\bar{\mathcal{M}}\right|^2 d_2(PS) = \frac{1}{3}\Delta_{\mu\mu'}\frac{-1}{M^4}\left(\frac{e_Q}{\pi^2}NI(\Lambda,M,m)\right)^2\left((ie)^2\frac{2\pi}{3}M^2\right)\Delta^{\mu\nu}g_{\nu\rho}\Delta^{\rho\rho'}g_{\rho'\nu'}\Delta^{\nu'\mu'}. \tag{4.39}$$

The leptonic decay width eventually reads from Eq. (4.19) :

$$\Gamma_{\ell\ell} = N^2\frac{e^2}{12\pi M^3}\left(\frac{e_Q}{\pi^2}I(\Lambda,M,m)\right)^2. \tag{4.40}$$

Numerical results

The value of N is in practice obtained by replacing $\Gamma_{\ell\ell}$ by its measured value, e_Q by $\frac{2e}{3}$ for c quarks and $\frac{-e}{3}$ for b quarks and, finally, by introducing the value obtained for I for the chosen value of Λ. The formulae to be used for the different quarkonia are shown in Tab. (4.1).

Meson	$\Gamma_{\ell\ell}$(keV)	N
J/ψ	5.40	$\sqrt{\frac{(5.4\times10^{-6})27\pi^5 M_{J/\psi}^3}{e^4 I(\Lambda,M_{J/\psi},m_c)^2}}$
ψ'	2.12	$\sqrt{\frac{(2.12\times10^{-6})27\pi^5 M_{\psi'}^3}{e^4 I(\Lambda,M_{\psi'},m_c)^2}}$
$\Upsilon(1S)$	1.31	$\sqrt{\frac{(1.31\times10^{-6})108\pi^5 M_{\Upsilon(1S)}^3}{e^4 I(\Lambda,M_{\Upsilon(1S)},m_b)^2}}$
$\Upsilon(2S)$	0.57	$\sqrt{\frac{(0.57\times10^{-6})108\pi^5 M_{\Upsilon(2S)}^3}{e^4 I(\Lambda,M_{\Upsilon(2S)},m_b)^2}}$
$\Upsilon(3S)$	0.48	$\sqrt{\frac{(0.48\times10^{-6})108\pi^5 M_{\Upsilon(3S)}^3}{e^4 I(\Lambda,M_{\Upsilon(3S)},m_b)^2}}$

Table 4.1: Formulas to be used to determine N.

We sketch some plots of N for the J/ψ and for the $\Upsilon(1S)$ to show its dependence on Λ and m_Q and the value it actually takes. The values obtained are also given in tables in Appendix B.1 and will be used in the production calculations presented in the following.

We have chosen the range of size of the mesons, *i.e.* Λ, following BSE studies [91] and other phenomenological models [74, 75], where the commonly accepted values for the J/ψ are from 1 to 2.4 GeV, and for the $\Upsilon(1S)$ from 3.0 to 6.5 GeV.

For illustration, we show in Tab. (4.2) several values of Λ obtained with BSE [91], accompanied with the vertex-function normalisation.

[7] Recall that the projector $\Delta_{\mu\nu}$ satisfies $\Delta_{\mu\nu}\Delta^{\mu\nu} = 3$ and $\Delta_{\mu\nu}\Delta^{\mu\nu'} = \Delta_{\nu}{}^{\nu'}$.

m_c (GeV)	Vertex functions			
	Gaussian		Dipole	
	N	Λ (GeV)	N	Λ (GeV)
1.6	1.59	2.34	1.33	2.87
1.7	2.28	2.08	1.87	2.54
1.87	3.31	1.97	2.76	2.31

Table 4.2: Set of values for m_c, Λ and N obtained for the J/ψ within BSE approach [91].

To what concerns the ψ', we give the results for Λ=1.8 GeV, $m_c = 1.87$ GeV and a gaussian vertex function (Tab. (4.3)). The constraint for the node position (Eq. (4.18)) gives $a_{node} = 1.46$ GeV for these values of Λ and m_c. The normalisation $N' = 16.36$ will then be the value that we shall retain for the numerical applications. Note that the normalisation is strongly dependent on the node position; it is even possible to make the decay width vanish, with the consequence of obtaining an infinite value for N.

a_{node} (GeV)	N'
0.8	2.02
1.46	16.36
2.0	4.12

Table 4.3: Normalisation for the ψ' as a function of a_{node}.

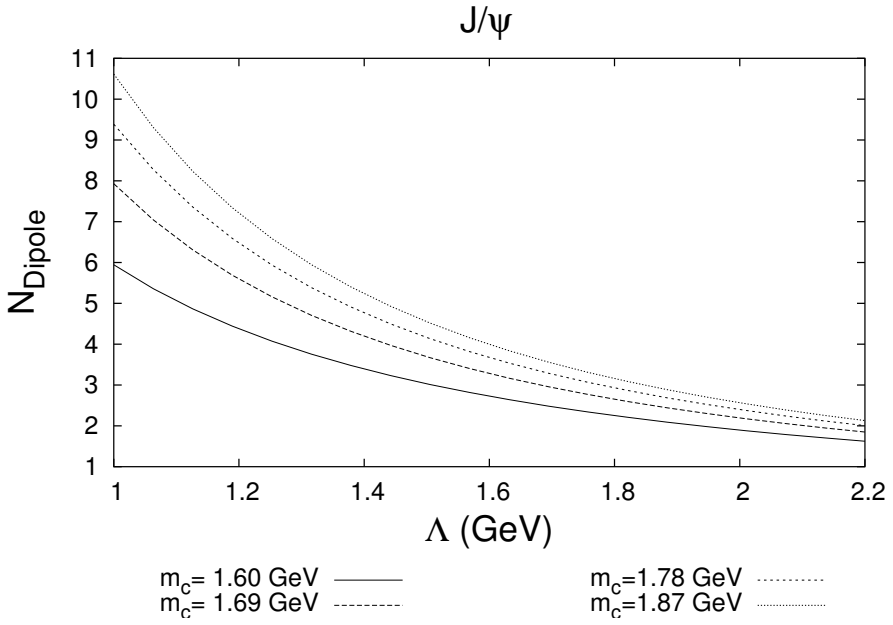

Figure 4.6: Normalisation for a dipolar form for J/ψ as a function of Λ.

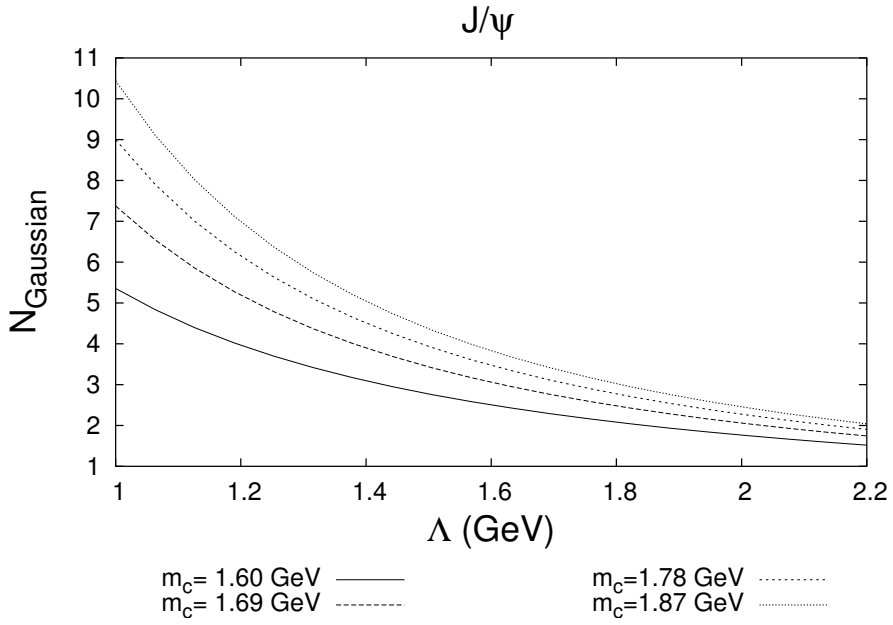

Figure 4.7: Normalisation for a gaussian form for J/ψ as a function of Λ.

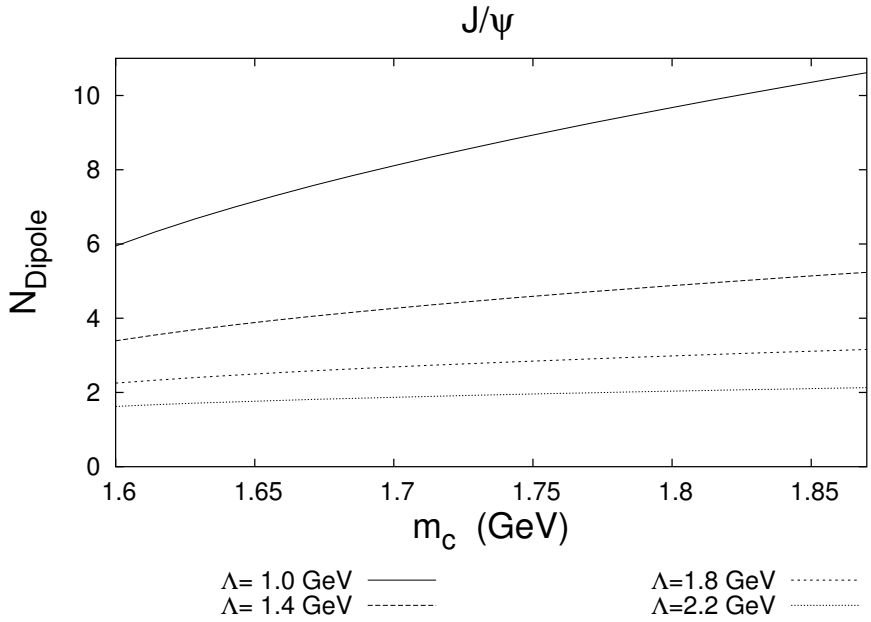

Figure 4.8: Normalisation for a dipolar form for J/ψ as a function of the c-quark mass.

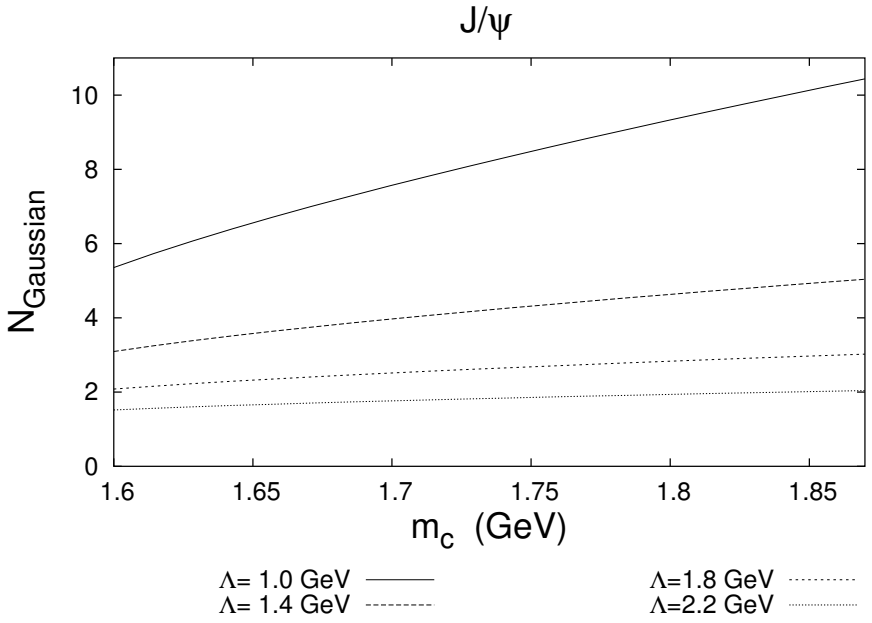

Figure 4.9: Normalisation for a gaussian form for J/ψ as a function of the c-quark mass.

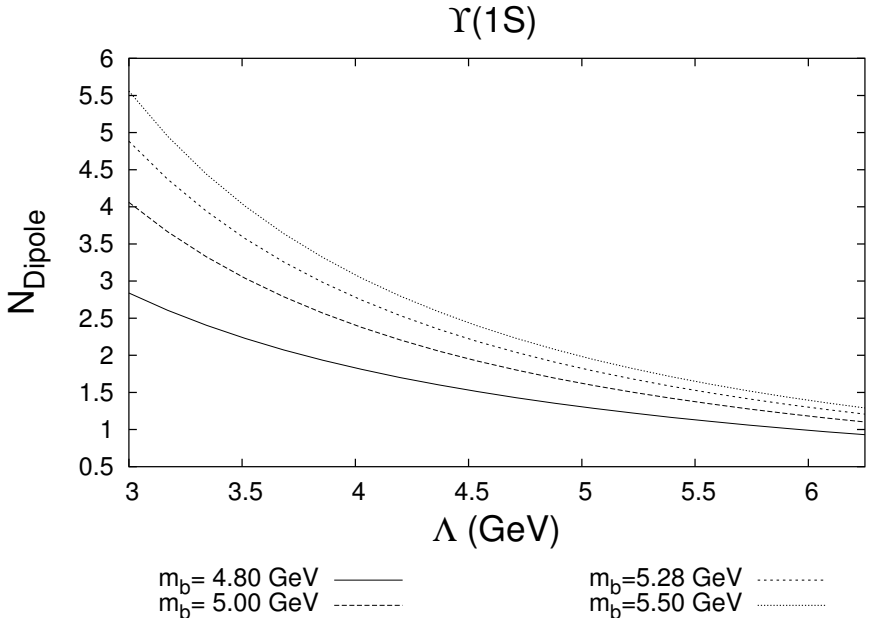

Figure 4.10: Normalisation for a dipolar form for $\Upsilon(1S)$ as a function of Λ.

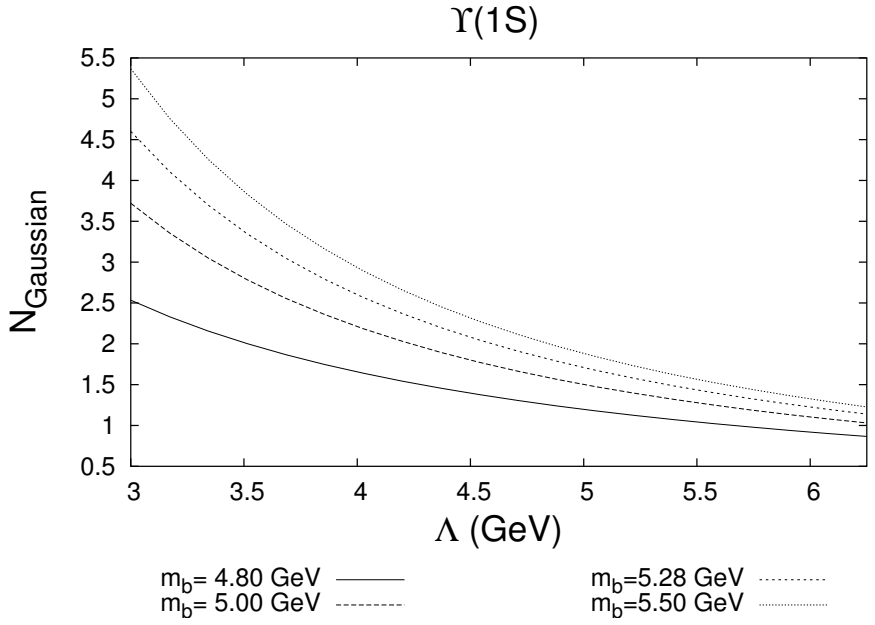

Figure 4.11: Normalisation for a gaussian form for $\Upsilon(1S)$ as a function of Λ.

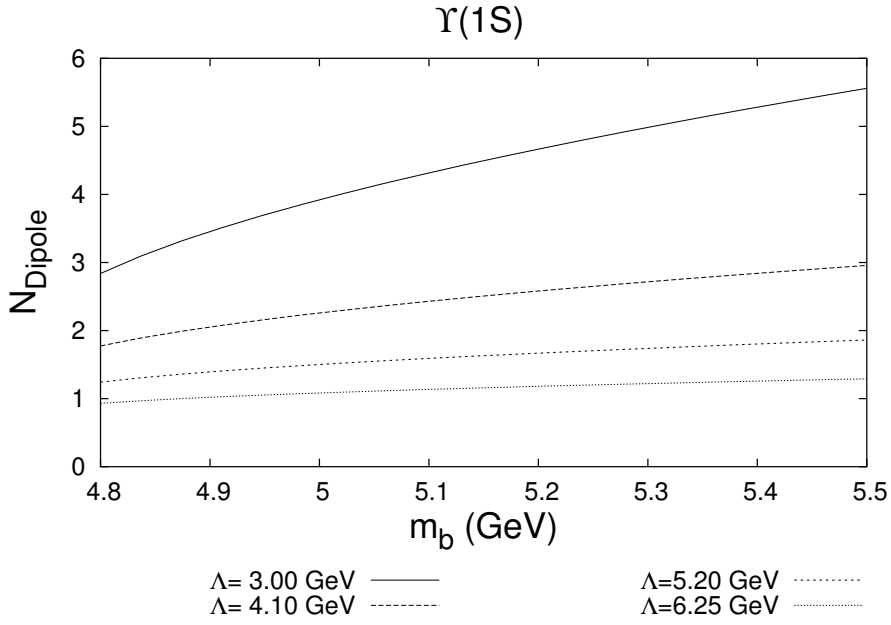

Figure 4.12: Normalisation for a dipolar form for $\Upsilon(1S)$ as a function of the b-quark mass.

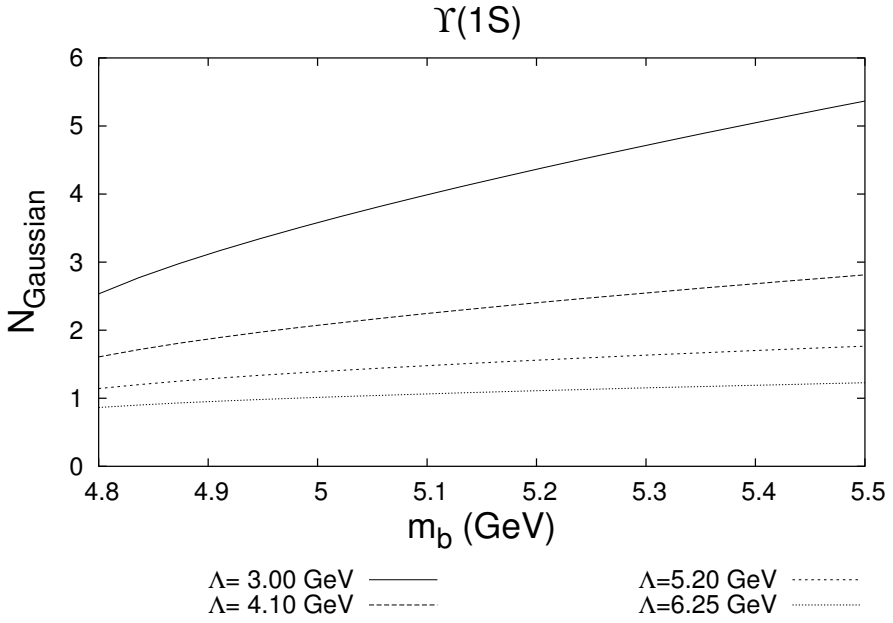

Figure 4.13: Normalisation for a gaussian form for $\Upsilon(1S)$ as a function of the b-quark mass.

4.4 Another point of view

In appendix B.2, we give some details about another method for determining the parameters of the vertex function. The latter relies on a Wick rotation of the relative momentum in order to work in Euclidean space. This procedure is absolutely common among the community of physicists which employ the Bethe-Salpeter equation and the Dyson-Schwinger equation to obtain the mass, the normalisation and the decay width of mesons.

We have been unable to justify this Wick rotation, especially in the case of the gaussian vertex function which reaches infinite values when $|k_0|^2 \to \infty$ and $|\mathcal{I}m\ k_0| > |\mathcal{R}e\ k_0|$. However, as one can see in Tab. (4.2), the results are similar to the ones obtained by our method and considering that this more classical method also gives Λ, m and N, we have thought useful for the reader to sketch some of its results. This can be seen as an *a posteriori* justification for the values of the parameters that we used, such as $\Lambda = 1.8$ GeV for m_c=1.87 GeV.

Chapter 5

Bound states and gauge invariance

As already mentioned in the previous chapter, in order to tackle processes involving bound-states, we shall phenomenologically generalise the Feynman rules for point-like particles to bound states by introducing vertex functions or form factors, keeping by hypothesis the same Dirac structure as for the corresponding point-like particle.

However, before using this formalism, one needs to deal with gauge invariance. Indeed, if we consider the production of a bound state associated with a photon or a gluon[1], this may couple with the constituent before the binding but also after, even though the bound state is neutral for the considered interaction. In the framework of Bethe-Salpeter equations (BSE) [70], one has to go back to the details of the interactions occurring in the bound state. We have to take into consideration which interactions occur and which type of possible diagram we shall have. This renders this study cumbersome [93, 94].

In the approach we follow, which we refer to as "phenomenological", gauge invariance is of course also broken. The vertex functions get different values for different kinematical configurations and the different diagrams, contributing at a given order in the expansion parameter, have different weights. As one knows, only the sum of the whole set of diagrams at a given order provides gauge-invariant results. Therefore gauge invariance is broken[2].

The aim of this chapter is to introduce the reader to our method to restore gauge invariance. We shall also choose a phenomenological point of view. Indeed our method is based on the introduction of effective new 4-particle vertices as a supplement to the 3-particle ones. We shall also show what constraints these effective new vertices have to satisfy.

First we shall present our derivation for a pseudoscalar particle, produced in association with a photon. Compared to our final application to heavy quarkonium production (*e.g.* J/ψ and Υ), this brings two main simplifications to the discussion: the absence of colour factors and a single vector particle, namely the photon. Thence we shall give a similar derivation for vector-meson production with a gluon. Finally, we shall state that, as there is an unconstrained degree of freedom in this restoration, we are free to add any suitable contribution to the amplitude. This will be accompanied with the derivation of the general form for these.

As said above, we consider the production of a bound state $\mathcal{Q}$ associated with a photon

[1] This depends of course on the bound-state content: quark, lepton,...

[2] To the exception of the decay process of the previous chapter.

or a gluon, the simplest processes are therefore $q\bar{q} \to \mathcal{Q}\gamma$ or $q\bar{q} \to \mathcal{Q}g$. We shall consider these here and this will be used in the calculation of the imaginary part of the amplitude for $gg \to Vg$ as done in the next chapter.

5.1 The simpler case of $q\bar{q} \to X_0\gamma$

We start from the usual amplitude at leading order (LO) for $q\bar{q} \to X_0\gamma$, where X_0 stands for a pseudoscalar structureless (point) particle and γ for a photon:

$$\begin{aligned}\mathcal{M} &= -i\,g\,e\,\underbrace{\bar{u}(p')}_{\bar{v}(-p')}V^{\mu}_{point}\varepsilon^{\star}_{\mu}(q)u(p)\\ &= -i\,g\,e\,\bar{u}(p')\left(\frac{\gamma^5((\not{p}-\not{q})+m)\gamma^{\mu}}{(p-q)^2-m^2}+\frac{\gamma^{\mu}((\not{p}'+\not{q})+m)\gamma^5}{(p'+q)^2-m^2}\right)\varepsilon^{\star}_{\mu}(q)u(p),\end{aligned} \tag{5.1}$$

where the momenta are defined as in Fig. 5.1, e is the QED charge and g is the $q\bar{q}X_0$ coupling. To emphasise the different Dirac structures appearing in it, we can rewrite it as:

$$\bar{u}(p')V^{\mu}_{point}\varepsilon^{\star}_{\mu}(q)u(p) = \bar{u}(p')\left(\alpha\gamma^5(\not{p}-\not{q})\gamma^{\mu}+\beta\gamma^5\gamma^{\mu}+\delta\gamma^{\mu}(\not{p}'+\not{q})\gamma^5+\lambda\gamma^{\mu}\gamma^5\right)\varepsilon^{\star}_{\mu}(q)u(p). \tag{5.2}$$

The factors $\alpha,\ldots,\lambda$ are functions of scalar products of momenta of the problem and take the following values in this case:

$$\begin{aligned}\alpha_{point} &\equiv \frac{1}{(p-q)^2-m^2} = P_1^{-1},\ \beta_{point} \equiv \frac{m}{(p-q)^2-m^2} = mP_1^{-1},\\ \delta_{point} &\equiv \frac{1}{(p'+q)^2-m^2} = P_2^{-1},\ \lambda_{point} \equiv \frac{m}{(p'+q)^2-m^2} = mP_2^{-1}.\end{aligned} \tag{5.3}$$

As announced, should we generalise this amplitude in order to describe the production of a bound state, the introduction of vertex functions would break gauge invariance. To restore the latter, we may add to these two diagrams a new contribution, constructed from a new vertex. This new vertex would account then for missing contributions, akin to direct interactions between the photon and the bound state, X_0. We shall call it V_4^{μ}.

In turn, this novel vertex has to satisfy constraints, *e.g.* to have the same symmetries as the sum of the previous contributions (which we shall refer to as the *point* ones). To enforce this symmetry constraint, we shall merely impose it on the partial amplitude built only from this effective vertex.

A first constraint comes from charge conjugation which can be assimilated to the crossing of the quark and the antiquark and reads (denoting the transformation $\mathcal{T}$):

$$V^{\mu}(p,p',q,P,m) = \mathcal{T}(V^{\mu}(p,p',q,P,m)) = \gamma^0 V^{\mu\dagger}(-p',-p,q,P,-m)\gamma^0. \tag{5.4}$$

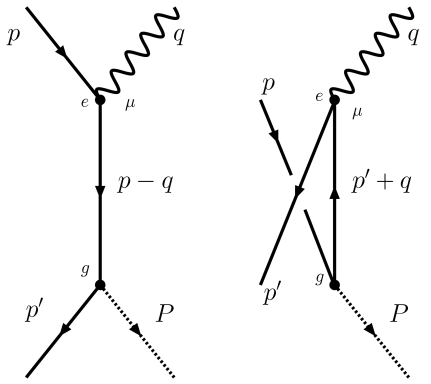

(a) Direct (b) Crossed

Figure 5.1: Feynman diagrams for the leading order contributions for $q\bar{q} \to X_0\gamma$.

Indeed, returning to the usual form for the amplitude (where we omitted the spinors u, the polarisation vector ε and the other factors),

$$V^{\mu}_{point} = \frac{\gamma^5((\not{p} - \not{q}) + m)\gamma^{\mu}}{(p-q)^2 - m^2} + \frac{\gamma^{\mu}((\not{p}' + \not{q}) + m)\gamma^5}{(p'+q)^2 - m^2}, \tag{5.5}$$

and using the following well-known relations, $(\gamma^5)^{\dagger} = \gamma^5$, $\gamma^{\mu}\gamma^5 = -\gamma^5\gamma^{\mu}$, $(\gamma^{\mu})^{\dagger} = \gamma^0\gamma^{\mu}\gamma^0$, we get:

$$\begin{aligned}\mathcal{T}(V^{\mu}) = \gamma^0 V^{\mu\dagger}(-p', -p, q, P, -m)\gamma^0 &= \frac{\gamma^{\mu}((-\not{p}' - \not{q}) - m)(-\gamma^5)}{(-p'-q)^2 - m^2} + \frac{(-\gamma^5)((-\not{p} + \not{q}) - m)\gamma^{\mu}}{(-p+q)^2 - m^2} \\ &= V^{\mu}(p, p', q, P, m).\end{aligned} \tag{5.6}$$

To sum up, the operation $\mathcal{T}(\cdot) = \gamma^0(\cdot)^{\dagger}(-p', -p, q, P, -m)\gamma^0$ should have no effect on the sought-after gauge-invariance restoring sub-amplitude:

$$V^{\mu}_4(p, p', q, P, m) = \gamma^0 V^{\mu\dagger}_4(-p', -p, q, P, -m)\gamma^0. \tag{5.7}$$

In the following, instead of deriving directly the effective vertex restoring gauge invariance in cases where the $q\bar{q}X_0$ vertex factors are simply the *point* ones multiplied by a function (this procedure is illustrated in Fig. 5.2), we prefer to derive explicit and general constraints expressing how gauge invariance would be broken and consequently how to restore it taking into account the above symmetry.

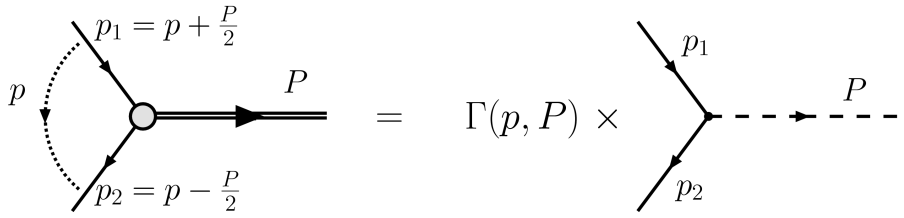

Figure 5.2: Phenomenological vertex obtained by multiplying a *point* vertex, representing a structureless particle, by a vertex function (or form factor).

These explicit and general constraints will actually relate the parameters $\alpha, \ldots, \lambda$. Having these constraints at hand, it will then be easier to construct our effective contribution from the general expression of Eq. (5.2). We shall simply input in Eq. (5.2) $\alpha, \ldots, \lambda$ fulfilling the obtained relations between them.

5.1.1 Symmetry: general constraints

In order to extract such relations for the symmetry of Eq. (5.4), we shall first rewrite the amplitude Eq. (5.2) by ordering the Dirac structures to insure immediate identifications of the factors of the latter structures.

$$\begin{aligned} V^\mu =& \alpha\gamma^5(\not{p} - \not{q})\gamma^\mu + \beta\gamma^5\gamma^\mu + \delta\gamma^\mu(\not{p}' + \not{q})\gamma^5 + \lambda\gamma^\mu\gamma^5 \\ =& -\alpha\gamma^5\gamma^\mu\not{p} + 2\alpha\gamma^5 p^\mu - \alpha\gamma^5\gamma^\mu\not{q} - 2\alpha\gamma^5 q^\mu\beta\gamma^5\gamma^\mu - \delta\not{p}'\gamma^\mu\gamma^5 \\ & + 2\delta p'^\mu\gamma^5 + \delta\gamma^\mu\not{q}\gamma^5 + \lambda\gamma^\mu\gamma^5 \\ \overset{(*)}{=}& m\alpha\gamma^\mu\gamma^5 + 2\alpha\gamma^5 p^\mu - \alpha\gamma^\mu\gamma^5\not{q} - 2\alpha\gamma^5 q^\mu - \beta\gamma^\mu\gamma^5 - m\delta\gamma^\mu\gamma^5 + 2\delta\gamma^5 p'^\mu \\ & - \delta\gamma^\mu\gamma^5\not{q} + \lambda\gamma^\mu\gamma^5. \end{aligned} \tag{5.8}$$

The equality $(*)$ is obtained by means of Dirac equations for the on-shell quark and antiquark: $\not{p}u(p) = mu(p)$ and $\bar{u}(p')\not{p}' = m\bar{u}(p')$ (or $\bar{v}(-p')(-\not{p}') = -m\bar{v}(-p')$).

By inspection of Eq. (5.8), we see that we only have three independent Dirac structures: γ^5, $\gamma^\mu\gamma^5$ and $\gamma^\mu\gamma^5\not{q}$. We have however to keep in mind that p, p' and q are independent, and that the identification must be true for all their values.

Schematically, we shall write:

Structures	Factors
γ^5	$2\alpha p^\mu - 2\alpha q^\mu + 2\delta p'^\mu$
$\gamma^\mu\gamma^5$	$m\alpha - \beta - m\delta + \lambda$
$\gamma^\mu\gamma^5\not{q}$	$-\alpha - \delta$

Now, we shall apply the transformation $\mathcal{T}(\cdot) = \gamma^0(\cdot)^\dagger(-p', -p, q, V, -m)\gamma^0 = \gamma^0(\cdot)^\dagger_{1\to 2}\gamma^0$ to the different structures and their coefficients. For the structures, we have

$$\begin{aligned}
\gamma^5 &\to \gamma^0(\gamma^5)^\dagger\gamma^0 = -\gamma^5 \\
\gamma^\mu\gamma^5 &\to \gamma^0(\gamma^\mu\gamma^5)^\dagger\gamma^0 = \gamma^0(\gamma^5)^\dagger\gamma^0\gamma^\mu\gamma^0\gamma^0 = -\gamma^5\gamma^\mu = \gamma^\mu\gamma^5 \\
\gamma^\mu\gamma^5\not{q} &\to \gamma^0(\gamma^\mu\gamma^5\not{q})^\dagger\gamma^0 = \gamma^0\gamma^0\not{q}\gamma^0(\gamma^5)^\dagger\gamma^0\gamma^\mu\gamma^0\gamma^0 = \not{q}\gamma^\mu\gamma^5 = \gamma^\mu\gamma^5\not{q} + 2q^\mu\gamma^5,
\end{aligned} \tag{5.9}$$

and for the coefficients[3]:

$$\begin{aligned}
2\alpha_1 p^\mu - 2\alpha_1 q^\mu + 2\delta_1 p'^\mu &\to -2\alpha_2 p'^\mu - 2\alpha_2 q^\mu - 2\delta_2 p^\mu \\
m\alpha_1 - \beta_1 - m\delta_1 + \lambda_1 &\to -m\alpha_2 - \beta_2 + m\delta_2 + \lambda_2 \\
-\alpha_1 - \delta_1 &\to -\alpha_2 - \delta_2
\end{aligned} \tag{5.10}$$

Finally, we get,

Structures	Factors 1	Factors 2
γ^5	$2\alpha_1 p^\mu - 2\alpha_1 q^\mu + 2\delta_1 p'^\mu$	$2\alpha_2 p'^\mu + 2\alpha_2 q^\mu + 2\delta_2 p^\mu - (\alpha_2 + \delta_2)2q^\mu$
$\gamma^\mu\gamma^5$	$m\alpha_1 - \beta_1 - m\delta_1 + \lambda_1$	$-m\alpha_2 - \beta_2 + m\delta_2 + \lambda_2$
$\gamma^\mu\gamma^5\not{q}$	$-\alpha_1 - \delta_1$	$-\alpha_2 - \delta_2$

which gives 4 different identities:

$$\begin{aligned}
\alpha_1 &= \delta_2 \\
\delta_1 &= \alpha_2 \\
m\alpha_1 - \beta_1 - m\delta_1 + \lambda_1 &= -m\alpha_2 - \beta_2 + m\delta_2 + \lambda_2 \\
-\alpha_1 - \delta_1 &= -\alpha_2 - \delta_2
\end{aligned} \tag{5.11}$$

In short, we have

$$\begin{aligned}
\alpha_1 &= \delta_2 \\
\delta_1 &= \alpha_2 \\
-\beta_1 + \lambda_1 &= -\beta_2 + \lambda_2
\end{aligned} \tag{5.12}$$

These three last equations contain all the constraints in terms of $\alpha, \ldots, \lambda$, coming from Eq. (5.4). The first thing to notice is that the *point* case obviously fulfils these conditions. Indeed, noticing that $P_1 \xrightarrow{1\to 2} P_2$,

$$\begin{aligned}
&1)\ \delta_{point,1} = P_2^{-1} \Rightarrow \delta_{point,2} = P_1^{-1} = \alpha_{point,1}, \\
&2)\ \alpha_{point,1} = P_1^{-1} \Rightarrow \alpha_{point,2} = P_2^{-1} = \delta_{point,1}, \\
&3)\ -\beta_{point,1} + \lambda_{point,1} = -mP_1^{-1} + mP_2^{-1} \\
&\quad \Rightarrow -\beta_{point,2} + \lambda_{point,2} = -(-m)P_2^{-1} + (-m)P_1^{-1} = \lambda_{point,1} - \beta_{point,1}.
\end{aligned} \tag{5.13}$$

[3] The indices 1 and 2 stand for the two sets of variables (p, p', q, V, m) and $(-p', -p, q, V, -m)$ for which these factors are to be evaluated, *e.g.* $\alpha_1 = \alpha(p, p', q, V, m)$ and $\alpha_2 = \alpha(-p', -p, q, V, -m)$.

The most important result is that we now have a means to deduce in a straightforward way whether or not given contributions, for instance the generalisation of these *point* contributions to bound state ones, have the symmetry required.

5.1.2 Gauge invariance: general constraints

$\mathcal{M}$, the amplitude under consideration in Eq. (5.1) involves $\varepsilon^{\star}_{\mu}(q)$, the polarisation vector of the photon. Being a four-vector, the latter possesses four degrees of freedom, one is removed by the orthogonality condition:

$$\varepsilon^{\star}_{\mu}(q)q^{\mu} = 0, \tag{5.14}$$

three remain, whereas we know that photons have only two. Supposing the photon travels in the z direction, one possible choice for these two polarisations could be

$$\varepsilon^{\mu}_{x} = (0,1,0,0) \text{ and } \varepsilon^{\mu}_{y} = (0,0,1,0) \tag{5.15}$$

The third degree of freedom can be expressed by noticing that any new vector obtained by a shift in the photon momentum direction q is also valid:

$$\varepsilon'^{\mu} = \varepsilon^{\mu}_{x,y} + \chi q^{\mu}, \tag{5.16}$$

A unique definition of the polarisation vectors is then only achieved by imposing a further condition upon χ. This condition is equivalent to fixing the gauge (see *e.g.* [92]), or equivalently, two different values of χ correspond to two different gauges [4] .

Gauge invariance of an amplitude $\mathcal{M}$ involving n external photons is therefore realised by the absence of χ in its expression. Hence, as χ appears solely in association with[5] q^{μ}, *a necessary condition for a gauge-invariant result* resides in the current-conservation condition:

$$V_{\mu_1\ldots\mu_n} q_i^{\mu_i} = 0, \forall i, \tag{5.17}$$

defining $V_{\mu_1\ldots\mu_n}$ by $\mathcal{M} = V_{\mu_1\ldots\mu_n} \prod_i \varepsilon^{\mu_i}(q_i)$.

To what concerns $\mathcal{M}$ of Eq. (5.1), the requested condition reads

$$V^{\mu} q_{\mu} = 0. \tag{5.18}$$

We shall perform the same ordering as before but for the amplitude V^{μ} contracted with q_{μ}, the momentum of the photon. As the contraction vanishes, it will be in turn expressed in terms of identities for the coefficients $\alpha, \beta, \delta, \lambda$.

[4] Let Λ be the gauge-transformation parameter such that $A'^{\mu} = A^{\mu} + \partial^{\mu}\Lambda(x)$. The wave function transforms like $\psi' = e^{i\Lambda(x)}\psi$ and the polarisation vector like $\varepsilon^{\mu}e^{ikx} = \varepsilon^{\mu}e^{ikx} + q^{\mu}\int \Lambda(x)e^{ikx}dx$. We may then identify χ with $\int \Lambda(x)e^{ikx}dx$.

[5] μ is the index of the photon for which we look at gauge-invariance or current conservation.

$$\begin{aligned} 0 = V^\mu q_\mu =& \alpha\gamma^5(\not{p} - \not{q})\not{q} + \beta\gamma^5\not{q} + \delta\not{q}(\not{p}' + \not{q})\gamma^5 + \lambda\not{q}\gamma^5 \\ =& -\alpha\gamma^5\not{q}\not{p} + 2\alpha\gamma^5 p.q - \alpha\gamma^5 q^2 + \beta\gamma^5\not{q} - \delta\not{p}'\not{q}\gamma^5 \\ &+ 2\delta p'.q\gamma^5 + \delta q^2\gamma^5 - \lambda\gamma^5\not{q} \\ =& -m\alpha\gamma^5\not{q} + 2\alpha p.q\gamma^5 - \alpha q^2\gamma^5 + \beta\gamma^5\not{q} + m\delta\gamma^5\not{q} + 2\delta p'.q\gamma^5 + \delta q^2\gamma^5 - \lambda\gamma^5\not{q} \end{aligned} \tag{5.19}$$

Finally we get,

Structures	Factors
γ^5	$2\alpha p.q - \alpha q^2 + \delta q^2 + 2\delta p'.q$
$\gamma^5\not{q}$	$-m\alpha + \beta + m\delta - \lambda$

And we can write –the two factors (right column of the last table) being identically zero–

$$-\alpha P_1 + \delta P_2 = 0 \tag{5.20}$$

$$\beta - \lambda = m(\alpha - \delta) \tag{5.21}$$

We may check that the *point* case follows these relations. This is straightforward since

$$\begin{aligned} &1)\ -\alpha_{point}P_1 + \delta_{point}P_2 = -P_1^{-1}P_1 + P_2^{-1}P_2 = 0, \\ &2)\ \beta_{point} - \lambda_{point} = mP_1^{-1} - mP_2^{-1} = m(\alpha_{point} - \delta_{point}). \end{aligned} \tag{5.22}$$

5.1.3 Restoring gauge invariance for the "phenomenological approach"

Having at our disposal the latter constraints, we are now ready to construct an effective 4-particle vertex that will restore gauge invariance for the cases where a bound-state vertex function enters the calculation.

The values of $\alpha, \beta, \delta, \lambda$ for our "phenomenological approach", where we introduce a 3-particle vertex function Γ ($V_3 = \Gamma\gamma^5$), are easily shown to be:

$$\alpha = \frac{\Gamma_1}{P_1},\ \beta = \frac{m\Gamma_1}{P_1}, \delta = \frac{\Gamma_2}{P_2}, \lambda = \frac{m\Gamma_2}{P_2}, \tag{5.23}$$

where $\Gamma_1 = \Gamma(2p - q)$ and $\Gamma_2 = \Gamma(2p' + q)$. This amounts to the following modifications compared to the point case:

$$\alpha = \alpha_{point} \times \Gamma_1,\ \beta = \beta_{point} \times \Gamma_1,\ \delta = \delta_{point} \times \Gamma_2,\ \lambda = \lambda_{point} \times \Gamma_2. \tag{5.24}$$

We directly see that Eq. (5.21) is automatically satisfied by this choice contrarily to Eq. (5.20) for $\Gamma_1 \neq \Gamma_2$. This is actually true as long as $\beta = m\alpha$ and $\lambda = m\delta$. *We have thus expressed through one single relation* (Eq. (5.20)) *involving one single Dirac structure* (γ^5) *the breaking of gauge invariance.*

The fact that Eq. (5.21) is satisfied shows us that either the effective 4-particle vertex should not contribute to this equation – no term in $\gamma^5\gamma^\mu$ at all (before contraction with q^μ) –, or that its contribution should be transverse, *i.e.* should vanish when contracted with q^μ.

Concerning the crossing symmetry, let us first analyse the constraint $\alpha_1 = \delta_2$: the symmetry of the vertex function, $\Gamma_1 \xrightarrow{1\to 2} \Gamma_2$, and $\alpha_{point,1} = \delta_{point,2}$ imply that the latter also holds in the "phenomenological approach". The same is true for the other symmetry relations as can easily be seen.

Let us turn back to the derivation of the new vertex. For simplicity, we shall first introduce terms that explicitly do not contribute to Eq. (5.21). On the other hand, Eq. (5.20) is not satisfied by our approach and corrections from the 4-particle vertex should then appear in this equation, *i.e.* with a γ^5 Dirac matrix for sole Dirac structure. This implies that it should be of the general form $k^\mu\gamma^5$. The vertex should as well satisfy the symmetry relation $V_4^\mu(p,p',q,V,m) = \mathcal{T}(V_4^\mu) = \gamma^0 V_4^\dagger(-p',-p,q,V,-m)\gamma^0$.

First solutions

Setting k^μ to $(p+p')^\mu$ in $k^\mu\gamma^5$, defining η as a multiplicative factor, we can take $2\eta(p+p')^\mu\gamma^5$ which can be rewritten as:

$$2\eta(p+p')^\mu\gamma^5 = \eta(2p'^\mu\gamma^5 - m\gamma^\mu\gamma^5 + 2p^\mu\gamma^5 - \gamma^5\gamma^\mu m) = \eta(\gamma^\mu \not{p}'\gamma^5 + \gamma^5 \not{p}\gamma^\mu). \tag{5.25}$$

As we have seen, under the transformation $\mathcal{T}$, γ^5 changes to $-\gamma^5$ and $\eta_1(p+p')$ will give $-\eta_2(p'+p)$, therefore, we have to impose that

$$\eta_1 = \eta_2. \tag{5.26}$$

Concerning gauge invariance, a similar equation to Eq. (5.20), with this new term added and with the values of α and δ for the "phenomenological approach", reads

$$0 = -\alpha P_1 + \delta P_2 + \eta(p+p').q\gamma^5 = -\frac{\Gamma_1}{P_1}P_1 + \frac{\Gamma_2}{P_2}P_2 + 2\eta(p+p').q\gamma^5, \tag{5.27}$$

Solving for η, this determines the effective vertex:

$$V_4^\mu = 2\eta(p+p')^\mu\gamma^5 = \frac{\Gamma_1 - \Gamma_2}{(p+p').q}\gamma^5(p+p')^\mu \tag{5.28}$$

We also see that η satisfies the symmetry relation Eq. (5.26) as Γ_1 transforms into Γ_2.

The similar vertex

$$V_4^\mu = \frac{\Gamma_1 - \Gamma_2}{(p-p').q}\gamma^5(p-p')^\mu \tag{5.29}$$

will suit also. Contracted with q^μ, it indeed gives $(\Gamma_1 - \Gamma_2)\gamma^5$ as required to guarantee gauge invariance. The symmetry constraint requires η to be odd in $\mathcal{T}$. This is also verified as $\eta = \frac{\Gamma_1 - \Gamma_2}{2(p-p').q}$.

If we consider a virtual photon, *i.e.*with $q^2 \neq 0$, we can also choose

$$V_4^\mu = \frac{\Gamma_1 - \Gamma_2}{q^2}\gamma^5 q^\mu, \tag{5.30}$$

nevertheless $V_4^\mu \varepsilon(q)_\mu = 0$ due to $\varepsilon_\mu(q)q^\mu = 0$.

Singularity structure

Now that we have seen that different choices are possible, let us turn to another issue, *i.e.* the singularity structure of the 4-particle vertex. Indeed the above mentioned vertices have all different denominators, with a different singularity structure, whereas we shall demand that the gauge-invariance restoring contribution does not introduce new singularities in the problem. The easiest way to insure this is to limit our choice to vertices with the same denominators as the ones already in the problem.

Of course any combination of the previous solutions is also correct. Thus any structure that would not contribute to Eq. (5.20) and Eq. (5.21) and with the correct symmetry can be added to them. This freedom will be discussed thoroughly for the $q\bar{q} \to V_0 g$ case (see section 5.3).

Since all structures similar to $\frac{\Gamma_1 - \Gamma_2}{k.q}\gamma^5 k^\mu$ will satisfy the gauge-invariance constraint, it is sufficient to concentrate on its symmetry. Since the odd character of $(\Gamma_1 - \Gamma_2)$ is compensated by γ^5, it is obvious that any combination of the vectors of the problem will yield a correct k (since k is both in the numerator and in the denominator).

If we choose $k^\mu = p^\mu(p'.q) + p'^\mu(p.q)$, we get

$$V_4^\mu = (\Gamma_1 - \Gamma_2)\frac{p^\mu(p'.q) + p'^\mu(p.q)}{2(p'.q)(p.q)}\gamma^5 = (\Gamma_1 - \Gamma_2)\left(\frac{p^\mu}{2(p.q)} + \frac{p'^\mu}{2(p'.q)}\right) \tag{5.31}$$

Except for the term q^2, the denominators of this solution are equivalent to the propagators of the problem. For $q^2 = 0$, they do not bring any new singularities in the problem. But we look for a more general case...

A slight different choice for k^μ gives:

$$\begin{aligned} V_4^\mu =& (\Gamma_1 - \Gamma_2)\frac{(2p-q)^\mu(2p'.q + q^2) + (2p'+q)^\mu(2p.q - q^2)}{2(2p'.q + q^2)(2p.q - q^2)}\gamma^5 \\ =& (\Gamma_1 - \Gamma_2)\left(\frac{(-2p+q)^\mu}{2P_1} + \frac{(2p'+q)^\mu}{2P_2}\right)\gamma^5 \end{aligned} \tag{5.32}$$

The great advantage of this vertex, contrarily to Eq. (5.31), is that it does not introduce new singularities in the problem for any value of q^2. It can therefore be used in model calculation for pion structure functions where the probing photon is off-shell [95, 96].

5.2 Derivation of an effective vertex for $q\bar{q} \to V_0 g$

We shall here deal with a vector particle and with a gluon field. We start from the amplitude at LO which we rewrite in a simplified form comparable to Eq. (5.1):

$$\begin{aligned}\mathcal{M} &= -i\, g\, g_s\, T^a_{ji}\delta_{kj}\, \underbrace{\bar{u}(p')}_{\bar{v}(-p')} V^{\mu\nu}\varepsilon^\star_\mu(q)\varepsilon^\star_\nu(P)u(p) \\ &= -i\, g\, g_s\, T^a_{ki}\bar{u}(p')\left(\frac{\gamma^\nu((\not{p}-\not{q})+m)\gamma^\mu}{(p-q)^2-m^2} + \frac{\gamma^\mu((\not{p}'+\not{q})+m)\gamma^\nu}{(p'+q)^2-m^2}\right)\varepsilon^\star_\mu(q)\varepsilon^\star_\nu(P)u(p),\end{aligned} \tag{5.33}$$

where the momenta are defined as in Fig. 5.3, g_s is the QCD coupling, g the $q\bar{q}V^0$ coupling, T^a the colour matrices and δ_{kj} the colour factor for a singlet state. To emphasise the different structures[6] appearing in it, we can rewrite it as :

$$\begin{aligned}\bar{u}(p')V^{\mu\nu}\varepsilon^\star_\mu(q)\varepsilon^\star_\nu(P)u(p) = \bar{u}(p')\,(&\alpha\gamma^\nu(\not{p}-\not{q})\gamma^\mu + \beta\gamma^\nu\gamma^\mu + \\ &\delta\gamma^\mu(\not{p}'+\not{q})\gamma^\nu + \lambda\gamma^\mu\gamma^\nu + \kappa g^{\mu\nu})\,\varepsilon^\star_\mu(q)\varepsilon^\star_\nu(P)u(p).\end{aligned} \tag{5.34}$$

Note that we have added a new structure $g^{\mu\nu}$ to get a more general discussion in the following.

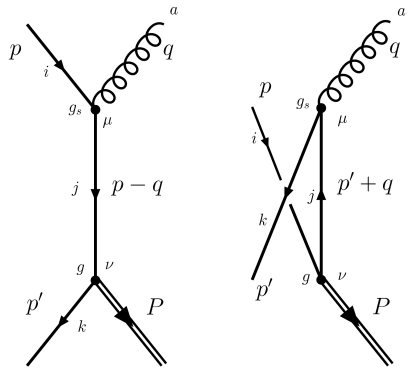

(a) Direct (b) Crossed

Figure 5.3: Feynman diagrams for the leading order contribution of $q\bar{q} \to V_0 g$.

The factors $\alpha, \ldots, \kappa$, then take the following values in the QCD perturbative case for point-like particles:

[6] Note that these are not necessarily independent.

$$\begin{aligned} \alpha_{point} &= \frac{1}{(p-q)^2-m^2} \equiv P_1^{-1},\ \beta_{point} = \frac{1}{(p-q)^2-m^2} \equiv mP_1^{-1}, \\ \delta_{point} &= \frac{1}{(p'+q)^2-m^2} \equiv P_2^{-1},\ \lambda_{point} = \frac{m}{(p'+q)^2-m^2} \equiv mP_2^{-1}, \\ \kappa_{point} &= 0, \end{aligned} \tag{5.35}$$

with the short notations for the propagator denominators ($p^2 = m^2, p'^2 = m^2, q^2 = 0$),

$$P_1^{-1} = \frac{1}{(p-q)^2-m^2} = \frac{-1}{2p.q} \text{ and } P_2^{-1} = \frac{1}{(p'+q)^2-m^2} = \frac{1}{2p'.q}. \tag{5.36}$$

Similarly to the pseudoscalar case, we work out a first constraint from the quark crossing symmetry, which reads:

$$V^{\mu\nu}(p,p',q,P,m) = -\gamma^0 V^{\mu\nu\dagger}(-p',-p,q,P,-m)\gamma^0. \tag{5.37}$$

Indeed, returning to the usual form for the amplitude (where we omitted the spinors u, the polarisation vectors ε and the other factors),

$$V^{\mu\nu} = \frac{\gamma^\nu((\not{p}-\not{q})+m)\gamma^\mu}{(p-q)^2-m^2} + \frac{\gamma^\mu((\not{p}'+\not{q})+m)\gamma^\nu}{(p'+q)^2-m^2}, \tag{5.38}$$

and using the following well-known relations , $\gamma^\mu\gamma^\nu = -\gamma^\nu\gamma^\mu + 2g^{\mu\nu}$, $(\gamma^\mu)^\dagger = \gamma^0\gamma^\mu\gamma^0$, we get:

$$\begin{aligned} \mathcal{T}(V^{\mu\nu}) = \gamma^0 V^{\mu\nu\dagger}(-p',-p,q,P,-m)\gamma^0 &= \frac{\gamma^\mu((-\not{p}'-\not{q})-m)\gamma^\nu}{(-p'-q)^2-m^2} + \frac{\gamma^\nu((-\not{p}+\not{q})-m)\gamma^\mu}{(-p+q)^2-m^2} \\ &= -V^{\mu\nu}(p,p',q,P,m). \end{aligned} \tag{5.39}$$

Note the change of sign compared to the pseudoscalar case (Eq. (5.4)).

5.2.1 Symmetry: general constraints

As for the pseudoscalar case, we shall now extract from Eq. (5.37) relations between the parameters $\alpha,\ldots,\kappa$. Using the relations $\gamma^\mu\not{q}\gamma^\nu = 2\gamma^\mu q^\nu - \gamma^\mu\gamma^\nu\not{q} = 2\gamma^\mu q^\nu - 2g^{\mu\nu}\not{q} + \gamma^\nu\gamma^\mu\not{q}$,

$$\begin{aligned} V^{\mu\nu} &= \alpha\gamma^\nu(\not{p}-\not{q})\gamma^\mu + \beta\gamma^\nu\gamma^\mu + \delta\gamma^\mu(\not{p}'+\not{q})\gamma^\nu + \lambda\gamma^\mu\gamma^\nu + \kappa g^{\mu\nu} \\ &= 2\alpha\gamma^\nu(p-q)^\mu + \alpha\gamma^\mu\gamma^\nu(\not{p}-\not{q}) - 2\alpha g^{\mu\nu}(\not{p}-\not{q}) - \beta\gamma^\mu\gamma^\nu + 2\beta g^{\mu\nu} + \lambda\gamma^\mu\gamma^\nu \\ &+ 2\delta p'^\mu\gamma^\nu - \delta\not{p}'\gamma^\mu\gamma^\nu + 2\delta\gamma^\mu q^\nu - \delta\gamma^\mu\gamma^\nu\not{q} + \kappa g^{\mu\nu} \\ &\overset{(*)}{=} 2\alpha\gamma^\nu(p-q)^\mu + m\alpha\gamma^\mu\gamma^\nu - \alpha\gamma^\mu\gamma^\nu\not{q} - 2m\alpha g^{\mu\nu} + 2\alpha g^{\mu\nu}\not{q} - \beta\gamma^\mu\gamma^\nu + 2\beta g^{\mu\nu} \\ &+ \lambda\gamma^\mu\gamma^\nu + 2\delta p'^\mu\gamma^\nu - m\delta\gamma^\mu\gamma^\nu + 2\delta\gamma^\mu q^\nu - \delta\gamma^\mu\gamma^\nu\not{q} + \kappa g^{\mu\nu}. \end{aligned} \tag{5.40}$$

The equality $(*)$ is obtained by means of Dirac equations for the on-shell quark and antiquark: $\not{p}u(p) = mu(p)$ and $\bar{u}(p')\not{p}' = mu(p')$.

By inspection of Eq. (5.40), we see that we have to deal with six Dirac structures: γ^μ, γ^ν, $\gamma^\mu\gamma^\nu$, $\gamma^\mu\gamma^\nu\not{q}$, $g^{\mu\nu}$ and $g^{\mu\nu}\not{q}$; we also have to keep in mind that p, p' and q are independent, and that the identification is expected to be true for all their values.

Schematically, to help the identification, we shall write:

Structures	Factors
γ^ν	$2\alpha p^\mu - 2\alpha q^\mu + 2\delta p'^\mu$
γ^μ	$2\delta q^\nu$
$\gamma^\mu\gamma^\nu$	$m\alpha - \beta - m\delta + \lambda$
$\gamma^\mu\gamma^\nu\not{q}$	$-\alpha - \delta$
$g^{\mu\nu}$	$-2m\alpha + 2\beta + \kappa$
$g^{\mu\nu}\not{q}$	2α

Now, we shall apply the transformation $-\mathcal{T}(\cdot) = -\gamma^0(\cdot)^\dagger(-p', -p, q, P, -m)\gamma^0$ to the different structures and their coefficients. We obtain

$$\begin{aligned}
\gamma^\nu &\to -\gamma^0(\gamma^\nu)^\dagger\gamma^0 = -\gamma^\nu,\\
\gamma^\mu &\to -\gamma^0(\gamma^\mu)^\dagger\gamma^0 = -\gamma^\mu,\\
\gamma^\mu\gamma^\nu &\to -\gamma^\nu\gamma^\mu = \gamma^\mu\gamma^\nu - 2g^{\mu\nu},\\
\gamma^\mu\gamma^\nu\not{q} &\to -\not{q}\gamma^\nu\gamma^\mu = \gamma^\nu\not{q}\gamma^\mu - 2q^\nu\gamma^\mu = \gamma^\mu\gamma^\nu\not{q} - 2g^{\mu\nu}\not{q},\\
g^{\mu\nu} &\to -g^{\mu\nu},\\
g^{\mu\nu}\not{q} &\to -g^{\mu\nu}\not{q},
\end{aligned} \tag{5.41}$$

and for the coefficients[7]:

$$\begin{aligned}
2\alpha_1 p^\mu - 2\alpha_1 q^\mu + 2\delta_1 p'^\mu &\to -2\alpha_2 p'^\mu - 2\alpha_2 q^\mu - 2\delta_2 p^\mu,\\
2\delta_1 q^\nu &\to 2\delta_2 q^\nu,\\
m\alpha_1 - \beta_1 - m\delta_1 + \lambda_1 &\to -m\alpha_2 - \beta_2 + m\delta_2 + \lambda_2,\\
-\alpha_1 - \delta_1 &\to -\alpha_2 - \delta_2,\\
-2m\alpha_1 + 2\beta_1 + \kappa_1 &\to 2m\alpha_2 + 2\beta_2 + \kappa_2,\\
2\alpha_1 &\to 2\alpha_2.
\end{aligned} \tag{5.42}$$

Finally, we get,

Structures	Factors 1	Factors 2
γ^ν	$2\alpha_1 p^\mu - 2\alpha_1 q^\mu + 2\delta_1 p'^\mu$	$2\alpha_2 p'^\mu - 2\delta_2 q^\mu + 2\delta_2 p^\mu$
γ^ν	$2\delta_1 q^\nu$	$2\alpha_2 q^\nu$
$\gamma^\mu\gamma^\nu$	$m\alpha_1 - \beta_1 - m\delta_1 + \lambda_1$	$-m\alpha_2 - \beta_2 + m\delta_2 + \lambda_2$
$\gamma^\mu\gamma^\nu\not{q}$	$-\alpha_1 - \delta_1$	$-\alpha_2 - \delta_2$
$g^{\mu\nu}$	$-2m\alpha_1 + 2\beta_1 + \kappa_1$	$-2m\delta_2 - 2\lambda_2 - \kappa_2$
$g^{\mu\nu}\not{q}$	$2\alpha_1$	$2\delta_2$

[7] The minus sign of the transformation $-\gamma^0(\cdot)^\dagger_{1\to 2}\gamma^0$ is already taken into account in the transformation laws for the structures.

which gives the following 8 identities relating $\alpha, \ldots, \kappa$ out of which 5 are independent:

$$\begin{aligned}
2\alpha_1 &= 2\delta_2, \\
-2\alpha_1 &= -2\delta_2, \\
2\delta_1 &= 2\alpha_2, \\
2\delta_1 &= 2\alpha_2, \\
m\alpha_1 - \beta_1 - m\delta_1 + \lambda_1 &= -m\alpha_2 - \beta_2 + m\delta_2 + \lambda_2, \\
-\alpha_1 - \delta_1 &= -\alpha_2 - \delta_2, \\
-2m\alpha_1 + 2\beta_1 + \kappa_1 &= -2m\delta_2 - 2\lambda_2 - \kappa_2 \\
2\alpha_1 &= 2\delta_2.
\end{aligned} \tag{5.43}$$

These relations reduce to 4 conditions:

$$\begin{aligned}
\alpha_1 &= \delta_2, \\
\delta_1 &= \alpha_2, \\
-\beta_1 + \lambda_1 &= -\beta_2 + \lambda_2, \\
2(\beta_1 + \lambda_2) &= -(\kappa_1 + \kappa_2)
\end{aligned} \tag{5.44}$$

Let us check that the *point* case fulfils these conditions.

$$\begin{aligned}
&1)\ \delta_{point,1} = P_2^{-1} \Rightarrow \delta_{point,2} = P_1^{-1} = \alpha_{point,1}, \\
&2)\ \alpha_{point,1} = P_1^{-1} \Rightarrow \alpha_{point,2} = P_2^{-1} = \delta_{point,1}, \\
&3)\ -\beta_{point,1} + \lambda_{point,1} = -mP_1^{-1} + mP_2^{-1} \\
&\quad \Rightarrow -\beta_{point,2} + \lambda_{point,2} = -(-m)P_2^{-1} + (-m)P_1^{-1} = \lambda_{point,1} - \beta_{point,1}, \\
&4)\ -(\kappa_{point,1} + \kappa_{point,2}) = 0 = 2(\beta_{point,1} + \lambda_{point,2}) = mP_1^{-1} + (-m)P_1^{-1}.
\end{aligned} \tag{5.45}$$

We have as in the pseudoscalar case a means to deduce in a straightforward way whether or not given contributions, for instance the generalisation of these *point* contributions to bound state ones, have the symmetry required.

5.2.2 Gauge invariance: general constraints

If we now turn to gauge invariance, we shall perform the same ordering but for the amplitude $V^{\mu\nu}$ contracted with q_μ, the momentum of the gluon. Current conservation implies that the contraction should then vanish. This annulment is in turn expressed in terms of identities for the coefficients $\alpha, \beta, \delta, \lambda, \kappa$.

$$\begin{aligned} 0 = V^{\mu\nu}q_\mu =& \alpha\gamma^\nu(\not p - \not q)\not q + \beta\gamma^\nu\not q + \delta\not q(\not p' + \not q)\gamma^\nu + \lambda\not q\gamma^\nu + \kappa q^\nu \\ =& -\alpha\gamma^\nu\not q\not p + 2\alpha\gamma^\nu p.q - \alpha\gamma^\nu q^2 + \beta\gamma^\nu\not q - \delta\not p'\not q\gamma^\nu \\ &+ 2\delta p'.q\gamma^\nu + \delta q^2\gamma^\nu + 2\lambda q^\nu - \lambda\gamma^\nu\not q + \kappa q^\nu \\ =& -m\alpha\gamma^\nu\not q + 2\alpha p.q\gamma^\nu - \alpha q^2\gamma^\nu + \beta\gamma^\nu\not q - 2m\delta q^\nu + m\delta\gamma^\nu\not q \\ &+ 2\delta p'.q\gamma^\nu + \delta q^2\gamma^\nu + 2\lambda q^\nu - \lambda\gamma^\nu\not q + \kappa q^\nu \end{aligned} \tag{5.46}$$

We are left with 3 independent structures, γ^ν, $\gamma^\nu\not q$ and q^ν with the following coefficients:

Structures	Factors
γ^ν	$2\alpha p.q - \alpha q^2 + 2\delta p'.q + \delta q^2$
$\gamma^\nu\not q$	$-m\alpha + \beta + m\delta - \lambda$
q^ν	$-2m\delta + 2\lambda + \kappa$

This gives

$$-\alpha P_1 + \delta P_2 = 0 \tag{5.47}$$

$$\beta - \lambda = m(\alpha - \delta) \tag{5.48}$$

$$\kappa = 2(m\delta - \lambda) \tag{5.49}$$

The *point* case follows these relations. Indeed,

$$\begin{aligned} &1)\ -\alpha_{point}P_1 + \delta_{point}P_2 = -P_1^{-1}P_1 + P_2^{-1}P_2 = 0 \\ &2)\ \beta_{point} - \lambda_{point} = mP_1^{-1} - mP_2^{-1} = m(\alpha_{point} - \delta_{point}) \\ &3)\ 2(m\delta_{point} - \lambda_{point}) = 2(mP_2^{-1} - mP_2^{-1}) = 0 = \kappa_{point} \end{aligned} \tag{5.50}$$

5.2.3 Restoring gauge invariance for the "phenomenological approach"

Let us construct an effective 4-particle vertex restoring gauge invariance, broken by the "phenomenological approach". If we introduce a 3-particle vertex function Γ ($V_3^\nu = \Gamma\gamma^\nu$), the values of $\alpha, \beta, \delta, \lambda$ are :

$$\alpha = \frac{\Gamma_1}{P_1},\ \beta = \frac{m\Gamma_1}{P_1}, \delta = \frac{\Gamma_2}{P_2}, \lambda = \frac{m\Gamma_2}{P_2}, \kappa = 0. \tag{5.51}$$

where $\Gamma_1 = \Gamma((2p-q)^2)$ and $\Gamma_2 = \Gamma((2p'+q)^2)$.

$$\alpha = \alpha_{point} \times \Gamma_1,\ \beta = \beta_{point} \times \Gamma_1,\ \delta = \delta_{point} \times \Gamma_2,\ \lambda = \lambda_{point} \times \Gamma_2. \tag{5.52}$$

From the point of view of gauge invariance, we directly see that Eq. (5.48) and Eq. (5.49) are automatically satisfied by our phenomenological 3-point vertex contrarily to Eq. (5.47) at least as long as $\Gamma_1 \neq \Gamma_2$. Concerning the symmetry under $-\mathcal{T}$, it can easily be seen that it is also satisfied.

The single relation Eq. (5.47) derived from coefficient identification of one single Dirac structure (γ^ν) will be also our starting point to restore gauge invariance in this case. However we shall proceed bearing in mind not to add any contribution to Eq. (5.48) and Eq. (5.49), *i.e.* no term in $\gamma^\nu\gamma^\mu$ at all (before contraction with q^μ), or only a transverse one (vanishing due to the contraction).

First solution

Starting from contribution whose Dirac structure is γ^ν, we can choose the following one (with the multiplicative factor η):

$$2\eta(p+p')^\mu\gamma^\nu = \eta(2p'^\mu\gamma^\nu - m\gamma^\mu\gamma^\nu + 2p^\mu\gamma^\nu - \gamma^\nu\gamma^\mu m) = \eta(\gamma^\mu \not{p}'\gamma^\nu + \gamma^\nu \not{p}\gamma^\mu). \tag{5.53}$$

As we have seen, under the transformation $-\mathcal{T}(\cdot)$, γ^ν changes to $-\gamma^\nu$ and $\eta_1(p+p')$ changes[8] to $-\eta_2(p'+p)$, therefore, we have to impose that

$$\eta_1 = \eta_2. \tag{5.54}$$

Concerning gauge invariance, the introduction of this new contribution adds a new term to Eq. (5.47):

$$0 = -\alpha P_1 + \delta P_2 + 2\eta(p+p').q = -\frac{\Gamma_1}{P_1}P_1 + \frac{\Gamma_2}{P_2}P_2 + 2\eta(p+p').q. \tag{5.55}$$

Solving for η, we have:

$$V_4^{\mu\nu} = 2\eta(p+p')^\mu\gamma^\nu = \frac{\Gamma_1 - \Gamma_2}{(p+p').q}\gamma^\nu(p+p')^\mu, \tag{5.56}$$

η being $\frac{\Gamma_1-\Gamma_2}{2(p+p').q}$. We in turn see that η satisfies the symmetry relation Eq. (5.54) as Γ_1 transforms into Γ_2.

The similar vertex

$$V_4^{\mu\nu} = \frac{\Gamma_1 - \Gamma_2}{(p-p').q}\gamma^\nu(p-p')^\mu \tag{5.57}$$

also satisfies all the criteria. Contracted with q^μ, it indeed gives $(\Gamma_1 - \Gamma_2)\gamma^\nu$ as required to obtain gauge invariance. The symmetry constraint would then require η to be odd. This is also verified as $\eta = \frac{\Gamma_1-\Gamma_2}{2(p-p').q}$.

As in the pseudoscalar case, if we consider a virtual gluon, *i.e.* with $q^2 \neq 0$, we might have also chosen

$$V_4^{\mu\nu} = \frac{\Gamma_1 - \Gamma_2}{q^2}\gamma^\nu q^\mu, \tag{5.58}$$

which does not contribute due to $\varepsilon_\mu(q)q^\mu = 0$.

[8] The minus sign of $-\mathcal{T}(\cdot)$ is considered only the transformation of the structure.

Generalising...

Similarly to the pseudoscalar case, where $\frac{\Gamma_1-\Gamma_2}{k.q}\gamma^5 k^\mu$ was a possible gauge-invariance restoring vertex for any k, we have here $\frac{\Gamma_1-\Gamma_2}{k.q}\gamma^\nu k^\mu$.

If we choose $k^\mu = p^\mu(p'.q) + p'^\mu(p.q)$, we get

$$\begin{aligned} V_4^{\mu\nu} &= (\Gamma_1-\Gamma_2)\frac{p^\mu(p'.q)+p'^\mu(p.q)}{2(p'.q)(p.q)}\gamma^\nu = (\Gamma_1-\Gamma_2)\left(\frac{p^\mu}{2(p.q)}+\frac{p'^\mu}{2(p'.q)}\right)\gamma^\nu \\ &= (\Gamma_1-\Gamma_2)\left(\frac{p^\mu}{P_1}-\frac{p'^\mu}{P_2}\right)\gamma^\nu \end{aligned} \tag{5.59}$$

In this case, this choice contains the same propagators as the *point* case: it cannot introduce new singularities in the problem. As before, there exist also choices of k to make appear the denominator of the problem when $q^2 \neq 0$, *i.e.* for an off-shell gluon. If we choose $k^\mu = (2p-q)^\mu(2p'.q+q^2) + (2p'+q)^\mu(2p.q-q^2)$, we get

$$\begin{aligned} V_4^{\mu\nu} &= (\Gamma_1-\Gamma_2)\frac{(2p-q)^\mu(2p'.q+q^2)+(2p'+q)^\mu(2p.q-q^2)}{2(2p'.q+q^2)(2p.q-q^2)}\gamma^\nu \\ &= \frac{(\Gamma_1-\Gamma_2)}{2}\left(\frac{(2p-q)^\mu}{2p.q-q^2}+\frac{(2p'+q)^\mu}{2p'.q+q^2}\right)\gamma^\nu = (\Gamma_1-\Gamma_2)\left(\frac{(2p-q)^\mu}{2P_1}-\frac{(2p'+q)^\mu}{2P_2}\right)\gamma^\nu, \end{aligned} \tag{5.60}$$

suitable for an off-shell gluon.

The choice of Eq. (5.59) associated with the contributions derived from our phenomenological 3-point vertex will be what we shall refer to as the Gauge-Invariant Phenomenological Approach (GIPA). The latter will be considered as our benchmark for the study of non-static effects and will be studied in details when applied to the calculation of the quarkonium cross section at the Tevatron and at RHIC in chapter 6.

5.3 Autonomous contributions for $q\bar{q} \to V_0 g$

Following the discussion for $q\bar{q} \to V_0 g$, we may generalise the vertex by adding new contributions that are gauge-invariant. This is in fact equivalent to what is implicitly done when passing from one gauge-invariance restoring contribution to another .

For this reason we shall derive here a generic form for a gauge-invariant contribution that can be added to the amplitude for the bound state. We shall nevertheless restrain ourselves to certain class of contributions that satisfy reasonable constraints, namely

- They should vanish for a structureless bound state, that is when $\Gamma_1 = \Gamma_2$.
- The colour factors, as well as the coupling constant from QCD, are to be the same as in the corresponding perturbative contribution with the same external particles.
- Once again, no new singularities can be brought into the problem.

- The new contributions should have the same symmetries under quark crossing as the structureless ones.

As we are dealing with two vectors particles and two of spin 1/2, we have have to have the following generic form for the amplitude

$$\bar{u}(p')V^{\mu\nu}\varepsilon^{\star}_{\mu}(q)\varepsilon^{\star}_{\nu}(P)u(p), \tag{5.61}$$

$\varepsilon^{\star}_{\mu}(q)$ is the gluon helicity vector and $\varepsilon^{\star}_{\nu}(P)$ that of the vector meson.

The only independent tensorial structures that we can introduce are made of Dirac matrices and of the momenta of the problem. From momentum conservation, we might choose: P, q and $p+p'$ (recall that $p-p'=q+P$). Therefore, $V^{\mu\nu}$ could be constructed from a product like the following

$$V^{\mu\nu} = (\Gamma_1 - \Gamma_2) \begin{pmatrix} \gamma^{\mu} \\ P^{\mu} \\ q^{\mu} \\ (p+p')^{\mu} \end{pmatrix} \otimes \begin{pmatrix} \gamma^{\nu} \\ P^{\nu} \\ q^{\nu} \\ (p+p')^{\nu} \end{pmatrix}, \tag{5.62}$$

and with $g^{\mu\nu}$, but this simple combination does not insure gauge-invariance.

The latter can be insured by use of the projector $\mathcal{P}^{\mu}_{\ \mu'} = g^{\mu}_{\ \mu'} - \frac{P^{\mu}q_{\mu'}}{q.P}$. For $g^{\mu\nu}$, this gives $V^{\mu\nu} = (\Gamma_1 - \Gamma_2)(g^{\mu\nu} - \frac{P^{\mu}q^{\nu}}{q.P})$. As the index of the bound-state ν is not affected by the gauge constraints, let us consider the factors in Eq. (5.62) with index μ first:

$$\mathcal{P}^{\mu}_{\ \mu'} \begin{pmatrix} \gamma^{\mu'} \\ P^{\mu'} \\ q^{\mu'} \\ (p+p')^{\mu'} \end{pmatrix} = \begin{pmatrix} \gamma^{\mu} - \frac{P^{\mu}\not{q}}{q.P} \\ 0 \\ q^{\mu} \\ (p+p')^{\mu} - \frac{P^{\mu}(p+p').q}{q.P} \end{pmatrix} \tag{5.63}$$

We can drop q^{μ} as the μ index is the one of the gluon and $\varepsilon(q).q = 0$. We do the same for P^{ν} ($\varepsilon(P).P = 0$) and finally for P^{μ}. Indeed because the gluon is real and thus transverse, we have $\varepsilon(q).k = 0$ for all time-like vectors, k, like $q+P$ –which reduce to $(\sqrt{s},0,0,0)$ in the CM frame–. $\varepsilon(q).(q+P) = 0$ and $\varepsilon(q).q = 0$ obviously give $\varepsilon(q).P = 0$. We therefore have

$$V^{\mu\nu} = (\Gamma_1 - \Gamma_2) \begin{pmatrix} \gamma^{\mu} \\ 0 \\ 0 \\ (p+p')^{\mu} \end{pmatrix} \otimes \begin{pmatrix} \gamma^{\nu} \\ 0 \\ q^{\nu} \\ (p+p')^{\nu} \end{pmatrix}. \tag{5.64}$$

This drives us to the generic contribution :

$$V^{\mu\nu} = (\Gamma_1 - \Gamma_2)(\alpha_1\gamma^{\nu} + \alpha_2 q^{\nu} + \alpha_3(p+p')^{\nu})(\beta_1\gamma^{\mu} + \beta_3(p+p')^{\mu}) + \xi g^{\mu\nu} \tag{5.65}$$

Please remember that the latter expression is without terms that explicitly do not contribute due to contraction with helicity vectors of the bound-state and of the gluon. $V^{\mu\nu}$ in Eq. (5.65) is not meant to verify current conservation as is. We would rather write to be complete:

$$\begin{aligned} V^{\mu\nu} =&(\Gamma_1 - \Gamma_2)((\alpha_1\gamma^\nu + \alpha_2 P^\nu + \alpha_3 q^\nu + \alpha_4(p+p')^\nu) \\ &(\beta_1(\gamma^\mu - \frac{P^\mu \not{q}}{q.P}) + \beta_2 q^\mu + \beta_3((p+p')^\mu - \frac{P^\mu(p+p').q}{q.P}) + \xi(g^{\mu\nu} - \frac{P^\mu q^\nu}{q.P})) \end{aligned} \tag{5.66}$$

As long as the coefficients $\alpha, \beta, \gamma, \kappa, \lambda, \xi$ are not singular anywhere, the second condition that we required is satisfied. To what concerns the crossing symmetry, first let us recall that $\Gamma_1 - \Gamma_2$ changes signs since $\Gamma_1 \xrightarrow{1\to 2} \Gamma_2$, the rest of the expression must then also change sign. Under $-\mathcal{T}(\cdot)$, we have:

$$\begin{array}{rlrl} \gamma^\mu P^\nu \to & -\gamma^\mu P^\nu & \gamma^\mu q^\nu & \to -\gamma^\mu q^\nu \\ \gamma^\mu(p+p')^\nu \to & +\gamma^\mu(p+p')^\nu & (p+p')^\mu(p+p')^\nu & \to -(p+p')^\mu(p+p')^\nu \\ P^\mu q^\mu \to & -P^\mu q^\mu & P^\mu(p+p')^\nu & \to +P^\mu(p+p')^\nu \\ \gamma^\mu\gamma^\nu \to & +\gamma^\mu\gamma^\nu - 2g^{\mu\nu} & g^{\mu\nu} & \to -g^{\mu\nu} \end{array} \tag{5.67}$$

the other combinations are trivially obtained from these. As we required them to change sign, to cancel that of $\Gamma_1 - \Gamma_2$, we have to impose that $\gamma^\mu(p+p')^\nu$ as well as $q^\mu(p+p')^\nu$ have coefficients changing sign contrary to $(p+p')^\mu(p+p')^\nu$, whose coefficient can be a constant.

On the other hand, we have to rule out $\gamma^\mu\gamma^\nu$, the term $-2g^{\mu\nu}$ cannot be cancelled by the terms proportional to $g^{\mu\nu}$. Only more complicated combination starting from a more general product:

$$V^{\mu\nu} = (\Gamma_1 - \Gamma_2) \begin{pmatrix} \gamma^\mu \\ P^\mu \\ q^\mu \\ (p+p')^\mu \end{pmatrix} \otimes \begin{pmatrix} I \\ \not{q} \\ \not{P} \\ (\not{p} + \not{p}') \end{pmatrix} \otimes \begin{pmatrix} \gamma^\nu \\ P^\nu \\ q^\nu \\ (p+p')^\nu \end{pmatrix}, \tag{5.68}$$

would allow to have terms including $\gamma^\mu\gamma^\nu$.

For a first approach, we shall retain here only vertices with a constant multiplicative factor. This enables us to drop some terms in Eq. (5.65) which eventually becomes:

$$V^{\mu\nu} = (\Gamma_1 - \Gamma_2)(\alpha\,\gamma^\mu q^\nu + \beta\,(p+p')^\mu(p+p')^\nu + \xi\,g^{\mu\nu}). \tag{5.69}$$

5.3.1 Our Feynman rules

Considering the process $q\bar{q} \to V_0 g$ in the GIPA, where the $q\bar{q}V_0$ vertex is $\Gamma(p_{rel}^2, P)\gamma^\mu$ (p_{rel} is the relative momentum of the quark and the antiquark and P the momentum of V_0), the choice given by Eq. (5.59) is written explicitly in the first line of Tab. (5.1).

To what concerns autonomous contributions, we limit ourselves to the ones where the free multiplicative factor is a constant. The Feynman rules for these three possible choices derived in Eq. (5.69) are also given in Tab. (5.1).

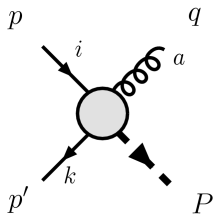	$= -ig_s T^a_{ki}(\Gamma_{(2p+q)} - \Gamma_{(2p'-q)}) \left[\frac{p^\mu}{(p-q)^2-m^2} + \frac{p'^\mu}{(p'+q)^2-m^2}\right] \gamma^\nu$ $= -ig_s T^a_{ki} \frac{(\Gamma_{(2p+q)}-\Gamma_{(2p'-q)})}{2} \left[\frac{p^\mu}{p.q} + \frac{p'^\mu}{p'.q}\right] \gamma^\nu$	cf.Eq. (5.59)
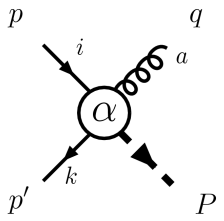	$= -i\, g_s\, T^a_{ki}\, \alpha\, (\Gamma_{(2p+q)} - \Gamma_{(2p'-q)}) \gamma^\mu q^\nu$	First term in Eq. (5.69)
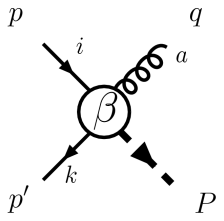	$= -i\, g_s\, T^a_{ki}\, \beta\, (\Gamma_{(2p+q)} - \Gamma_{(2p'-q)})(p+p')^\mu (p+p')^\nu$	Second term in Eq. (5.69)
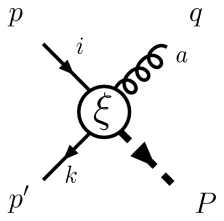	$= -i\, g_s\, T^a_{ki}\, \xi\, (\Gamma_{(2p+q)} - \Gamma_{(2p'-q)}) g^{\mu\nu}$	Third term in Eq. (5.69)

Table 5.1: Feynman rules for one choice of gauge-invariance restoring vertex (first line) and for the three possible choices of autonomous contributions with a constant multiplicative factor.

Chapter 6

J/ψ and Υ production at RHIC and at the Tevatron

We shall now calculate the inclusive polarised cross sections for $pp \to \psi X$ (or $p\bar{p} \to \psi X$) and $p\bar{p} \to \Upsilon X$ (or $pp \to \Upsilon X$) in the experimental conditions of the Tevatron collider based at Fermilab and RHIC at BNL. As already mentioned, the Tevatron is a collider with two beams of equal energy, one of protons and one of antiprotons. The energy in center of momentum frame amounts[1] to 1.8 TeV. There exist two main detectors operating on this collider, CDF and D$\emptyset$. We shall here solely consider the results coming from the CDF collaboration as their analysis reckon, oppositely to that of D$\emptyset$, on a central magnet which enables to identify the charges of the detected particles. As a consequence, their results are slightly more reliable. Concerning RHIC, we shall focus on the PHENIX analysis for pp collisions at $\sqrt{s} = 200$ GeV.

The main study of the CDF analysis, as seen in chapter 2, has been centered on J/ψ, ψ' and the $\Upsilon(nS)$. For the latter, the direct production has been extracted only for $\Upsilon(1S)$. The P_T range was from 5 to 20 GeV and the pseudorapidity range from -0.6 to 0.6 for ψ and from -0.4 to 0.4 Υ. PHENIX studied only total J/ψ production in the central region $|y| \leq 0.35$ and in the forward one $-2.2 \leq y \leq -1.2$. The P_T range was much smaller, from 0.4 GeV to 5.5 GeV.

In those conditions (very high energy and hadron beams), we have already explained that that the main partonic contribution will be gluon fusion. Therefore, one can easily convince oneself that *a priori* the LO sub-process to produce J/ψ and Υ (generically denoted $\mathcal{Q}$) at medium transverse momentum should be $gg \to \mathcal{Q}g$, where the final state gluon is required to provide with the desired transverse momentum.

We first explain the kinematics, underlining the link between the hadronic cross section and the partonic one. The latter is then expressed in terms of helicity amplitudes, which will enable us to calculate the polarisation parameter α_{pol} measured by CDF (see section 2.5).

[1] In run I where the data were taken.

6.1 Generalities on the kinematics

The link between the partonic cross sections and the hadronic ones relies on the following general formula:

$$E\frac{d^3\sigma}{dP^3} = \int_0^1 dx_1 dx_2 \; G_1(x_1) \; G_2(x_2) \; \frac{\hat{s}}{\pi}\frac{d\sigma}{d\hat{t}}\delta(\hat{s}+\hat{t}+\hat{u}-M^2), \tag{6.1}$$

where $P = (E, \vec{P})$ is the momentum of the meson in the c.m. frame of the colliding hadrons. Note on the way that these variables are experimentally accessible. The functions G_i are the parton distribution functions, which give the probability that a parton i take a momentum fraction x_i off the parent hadron.

In the c.m. frame of the colliding hadrons, introducing the rapidity y, the transverse momentum $\vec{P}_T = (P_x, P_y)$ and the transverse energy[2] $E_T = \sqrt{P_T^2 + M^2}$, we may decompose P as follows (satisfying the on-shell constraint $P^2 = M^2$):

$$P = (\sqrt{M^2 + P_x^2 + P_y^2}\cosh y, P_x, P_y, \sqrt{M^2 + P_x^2 + P_y^2}\sinh y) = (E_T \cosh y, \vec{P}_T, E_T \sinh y), \tag{6.2}$$

with

$$y = \frac{1}{2}\ln\left(\frac{E+P_z}{E-P_z}\right) = \tanh^{-1}\left(\frac{P_z}{E}\right). \tag{6.3}$$

Now, let us express the measure d^3P in terms of the variables P_T and y, *i.e.* $d^3P = dP_z\, d\vec{P}_T = dP_z\, d\phi\, P_T\, dP_T$. As we want to keep P_T, we shall only express the z-component in terms of y, in order to get $\frac{dP_z}{dy}$:

$$P_z = E_T \sinh y \Rightarrow \left|\frac{dP_z}{dy}\right| = E_T \cosh y \equiv E, \tag{6.4}$$

which enables us to rewrite the integration element as:

$$E\frac{d^3\sigma}{dP^3} = \frac{d^3\sigma}{dy P_T dP_T d\phi}, \tag{6.5}$$

As the integrand is symmetric in ϕ, we obtain the double-differential cross section upon P_T and y from Eq. (6.1):

$$\frac{d\sigma}{dy dP_T} = \int_0^1 dx_1 dx_2 G_1(x_1) G_2(x_2) 2\hat{s} P_T \frac{d\sigma}{d\hat{t}}\delta(\hat{s}+\hat{t}+\hat{u}-M^2). \tag{6.6}$$

When there might be an ambiguity, the Mandelstam variables relative to the partonic process are discriminated from the hadronic ones by circumflexes. To simplify the notations,

[2] $P_T \equiv |\vec{P}_T|$

especially when dealing uniquely with partonic processes, we shall sometimes drop the circumflexes, as in the next section.

At this stage, we can perform the integration upon x_2 (or x_1) using the delta function, which gives us the jacobian:

$$\frac{1}{\left|\frac{d(\hat{s}+\hat{t}+\hat{u}-M^2)}{dx_2}\right|}. \tag{6.7}$$

To evaluate the latter, we have to express $\hat{s}$, $\hat{t}$ and $\hat{u}$ in terms of x_1, x_2, P_T and y. If the momenta of the initial gluons are k_1 and k_2 and that of the final ones is k_4 (see Fig. 6.1), we have:

$$\begin{aligned} \hat{s} &= (k_1 + k_2)^2 = (q + P)^2, \\ \hat{t} &= (k_1 - P)^2 = (k_2 - q)^2, \\ \hat{u} &= (k_1 - q)^2 = (k_2 - P)^2. \end{aligned} \tag{6.8}$$

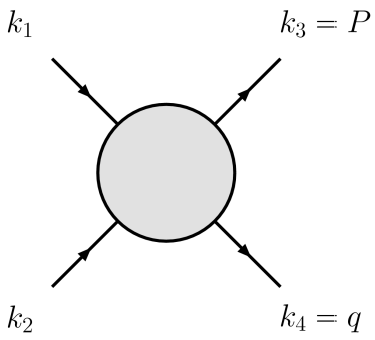

Figure 6.1: Definition of k_1, k_2, k_3 (P) and k_4 (q).

Defining the momenta of the two hadrons as p_1 and p_2, we may always choose the axis such as to suppress their transverse components (along the x and y axes for definiteness). For massless initial hadrons, we then have in their c.m. frame

$$\begin{aligned} p_1 &= (\frac{\sqrt{s}}{2}, 0, 0, \frac{\sqrt{s}}{2}), \\ p_2 &= (\frac{\sqrt{s}}{2}, 0, 0, -\frac{\sqrt{s}}{2}). \end{aligned} \tag{6.9}$$

Now, by definition of the momentum fractions x_1 and x_2:

$$\hat{s} = (k_1 + k_2)^2 = \frac{s}{4}(x_1 + x_2, 0, 0, x_1 - x_2)^2 = s x_1 x_2, \tag{6.10}$$

and

$$\begin{aligned} \hat{t} = (k_1 - P)^2 &= \underbrace{k_1^2}_{0} + \underbrace{P^2}_{M^2} - 2\underbrace{k_1}_{x_1 p_1} \cdot P \\ &= M^2 - 2x_1 \frac{\sqrt{s}}{2}(E - P_z). \end{aligned} \tag{6.11}$$

From Eq. (6.2), we have $(E - P_z) = E_T(\cosh y - \sinh y) = E_T e^{-y}$ and

$$\hat{t} = M^2 - x_1 e^{-y}\sqrt{s}E_T. \tag{6.12}$$

Similarly, we get

$$\hat{u} = M^2 - x_2 e^{y}\sqrt{s}E_T. \tag{6.13}$$

Writing down $\hat{s} + \hat{t} + \hat{u} - M^2 = sx_1x_2 + M^2 - x_1e^{-y}\sqrt{s}E_T - x_2e^{y}\sqrt{s}E_T$ and solving for x_2, we obtain:

$$x_2 = \frac{x_1E_T\sqrt{s}e^{-y} - M^2}{\sqrt{s}(\sqrt{s}x_1 - E_Te^{y})}. \tag{6.14}$$

For completeness, solving for x_1 we have

$$x_1 = \frac{x_2E_T\sqrt{s}e^{y} - M^2}{\sqrt{s}(\sqrt{s}x_2 - E_Te^{-y})}. \tag{6.15}$$

We also easily compute the jacobian of the δ integration:

$$\frac{1}{\left|\frac{d(\hat{s}+\hat{t}+\hat{u}-M^2)}{dx_2}\right|} = \frac{1}{\sqrt{s}(\sqrt{s}x_1 - E_Te^{y})}. \tag{6.16}$$

As x_2 is now a function of x_1, we are left with a one-dimensional integration which is restricted by

$$0 \leq x_2 \leq 1. \tag{6.17}$$

Supposing that[3] $x_1 \geq \frac{E_Te^y}{\sqrt{s}}$, we get the following condition:

$$x_1 \geq \frac{E_T\sqrt{s}e^{y} - M^2}{\sqrt{s}(E_Te^{-y} - \sqrt{s})} \equiv x_1^{min}. \tag{6.18}$$

Therefore, the double differential cross section upon P_T and y takes the following form:

$$\frac{d\sigma}{dydP_T} = \int_{x_1^{min}}^{1} dx_1 \frac{2\hat{s}P_TG_1(x_1)G_2(x_2(x_1))}{\sqrt{s}(\sqrt{s}x_1 - E_Te^{y})}\frac{d\sigma}{d\hat{t}}. \tag{6.19}$$

The last step is now to relate the partonic differential cross section $\frac{d\sigma}{d\hat{t}}$ to the amplitude calculated from our model. To this end, we use the well-known formula:

$$\frac{d\sigma}{d\hat{t}} = \frac{1}{16\pi\hat{s}^2}|\overline{\mathcal{M}}|^2, \tag{6.20}$$

where $|\overline{\mathcal{M}}|^2$ is the squared amplitude averaged on the initial spin and colour degrees of freedom and summed over the final ones for an unpolarised cross section, or averaged only for the colour for polarised cross sections.

The calculation of the latter amplitude within the framework of our model is the subject the following section.

[3] The conditions $\hat{t} \leq 0$ and $\hat{u} \leq 0$ give $x_1 \geq \frac{M^2e^y}{\sqrt{s}E_T}$ and $x_2 \geq \frac{M^2e^{-y}}{\sqrt{s}E_T}$ which are always less restrictive than $x_1 \geq \frac{E_Te^y}{\sqrt{s}}$ and $x_2 \geq \frac{E_Te^{-y}}{\sqrt{s}}$ for $P_T \neq 0$. Furthermore, as long as $|y|$ is not of the order of $\ln(\frac{\sqrt{s}}{P_T})$ ($|y| = 3.8$ at $P_T = 40$ GeV), $x_1 \geq \frac{E_Te^y}{\sqrt{s}}$ is always less restrictive than Eq. (6.18).

6.2 Amplitude for $gg \to {}^3S_1 g$

In this section, we shall give our procedure to calculate the imaginary of the amplitude for $gg \to {}^3S_1 g$ in our formalism through Cutkovsky rules. We shall consider this amplitude at leading order in α_s.

First, we further develop the kinematics to avoid any ambiguity and we derive expressions for the polarisation vectors of all particles. Then we write down the expressions for the helicity amplitudes. The cutting rules impose further constraints on the internal kinematics, which we give. We then organise the calculation by classifying the integrals that enter the amplitude.

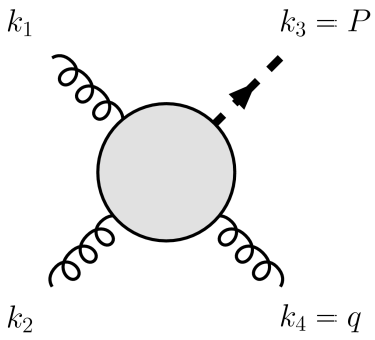

Figure 6.2: Kinematics of the process $gg \to {}^3S_1 g$.

6.2.1 Further kinematics and polarisation vectors

The momenta of the particles are as shown in Fig. 6.2. The on-shellness conditions are then: $k_1^2 = k_2^2 = k_4^2 = 0$, $k_3^2 = M^2$. The Mandelstam variables are defined as usual (dropping the circumflexes)

$$s = (k_1 + k_2)^2 = 2k_1.k_2 = (k_3 + k_4)^2 = M^2 + 2k_3.k_4\,, \tag{6.21}$$
$$t = (k_1 - k_3)^2 = -2k_1.k_3 + M^2 = (k_2 - k_4)^2 = -2k_2.k_4\,, \tag{6.22}$$
$$u = (k_1 - k_4)^2 = -2k_1.k_4 = (k_2 - k_3)^2 = -2k_2.k_3 + M^2\,, \tag{6.23}$$
$$s + t + u = M^2\,. \tag{6.24}$$

and all scalar products, $k_i.k_j$, are functions of the latter:

$$k_1.k_2 = \frac{s}{2}\,, k_1.k_3 = \frac{M^2 - t}{2}\,, k_1.k_4 = -\frac{u}{2}, \tag{6.25}$$
$$k_2.k_3 = \frac{M^2 - u}{2}\,, k_2.k_4 = -\frac{t}{2}\,, k_3.k_4 = \frac{s - M^2}{2}\,. \tag{6.26}$$

In order to compute polarised cross sections, we have to introduce explicitly the polarisation vectors for the vector meson and for the gluons. It is however sufficient to determine

for all polarisations the scalar product between these vectors and the other vectors of the problem, *i.e.* $k_1, \ldots, k_4$.

Let $\varepsilon_i \equiv \varepsilon(k_i)$ be the polarisation vector of the different particles considered in the present case, we shall perform a Sudakov decomposition of these along the momenta of the problem and along a vector ϵ_T ($\epsilon_T.\epsilon_T = -1$) orthogonal to the plane of the scattering.

A generic helicity vector ε_i^h, where i is the particle label ($i = 1, ..4$), h the helicity state (T_1 or T_2 for the gluons and T_1, T_2 or L for the vector meson), then becomes:

$$\varepsilon_i^h = a_i^h k_1 + b_i^h k_2 + c_i^h k_4 + d_i^h \epsilon_T. \tag{6.27}$$

We first impose that each vector be orthogonal to the momentum of the particle it describes:

$$k_i.\varepsilon_i^h = 0, \tag{6.28}$$

for all polarisation h.

Then we require that vectors of different helicities ($h \neq h'$) and of one given particle be orthogonal to each other:

$$\varepsilon_i^h.\varepsilon_i^{h'} = 0. \tag{6.29}$$

We in turn impose the correct normalisations,

$$(\varepsilon_i^h)^2 = -1. \tag{6.30}$$

The previous conditions are valid for all polarisations. In the case of the transverse ones, we shall introduce this transverse property by requiring that only spatial components remain. In other words, the scalar product between transverse polarisations and a vector of the generic form $v = (v_0, 0, 0, 0)$ should vanish.

In the c.m. frame (of the gluons), $k_1 + k_2$ or $k_3 + k_4$ have the latter property since $k_1 + k_2 = k_3 + k_4 = (\sqrt{s}, 0, 0, 0)$, and thus the condition for transverse polarisations becomes:

$$(k_1 + k_2).\varepsilon_i^T = (k_3 + k_4).\varepsilon_i^T = 0, \tag{6.31}$$

Taking into account the conditions of Eq. (6.28), we then derive

$$\begin{aligned} \varepsilon_1^T.k_2 &= 0, \\ \varepsilon_2^T.k_1 &= 0, \\ \varepsilon_3^T.k_4 &= 0, \\ \varepsilon_4^T.k_3 &= 0. \end{aligned} \tag{6.32}$$

Here, we are free to choose $\varepsilon_i^{T_1}$ to be a vector orthogonal to all the others, namely

$$\varepsilon_1^{T_1} = \varepsilon_2^{T_1} = \varepsilon_3^{T_1} = \varepsilon_4^{T_1} = \epsilon_T, \tag{6.33}$$

since this satisfies all conditions cited above.

Having fixed $\varepsilon_i^{T_1}$, we shall determine $\varepsilon_i^{T_2}$ imposing $\varepsilon_i^{T_1}.\varepsilon_i^{T_2} = 0$. We have:

$$\begin{aligned} a_1^{T_2} = a_2^{T_2} = a_3^{T_2} = a_4^{T_2} &= \sqrt{\frac{s}{ut}}\frac{t}{s}, \\ b_1^{T_2} = b_2^{T_2} = -b_3^{T_2} = -b_4^{T_2} &= \sqrt{\frac{s}{ut}}\frac{u}{s}, \\ c_1^{T_2} = c_2^{T_2} &= \sqrt{\frac{s}{ut}}, \\ c_3^{T_2} = c_4^{T_2} &= \sqrt{\frac{s}{ut}}\frac{(t-u)}{t+u}, \\ d_1^{T_2} = d_2^{T_2} = d_3^{T_2} = d_4^{T_2} &= 0. \end{aligned} \tag{6.34}$$

Finally, requiring $\varepsilon_3^{T_1}.\varepsilon_3^L = 0 = \varepsilon_3^{T_2}.\varepsilon_3^L$, we fully determine ε_3^L:

$$a_3^L = \frac{1}{M}, b_3^L = \frac{1}{M}, c_3^L = -\frac{1}{M}\frac{s+M^2}{s-M^2}, d_3^L = 0. \tag{6.35}$$

Thus, the complete expressions of the polarisation vectors are the following:

$$\begin{aligned} \varepsilon_1^{T_1} = \varepsilon_2^{T_1} = \varepsilon_3^{T_1} = \varepsilon_4^{T_1} &= \epsilon_T, \\ \varepsilon_1^{T_2} &= \sqrt{\frac{1}{stu}}\left(tk_1 + uk_2 + sk_4\right) = \varepsilon_2^{T_2}, \\ \varepsilon_3^{T_2} &= \sqrt{\frac{1}{stu}}\left(tk_1 - uk_2 + \left(\frac{s(t-u)}{t+u}\right)k_4\right) = \varepsilon_4^{T_2}, \\ \varepsilon_3^L &= \frac{1}{M}\left(k_1 + k_2 - \left(\frac{s+M^2}{s-M^2}\right)k_4\right), \end{aligned} \tag{6.36}$$

Compatibility with the standard choice

We shall show here that our result can give in a non-covariant form the standard choice for instance taken in [50, 51]. Let us do that for the longitudinal meson polarisation vector. We have with the notations explained above:

$$\varepsilon_3^L = \frac{1}{M}\left(k_1 + k_2 - \left(\frac{s+M^2}{s-M^2}\right)k_4\right) \tag{6.37}$$

whereas the standard choice used in [50, 51] is in the meson rest frame ($k_3 = (M, 0, 0, 0,)$):

$$\varepsilon_3^L = (0, 0, 0, 1), \tag{6.38}$$

First we rewrite ε_3^L in terms of k_3, this gives

$$\varepsilon_3^L = \frac{1}{M}\left(k_3 - \frac{2M^2}{s-M^2}k_4\right). \tag{6.39}$$

Choosing the z-axis direction to be the same as $-\vec{k}_4$, we have $k_4 = (k_{4,0}, 0, 0, -|k_{4,z}|)$, which, for an on-shell gluon, gives $k_4 = (k_{4,0}, 0, 0, -k_{4,0})$. We are thus left to determine $k_{4,0}$, which is given by

$$s = (k_3 + k_4)^2 = M^2 + 0 + 2k_3.k_4 = M^2 + 2Mk_{4,0} \;\Rightarrow k_{4,0} = \frac{s - M^2}{2M} \tag{6.40}$$

Finally, we have

$$\varepsilon_3^L = \frac{1}{M}((M, 0, 0, 0,) - (M, 0, 0, -M)) = (0, 0, 0, 1). \tag{6.41}$$

6.2.2 Expressions for the amplitude

As we shall consider only its imaginary part, the amplitude of the process can be diagrammatically presented by a product of two scattering amplitudes $gg \to q\bar{q}$ and $q\bar{q} \to \mathcal{Q}g$ where we put the quark lines with momenta $\ell + k_1$ and $\ell - k_2$ (Fig. 6.3) on their mass shell, so that they satisfy the relations: $(\ell + k_1)^2 = m^2$, $(\ell - k_2)^2 = m^2$, or equivalently we replace their propagators by δ functions:

$$\begin{aligned} \frac{1}{(\ell + k_1)^2 - m^2} \frac{1}{(\ell - k_2)^2 - m^2} &\to \frac{1}{2}(2\pi)^2 \delta^+((\ell + k_1)^2 - m^2)\delta^-((\ell - k_2)^2 - m^2) \\ &= \frac{1}{2}(2\pi)^2 \delta(2\ell.(k_1 + k_2))\delta(\ell^2 + 2\ell.k_1 - m^2) \times \\ &\times \theta(\ell^0 + k_1^0)\theta(-\ell^0 + k_2^0), \end{aligned} \tag{6.42}$$

where the factor $\frac{1}{2}$ comes from $\Im m\mathcal{A} = \frac{1}{2}\mathrm{Disc}(\mathcal{A})$, and the discontinuity is obtained with the introduction of the above-mentioned δ functions.

At leading order in α_s (g_s), we have three diagrams for $gg \to q\bar{q}$ and also three for $q\bar{q} \to \mathcal{Q}g$, in our framework. The six diagrams[4] are drawn in Fig. 6.3.

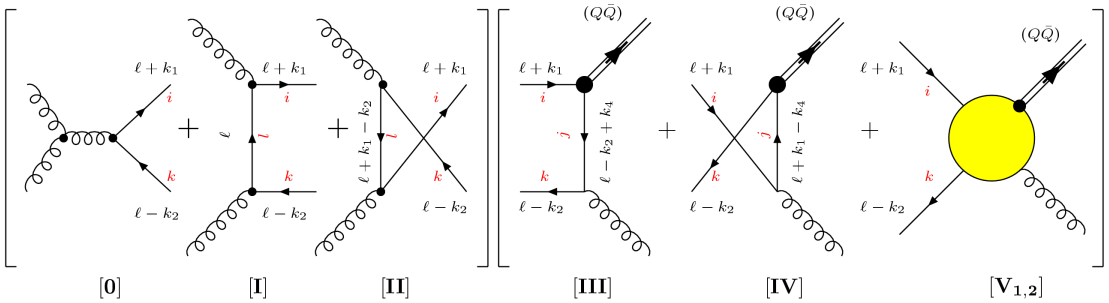

Figure 6.3: Different contributions to the imaginary part of the amplitude for $q\bar{q} \to \mathcal{Q}g$.

[4] Compared to notations used for the derivation of the gauge-invariance restoring vertices (chapter 5), we have $p \to \ell + k_1$, $p' \to \ell - k_2$, $q \to k_4$ and $P \to k_3$.

These scattering amplitudes have the following explicit forms, where p, q, r and s are the helicity states of the particles,

$$
\begin{aligned}
[\mathbf{O}] &= (-g_s) f^{abd} \bar{u}(\ell + k_1) \left[(k_1 - k_2)^\tau g^{\mu\nu} + (k_1 + 2k_2)^\mu g^{\nu\tau} - (2k_1 + k_2)^\nu g^{\tau\mu} \right] \times \\
&\times \quad \frac{-i g_{\tau\tau'} \delta_{dd'}}{(k_1 + k_2)^2} (-i g_s T^{d'}_{ik}) \gamma^{\tau'} u(\ell + k_1) \varepsilon^p_\mu(k_1) \varepsilon^q_\nu(k_2) \qquad (6.43) \\
&= g_s^2 \frac{f^{abd} T_d}{s} \bar{u}(\ell - k_2) \left[(\not{k}_1 - \not{k}_2) g^{\mu\nu} + (k_1 + 2k_2)^\mu \gamma^\nu - (2k_1 + k_2)^\nu \gamma^\mu \right] u(\ell + k_1) \times \\
&\times \quad \varepsilon^p_\mu(k_1) \varepsilon^q_\nu(k_2), \qquad (6.44) \\
[\mathbf{I}] &= (-i g_s)^2 T^a_{il} T^b_{lk} \bar{u}(\ell - k_2) \frac{i \left[\gamma^\mu (\not{\ell} + m) \gamma^\nu \right]}{\ell^2 - m^2} u(\ell + k_1) \varepsilon^p_\mu(k_1) \varepsilon^q_\nu(k_2), \qquad (6.45) \\
[\mathbf{II}] &= (-i g_s)^2 T^b_{il} T^a_{lk} \bar{u}(\ell - k_2) \frac{i \left[\gamma^\nu \left((\not{\ell} + \not{k}_1 - \not{k}_2) + m \right) \gamma^\mu \right]}{(\ell + k_1 - k_2)^2 - m^2} u(\ell + k_1) \varepsilon^p_\mu(k_1) \varepsilon^q_\nu(k_2), \qquad (6.46) \\
[\mathbf{III}] &= (-i g_s T^c_{kj}) (-i \Gamma_1 \delta^{ji}) \bar{u}(\ell - k_2) \frac{i \left[\gamma^\sigma \left((\not{\ell} - \not{k}_2 + \not{k}_4) + m \right) \gamma^\rho \right]}{(\ell - k_2 + k_4)^2 - m^2} u(\ell + k_1) \times \\
&\times \quad \varepsilon^{r\star}_\rho(k_3) \varepsilon^{s\star}_\sigma(k_4), \qquad (6.47) \\
[\mathbf{IV}] &= (-i \Gamma_2 \delta^{kj}) (-i g_s T^c_{ji}) \bar{u}(\ell - k_2) \frac{i \left[\gamma^\rho \left((\not{\ell} + \not{k}_1 - \not{k}_4) + m \right) \gamma^\sigma \right]}{(\ell + k_1 - k_4)^2 - m^2} u(\ell + k_1) \times \\
&\times \quad \varepsilon^{r\star}_\rho(k_3) \varepsilon^{s\star}_\sigma(k_4), \qquad (6.48) \\
[\mathbf{V}] &= [\mathbf{V_1}] + [\mathbf{V_2}] \qquad (6.49) \\
[\mathbf{V_1}] &= -i \left(\Gamma_1 - \Gamma_2 \right) (-i g_s) T^c_{ki} \bar{u}(\ell - k_2) \gamma^\rho \frac{i(\ell^\sigma + k_1^\sigma)}{(\ell + k_1 - k_4)^2 - m^2} u(\ell + k_1) \times \\
&\times \quad \varepsilon^{r\star}_\rho(k_3) \varepsilon^{s\star}_\sigma(k_4), \qquad (6.50) \\
[\mathbf{V_2}] &= -i \left(\Gamma_1 - \Gamma_2 \right) (-i g_s) T^c_{ki} \bar{u}(\ell - k_2) \gamma^\rho \frac{-i(\ell^\sigma - k_2^\sigma)}{(\ell - k_2 + k_4)^2 - m^2} u(\ell + k_1) \times \\
&\times \quad \varepsilon^{r\star}_\rho(k_3) \varepsilon^{s\star}_\sigma(k_4). \qquad (6.51)
\end{aligned}
$$

Before going further, let us draw the reader's attention to some points concerning these amplitudes:

- Gauge invariance imposes that $([\mathbf{0}] + [\mathbf{I}] + [\mathbf{II}]) \varepsilon^\nu(k_2) k_1^\mu = 0$ and not simply $([\mathbf{0}] + [\mathbf{I}] + [\mathbf{II}]) k_1^\mu = 0$. The same remark holds also for k_2. Indeed, using the Dirac equation for the on-shell quarks, we have $([\mathbf{0}] + [\mathbf{I}] + [\mathbf{II}]) k_1^\mu = i g_s^2 [T^a, T^b] \bar{u}(\ell + k_1) \frac{k_2^\nu}{s} \not{k}_1 u(\ell - k_2)$ which is orthogonal to $\varepsilon_\nu(k_2)$. Their product therefore vanishes.

- Gauge invariance for the right part is insured by the introduction of the diagrams $[\mathbf{V_1}]$ and $[\mathbf{V_2}]$ that come from the choice of the following gauge-invariance restoring vertex derived in section 5.2.3, Eq. (5.59) (see also Tab. (5.1))

$$
(\Gamma_1 - \Gamma_2) \left(\frac{p^\mu}{P_1} - \frac{p'^\mu}{P_2} \right) \gamma^\nu \to (\Gamma_1 - \Gamma_2) \left(\frac{\ell^\sigma + k_1^\sigma}{(\ell + k_1 - k_4)^2 - m^2} + \frac{-(\ell^\sigma - k_2^\sigma)}{(\ell - k_2 + k_4)^2 - m^2} \right) \gamma^\rho \qquad (6.52)
$$

- We have split the contribution [**V**] in two parts as they contain two different propagators.
- We have chosen to omit the $\frac{1}{\sqrt{3}}$ factor in the colour factor for the quark-antiquark-meson vertex. Of course, the same choice has been made during the normalisation procedure (cf. Eq. (4.21)).
- The contributions of the triple-gluon vertex [**0**] will vanish when contracted with the right part of the diagram due to Furry's theorem. Indeed, a loop with an odd number of vertices of vectors particles vanishes. We have nevertheless checked numerically that it was the case, also for the gauge-invariance restoring vertex [**V**].
- This set of contribution is what we shall refer to as the Gauge-Invariant Phenomenological Approach (GIPA).

The vertex functions depend on the relative momentum of the quarks at the vertices as follows

$$\Gamma_1 = \Gamma\left(\ell + \frac{1}{2}\left(k_1 - k_2 + k_4\right)\right)\ ,\ \Gamma_2 = \Gamma\left(\ell + k_1 - \frac{1}{2}k_4\right)\ . \tag{6.53}$$

Multiplying the amplitudes from the right with the ones from the left and taking the trace in Dirac matrix space and in colour space, we define the following quantities[5] :

$$\begin{aligned}\mathrm{tr}^{pqrs}_{I-III} =& -g_s^3 \mathrm{Tr}\left[T^a T^b T^c\right] \mathrm{Tr}\left[\gamma^\mu\left(\not{\ell}+m\right)\gamma^\nu((\not{\ell}-\not{k}_2)+m)\right.\\ &\left.\times\gamma^\sigma\left((\not{\ell}-\not{k}_2+\not{k}_4)+m\right)\gamma^\rho((\not{\ell}+\not{k}_1)+m)\right]\varepsilon^p_\mu(k_1)\varepsilon^q_\nu(k_2)\varepsilon^{r\star}_\rho(k_3)\varepsilon^{s\star}_\sigma(k_4)\end{aligned} \tag{6.54}$$

$$\begin{aligned}\mathrm{tr}^{pqrs}_{I-IV} =& -g_s^3 \mathrm{Tr}\left[T^a T^b T^c\right] \mathrm{Tr}\left[\gamma^\mu\left(\not{\ell}+m\right)\gamma^\nu((\not{\ell}-\not{k}_2)+m)\right.\\ &\left.\times\gamma^\rho\left((\not{\ell}+\not{k}_1-\not{k}_4)+m\right)\gamma^\sigma((\not{\ell}+\not{k}_1)+m)\right]\varepsilon^p_\mu(k_1)\varepsilon^q_\nu(k_2)\varepsilon^{r\star}_\rho(k_3)\varepsilon^{s\star}_\sigma(k_4)\end{aligned} \tag{6.55}$$

$$\begin{aligned}\mathrm{tr}^{pqrs}_{II-III} =& -g_s^3 \mathrm{Tr}\left[T^b T^a T^c\right] \mathrm{Tr}\left[\gamma^\nu\left((\not{\ell}+\not{k}_1-\not{k}_2)+m\right)\gamma^\mu((\not{\ell}-\not{k}_2)+m)\right.\\ &\left.\times\gamma^\sigma\left((\not{\ell}-\not{k}_2+\not{k}_4)+m\right)\gamma^\rho((\not{\ell}+\not{k}_1)+m)\right]\varepsilon^p_\mu(k_1)\varepsilon^q_\nu(k_2)\varepsilon^{r\star}_\rho(k_3)\varepsilon^{s\star}_\sigma(k_4)\end{aligned} \tag{6.56}$$

$$\begin{aligned}\mathrm{tr}^{pqrs}_{II-IV} =& -g_s^3 \mathrm{Tr}\left[T^b T^a T^c\right] \mathrm{Tr}\left[\gamma^\nu\left((\not{\ell}+\not{k}_1-\not{k}_2)+m\right)\gamma^\mu((\not{\ell}-\not{k}_2)+m)\right.\\ &\left.\times\gamma^\rho\left((\not{\ell}+\not{k}_1-\not{k}_4)+m\right)\gamma^\sigma((\not{\ell}+\not{k}_1)+m)\right]\varepsilon^p_\mu(k_1)\varepsilon^q_\nu(k_2)\varepsilon^{r\star}_\rho(k_3)\varepsilon^{s\star}_\sigma(k_4)\end{aligned} \tag{6.57}$$

$$\begin{aligned}\mathrm{tr}^{pqrs}_{I-V_1} =& -g_s^3 \mathrm{Tr}\left[T^a T^b T^c\right] \mathrm{Tr}\left[\gamma^\mu\left(\not{\ell}+m\right)\gamma^\nu((\not{\ell}-\not{k}_2)+m)\right.\\ &\left.\times\gamma^\rho((\not{\ell}+\not{k}_1)+m)\right]\left(\ell^\sigma + k_1^\sigma\right)\varepsilon^p_\mu(k_1)\varepsilon^q_\nu(k_2)\varepsilon^{r\star}_\rho(k_3)\varepsilon^{s\star}_\sigma(k_4)\end{aligned} \tag{6.58}$$

$$\begin{aligned}\mathrm{tr}^{pqrs}_{I-V_2} =& -g_s^3 \mathrm{Tr}\left[T^a T^b T^c\right] \mathrm{Tr}\left[\gamma^\mu\left(\not{\ell}+m\right)\gamma^\nu((\not{\ell}-\not{k}_2)+m)\right.\\ &\left.\times\gamma^\rho((\not{\ell}+\not{k}_1)+m)\right](-)\left(\ell^\sigma - k_2^\sigma\right)\varepsilon^p_\mu(k_1)\varepsilon^q_\nu(k_2)\varepsilon^{r\star}_\rho(k_3)\varepsilon^{s\star}_\sigma(k_4)\end{aligned} \tag{6.59}$$

$$\begin{aligned}\mathrm{tr}^{pqrs}_{II-V_1} =& -g_s^3 \mathrm{Tr}\left[T^b T^a T^c\right] \mathrm{Tr}\left[\gamma^\nu\left((\not{\ell}+\not{k}_1-\not{k}_2)+m\right)\gamma^\mu((\not{\ell}-\not{k}_2)+m)\right.\\ &\left.\times\gamma^\rho((\not{\ell}+\not{k}_1)+m)\right]\left(\ell^\sigma + k_1^\sigma\right)\varepsilon^p_\mu(k_1)\varepsilon^q_\nu(k_2)\varepsilon^{r\star}_\rho(k_3)\varepsilon^{s\star}_\sigma(k_4)\end{aligned} \tag{6.60}$$

[5] Note that the following quantities are defined so that they contain neither the denominator of the quarks propagators nor the meson vertex function.

$$\begin{aligned}\mathrm{tr}^{pqrs}_{II-V_2} = &- g_s^3 \mathrm{Tr}\left[T^b T^a T^c\right] \mathrm{Tr}\left[\gamma^\nu \left((\not{\ell} + \not{k}_1 - \not{k}_2) + m\right) \gamma^\mu ((\not{\ell} - \not{k}_2) + m)\right. \\ &\left. \times \gamma^\rho ((\not{\ell} + \not{k}_1) + m)\right] (-)(\ell^\sigma - k_2^\sigma) \varepsilon^p_\mu(k_1) \varepsilon^q_\nu(k_2) \varepsilon^{r\star}_\rho(k_3) \varepsilon^{s\star}_\sigma(k_4)\end{aligned} \tag{6.61}$$

Using the latter quantities, it is now straightforward to rewrite the different contributions to the imaginary of $gg \to {}^3S_1 g$ by including the integration over the internal quarks momenta constrained by the two δ functions coming from the cutting rules which is designated by $d_{PS} = \frac{d^4\ell}{8\pi^2}\delta(2\ell.(k_1+k_2))\delta(\ell^2 + 2\ell.k_1 - m^2)\theta(\ell^0 + k_1^0)\theta(-\ell^0 + k_2^0)$ in the following,

$$\begin{aligned}
[\mathbf{I}][\mathbf{III}](p,q,r,s) &= \int d_{PS} \Gamma_1 \mathrm{tr}^{pqrs}_{I-III} \frac{1}{\ell^2 - m^2} \frac{1}{(\ell - k_2 + k_4)^2 - m^2} \\
[\mathbf{I}][\mathbf{IV}](p,q,r,s) &= \int d_{PS} \Gamma_2 \mathrm{tr}^{pqrs}_{I-IV} \frac{1}{\ell^2 - m^2} \frac{1}{(\ell + k_1 - k_4)^2 - m^2} \\
[\mathbf{II}][\mathbf{III}](p,q,r,s) &= \int d_{PS} \Gamma_1 \mathrm{tr}^{pqrs}_{II-III} \frac{1}{(\ell + k_1 - k_2)^2 - m^2} \frac{1}{(\ell - k_2 + k_4)^2 - m^2} \\
[\mathbf{II}][\mathbf{IV}](p,q,r,s) &= \int d_{PS} \Gamma_2 \mathrm{tr}^{pqrs}_{II-IV} \frac{1}{(\ell + k_1 - k_2)^2 - m^2} \frac{1}{(\ell + k_1 - k_4)^2 - m^2} \\
[\mathbf{I}][\mathbf{V_1}](p,q,r,s) &= \int d_{PS} \left(\Gamma_1 - \Gamma_2\right) \mathrm{tr}^{pqrs}_{I-V_1} \frac{1}{\ell^2 - m^2} \frac{1}{(\ell + k_1 - k_4)^2 - m^2} \\
[\mathbf{I}][\mathbf{V_2}](p,q,r,s) &= \int d_{PS} \left(\Gamma_1 - \Gamma_2\right) \mathrm{tr}^{pqrs}_{I-V_2} \frac{1}{\ell^2 - m^2} \frac{1}{(\ell - k_2 + k_4)^2 - m^2} \\
[\mathbf{II}][\mathbf{V_1}](p,q,r,s) &= \int d_{PS} \left(\Gamma_1 - \Gamma_2\right) \mathrm{tr}^{pqrs}_{II-V_1} \frac{1}{(\ell + k_1 - k_2)^2 - m^2} \frac{1}{(\ell + k_1 - k_4)^2 - m^2} \\
[\mathbf{II}][\mathbf{V_2}](p,q,r,s) &= \int d_{PS} \left(\Gamma_1 - \Gamma_2\right) \mathrm{tr}^{pqrs}_{II-V_2} \frac{1}{(\ell + k_1 - k_2)^2 - m^2} \frac{1}{(\ell - k_2 + k_4)^2 - m^2}
\end{aligned} \tag{6.62}$$

The full polarised amplitude of $gg \to {}^3S_1 g$ is given by summing all these expressions.

6.2.3 Integration over internal kinematics

To extract explicit forms for the conditions constraining the integration phase space, we shall decompose the vector ℓ along three independent light-cone vectors k_1, k_2, k_4 and ϵ_T

$$\ell = \bar{x} k_1 + \bar{y} k_2 + \bar{z} k_4 + \lambda \epsilon_T. \tag{6.63}$$

In terms of these new variables $(\bar{x}, \bar{y}, \bar{z}, \lambda)$, we can rewrite the element of integration $d^4\ell$ as

$$d^4\ell = \frac{1}{2}\sqrt{stu}\; d\bar{x}\, d\bar{y}\, d\bar{z}\, d\lambda = \frac{1}{4}\sqrt{stu}\, d\bar{x}\, d\bar{y}\, d\bar{z}\, \frac{1}{\sqrt{\lambda^2}} \left[d\lambda^2\, (\cdot)|_{\sqrt{\lambda}=\lambda^2} + d\lambda^2\, (\cdot)|_{\sqrt{\lambda}=-\lambda^2}\right]. \tag{6.64}$$

From Eq. (6.63) and Eq. (6.21)-Eq. (6.23), we find

$$\begin{aligned}
\ell^2 &= (\bar{x}\bar{y})s - (\bar{x}\bar{z})u - (\bar{y}\bar{z})t + \lambda^2\epsilon_T^2, && (6.65)\\
\ell.k_1 &= \frac{1}{2}(\bar{y}s - \bar{z}u), && (6.66)\\
\ell.k_2 &= \frac{1}{2}(\bar{x}s - \bar{z}t), && (6.67)\\
\ell.k_3 &= \frac{1}{2}(\bar{x}(s+u) + \bar{y}(s+t) - \bar{z}(u+t)), && (6.68)\\
\ell.k_4 &= -\frac{1}{2}(\bar{x}u + \bar{y}t), && (6.69)
\end{aligned}$$

and

$$\delta(2\ell.(k_1+k_2)) = \frac{1}{(u+t)}\,\delta\left(\bar{z} - \frac{s}{u+t}(\bar{x}+\bar{y})\right). \qquad (6.70)$$

The integration over $\bar{z}$ can thus be done. The second δ-function in Eq. (6.42) allows to integrate over λ^2:

$$\delta((\ell+k_1)^2 - m^2) = \delta\left(\lambda^2 + \left[\frac{su}{u+t}(\bar{x}^2+\bar{x}) + \frac{st}{u+t}(\bar{y}^2-\bar{y}) + m^2\right]\right) \qquad (6.71)$$

We have for $d^4\ell$:

$$\begin{aligned}
\int d^4\ell(\cdot) &= \frac{1}{4}\frac{\sqrt{stu}}{u+t}\int (d\bar{x}d\bar{y})d\bar{z}\delta\left(\bar{z} - \frac{s}{u+t}(\bar{x}+\bar{y})\right)\frac{d(\lambda^2)}{\sqrt{\lambda^2}}\delta\left(\lambda^2 + [..]\right)(\cdot)\\
&= \frac{1}{4}\frac{\sqrt{stu}}{u+t}\int (d\bar{x}d\bar{y})\,\frac{1}{\sqrt{-\frac{su}{u+t}\left[\bar{x}^2+\bar{x}+\frac{t}{u}(\bar{y}^2-\bar{y})+\frac{u+t}{su}m^2\right]}}(\cdot)|_{...}\\
&= \frac{1}{4}\frac{\sqrt{stu}}{u+t}\int (d\bar{x}d\bar{y})\,\frac{1}{\sqrt{\lambda^2}}(\cdot)|_{...}\,. && (6.72)
\end{aligned}$$

We can rewrite the latter square root (*i.e.* λ),

$$\sqrt{\frac{-su}{u+t}\left[\bar{x}^2+\bar{x}+\frac{t}{u}(\bar{y}^2-\bar{y})+\frac{u+t}{su}m^2\right]} = \sqrt{\frac{-su}{u+t}(\bar{x}-\bar{x}_1(\bar{y}))(\bar{x}-\bar{x}_2(\bar{y}))} \qquad (6.73)$$

so that the condition $\bar{x}_2(\bar{y}) \leq \bar{x} \leq \bar{x}_1(\bar{y})$ giving the limits of integration over $\bar{x}$ appears clearly:

$$\bar{x}_{1,2}(\bar{y}) = -\frac{1}{2} \pm \frac{1}{2}\sqrt{1 - 4\frac{t}{u}\left(\bar{y}^2 - \bar{y} + \frac{u+t}{st}m^2\right)}\,. \qquad (6.74)$$

From this expression we also have a constraint upon the $\bar{y}$-integration. Similarly, the latter square root can be rewritten:

$$\sqrt{1 - 4\frac{t}{u}\left(\bar{y}^2 - \bar{y} + \frac{u+t}{st}m^2\right)} = \sqrt{-4\frac{t}{u}(\bar{y}-\bar{y}_1)(\bar{y}-\bar{y}_2)}. \qquad (6.75)$$

We see that if $t/u \geq 0$, then the expression is real for $\bar{y}_2 \leq \bar{y} \leq \bar{y}_1$, where

$$\bar{y}_{1,2} = \frac{1}{2} \pm \frac{1}{2}\sqrt{\frac{u+t}{t}\,\frac{s-4m^2}{s}} = \frac{1}{2} \pm \frac{1}{2}\frac{\sqrt{(s-M^2)(s-4m^2)}}{\sqrt{-st}} \tag{6.76}$$

From the boundary values $\bar{y}_1$ and $\bar{y}_2$, we also infer that $s \geq M^2$ and $s \geq 4m^2$. The integral from Eq. (6.72) then becomes:

$$\begin{aligned}\int d^4\ell\ (\cdot) &= \frac{1}{4}\frac{\sqrt{stu}}{u+t}\ \int_{\bar{y}_2}^{\bar{y}_1} d\bar{y} \int_{\bar{x}_2(\bar{y})}^{\bar{x}_1(\bar{y})} d\bar{x}\ \frac{1}{\sqrt{-\frac{su}{u+t}(\bar{x}-\bar{x}_1(\bar{y}))(\bar{x}-\bar{x}_2(\bar{y}))}}(\cdot)|_{\ldots} \\ &= \frac{1}{4}\frac{\sqrt{stu}}{u+t}\ \int [d\bar{x}d\bar{y}]\ \frac{1}{\sqrt{-\frac{su}{u+t}(\bar{x}-\bar{x}_1(\bar{y}))(\bar{x}-\bar{x}_2(\bar{y}))}}(\cdot)|_{\ldots}\end{aligned} \tag{6.77}$$

6.2.4 Organising the integration

In the same fashion, we rewrite the propagators in terms of the new variables of integration $(\bar{x}, \bar{y}, \bar{z}, \lambda)$:

$$\frac{1}{(\ell^2-m^2)} = \frac{u+t}{su}\,\frac{1}{\bar{x}-\frac{t}{u}\bar{y}} = -\frac{u+t}{st}\,\frac{1}{\bar{y}-\frac{u}{t}\bar{x}}\,, \tag{6.78}$$

$$\frac{1}{((\ell+k_1-k_2)^2-m^2)} = -\frac{u+t}{su}\,\frac{1}{\bar{x}-\frac{t}{u}\bar{y}+\frac{u+t}{u}} = \frac{u+t}{st}\,\frac{1}{\bar{y}-\frac{u}{t}\bar{x}-\frac{u+t}{t}}\,, \tag{6.79}$$

$$\frac{1}{((\ell-k_2+k_4)^2-m^2)} = -\frac{1}{u}\,\frac{1}{\bar{x}+\frac{t}{u}(\bar{y}-1)} = \frac{1}{t}\,\frac{1}{\bar{y}-1+\frac{u}{t}\bar{x}}\,, \tag{6.80}$$

$$\frac{1}{((\ell+k_1-k_4)^2-m^2)} = \frac{1}{u}\,\frac{1}{\bar{x}+\frac{t}{u}\bar{y}+1} = \frac{1}{t}\,\frac{1}{\bar{y}+\frac{u}{t}(\bar{x}+1)}\,, \tag{6.81}$$

$$\tag{6.82}$$

Concerning the vertex factors Γ_i, as discussed previously, we shall employ either the dipolar form or the gaussian form both with the shifted argument $p^2_{i,sh} = p_i^2 - \frac{(p_i.k_3)^2}{M^2}$ instead of p_i^2: The relative momentum squared p_i^2 is calculated from the momenta at the meson vertex

$$\begin{aligned}p_1^2 &= \frac{-u\bar{x}-t(\bar{y}-1)}{2} + m^2 - \frac{M^2}{4} = -\frac{s-4m^2+(2\bar{x}+1)u+(2\bar{y}-1)t}{4} \\ p_2^2 &= \frac{u(\bar{x}+1)+t\bar{y}}{2} + m^2 - \frac{M^2}{4} = -\frac{s-4m^2-(2\bar{x}+1)u-(2\bar{y}-1)t}{4}\end{aligned} \tag{6.83}$$

and we therefore obtain the following expressions for the argument of the vertex functions at the considered relative momenta:

$$\begin{aligned}p^2_{1,sh} &= \left(\frac{s-4m^2+(2\bar{x}+1)u+(2\bar{y}-1)t}{4} + \frac{(u\bar{x}+t(\bar{y}-1))^2}{4M^2}\right) \\ p^2_{2,sh} &= \left(\frac{s-4m^2-(2\bar{x}+1)u-(2\bar{y}-1)t}{4} + \frac{(u(\bar{x}+1)+t\bar{y}-M^2)^2}{4M^2}\right)\end{aligned} \tag{6.84}$$

and

$$\Gamma_i = \frac{N}{(1+\frac{p_{i,sh}^2}{\Lambda^2})^2} \text{ or } \Gamma_i = N\exp(-\frac{p_{i,sh}^2}{\Lambda^2}). \tag{6.85}$$

All integrals that we have to calculate can be recast in the following forms:

$$\begin{aligned}\int d_{PS} \quad & \frac{1}{(\ell^2-m^2)}\frac{1}{((\ell-k_2+k_4)^2-m^2)}\Gamma_i\times[\ldots] = -\frac{1}{8\pi^2}\frac{\sqrt{stu}}{4(u+t)} \\ & \frac{u+t}{su^2}\int[d\bar{x}d\bar{y}]\frac{1}{\sqrt{\lambda^2}}\frac{1}{\bar{x}-\frac{t}{u}\bar{y}}\frac{1}{\bar{x}+\frac{t}{u}(\bar{y}-1)}\Gamma_i\times[\ldots]\end{aligned} \tag{6.86}$$

$$\begin{aligned}\int d_{PS} \quad & \frac{1}{(\ell^2-m^2)}\frac{1}{((\ell+k_1-k_4)^2-m^2)}\Gamma_i\times[\ldots] = \frac{1}{8\pi^2}\frac{\sqrt{stu}}{4(u+t)} \\ & \frac{u+t}{su^2}\int[d\bar{x}d\bar{y}]\frac{1}{\sqrt{\lambda^2}}\frac{1}{\bar{x}-\frac{t}{u}\bar{y}}\frac{1}{\bar{x}+\frac{t}{u}\bar{y}+1}\Gamma_i\times[\ldots]\end{aligned} \tag{6.87}$$

$$\begin{aligned}\int d_{PS} \quad & \frac{1}{((\ell+k_1-k_2)^2-m^2)}\frac{1}{((\ell-k_2+k_4)^2-m^2)}\Gamma_i\times[\ldots] = \frac{1}{8\pi^2}\frac{\sqrt{stu}}{4(u+t)} \\ & \frac{u+t}{su^2}\int[d\bar{x}d\bar{y}]\frac{1}{\sqrt{\lambda^2}}\frac{1}{\bar{x}-\frac{t}{u}\bar{y}-\frac{u+t}{u}}\frac{1}{\bar{x}+\frac{t}{u}(\bar{y}-1)}\Gamma_i\times[\ldots]\end{aligned} \tag{6.88}$$

$$\begin{aligned}\int d_{PS} \quad & \frac{1}{((\ell+k_1-k_2)^2-m^2)}\frac{1}{((\ell+k_1-k_4)^2-m^2)}\Gamma_i\times[\ldots] = -\frac{1}{8\pi^2}\frac{\sqrt{stu}}{4(u+t)} \\ & \frac{u+t}{su^2}\int[d\bar{x}d\bar{y}]\frac{1}{\sqrt{\lambda^2}}\frac{1}{\bar{x}-\frac{t}{u}\bar{y}-\frac{u+t}{u}}\frac{1}{\bar{x}+\frac{t}{u}\bar{y}+1}\Gamma_i\times[\ldots],\end{aligned} \tag{6.89}$$

with $\lambda = \pm\sqrt{-\frac{su}{u+t}(\bar{x}-\bar{x}_1(\bar{y}))(\bar{x}-\bar{x}_2(\bar{y}))}$ in $[\ldots]$.

Let us introduce a short-hand notation for the denominators, the vertex functions and the jacobian $\frac{1}{\sqrt{\lambda^2}}$:

$$D_3(d_i,e_j,\Gamma_k) \equiv \frac{1}{\sqrt{\lambda^2}}\frac{1}{\bar{x}+d_i}\frac{1}{\bar{x}+e_j}\Gamma_k \tag{6.90}$$

with

$$d_1 = -\frac{t}{u}\bar{y}\,, \tag{6.91}$$

$$d_2 = -\frac{t}{u}\bar{y}+\frac{u+t}{u}\,, \tag{6.92}$$

$$e_1 = +\frac{t}{u}(\bar{y}-1)\,, \tag{6.93}$$

$$e_2 = +\frac{t}{u}\bar{y}+1\,. \tag{6.94}$$

defined so that

$$\begin{aligned}
\frac{1}{(\ell^2 - m^2)} &= \frac{u+t}{su}\,\frac{1}{\bar{x}+d_1}\,,\\
\frac{1}{((\ell+k_1-k_2)^2 - m^2)} &= -\frac{u+t}{su}\,\frac{1}{\bar{x}+d_2}\,,\\
\frac{1}{((\ell-k_2+k_4)^2 - m^2)} &= -\frac{1}{u}\,\frac{1}{\bar{x}+e_1}\,,\\
\frac{1}{((\ell+k_1-k_4)^2 - m^2)} &= \frac{1}{u}\,\frac{1}{\bar{x}+e_2}\,,
\end{aligned} \tag{6.95}$$

The amplitudes can then be written as[6]:

$$[\mathbf{I}][\mathbf{III}](p,q,r,s) = -\mathcal{C}\int [d\bar{x}d\bar{y}] D_3(d_1,e_1,\Gamma_1)\mathrm{tr}^{pqrs}_{I-III} \tag{6.96}$$

$$[\mathbf{I}][\mathbf{IV}](p,q,r,s) = +\mathcal{C}\int [d\bar{x}d\bar{y}] D_3(d_1,e_2,\Gamma_2)\mathrm{tr}^{pqrs}_{I-IV} \tag{6.97}$$

$$[\mathbf{II}][\mathbf{III}](p,q,r,s) = +\mathcal{C}\int [d\bar{x}d\bar{y}] D_3(d_2,e_1,\Gamma_1)\mathrm{tr}^{pqrs}_{II-III} \tag{6.98}$$

$$[\mathbf{II}][\mathbf{IV}](p,q,r,s) = -\mathcal{C}\int [d\bar{x}d\bar{y}] D_3(d_2,e_2,\Gamma_2)\mathrm{tr}^{pqrs}_{I-IV} \tag{6.99}$$

$$[\mathbf{I}][\mathbf{V_1}](p,q,r,s) = +\mathcal{C}\int [d\bar{x}d\bar{y}] \left[D_3(d_1,e_2,\Gamma_1) - D_3(d_1,e_2,\Gamma_2)\right]\mathrm{tr}^{pqrs}_{I-V_1} \tag{6.100}$$

$$[\mathbf{I}][\mathbf{V_2}](p,q,r,s) = -\mathcal{C}\int [d\bar{x}d\bar{y}] \left[D_3(d_1,e_1,\Gamma_1) - D_3(d_1,e_1,\Gamma_2)\right]\mathrm{tr}^{pqrs}_{I-V_2} \tag{6.101}$$

$$[\mathbf{II}][\mathbf{V_1}](p,q,r,s) = -\mathcal{C}\int [d\bar{x}d\bar{y}] \left[D_3(d_2,e_2,\Gamma_1) - D_3(d_2,e_2,\Gamma_2)\right]\mathrm{tr}^{pqrs}_{II-V_1} \tag{6.102}$$

$$[\mathbf{II}][\mathbf{V_2}](p,q,r,s) = +\mathcal{C}\int [d\bar{x}d\bar{y}] \left[D_3(d_2,e_1,\Gamma_1) - D_3(d_2,e_1,\Gamma_2)\right]\mathrm{tr}^{pqrs}_{II-V_2} \tag{6.103}$$

with

$$\mathcal{C} = \frac{1}{32\pi^2}\frac{\sqrt{stu}}{su^2} \tag{6.104}$$

Apart from the denominators and the vertex function in D_3, the only dependence on $[\bar{x}\bar{y}]$ left is contained in the tr_{X-Y} – through scalar products involving ℓ. Indeed, as we have seen, the decomposition of ℓ will introduce $\bar{x}$, $\bar{y}$, $\bar{z}$ and λ factors. The $\bar{z}$ factors are dropped in favour of $\bar{x}$ and $\bar{y}$. On the other hand, as λ has non-linear dependence on $\bar{x}$ and $\bar{y}$, we shall keep it explicitly.

It is also easy to convince oneself that we can decompose any tr_{X-Y} as:

$$tr_{X-Y} = \sum_{l,m,n} K^{tr_{X-Y}}_{l,m,n}\lambda^l \bar{x}^m \bar{y}^n, \tag{6.105}$$

[6] the + or − signs before $\mathcal{C}$ simply come from Eq. (6.95).

where $l, m, n = (0, 1, 2, 3, 4)$ and $l + m + n \leq 4$. This follows simply from the number of ℓ in each tr_{X-Y}. Nothing here will be stated about $K_{l,m,n}^{tr_{X-Y}}$, except that they do not contain $\bar{x}$ and $\bar{y}$, *i.e.* the integration variables.

Therefore, we are simply to perform one type of integrals

$$\begin{aligned} I(d_i, e_j, \Gamma_k; l, m, n) &\equiv \int [d\bar{x}d\bar{y}] \lambda^l \bar{x}^m \bar{y}^n D_3(d_i, e_j, \Gamma_k) \qquad (6.106) \\ &= \int [d\bar{x}d\bar{y}] \frac{\lambda^l \bar{x}^m \bar{y}^n}{\sqrt{-\frac{su}{u+t}(\bar{x} - \bar{x}_1(\bar{y}))(\bar{x} - \bar{x}_2(\bar{y}))}} \frac{1}{\bar{x} + d_i} \frac{1}{\bar{x} + e_j} \Gamma_k \\ &= \int [d\bar{x}d\bar{y}] \frac{\lambda^l \bar{x}^m \bar{y}^n}{\sqrt{\lambda^2}} \frac{1}{\bar{x} + d_i} \frac{1}{\bar{x} + e_j} \Gamma_k \,. \qquad (6.107) \end{aligned}$$

We already know that the integrals will vanish for l odd, as the two branches of the integrals over λ^2 cancel each other.

From this feature, we can also draw some conclusions on some helicity amplitudes. Indeed, the only way to make λ appear and not λ^2 is through the scalar product $\ell.\epsilon_T = \lambda$; all other possible scalar products with ℓ (see Eq. (6.65)) do not involve an odd power of λ. Since ϵ_T appears solely in $\varepsilon_i^{T_1}$, we can check that all amplitudes with an odd number of particles polarised along ϵ_T (vector orthogonal to the collision plane) vanish, as should be.

6.3 Polarised cross sections

Combining Eq. (6.105) with the expressions for the polarised amplitudes as in Eq. (6.96) and the generic expression for the integrals on the internal phase space Eq. (6.106), we have

$$\mathcal{M}(p, q, r, s) = \sum_{X,Y} [\mathbf{X}][\mathbf{Y}](p, q, r, s) = \sum_{X,Y} \sum_{l,m,n} K_{l,m,n}^{tr_{X-Y}^{pqrs}} I(d_i, e_j, \Gamma_k; l, m, n), \qquad (6.108)$$

the coefficients $K_{l,m,n}^{tr_{X-Y}^{pqrs}}$ are determined by FORM [97] and are functions[7] of $\hat{s}$, $\hat{t}$ and $\hat{u}$ whereas the integrals $I(d_i, e_j, \Gamma_k; l, m, n)$ are performed numerically for each sets of $\hat{s}$, $\hat{t}$ and $\hat{u}$ after having chosen the parameter defining Γ.

Squaring the sum of the expressions $[\mathbf{X}][\mathbf{Y}](p, q, r, s)$, multiplying them by $\frac{1}{64}$ for the averaging on initial colour, by $\frac{1}{4}$ for the averaging on initial spin, we get $|\overline{\mathcal{M}}(p, q, r, s)|^2$ to be plugged into Eq. (6.20). This in turn gives the polarised differential cross section $\frac{d\sigma(p,q,r,s)}{d\hat{t}}$.

As we are concerned with the polarisation effects only for the vector meson, we shall sum the various helicity contributions for the gluons and define the following polarised cross

[7] As now, we are dealing back with hadronic and partonic processes, we put the circumflexes back for the partonic Mandelstam variables.

sections:

$$\begin{aligned}\frac{d\sigma_{T_1}}{d\hat{t}} &= \sum_{p,q,s=T_1,T_2} \frac{d\sigma(p,q,T_1,s)}{d\hat{t}} \\ \frac{d\sigma_{T_2}}{d\hat{t}} &= \sum_{p,q,s=T_1,T_2} \frac{d\sigma(p,q,T_2,s)}{d\hat{t}} \\ \frac{d\sigma_{L}}{d\hat{t}} &= \sum_{p,q,s=T_1,T_2} \frac{d\sigma(p,q,L,s)}{d\hat{t}}\end{aligned} \tag{6.109}$$

The hadronic cross sections are therefore obtained with

$$\frac{d\sigma_h}{dydP_T} = \int_{x_1^{min}}^{1} dx_1 \frac{2\hat{s}P_T G_1(x_1)G_2(x_2(x_1))}{\sqrt{s}(\sqrt{s}x_1 - E_T e^y)} \frac{d\sigma_h}{d\hat{t}}, \tag{6.110}$$

for $h = T_1, T_2$ or L. Specifying s, y and P_T, we get the final result.

6.4 Numerical results and comparison with the CSM

The most natural comparison of our calculation is with the LO CSM predictions. Indeed, the structure of that calculation is similar to that of our model with solely the imaginary part of the amplitude. We recall here that the two quarks forming the meson are put on their mass shell in the CSM.

The comparison will be done with the unpolarised partonic cross section for $gg \to {}^3S_1 g$ obtained in [24]:

$$\frac{d\sigma}{d\hat{t}} = \frac{20\pi^2 M\alpha_s^3 |\psi(0)|^2}{9\hat{s}^2} \frac{[\hat{s}^2(\hat{s}-M^2)^2] + \left[\hat{t}^2(\hat{t}-M^2)^2\right] + [\hat{u}^2(\hat{u}-M^2)^2]}{(\hat{s}-M^2)^2(\hat{t}-M^2)^2(\hat{u}-M^2)^2}.$$

We shall use the gluon pdf's from CTEQ6LO fit [98] and MRST2001LO [99] evaluated at the scale $Q = \sqrt{M^2 + P_T^2}$. The coupling constant is computed as

$$\alpha_s(Q) = \frac{12\pi}{23\log(\frac{Q^2}{0.165^2})} \tag{6.111}$$

with 5 active flavours and $\Lambda_{QCD} = 0.165$ GeV [98]. Indeed, Q is above m_b as soon as P_T reaches 3-3.5 GeV for the J/ψ .

6.4.1 J/ψ at the Tevatron

Setting $\sqrt{s}$ to 1800 GeV and considering the cross section in the range $|\eta| < 0.6$, we get the following results for J/ψ production at the Tevatron in the experimental conditions of the CDF collaboration whose measurements are detailed in chapter 2. The first plot (see Fig. 6.4) shows our prediction (σ_{TOT}, σ_T and σ_L) for $m_c = 1.87$ GeV and $\Lambda = 1.8$ GeV to be

compared with the LO CSM (which does not depend on m_c) and the CSM fragmentation. We see that our prediction for the imaginary part of the amplitude is lower than the LO CSM, except at large P_T and is mostly longitudinal.

On the other hand, these results include the gauge-invariance restoring vertex whose choice is arbitrary. The conclusion drawn here might be only relevant for the GIPA, *i.e.* the standard pQCD set of diagrams with a phenomenological vertex for $q\bar{q} \to \mathcal{Q}$ and the gauge-invariance restoring term of Eq. (5.59). Differences between possible choices of gauge-invariance restoring vertices are described by what we call autonomous contributions, their effects are analysed in the next section.

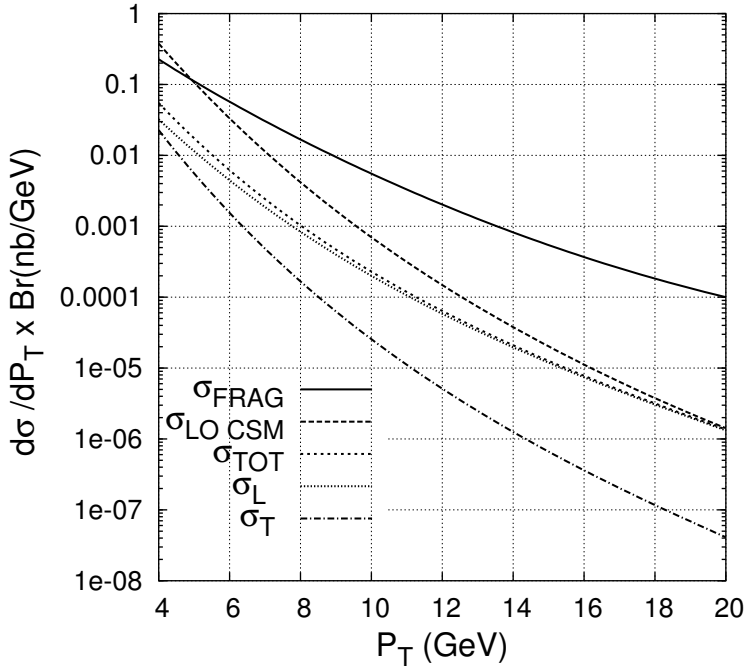

Figure 6.4: Polarised (σ_T and σ_L) and total (σ_{TOT}) cross sections obtained with a gaussian vertex functions, $m_c = 1.87$ GeV, $\Lambda = 1.8$ GeV and the MRST gluon distribution, to be compared with LO CSM and fragmentation CSM contributions.

Then, we illustrate (see Fig. 6.5 (a)) the effect due to a change in the form of the vertex functions, *i.e.* from a dipole to a gaussian. The effects due to a variation in Λ (see Fig. 6.5 (b)), m_c and Λ (see Fig. 6.5 (c)), due to a change in the scale $Q = \sqrt{M^2 + P_T^2}$ (see Fig. 6.5 (d)) are also shown.

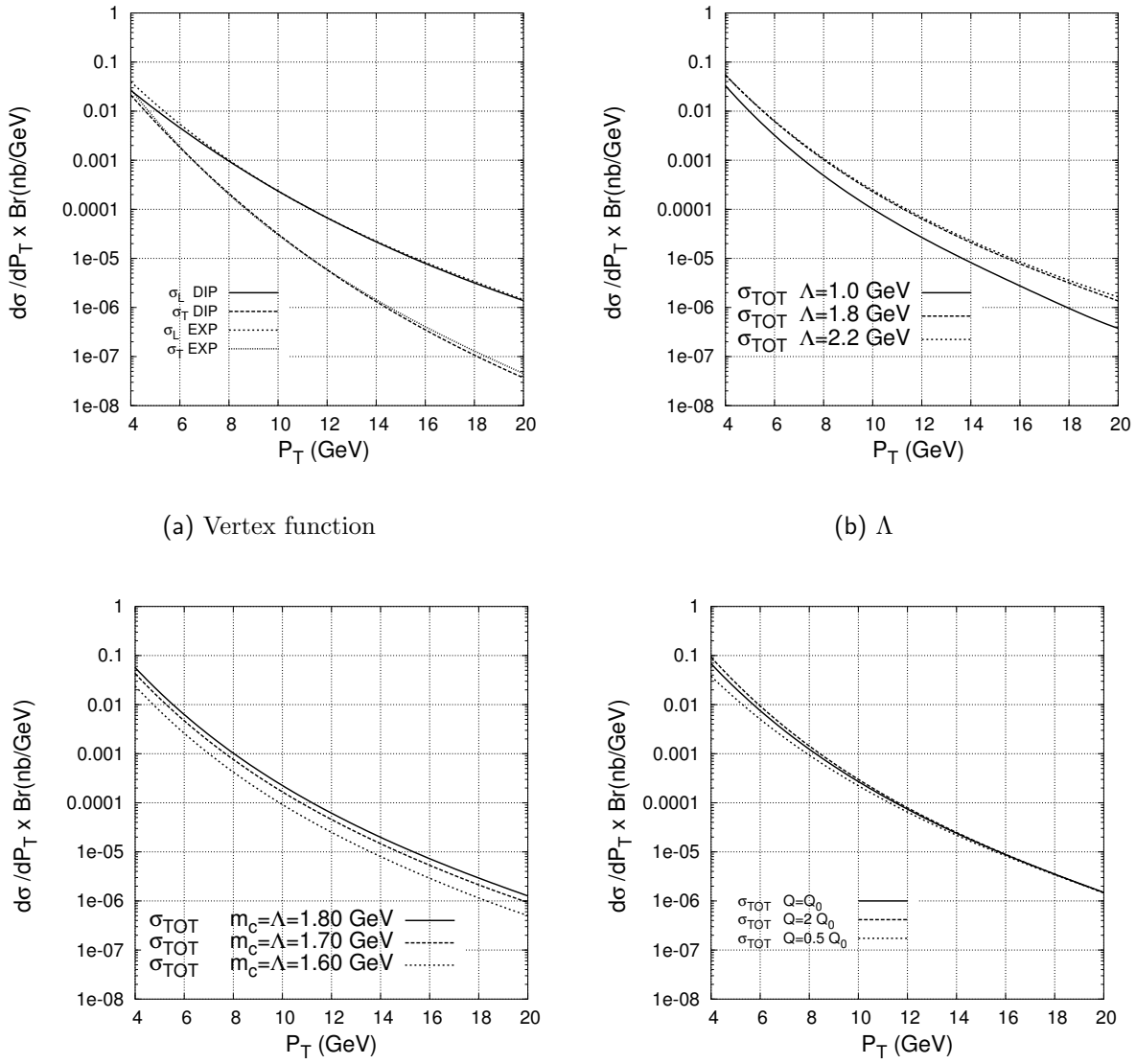

(a) Vertex function

(b) Λ

(c) Λ and m_c

(d) Scale

Figure 6.5: (a) Comparison between the cross section obtained with the dipole and the gaussian vertex functions (MRST); (b) Variation of the cross section due to a change in Λ for a fixed value of the quark mass (MRST); (c) Variation of the cross section due to a change in m_c and Λ (CTEQ); (d) Variation of the cross section due to a change of a factor two in the scale $Q = \sqrt{M^2 + P_T^2}$ (CTEQ).

As the changes in the vertex function illustrated above are of little influence on the final results, all the following plots for the J/ψ, unless specified differently, will be made for $m_c = 1.87$ GeV, $\Lambda = 1.8$ GeV, $Q = \sqrt{M^2 + P_T^2}$ and a gaussian vertex function.

6.4.2 $\Upsilon(1S)$ at the Tevatron

Here are similar plots for the $\Upsilon(1S)$ at the Tevatron ($\eta = 0$). The deviation of the GIPA with the CSM is slightly more marked, perhaps indicating that the deviation behaves like a power of $\frac{m_Q}{P_T}$. In the following, all plots for the $\Upsilon(1S)$, unless specified differently, will be made for $m_b = 5.28$ GeV, $\Lambda = 6.0$ GeV, $Q = \sqrt{M^2 + P_T^2}$ and a gaussian vertex function.

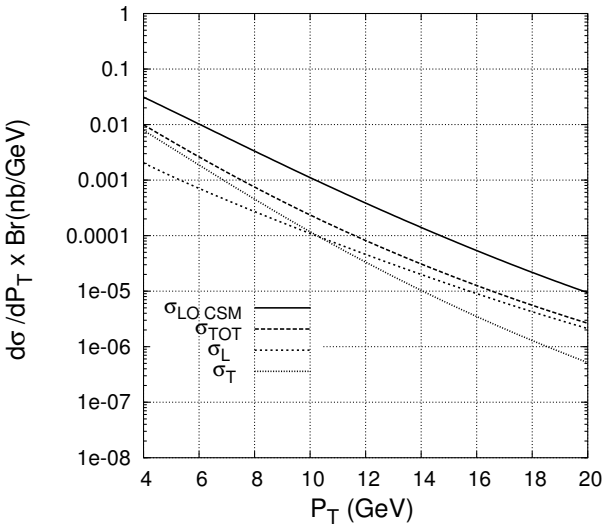

Figure 6.6: Polarised (σ_T and σ_L) and total (σ_{TOT}) cross sections obtained with a gaussian vertex functions, $m_b = 5.28$ GeV, $\Lambda = 6.0$ GeV and the CTEQ gluon distribution, to be compared with LO CSM and fragmentation CSM contributions

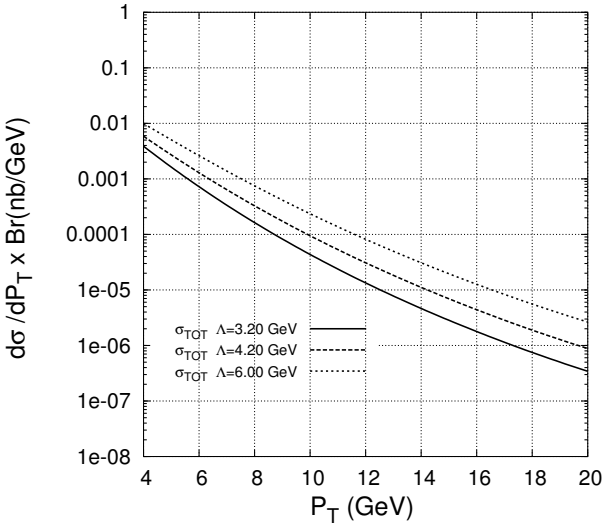

Figure 6.7: Variation of the cross section due to a change in Λ for a fixed value of the quark mass (CTEQ)

6.4.3 J/ψ at RHIC

Here are plots for the J/ψ at RHIC ($\sqrt{s} = 200$ GeV) (for $-0.5 < y < 0.5$).

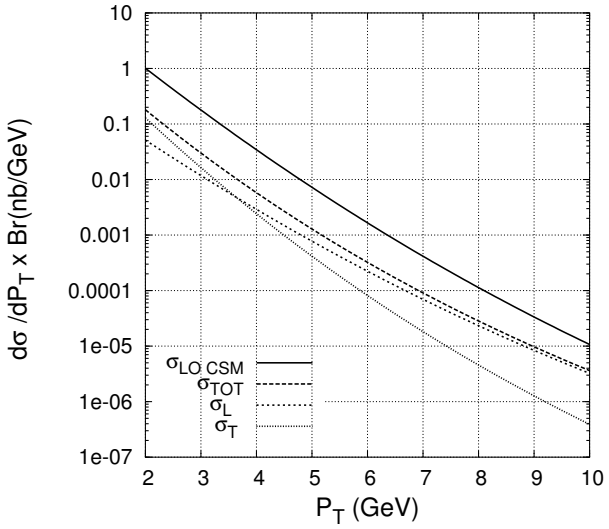

Figure 6.8: Polarised (σ_T and σ_L) and total (σ_{TOT}) cross sections obtained at $\sqrt{s} = 200$ GeV with a gaussian vertex functions, $m_c = 1.87$ GeV, $\Lambda = 1.8$ GeV and the CTEQ gluon distribution, to be compared with LO CSM.

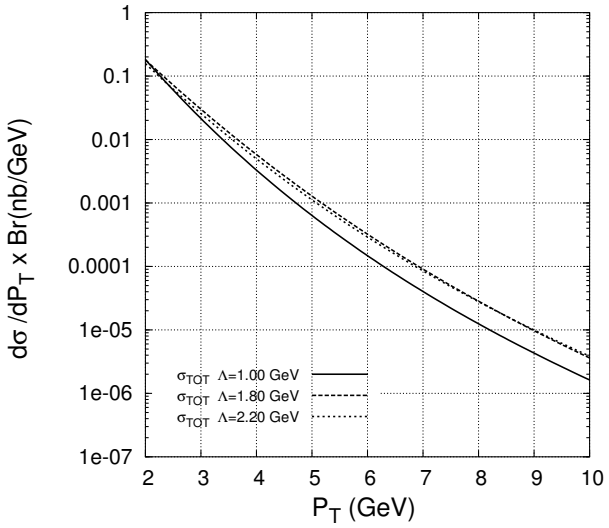

Figure 6.9: Polarised (σ_T and σ_L) and total (σ_{TOT}) cross sections obtained at $\sqrt{s} = 200$ GeV with a gaussian vertex functions, $m_c = 1.87$ GeV, $\Lambda = 1.8$ GeV and the CTEQ gluon distribution, to be compared with LO CSM.

6.4.4 ψ' at the Tevatron

Here we plot the cross section for the ψ' at $\sqrt{s} = 1800$ GeV with $m_c = 1.87$ GeV, $\Lambda = 1.8$ GeV and for three values of the node parameter a_{node}: 0.8, 1.46, 2.0 GeV (see Eq. (4.17) and Tab. (4.3)) We see that this parameter can have a significant influence. This comes from the fact that the normalisation strongly depends on the node position, whereas the production process is not very sensitive to this parameter.

In the following, we shall use $a_{node} = 1.46$ GeV, $m_c = 1.87$ GeV, $\Lambda = 1.8$ GeV and a gaussian vertex function.

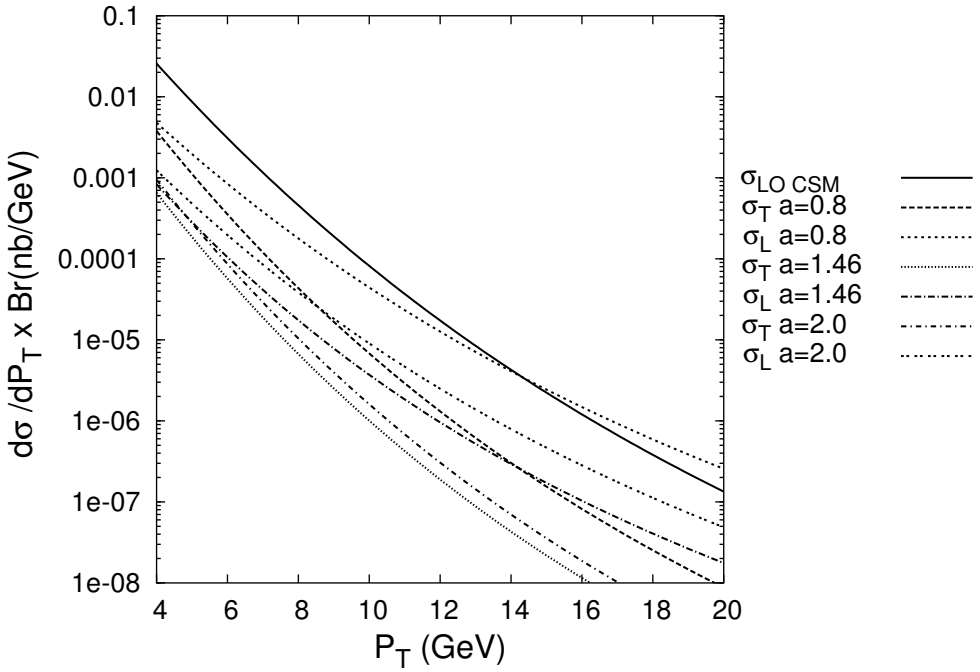

Figure 6.10: Polarised (σ_T and σ_L) cross sections obtained at $\sqrt{s} = 1800$ GeV with a gaussian vertex functions, $m_c = 1.87$ GeV, $\Lambda = 1.8$ GeV and the CTEQ gluon distribution for various values of a_{node}.

6.4.5 Taking stock of the situation

Following the discussion concerning the J/ψ at the Tevatron and RHIC, the Υ at the Tevatron and the ψ' at the Tevatron, we may draw some conclusions concerning the effects of changing the energy involved in the collision, the mass of the quarks and the internal structure of the quarkonium. We can first say that the main features of our predictions are not drastically affected by these changes.

To what concerns the deviation between the GIPA and the LO CSM, it seems that it is a permanent feature at low P_T. As we have said before, it indicates that the real part can be large. One important result of our study of non-static effects – or relativistic effects – is

the existence of a large uncertainty in ψ' production linked with the position of the node in the vertex function.

We have shown that it is possible to go beyond the static approximation and that our procedure does not show any instabilities and uncontrollable behaviour due to changes in m_q and Λ. Our procedure to normalise the vertex function also seems to work and to provide sensible values.

We have the hope that tuning the internal dynamics of the quarkonium in production processes could be applied to their study in media; for instance, to study their suppression due to an evolution in their size or due to an alteration of the binding of their constituting quarks.

However, numerous choices of gauge-invariance restoring vertices are possible. No firm conclusions should be drawn before we have an idea of the effects due to a change in them. The easiest way to get insights on this issue comes from the analysis of contributions that were derived in section 5.3. This is the subject of the following study.

6.5 Analysis of autonomous vertices

We now consider the contributions from autonomous vertices as in Eq. (5.65). We have simply to introduce sub-amplitude [**VI**], [**VII**], ..., whose expressions are obtained from the vertex chosen.

We limit ourselves to choices for the vertex coming from Eq. (5.69) with constant factors, we have therefore three possibilities, that we rewrite in the conventions of this chapter:

1. $(\Gamma_1 - \Gamma_2)\alpha\gamma^\mu q^\nu \to (\Gamma_1 - \Gamma_2)\alpha\gamma^\sigma k_4^\rho$ the "α-term"
2. $(\Gamma_1 - \Gamma_2)\beta\,(p+p')^\mu(p+p')^\nu \to (\Gamma_1 - \Gamma_2)\beta\,(2\ell + k_1 - k_2)^\rho(2\ell + k_1 - k_2)^\sigma$ the "β-term"
3. $(\Gamma_1 - \Gamma_2)\xi\, g^{\mu\nu} \to (\Gamma_1 - \Gamma_2)\xi\, g^{\rho\sigma}$ the "ξ-term"

Let us consider the first one. If we include it in our calculation, it will induce the following sub-amplitude to be added to the set [**III**] + [**IV**] + [**V**],

$$[\mathbf{VI}] = -i\alpha\,(\Gamma_1 - \Gamma_2)\,(-ig_s)T^c_{ki}\bar{u}(\ell - k_2)i\gamma^\sigma k_4^\rho u(\ell + k_1)\varepsilon_\rho^{r\star}(k_3)\varepsilon_\sigma^{s\star}(k_4). \tag{6.112}$$

Let us now have a closer look at the product $k_4^\rho\varepsilon_\rho^{r\star}(k_3)$. The latter is zero for $r = T$ (Eq. (6.32)), whereas for $r = L$ it is (Eq. (6.36))

$$\varepsilon^L(k_3).k_4 = \frac{\hat{s} - M^2}{2M}. \tag{6.113}$$

This contribution will thus produce solely longitudinal vector mesons. It is the ingredient needed for a possible solution of the polarisation issue. We shall come back to this fact when we analyse the numerical results.

In practice, the introduction of these contributions does not modify much the procedure to get the polarised cross section as explained in the previous sections. The main difference is the introduction of a new quantity

$$D_2(d_i,\Gamma_j) \equiv \frac{1}{\sqrt{\lambda^2}}\frac{1}{\bar{x}+d_i}\Gamma_k \tag{6.114}$$

which appears in the following new integrals,

$$[\mathbf{I}][\mathbf{VI}](p,q,r,s) = +\mathcal{C}'\int[d\bar{x}d\bar{y}]\,[D_2(d_1,\Gamma_1)-D_2(d_1,\Gamma_2)]\,\mathrm{tr}^{pqrs}_{I-VI} \tag{6.115}$$

$$[\mathbf{II}][\mathbf{VI}](p,q,r,s) = -\mathcal{C}'\int[d\bar{x}d\bar{y}]\,[D_2(d_2,\Gamma_1)-D_2(d_2,\Gamma_2)]\,\mathrm{tr}^{pqrs}_{II-VI}, \tag{6.116}$$

where $\mathcal{C}'$ is $\frac{1}{32\pi^2}\frac{\sqrt{\hat{s}\hat{t}\hat{u}}}{\hat{s}\hat{u}}$ and the quantities $\mathrm{tr}^{pqrs}_{I-VI}$ and $\mathrm{tr}^{pqrs}_{II-VI}$ are

$$\begin{aligned}\mathrm{tr}^{pqrs}_{I-VI} = &-\alpha g_s^3 \mathrm{Tr}\left[T^aT^bT^c\right]\mathrm{Tr}\left[\gamma^\mu\left(\not{\ell}+m\right)\gamma^\nu((\not{\ell}-\not{k}_2)+m)\right.\\ &\left.\times\gamma^\sigma((\not{\ell}+\not{k}_1)+m)\right]k_4^\rho\varepsilon^p_\mu(k_1)\varepsilon^q_\nu(k_2)\varepsilon^{r\star}_\rho(k_3)\varepsilon^{s\star}_\sigma(k_4)\end{aligned} \tag{6.117}$$

$$\begin{aligned}\mathrm{tr}^{pqrs}_{II-VI} = &-\alpha g_s^3 \mathrm{Tr}\left[T^bT^aT^c\right]\mathrm{Tr}\left[\gamma^\nu\left((\not{\ell}+\not{k}_1-\not{k}_2)+m\right)\gamma^\mu((\not{\ell}-\not{k}_2)+m)\right.\\ &\left.\times\gamma^\sigma((\not{\ell}+\not{k}_1)+m)\right]k_4^\rho\varepsilon^p_\mu(k_1)\varepsilon^q_\nu(k_2)\varepsilon^{r\star}_\rho(k_3)\varepsilon^{s\star}_\sigma(k_4)\end{aligned} \tag{6.118}$$

6.5.1 Numerical results

To get a first idea, we have introduced these vertices in the amplitude one by one with α, β or ξ equal[8] to 1. In Fig. 6.11, we show the individual contributions of these terms. Note that some of these produce only one helicity. One example already foreseen concerns the α-term whose transverse cross section is zero. However, if we want to fit the data, the autonomous vertices will need to be dominant, hence the GIPA and any interferences terms will not be important.

[8] Note that in this first application the coefficients α, β and ξ do not have the same dimension.

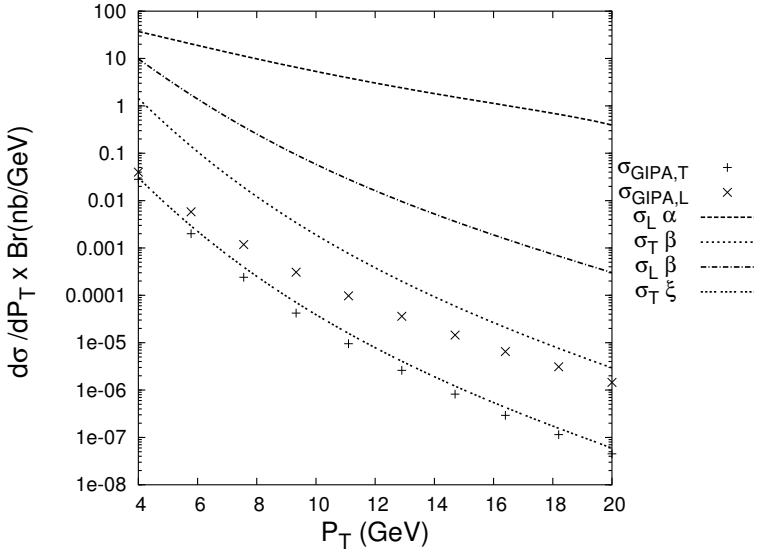

Figure 6.11: Polarised (σ_T and σ_L) cross sections for the J/ψ at the Tevatron obtained with three different autonomous vertices alone. Note that $\sigma_T^{\alpha} = \sigma_L^{\xi} = 0$.

The most striking result is that this latter contribution (α-term) has a slope compatible with the data. The contribution from the ξ-term has no longitudinal contribution[9] and its transverse component is slightly bigger than the GIPA. Yet, one might expect, since its dimension is lower, that the actual value of ξ would enhance it. The contribution of the β-term has no remarkable characteristic and considering its dimension, we do not expect β to enhance its contribution.

6.5.2 Fitting the data

We are then going to make use of these two unconstrained structures (α and ξ-terms). One is purely transverse whereas the other is purely longitudinal. This is a motivation to try to reproduce the behaviour of the polarisation parameter α_{pol} as measured by CDF (see section 2.5).

First we shall rescale the multiplicative factors α and ξ to get dimensionless parameters:

$$\begin{aligned} \alpha &\to \frac{\alpha}{\sqrt{\hat{s}} m_Q}, \\ \xi &\to \frac{\xi}{m_Q}. \end{aligned} \tag{6.119}$$

Note that this rescaling is purely arbitrary. It is far from obvious which quantity among $m_{\mathcal{Q}}$ (mass of the quarkonium), m_Q , Λ, Λ_{QCD}, $\sqrt{\hat{s}}$, ... is the most suitable. However, except for Λ_{QCD}, they are all of the same order. Besides, the uncertainties coming from the missing real part may modify the final values obtained in the fit.

[9] This can be also foreseen since $g^{\rho\sigma}\varepsilon_{\rho}^{r\star}(k_3)\varepsilon_{\sigma}^{s\star}(k_4) = \varepsilon^{r\star}(k_3).\varepsilon^{s\star}(k_4)$ is zero for $r = L$ (see section 6.2.1).

J/ψ at the Tevatron

Setting α to 8 and ξ to 37.5, we reproduce the cross section for J/ψ at $\sqrt{s} = 1800$ GeV [43] as displayed in Fig. 6.12. However since σ_L is much larger than σ_T for $P_T \gtrsim 10$ GeV, we predict that α_{pol} will be negative for $P_T \gtrsim 6$ GeV at variance with COM fragmentation predictions, for which α_{pol} is significantly positive. This fact can easily traced back to the steeper slope of the ξ-term compared to the α-term (see Fig. 6.11 (b)).

$\Upsilon(1S)$ at the Tevatron

Setting α to 8 and ξ to 10, we reproduce the cross section for $\Upsilon(1S)$ at $\sqrt{s} = 1800$ GeV [60] as shown in Fig. 6.13. We observe the same behaviour as in the J/ψ case to what concerns σ_L relative to σ_T and we predict that α_{pol} will be negative for $P_T \gtrsim 8$ GeV.

J/ψ at RHIC

Since the P_T range of the data [55] is not very wide and the error bars are rather large, we use the same values for α and ξ as for the Tevatron energy. Furthermore, our calculation (Fig. 6.14) agrees with the data, even though slightly improved agreement could be obtained with a different set of values for α and ξ. To what concerns polarisation, we predict that α_{pol} will be positive for $P_T \lesssim 4$ GeV and negative for larger values of P_T.

Note that our LO CSM curve includes solely gluon fusion at variance with curves of Nayak *et al.* [67] which include all parton-fusion processes.

ψ' at the Tevatron

Setting a_{node} to 1.46 GeV and α to 27.5, we get the cross section for ψ' at $\sqrt{s} = 1800$ GeV as shown in Fig. 6.15. This fits perfectly the data obtained by CDF [43]. There is no need to introduce any contribution from the ξ-term and we predict that the cross section is longitudinally polarised.

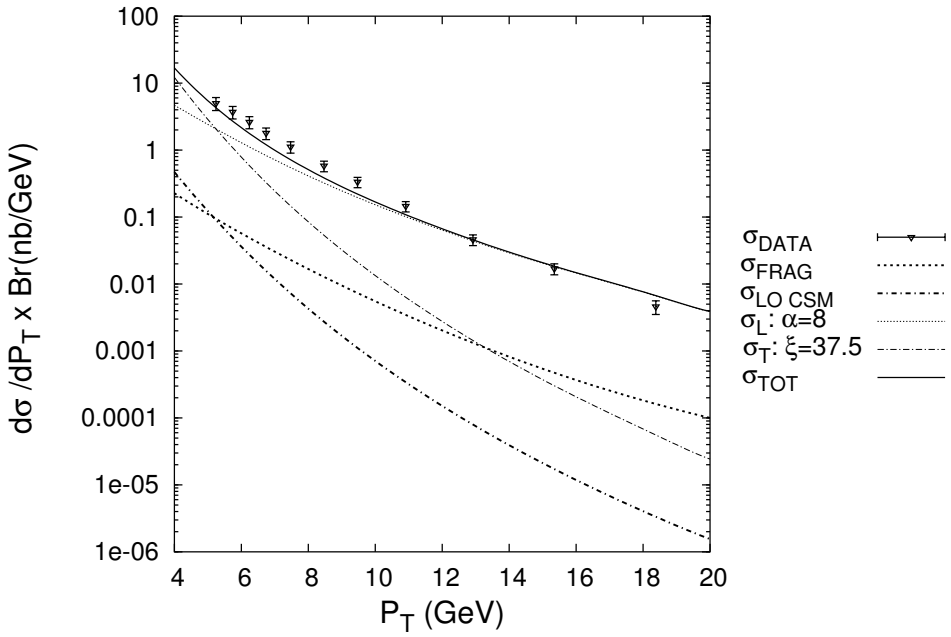

Figure 6.12: Polarised (σ_T and σ_L) and total (σ_{TOT}) cross sections obtained for J/ψ at $\sqrt{s} = 1800$ GeV with $\alpha = 8$ and $\xi = 37.5$ to be compared with LO CSM, the fragmentation CSM and to the data of CDF [43].

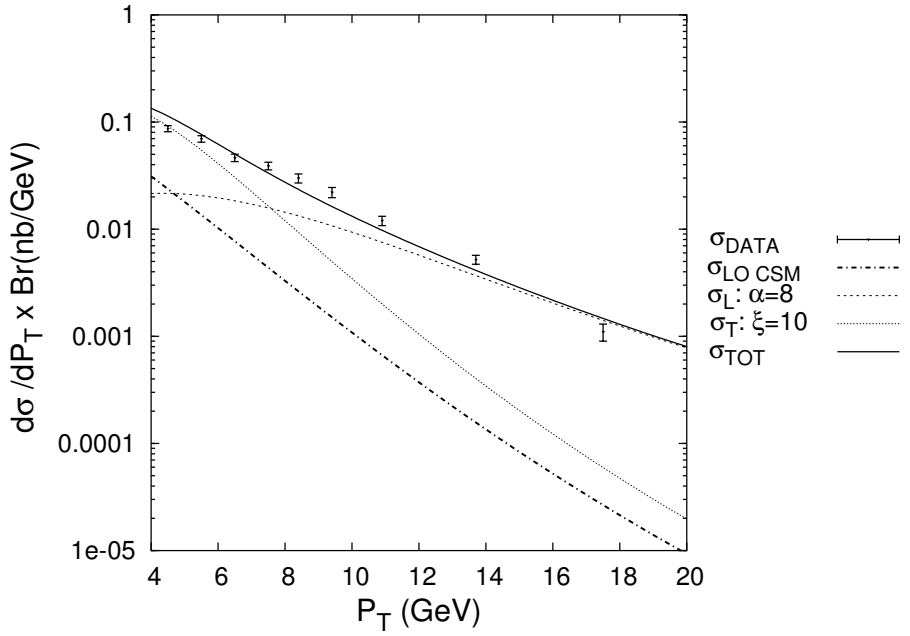

Figure 6.13: Polarised (σ_T and σ_L) and total (σ_{TOT}) cross sections obtained for $\Upsilon(1S)$ at $\sqrt{s} = 1800$ GeV with $\alpha = 8$ and $\xi = 10$ to be compared with LO CSM and to the data of CDF [60].

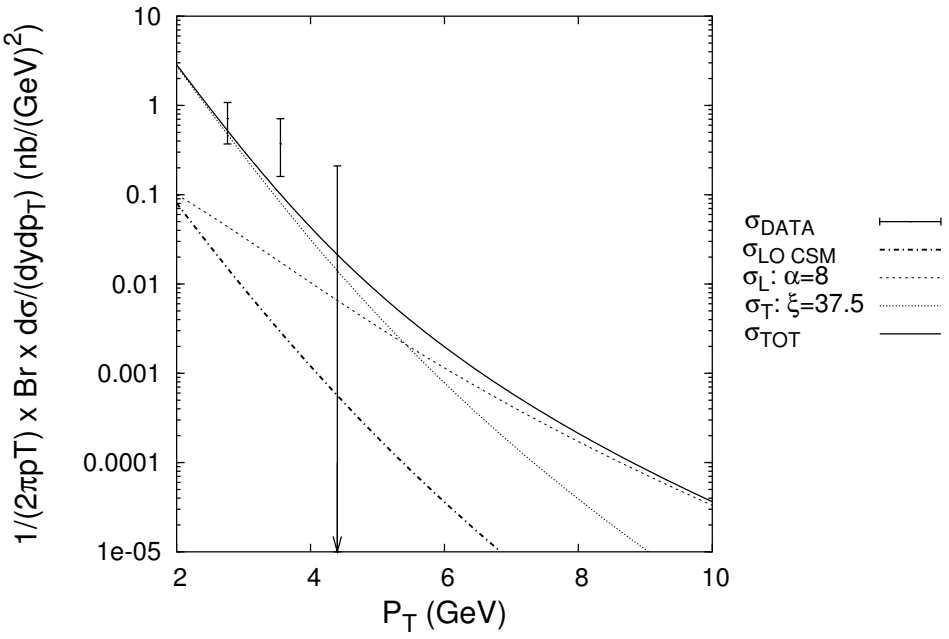

Figure 6.14: Polarised (σ_T and σ_L) and total (σ_{TOT}) cross sections obtained for J/ψ at $\sqrt{s} = 200$ GeV with $\alpha = 8$ and $\xi = 37.5$ to be compared with LO CSM and to the data of PHENIX [55].

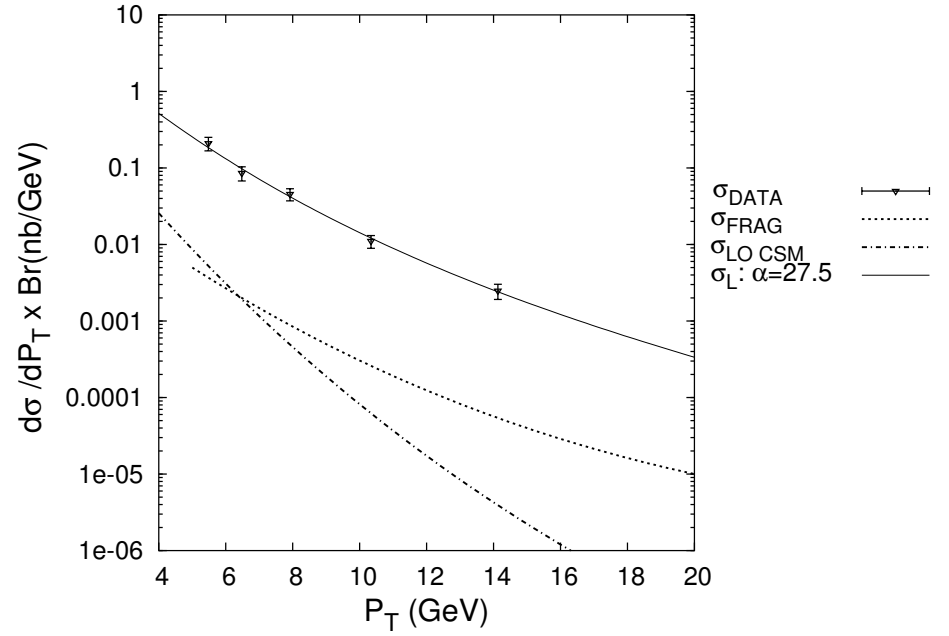

Figure 6.15: Polarised (σ_T and σ_L) and total (σ_{TOT}) cross sections obtained for ψ' at $\sqrt{s} = 1800$ GeV with $\alpha = 27.5$ to be compared with LO CSM, the fragmentation CSM and to the data of CDF [43].

6.5.3 Refining for the polarisation

Following the discussion of Tab. (1.14), we know that fragmentation-like processes should dominate for sufficiently large P_T. We have not yet included these in our calculation. Since the COM contribution is mainly transverse[10] and can account with appropriate LDME (Long-Distance Matrix Element) value for the CDF data [50], we are going to combine it with our contribution from the α-term which is purely longitudinal and which can also account for the data.

The amplitude to produce a ${}^3S_1$ quarkonium $\mathcal{Q}$ by fragmentation of a colour octet state ${}^3S_1^{(8)}$ is given by

$$|\mathcal{M}(gg \to {}^3S_1^{(8)} g \to {}^3S_1 g)|^2 = \overline{\sum_T} |\mathcal{A}(gg \to {}^3S_1^{(8)} g)|^2 \langle \mathcal{O}^{\mathcal{Q}}[{}^3S_1^{(8)}] \rangle \tag{6.120}$$

with for a transverse polarisation state [50]

$$\begin{aligned}\overline{\sum_T} |\mathcal{A}(gg \to {}^3S_1^{(8)} g)|^2 = -\frac{(4\pi\alpha_s)^3}{144M^3} \frac{\hat{s}^2}{(\hat{s}-M^2)^2} \left[(\hat{s}-M^2)^4 + \hat{t}^4 + \hat{u}^4 + 2M^4 \left(\frac{\hat{t}\hat{u}}{\hat{s}} \right)^2 \right] \times \\ \times \frac{27(\hat{s}\hat{t}+\hat{t}\hat{u}+\hat{u}\hat{s}) - 19M^4}{[(\hat{s}-M^2)(\hat{t}-M^2)(\hat{u}-M^2)]^2}\end{aligned} \tag{6.121}$$

and for a longitudinal polarisation state [50]

$$\overline{\sum_L} |\mathcal{A}(gg \to {}^3S_1^{(8)} g)|^2 = -\frac{(4\pi\alpha_s)^3}{144M^3} \frac{2M^2\hat{s}}{(\hat{s}-M^2)^2} (\hat{t}^2+\hat{u}^2)\hat{t}\hat{u} \frac{27(\hat{s}\hat{t}+\hat{t}\hat{u}+\hat{u}\hat{s}) - 19M^4}{[(\hat{s}-M^2)(\hat{t}-M^2)(\hat{u}-M^2)]^2} \tag{6.122}$$

and where the LDME $\langle \mathcal{O}^{\mathcal{Q}}[{}^3S_1^{(8)}] \rangle$ depends on $\mathcal{Q}$. The longitudinal cross section is suppressed by $\frac{\hat{s}}{M^2}$ and therefore always small compared to its transverse counterpart.

Combining our contribution and COM fragmentation with smaller coefficients (roughly decreasing the cross section of each contribution of a factor of 2), we should recover a good description of the measured cross section as a function of P_T but also a reasonable description of the evolution of the polarisation parameter $\alpha_{pol} = \frac{\sigma_T - 2\sigma_L}{\sigma_T + 2\sigma_L}$ as a function of P_T .

J/ψ at the Tevatron

Setting α to 4.2, ξ to 26.5 and $\langle \mathcal{O}^{J/\psi}({}^3S_1^{(8)}) \rangle$ to 4×10^{-3} GeV^3, we got the cross section for the J/ψ at $\sqrt{s} = 1800$ GeV shown in Fig. 6.16. This fits rather well the cross section measured by CDF [60]. To what concerns polarisation data [52], they are only available for prompt J/ψ and not for the direct component of the signal for which our prediction are relevant. However, we can say that we obtain the same trend (see Fig. 6.17).

[10] We shall not consider its longitudinal part in plots, even though we included it in our calculation for the sake of completeness, plotting them would have diminished the readability of the plots.

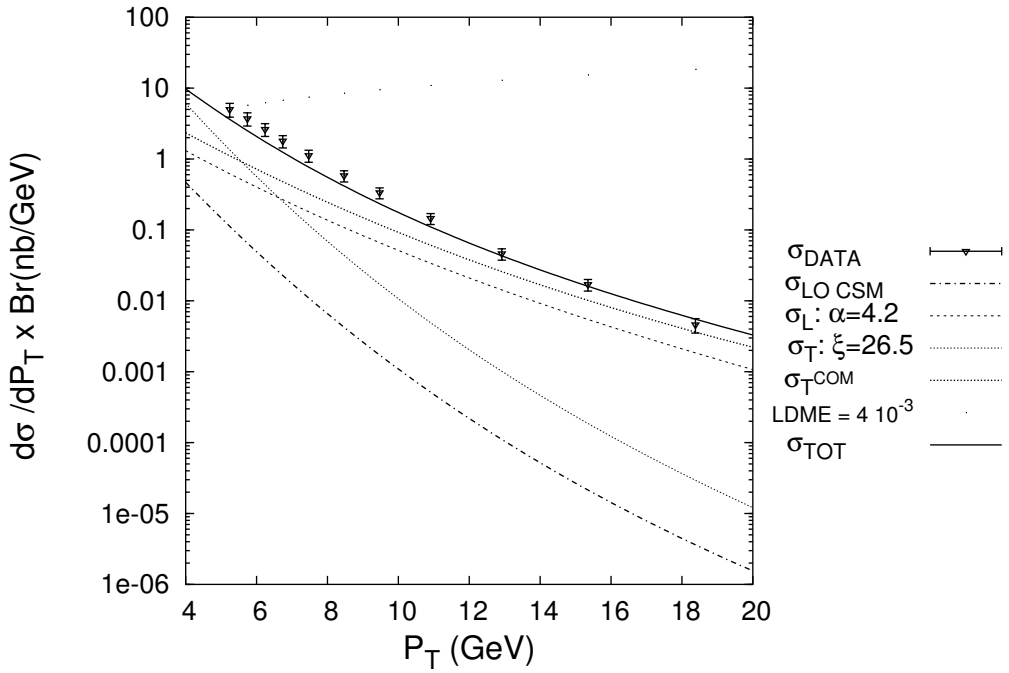

Figure 6.16: Various cross sections (see legend) obtained for the J/ψ at $\sqrt{s} = 1800$ GeV with $\alpha = 4.2$ and $\xi = 26.5$ and with a COM contribution with $\langle \mathcal{O}^{J/\psi}(^3S_1^{(8)}) \rangle = 4 \times 10^{-3}$ GeV^3 to be compared with LO CSM and to the data of CDF [43].

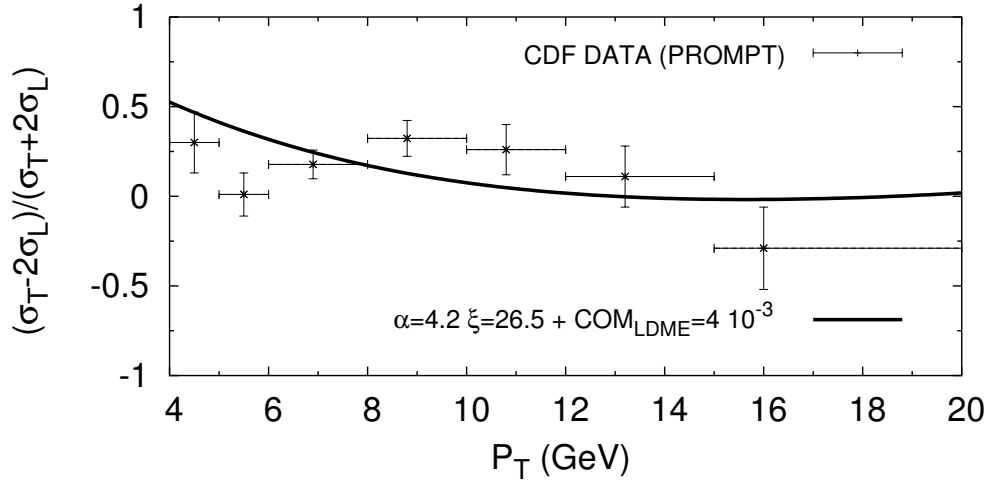

Figure 6.17: The polarisation parameter $\alpha_{pol} = \frac{\sigma_T - 2\sigma_L}{\sigma_T + 2\sigma_L}$ obtained for the J/ψ at $\sqrt{s} = 1800$ GeV with $\alpha = 4.2$ and $\xi = 26.5$ and with a COM contribution with $\langle \mathcal{O}^{J/\psi}(^3S_1^{(8)}) \rangle = 4 \times 10^{-3}$ GeV^3.

ψ' at the Tevatron

With $a_{node} = 1.46$ GeV, setting α to 17.5 and $\langle \mathcal{O}^{\psi'}({}^3S_1^{(8)}) \rangle$ to 4.5×10^{-3} GeV^3, we get the cross section for the ψ' at $\sqrt{s} = 1800$ GeV shown in Fig. 6.18 and the polarisation parameter α_{pol}, in Fig. 6.19. The agreement is quite good both for cross section and for the polarisation.

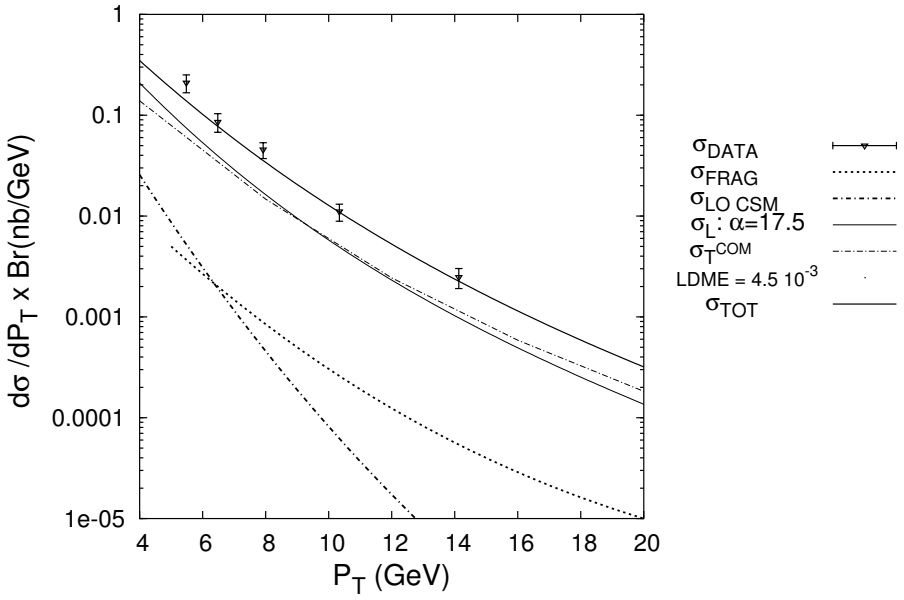

Figure 6.18: Various cross sections (see legend) obtained for ψ' at $\sqrt{s} = 1800$ GeV with $\alpha = 17.5$ and with a COM contribution with $\langle \mathcal{O}^{\psi'}({}^3S_1^{(8)}) \rangle = 4.5 \times 10^{-3}$ GeV^3 to be compared with LO CSM and to the data of CDF [43].

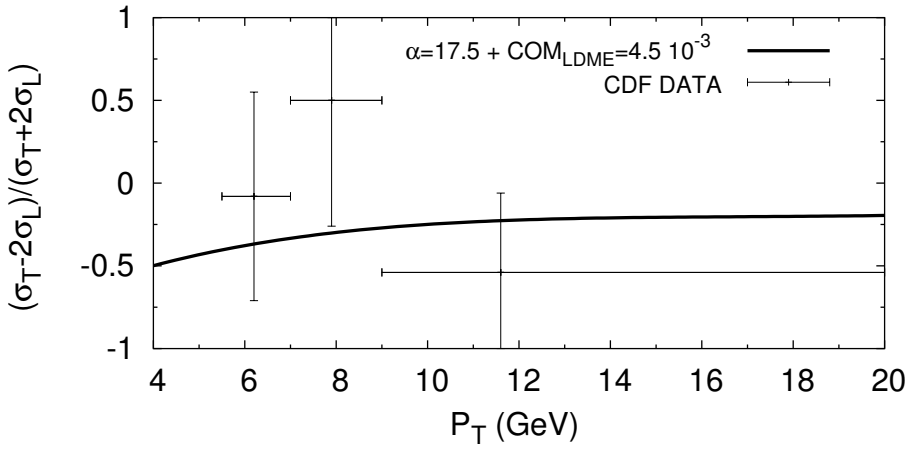

Figure 6.19: The polarisation parameter $\alpha_{pol} = \frac{\sigma_T - 2\sigma_L}{\sigma_T + 2\sigma_L}$ obtained for the ψ' at $\sqrt{s} = 1800$ GeV with $\alpha = 17.5$ and with a COM contribution with $\langle \mathcal{O}^{\psi'}({}^3S_1^{(8)}) \rangle = 4.5 \times 10^{-3}$ GeV^3, to be compared with the CDF measurements [52].

In brief

Our fitted values for α and ξ are:

1. Without COM contribution:
   - for the J/ψ at the Tevatron: α=8 – ξ=37.5
   - for the J/ψ at RHIC: cf. Tevatron
   - for the $\Upsilon(1S)$ at the Tevatron: α=8 – ξ=10
   - for the ψ' at the Tevatron: α=27 – ξ: $0 < \xi \lesssim 30$ (not constrained)
2. With COM contribution:
   - for the J/ψ at the Tevatron: α=4.2 – ξ=26.5 – $\langle \mathcal{O}^{J/\psi}(^3S_1^{(8)}) \rangle = 4.0 \times 10^{-3}$ GeV^3
   - for the ψ' at the Tevatron: α=17.5 – ξ: $0 < \xi \lesssim 30$ (not constrained) – $\langle \mathcal{O}^{\psi'}(^3S_1^{(8)}) \rangle = 4.5 \times 10^{-3}$ GeV^3

Chapter 7

Conclusions and outlook

"Use NRQCD !". I shall never forget this wise and humoristic reply of Eric Braaten to me when I asked him what to do to go beyond the CSM – and its static approximation – without having problems with gauge-invariance. Indeed, that approximation implying that whatever the hard part could be, the non-relativistic nature of the quarkonium should reduce the problem to a static one, was seriously disturbing me. Of course, NRQCD was a way to probe the internal dynamics of the quarkonium, but still, the quark in the bound state were always considered at rest.

Now, are we in position to reply that we could go beyond this static approximation and that we included relativistic effects in the calculation ? On the one hand, yes. We have introduced a relative momentum in the problem, we have tackled the issue of gauge invariance, we have constrained our model and we have applied it to processes for which the CSM was failing.

On the other hand, no. We have not calculated the real part of the amplitude and the contribution from the imaginary part is lower than the LO CSM at low P_T. However, we have shown that the choice of the gauge-invariance restoring vertex is not unique: this is the price to pay to introduce non-static effects. And, then, things are getting very interesting since we can reproduce the data, both from the Tevatron and from RHIC. This is the first time that a model can reproduce both the rate and the polarisation of the data.

What we did

Let us recall one by one the achievements of this thesis. As we have just said, our aim was to introduce non-static relativistic effects in the problem of hadroproduction of quarkonium, especially for the J/ψ, ψ' and the Υ for which data are numerous, reliable but in evident contradiction with the models derived from pQCD.

In chapter 3, we studied the theoretical uncertainties affecting the LO CSM, as an indication of those affecting all models. These uncertainties being a factor 3, our conclusion was that something new was to be introduced, like the colour-octet contributions brought in by NRQCD.

The way that we have chosen to introduce non-static effects was via a phenomenologi-

cal 3-particle vertex, made of a Dirac structure inferred from the quantum numbers of the considered quarkonium and a vertex function inspired by phenomenological arguments. Of course, the vertex function was to be constrained. Firstly, its size parameter – telling us how rapidly it falls when the relative momentum of the quarks inside the quarkonium increases – was chosen to be compatible with existing theoretical studies. Secondly, the factor multiplying the vertex – the normalisation N – was fixed to reproduce the leptonic decay width.

In the case of the ψ', we showed that the normalisation, or equivalently the decay width, was strongly affected by a change in the position of the node in the vertex function.

Whereas the choice of the vertex function was driven by phenomenological considerations, the method, which we have proposed to restore gauge invariance was based on a rigorous and *ab initio* derivation exposed in chapter 5. First, we stated how gauge invariance was broken by the introduction of a 3-particle vertex function in the case of a pseudoscalar bound state. This was followed by the description of how to restore gauge invariance, keeping in mind that this procedure, which introduces new 4-particle vertices in the calculation, was not unique.

We considered the same problem for vector particles associated with a gluon. The same conclusions were drawn, and we also studied in details how to parametrise the freedom left in the 4-particle vertex. Indeed, we have given simple and easily manageable Feynman rules for what we have called "autonomous" contributions, which correspond to different choices in the gauge-invariance restoring vertices. Note that the new contributions disappear in the case of point-like particles, for which there is no problem with gauge invariance.

In chapter 6, we have applied our model to the hadroproduction of quarkonia associated with a gluon, with the sole consideration of the imaginary part of the amplitude. This constraint comes from the necessity of having internal quark on-shell to derive the new vertices. We made the calculations, first, for one choice of a gauge-invariance restoring vertex, then, for the same contribution with autonomous vertices whose weights were fitted to reproduce the cross-sections and, finally, with the further addition of colour-octet fragmentation contributions to reproduce the polarisation data.

What we have obtained

The main result that we have obtained is that one autonomous contribution is naturally dominant and produces only longitudinally polarised quarkonia. Moreover, the P_T slope of this contribution is compatible with the data. Indeed, it is expected that any non vanishing scalar product with a helicity vector of a longitudinally polarised quarkonium should scale like $\hat{s}$, which, at threshold, is proportional to P_T^2. This explains why longitudinal components have a less steep slope.

If we combine this contribution with colour-octet fragmentation, which is also naturally large and produces only transversally polarised quarkonia, we can reach a perfect agreement with all existing data and with a minimal number of free parameters.

This combination with colour-octet fragmentation was actually motivated by the fact that we were missing fragmentation contributions, which are expected to be significant, due

to their P_T slope (see Fig. 1.14).

Our new contribution is the only one, which is able to produce only longitudinally polarised quarkonium.

Of course, we obtained other results. We have managed to introduce relativistic effects in the sense that we took account of contributions with nonzero relative momentum – non-static configurations – between the two constituent quarks. Our estimate of the imaginary part is lower than the LO CSM at low P_T, but of the same order at large P_T. We also got some interesting insights on the influence of the node of the $2S$ states.

More generally we have provided a formalism to study effects that come from the internal structure of the quarkonia and that were never considered before. One very interesting application would be to study the effect of a variation of the binding potential on the production cross-section of quarkonia. This variation of potential could for instance be introduced to study the influence of the quark-gluon plasma.

What we still miss

Even though these results are new, there are still some drawbacks. The first is the missing real part. If we take the LO CSM as a benchmark, the real part seems to be dominant over the imaginary part at low P_T. One way to calculate it would be to use dispersion relations. However, due to the expected asymptotic $\log \hat{s}$ behaviour of the partonic amplitude, we have to introduce a subtraction constant in the dispersion relation. Furthermore, this constant is a function of P_T. We could fix it by fitting the data at a given energy and make predictions for different energies. In the present situation, the data from RHIC have too small a P_T range to proceed through the analysis. The second missing point it that our description of the quarkonia does not take into account cuts in the vertices.

These missing contributions make us believe that the fits which we have made are reliable only up to a factor of order 3.

Another thing that we miss is an understanding of how the autonomous contributions arise. One of the three autonomous contributions that we have considered, namely the ξ-term ($g^{\mu\nu}$), could come from off-shell contributions. This can be seen easily by setting a different quark mass in the off-shell quark propagator in Eq. (5.33) and performing the classification of the different Dirac structures with their factors. However, for the other ones, we have currently no simple argument to motivate their presence, except that they exist in the standard contribution and that their slope in P_T is expected to be quite low, explaining why they dominate at large P_T.

What is expedient to do

A first necessary test of our formalism would be to apply it to production regimes other than hadroproduction. The application to photoproduction at HERA is the first that comes to mind. Moreover, results on photoproduction are compatible with NLO calculations within the CSM [53] and no contribution from colour-octet mechanisms are needed. In that context, a smaller value of the LDME's fixed by the fits on hadroproduction data would be welcome,

while our model provides with smaller ones. For all these reasons, we do plan to consider photoproduction in a close future.

Besides photoproduction, electroproduction is also expected to provide us with interesting tests and constraints. Compared to photoproduction, the kinematics would be slightly modified. There exist data from LEP and a comparison with those would also be useful.

Finally, in the case of B-factories, the situation is even more appealing, since both the CSM and the COM diagree with Belle data. For some observables, the discrepancy amounts to more than one order of magnitude. Let us mention the double-charm production, *e.g.* $e^+e^- \to J/\psi + \eta_c$, and the inclusive production rate. However, a confirmation from BaBar of theses discrepancies would be greatly welcome.

In a totally different context, another attractive application is the modelisation of Generalised Parton Distributions (GPD). In previous works, we have worked out these for the pion in a simple but rough model where the restoration of gauge invariance was achieved by symmetrising the vertex function $\Gamma_{(1,2)} \to \Gamma_1 + \Gamma_2$. The result were encouraging, however we have now the tools to greatly refine this model. An important asset of our approach is the possibility to cast off the obligation to work on the light cone.

Moreover, as mentioned a couple of times, the application to production in media is opportune. For some time now, J/ψ has been thought to be an ideal probe for quark-gluon plasma through its suppression. Besides the fact that the absolute rates are not completely understood – as we have seen throughout this work –, the way to introduce modification in the quark binding induced by the hadronic medium are not completely settled. Our formalism may be used to study these processes.

If we now turn back to the formalism rather than to its possible applications and tests, we are thinking to try to justify the presence of these autonomous 4-particle vertices from first principles, *e.g.* from standard perturbative Feynman rules applied to some typical sets of diagrams. We would then obtain an estimate of the free parameters α, β and ξ, possibly in a similar fashion than the velocity scaling rules in NRQCD.

Another direct improvement of our formalism would be of course the consideration of the real part of the amplitude. We have already addressed the possibility of making use of dispersion relation with the drawback which is the presence of arbitrary subtraction constants. Another way may be to generalise our gauge-invariance restoring vertices to off-shell quarks. Then, we would be in position to consider the real part at any $\hat{s}$ or to determine it at a precise value of $\hat{s}$, providing us with the value of the subtraction constants of the dispersion relations.

By showing that it was possible to *build* a model reproducing all available data on high-energy hadroproduction of quarkonia, we do believe that we have provided a new subject of discussion and research and, hopefully, shed some light on what may be considered to be the path to a resolution of this issue.

Appendix A

Acronyms and abbreviations

AGS	Alternating Gradient Synchrotron
BNL	Brookhaven National Laboratory
BSE	Bethe-Salpeter Equation
CDF	Collider Detector at Fermilab
CERN	Conseil Européen pour la Recherche Nucléaire
CES	Central Electromagnetic Strip chambers
c.m.	center-of-momentum
CMP	Central Muon Upgrade
CEM	Colour Evaporation Model
CLEO	CLEO(patra)[1] or Cornell's Largest Experimental Object (or Operation or Organization)
COM	Colour Octet Mechanism
CSM	Colour Singlet Model
CTC	Central Tracking System
DESY	Deutsches Elektronen-Synchrotron
DSE	Dyson-Schwinger Equation
EMC	ElectroMagnetic Calorimeter
FNAL	Fermi National Accelerator Laboratory (Fermilab)
GIPA	Gauge-Invariant Phenomenological Approach
GPD	Generalised Parton Distribution
HERA	Hadron Elektron Ring Anlage (Hadron Electron Ring Accelerator)
ISR	Intersecting Storage Rings
KEK	Kou Enerugii Butsurigaku Kenkyusho
LDME	Long-Distance Matrix Element
LEP	Large Electron - Positron (storage ring)
LO	Leading order

[1] Named sugested by Chris Day: short for Cleopatra

MuID	Muon IDentifier
MuTr	Muon Tracker
NLO	Next-to-Leading Order
NRQCD	Non Relativistic Quantum ChromoDynamics
pdf	parton distribution function
pQCD	perturbative Quantum ChromoDynamics
QCD	Quantum ChromoDynamics
QED	Quantum ElectroDynamics
RHIC	Relativistic Heavy Ion Collider
RICH	Ring Imaging Č(h)erenkov
SCI	Soft Colour Interactions
SLAC	Stanford Linear Accelerator
SPEAR	Stanford Positron Electron Accelerating Ring
SVX	Silicon Vertex Detector

Appendix B

Normalisation

B.1 Results relative to the normalisation

Λ	N	Λ	N
1.00	5.95	1.63	2.64
1.06	5.36	1.69	2.48
1.13	4.86	1.76	2.34
1.19	4.44	1.82	2.21
1.25	4.07	1.88	2.09
1.32	3.76	1.95	1.98
1.38	3.48	2.01	1.88
1.44	3.23	2.07	1.79
1.51	3.01	2.14	1.70
1.57	2.82	2.20	1.62

Table B.2: Normalisation for a dipolar form for J/ψ as a function of Λ for $m_c = 1.60$ GeV.

1.00	7.93	1.63	3.17
1.06	7.04	1.69	2.96
1.13	6.31	1.76	2.77
1.19	5.69	1.82	2.60
1.25	5.16	1.88	2.44
1.32	4.71	1.95	2.30
1.38	4.31	2.01	2.17
1.44	3.97	2.07	2.06
1.51	3.67	2.14	1.95
1.57	3.40	2.20	1.85

Table B.4: Normalisation for a dipolar form for J/ψ as a function of Λ for $m_c = 1.69$ GeV.

1.00	9.39	1.63	3.54
1.06	8.28	1.69	3.29
1.13	7.36	1.76	3.07
1.19	6.59	1.82	2.87
1.25	5.94	1.88	2.69
1.32	5.39	1.95	2.52
1.38	4.91	2.01	2.38
1.44	4.50	2.07	2.24
1.51	4.14	2.14	2.12
1.57	3.82	2.20	2.01

Table B.6: Normalisation for a dipolar form for J/ψ as a function of Λ for $m_c = 1.78$ GeV.

1.00	10.61	1.63	3.84
1.06	9.31	1.69	3.56
1.13	8.23	1.76	3.31
1.19	7.34	1.82	3.09
1.25	6.59	1.88	2.88
1.32	5.95	1.95	2.70
1.38	5.40	2.01	2.54
1.44	4.93	2.07	2.39
1.51	4.52	2.14	2.25
1.57	4.16	2.20	2.13

Table B.8: Normalisation for a dipolar form for J/ψ as a function of Λ for $m_c = 1.87$ GeV.

m_c	N	m_c	N
1.60	5.95	1.74	8.81
1.61	6.33	1.76	9.03
1.63	6.67	1.77	9.25
1.64	6.99	1.78	9.46
1.66	7.29	1.80	9.66
1.67	7.57	1.81	9.86
1.69	7.84	1.83	10.05
1.70	8.10	1.84	10.24
1.71	8.34	1.86	10.43
1.73	8.58	1.87	10.61

Table B.10: Normalisation for a dipolar form for J/ψ as a function of the c quark mass for $\Lambda = 1.0$ GeV.

1.60	3.39	1.74	4.54
1.61	3.55	1.76	4.63
1.63	3.69	1.77	4.71
1.64	3.82	1.78	4.79
1.66	3.94	1.80	4.87
1.67	4.05	1.81	4.95
1.69	4.16	1.83	5.02
1.70	4.26	1.84	5.09
1.71	4.36	1.86	5.17
1.73	4.45	1.87	5.24

Table B.12: Normalisation for a dipolar form for J/ψ as a function of the c quark mass for $\Lambda = 1.4$ GeV.

1.60	2.25	1.74	2.82
1.61	2.33	1.76	2.86
1.63	2.40	1.77	2.90
1.64	2.47	1.78	2.94
1.66	2.53	1.80	2.98
1.67	2.58	1.81	3.02
1.69	2.63	1.83	3.05
1.70	2.68	1.84	3.09
1.71	2.73	1.86	3.12
1.73	2.78	1.87	3.16

Table B.14: Normalisation for a dipolar form for J/ψ as a function of the c quark mass for $\Lambda = 1.8$ GeV.

1.60	1.62	1.74	1.94
1.61	1.67	1.76	1.97
1.63	1.71	1.77	1.99
1.64	1.75	1.78	2.01
1.66	1.78	1.80	2.03
1.67	1.81	1.81	2.05
1.69	1.84	1.83	2.07
1.70	1.87	1.84	2.09
1.71	1.90	1.86	2.11
1.73	1.92	1.87	2.13

Table B.16: Normalisation for a dipolar form for J/ψ as a function of the c quark mass for $\Lambda = 2.2$ GeV.

Λ	N	Λ	N
1.00	5.36	1.63	2.43
1.06	4.84	1.69	2.29
1.13	4.40	1.76	2.16
1.19	4.02	1.82	2.04
1.25	3.70	1.88	1.94
1.32	3.42	1.95	1.84
1.38	3.17	2.01	1.75
1.44	2.95	2.07	1.67
1.51	2.76	2.14	1.59
1.57	2.58	2.20	1.52

Table B.18: Normalisation for a gaussian form for J/ψ as a function of Λ for $m_c = 1.60$ GeV.

1.00	7.38	1.63	2.95
1.06	6.54	1.69	2.76
1.13	5.86	1.76	2.58
1.19	5.28	1.82	2.43
1.25	4.79	1.88	2.29
1.32	4.37	1.95	2.16
1.38	4.01	2.01	2.04
1.44	3.69	2.07	1.93
1.51	3.41	2.14	1.83
1.57	3.17	2.20	1.74

Table B.20: Normalisation for a gaussian form for J/ψ as a function of Λ for $m_c = 1.69$ GeV.

1.00	9.00	1.63	3.34
1.06	7.90	1.69	3.11
1.13	7.00	1.76	2.90
1.19	6.26	1.82	2.71
1.25	5.63	1.88	2.54
1.32	5.10	1.95	2.39
1.38	4.65	2.01	2.25
1.44	4.25	2.07	2.13
1.51	3.91	2.14	2.01
1.57	3.61	2.20	1.91

Table B.22: Normalisation for a gaussian form for J/ψ as a function of Λ for $m_c = 1.78$ GeV.

1.00	10.44	1.63	3.68
1.06	9.10	1.69	3.41
1.13	8.02	1.76	3.17
1.19	7.12	1.82	2.95
1.25	6.37	1.88	2.76
1.32	5.74	1.95	2.59
1.38	5.20	2.01	2.43
1.44	4.74	2.07	2.29
1.51	4.34	2.14	2.16
1.57	3.99	2.20	2.04

Table B.24: Normalisation for a gaussian form for J/ψ as a function of Λ for $m_c = 1.87$ GeV.

m_c	N	m_c	N
1.60	5.36	1.74	8.34
1.61	5.73	1.76	8.59
1.63	6.07	1.77	8.84
1.64	6.40	1.78	9.08
1.66	6.70	1.80	9.31
1.67	7.00	1.81	9.54
1.69	7.28	1.83	9.77
1.70	7.56	1.84	10.00
1.71	7.83	1.86	10.22
1.73	8.09	1.87	10.44

Table B.26: Normalisation for a gaussian form for J/ψ as a function of the c quark mass for $\Lambda = 1.0$ GeV.

1.60	3.09	1.74	4.26
1.61	3.25	1.76	4.36
1.63	3.38	1.77	4.45
1.64	3.51	1.78	4.54
1.66	3.63	1.80	4.63
1.67	3.75	1.81	4.71
1.69	3.86	1.83	4.79
1.70	3.97	1.84	4.88
1.71	4.07	1.86	4.96
1.73	4.17	1.87	5.04

Table B.28: Normalisation for a gaussian form for J/ψ as a function of the c quark mass for $\Lambda = 1.4$ GeV.

1.60	2.08	1.74	2.66
1.61	2.16	1.76	2.70
1.63	2.23	1.77	2.74
1.64	2.29	1.78	2.79
1.66	2.35	1.80	2.83
1.67	2.41	1.81	2.87
1.69	2.46	1.83	2.91
1.70	2.51	1.84	2.95
1.71	2.56	1.86	2.99
1.73	2.61	1.87	3.02

Table B.30: Normalisation for a gaussian form for J/ψ as a function of the c quark mass for $\Lambda = 1.8$ GeV.

1.60	1.52	1.74	1.84
1.61	1.56	1.76	1.87
1.63	1.60	1.77	1.89
1.64	1.64	1.78	1.91
1.66	1.67	1.80	1.94
1.67	1.70	1.81	1.96
1.69	1.73	1.83	1.98
1.70	1.76	1.84	2.00
1.71	1.79	1.86	2.02
1.73	1.82	1.87	2.04

Table B.32: Normalisation for a gaussian form for J/ψ as a function of the c quark mass for $\Lambda = 2.2$ GeV.

Λ	N	Λ	N
3.00	2.84	4.71	1.43
3.17	2.61	4.88	1.35
3.34	2.40	5.05	1.29
3.51	2.23	5.22	1.22
3.68	2.07	5.39	1.16
3.86	1.93	5.57	1.11
4.03	1.81	5.74	1.06
4.20	1.70	5.91	1.01
4.37	1.60	6.08	0.97
4.54	1.51	6.25	0.93

Table B.34: Normalisation for a dipolar form for $\Upsilon(1S)$ as a function of Λ for $m_b = 4.80$ GeV.

3.00	4.06	4.71	1.80
3.17	3.66	4.88	1.69
3.34	3.33	5.05	1.59
3.51	3.04	5.22	1.50
3.68	2.79	5.39	1.42
3.86	2.57	5.57	1.35
4.03	2.38	5.74	1.28
4.20	2.21	5.91	1.21
4.37	2.06	6.08	1.16
4.54	1.92	6.25	1.10

Table B.36: Normalisation for a dipolar form for $\Upsilon(1S)$ as a function of Λ for $m_b = 5.00$ GeV.

3.00	4.88	4.71	2.04
3.17	4.37	4.88	1.91
3.34	3.94	5.05	1.79
3.51	3.57	5.22	1.68
3.68	3.26	5.39	1.58
3.86	2.98	5.57	1.49
4.03	2.75	5.74	1.41
4.20	2.54	5.91	1.34
4.37	2.35	6.08	1.27
4.54	2.19	6.25	1.21

Table B.38: Normalisation for a dipolar form for $\Upsilon(1S)$ as a function of Λ for $m_b = 5.28$ GeV.

3.00	5.56	4.71	2.23
3.17	4.95	4.88	2.08
3.34	4.44	5.05	1.94
3.51	4.01	5.22	1.82
3.68	3.64	5.39	1.71
3.86	3.32	5.57	1.61
4.03	3.04	5.74	1.52
4.20	2.80	5.91	1.44
4.37	2.59	6.08	1.36
4.54	2.40	6.25	1.29

Table B.40: Normalisation for a dipolar form for $\Upsilon(1S)$ as a function of Λ for $m_b = 5.50$ GeV.

m_b	N	m_b	N
4.80	2.84	5.17	4.56
4.84	3.10	5.21	4.68
4.87	3.31	5.24	4.80
4.91	3.51	5.28	4.92
4.95	3.69	5.32	5.03
4.98	3.85	5.35	5.14
5.02	4.01	5.39	5.25
5.06	4.16	5.43	5.36
5.09	4.30	5.46	5.46
5.13	4.43	5.50	5.56

Table B.42: Normalisation for a dipolar form for $\Upsilon(1S)$ as a function of the b quark mass for $\Lambda = 3.00$ GeV.

4.80	1.77	5.17	2.53
4.84	1.89	5.21	2.59
4.87	1.99	5.24	2.64
4.91	2.08	5.28	2.69
4.95	2.16	5.32	2.74
4.98	2.23	5.35	2.78
5.02	2.30	5.39	2.83
5.06	2.36	5.43	2.87
5.09	2.42	5.46	2.92
5.13	2.48	5.50	2.96

Table B.44: Normalisation for a dipolar form for $\Upsilon(1S)$ as a function of the b quark mass for $\Lambda = 4.10$ GeV.

4.80	1.24	5.17	1.64
4.84	1.31	5.21	1.67
4.87	1.36	5.24	1.70
4.91	1.41	5.28	1.72
4.95	1.45	5.32	1.75
4.98	1.49	5.35	1.77
5.02	1.52	5.39	1.80
5.06	1.55	5.43	1.82
5.09	1.59	5.46	1.84
5.13	1.62	5.50	1.86

Table B.46: Normalisation for a dipolar form for $\Upsilon(1S)$ as a function of the b quark mass for $\Lambda = 5.20$ GeV.

4.80	0.93	5.17	1.17
4.84	0.97	5.21	1.18
4.87	1.00	5.24	1.20
4.91	1.03	5.28	1.21
4.95	1.05	5.32	1.23
4.98	1.07	5.35	1.24
5.02	1.10	5.39	1.25
5.06	1.11	5.43	1.27
5.09	1.13	5.46	1.28
5.13	1.15	5.50	1.29

Table B.48: Normalisation for a dipolar form for $\Upsilon(1S)$ as a function of the b quark mass for $\Lambda = 6.25$ GeV.

Λ	N	Λ	N
3.00	2.53	4.71	1.31
3.17	2.33	4.88	1.24
3.34	2.16	5.05	1.18
3.51	2.00	5.22	1.12
3.68	1.87	5.39	1.07
3.86	1.75	5.57	1.02
4.03	1.64	5.74	0.98
4.20	1.54	5.91	0.94
4.37	1.46	6.08	0.90
4.54	1.38	6.25	0.87

Table B.50: Normalisation for a gaussian form for $\Upsilon(1S)$ as a function of Λ for $m_b = 4.80$ GeV.

3.00	3.72	4.71	1.66
3.17	3.36	4.88	1.57
3.34	3.05	5.05	1.48
3.51	2.79	5.22	1.39
3.68	2.56	5.39	1.32
3.86	2.36	5.57	1.25
4.03	2.19	5.74	1.19
4.20	2.03	5.91	1.13
4.37	1.90	6.08	1.08
4.54	1.77	6.25	1.03

Table B.52: Normalisation for a gaussian form for $\Upsilon(1S)$ as a function of Λ for $m_b = 5.00$ GeV.

3.00	4.60	4.71	1.91
3.17	4.11	4.88	1.79
3.34	3.70	5.05	1.68
3.51	3.35	5.22	1.58
3.68	3.05	5.39	1.49
3.86	2.79	5.57	1.40
4.03	2.57	5.74	1.33
4.20	2.37	5.91	1.26
4.37	2.20	6.08	1.20
4.54	2.05	6.25	1.14

Table B.54: Normalisation for a gaussian form for $\Upsilon(1S)$ as a function of Λ for $m_b = 5.28$ GeV.

3.00	5.37	4.71	2.11
3.17	4.76	4.88	1.97
3.34	4.26	5.05	1.84
3.51	3.83	5.22	1.73
3.68	3.47	5.39	1.62
3.86	3.16	5.57	1.53
4.03	2.89	5.74	1.44
4.20	2.66	5.91	1.37
4.37	2.46	6.08	1.29
4.54	2.27	6.25	1.23

Table B.56: Normalisation for a gaussian form for $\Upsilon(1S)$ as a function of Λ for $m_b = 5.50$ GeV.

m_b	N	m_b	N
4.80	2.53	5.17	4.25
4.84	2.77	5.21	4.38
4.87	2.98	5.24	4.51
4.91	3.17	5.28	4.64
4.95	3.35	5.32	4.77
4.98	3.51	5.35	4.89
5.02	3.67	5.39	5.01
5.06	3.82	5.43	5.13
5.09	3.97	5.46	5.25
5.13	4.11	5.50	5.37

Table B.58: Normalisation for a gaussian form for $\Upsilon(1S)$ as a function of the b quark mass for $\Lambda = 3.00$ GeV.

4.80	1.61	5.17	2.35
4.84	1.72	5.21	2.41
4.87	1.81	5.24	2.46
4.91	1.89	5.28	2.52
4.95	1.97	5.32	2.57
4.98	2.04	5.35	2.62
5.02	2.11	5.39	2.67
5.06	2.17	5.43	2.72
5.09	2.24	5.46	2.77
5.13	2.30	5.50	2.81

Table B.60: Normalisation for a gaussian form for $\Upsilon(1S)$ as a function of the b quark mass for $\Lambda = 4.10$ GeV.

4.80	1.14	5.17	1.54
4.84	1.20	5.21	1.56
4.87	1.25	5.24	1.59
4.91	1.30	5.28	1.62
4.95	1.34	5.32	1.64
4.98	1.37	5.35	1.67
5.02	1.41	5.39	1.69
5.06	1.44	5.43	1.72
5.09	1.47	5.46	1.74
5.13	1.51	5.50	1.77

Table B.62: Normalisation for a gaussian form for $\Upsilon(1S)$ as a function of the b quark mass for $\Lambda = 5.20$ GeV.

4.80	0.87	5.17	1.10
4.84	0.90	5.21	1.11
4.87	0.93	5.24	1.13
4.91	0.96	5.28	1.14
4.95	0.98	5.32	1.16
4.98	1.00	5.35	1.17
5.02	1.02	5.39	1.19
5.06	1.04	5.43	1.20
5.09	1.06	5.46	1.21
5.13	1.08	5.50	1.23

Table B.64: Normalisation for a gaussian form for $\Upsilon(1S)$ as a function of the b quark mass for $\Lambda = 6.25$ GeV.

B.2 Determination of parameters: another approach

Usually, the complete procedure to be followed is to obtain from the gap equation[1] a relation between the quark mass and the bound-state mass; Λ – the paramater size– is determined from the leptonic decay width, whereas the normalisation N is determined by the fact that the residue of the bound-state propagator be 1 at the bound-state mass. The value obtained for the quark mass from the gap equation depends unfortunately on Λ. This imposes the use of an iterative method to solve these coupled equations.

In the following, we limit ourselves to the calculation of the leptonic decay width, to single out the few differences with our calculation but also to point out where there is a problem with the Wick rotation.

We present here the calculation of the decay width for the dipole vertex function. The same procedure can be applied for the gaussian; instead of using Feynman-parameter method to gather the denominators, one has therefore to use Schwinger ones, or equally the properties of the Laplace transform.

[1] which is another way to write down the BSE.

B.2.1 Leptonic decay width

From the Feynman rules and the vertex functions for the bound state, we have

$$\begin{aligned} iA^{\mu\nu} &= (-1)e_Q 3 \int \frac{d^4k}{(2\pi)^4} \mathrm{Tr}\left((i\Gamma(p_{rel}^2)\gamma^\mu) i \frac{\not{k} - \frac{1}{2}\not{P} + m}{(k-\frac{P}{2})^2 - m_c^2} (ie\gamma^\nu) i \frac{\not{k} + \frac{1}{2}\not{P} + m}{(k+\frac{P}{2})^2 - m_c^2} \right) \\ &= -3e_Q \int \frac{d^4k}{(2\pi)^4} \Gamma(p_{rel}^2) \frac{g^{\mu\nu}(M^2 + 4m^2 - 4k^2) + 8k^\mu k^\nu - 2P^\mu P^\nu}{((k-\frac{P}{2})^2 - m_c^2)((k+\frac{P}{2})^2 - m_c^2)} \end{aligned} \tag{B.1}$$

e_Q is the heavy quark charge, -1 comes for the fermionic loop, 3 is the colour factor.
Since $p_{rel} = k$, for the dipolar form of the vertex functions, we shall have

$$\Gamma(p_{rel}^2) = \frac{N}{(1 - \frac{k^2}{\Lambda^2})^2} \tag{B.2}$$

Bearing in mind that k^2 is $g_{\mu\nu}k^\mu k^\nu$ and defining:

$$\begin{aligned} I &\equiv \int \frac{d^4k}{(2\pi)^4} \Gamma(p_{rel}^2) \frac{1}{((k-\frac{P}{2})^2 - m_c^2)((k+\frac{P}{2})^2 - m_c^2)}, \\ I^{\mu\nu} &\equiv \int \frac{d^4k}{(2\pi)^4} \Gamma(p_{rel}^2) \frac{k^\mu k^\nu}{((k-\frac{P}{2})^2 - m_c^2)((k+\frac{P}{2})^2 - m_c^2)}, \end{aligned} \tag{B.3}$$

we have

$$A^{\mu\nu} = -2eN\Lambda^4 \left[(g^{\mu\nu}(M^2 + 4m^2) - 8P^\mu P^\nu) I - 4g^{\mu\nu} g_{\mu'\nu'} I^{\mu'\nu'} + 8I^{\mu\nu} \right] \tag{B.4}$$

Using the Feynman parametrisation for rational fractions, we have the following relation

$$\frac{1}{A_1^2 A_2 A_3} = \int_0^1 dxdydz\delta(x+y+z-1) \frac{6x}{(xA_1 + yA_2 + zA_3)^4}, \tag{B.5}$$

we may rewrite all the denominators as:

$$\frac{1}{(k^2 - \Lambda^2)^2((k-\frac{P}{2})^2 - m_c^2)((k+\frac{P}{2})^2 - m_c^2)} = \int_0^1 dxdydz\delta(x+y+z-1) \frac{6x}{D^4}, \tag{B.6}$$

with

$$\begin{aligned} D &= x(k^2 + \lambda^2) - y((k - \frac{P}{2})^2 - m_c^2) + z((k + \frac{P}{2})^2 - m_c^2) + (y+z)i\varepsilon \\ &= k^2 + (z-y)k.P - x\Lambda^2 + (y+z)(\frac{M^2}{4} - m^2) + (y+z)i\varepsilon \end{aligned} \tag{B.7}$$

.

The aim now is to get a complete square. To achieve this, we make use of the following change of variable

$$\begin{aligned}\ell \equiv k + \frac{z-y}{2}P \Rightarrow k &= \ell - \frac{z-y}{2}P \\ \Rightarrow k^2 &= \ell^2 + \frac{(z-y)^2}{4}M^2 - (z-y)\ell.P \\ \Rightarrow k.P &= \ell.P - \frac{z-y}{2}M^2,\end{aligned} \tag{B.8}$$

which cancels linear terms in the variable. Indeed, we have

$$\begin{aligned}D &= \ell^2 - \frac{(z-y)^2}{4}M^2 - x\Lambda^2 + (y+z)(\frac{M^2}{4} - m^2) + (y+z)i\varepsilon \\ &= \ell^2 - \Delta + (y+z)i\varepsilon,\end{aligned} \tag{B.9}$$

with

$$\Delta = \underbrace{(z-y)^2\frac{M^2}{4}}_{>0} + \underbrace{x\Lambda^2}_{>0} + (y+z)\underbrace{(m^2 - \frac{M^2}{4})}_{>0 \text{ if } m^2 > \frac{M^2}{4}}. \tag{B.10}$$

Now we have,

$$\begin{aligned}\int \frac{d^4k}{(2\pi)^4}\frac{\Gamma(p_{rel}^2)}{((k-\frac{P}{2})^2 - m_c^2)((k+\frac{P}{2})^2 - m_c^2)} &\to \int_0^1 dxdydz\delta(..)\int \frac{d^4\ell}{(2\pi)^4}\frac{6x}{(\ell^2-\Delta)^4}, \\ \int \frac{d^4k}{(2\pi)^4}\frac{k^\mu k^\nu\Gamma(p_{rel}^2)}{((k-\frac{P}{2})^2 - m_c^2)((k+\frac{P}{2})^2 - m_c^2)} &\to \int_0^1 dxdydz\delta(..)\int \frac{d^4\ell}{(2\pi)^4}\frac{6x\ell^\mu\ell^\nu}{(\ell^2-\Delta)^4}\end{aligned} \tag{B.11}$$

The previous lines implicitly require to make the Wick rotation one cannot trust as already explained.

The integration over $d^4\ell$ is carried out using these relations [102]:

$$\begin{aligned}\int \frac{d^4\ell}{(2\pi)^4}\frac{1}{(\ell^2-\Delta)^4} &= \frac{i}{(4\pi)^2}\frac{2!}{3!}\left(\frac{1}{\Delta}\right)^2 = \frac{i}{3(4\pi)^2}\left(\frac{1}{\Delta}\right)^2, \\ \int \frac{d^4\ell}{(2\pi)^4}\frac{\ell^\mu\ell^\nu}{(\ell^2-\Delta)^4} &= \frac{-1}{(4\pi)^2}i\frac{g^{\mu\nu}}{2}\frac{1!}{3!}\left(\frac{1}{\Delta}\right) = \frac{-i}{3(4\pi)^2}\frac{g^{\mu\nu}}{4}\left(\frac{1}{\Delta}\right).\end{aligned} \tag{B.12}$$

We are thus left with two types of integrals:

$$\begin{aligned}\int_0^1 dxdydz\delta(..)\frac{x}{\Delta} &\equiv A, \\ \int_0^1 dxdydz\delta(..)\frac{x}{\Delta^2} &\equiv B,\end{aligned} \tag{B.13}$$

in terms of which $A^{\mu\nu}$ reads :

$$\begin{aligned} A^{\mu\nu} &= -2eN\Lambda^4 \left(\frac{6}{3(4\pi)^2}\right)[(g^{\mu\nu}(M^2+4m^2) - 2P^\mu P^\nu)B \\ &\qquad - (8\left(\frac{g^{\mu\nu}A}{4}\right) - 4g^{\mu\nu}g_{\mu'\nu'}\left(\frac{g^{\mu'\nu'}A}{4}\right)] \\ &= \frac{-eN\Lambda^4}{4\pi^2}[g^{\mu\nu}((M^2{+}4m^2)B + 2A) - 2P^\mu P^\nu B]. \end{aligned} \tag{B.14}$$

The integration on z is done using the δ-function, which gives $z = 1-x-y$ and the remaining domain of integration on (x,y) is then restricted by $0 \leq 1-x-y \leq 0$, that is $0 \leq x \leq 1$ and $0 \leq y \leq 1-x$.

First, let us concentrate on A. Defining $\gamma^2 = m^2 - \frac{M^2}{4}$, we have

$$\begin{aligned} \int_0^1 \frac{4xdx}{M^2}\int_0^{1-x}\frac{dy}{\Delta_{z=1-x-y}} &= \int_0^1 \frac{4xdx}{M^2}\int_0^{1-x}\frac{dy}{((1-x)-2y)^2 + (x\Lambda^2 + (1-x)\gamma^2)\frac{4}{M^2})} \\ &= \int_0^1 \frac{xdx}{M^2}\int_0^{1-x}\frac{dy}{y^2 - y(1-x) + \frac{(1-x)^2}{4} + \frac{x\Lambda^2+(1-x)\gamma^2}{M^2})} \end{aligned} \tag{B.15}$$

In order to simplify the denominator, we make the following change of variable:

$$\begin{aligned} y' &= y - \frac{1-x}{2}, \\ y'_0 &= 0 - \frac{1-x}{2}, \\ y'_1 &= (1-x) - \frac{1-x}{2} = \frac{1-x}{2}. \end{aligned} \tag{B.16}$$

We thus obtain:

$$\begin{aligned} &\int_0^1 \frac{xdx}{M^2}\int_{-\frac{1-x}{2}}^{\frac{1-x}{2}}\frac{dy'}{y'^2 + \frac{x\Lambda^2+(1-x)\gamma^2)}{M^2}} = 2\int_0^1 \frac{xdx}{M^2}\int_0^{\frac{1-x}{2}}\frac{dy'}{y'^2 + \frac{x\Lambda^2+(1-x)\gamma^2)}{M^2}} \\ &\Rightarrow A = 2\int_0^1 \frac{xdx}{M^2}\frac{M}{\sqrt{\gamma^2 + x(\Lambda^2-\gamma^2)}}\arctan\left(\frac{(1-x)M}{2\sqrt{\gamma^2 + x(\Lambda^2-\gamma^2)}}\right). \end{aligned} \tag{B.17}$$

Acting in the same way with B, we may also write

$$B = 2\int_0^1 \frac{xdx}{M^2}\int_0^{\frac{1-x}{2}}\frac{dy'}{\left(y'^2 + \frac{x\Lambda^2+(1-x)\gamma^2)}{M^2}\right)^2}, \tag{B.18}$$

which, integrating by part gives $B = B_1 + B_2$ with:

$$\begin{aligned} B_1 &= \int_0^1 \frac{2x(1-x)dx}{(\gamma^2 + x(\Lambda^2-\gamma^2))\left(4(\gamma^2 + x(\Lambda^2-\gamma^2)) + M^2(1-x)^2\right),} \\ B_2 &= \frac{1}{M}\int_0^1 \frac{xdx}{(\gamma^2 + x(\Lambda^2-\gamma^2))^{\frac{3}{2}}}\arctan\left(\frac{(1-x)M}{2\sqrt{\gamma^2 + x(\Lambda^2-\gamma^2)}}\right). \end{aligned} \tag{B.19}$$

The latter three integrals are not computable analytically. We shall therefore use numerical method to obtain their value as function of Λ and M^2. In our approach, we recall that we have choosen to take m as the mass of the lowest-lying meson composed of a heavy quark Q.

On the other hand, we simply have

$$C^{\nu'\mu'} = (A^{\mu\nu})^\dagger = \frac{-eN\Lambda^4}{4\pi^2}[g^{\mu\nu}((M^2{+}4m^2)B + 2A) - 2P^\mu P^\nu B]. \tag{B.20}$$

From the Feynman rules, we have

$$\begin{aligned} B^{\rho\rho'} =& (ie)^2 \int d_2(PS)\mathrm{Tr}(\gamma^\rho(-\not{a} + m_\ell)\gamma^{\rho'}(\not{b} + m_\ell)) \\ & (ie)^2 \int d_2(PS)4(a.bg^{\rho\rho'} - a^\rho b^{\rho'} - a^{\rho'}b^\rho + g^{\rho\rho'}m_\ell^2) \end{aligned} \tag{B.21}$$

where a and b are the momenta of the lepton and antilepton ($a+b=P$), and m_ℓ their mass. As m_ℓ is much smaller than M and m, we shall neglect it.

To perform the integration on the two-particle phase space, we shall use the following well known relations [90][2]

$$\begin{aligned} \int d_2(PS)a^\alpha b^\beta =& \frac{\pi M^2}{24}\sqrt{\lambda}\left(g^{\alpha\beta}\lambda + 2\frac{P^\alpha P^\beta}{M^2}\left[1 + \frac{a^2}{M^2} + \frac{b^2}{M^2} - 2\frac{(a^2-b^2)^2}{M^4}\right]\right) \\ \simeq& \frac{\pi M^2}{24}\left(g^{\alpha\beta} + 2\frac{P^\alpha P^\beta}{M^2}\right), \\ \int d_2(PS)a.b = \int d_2(PS)a^\alpha b^\beta g_{\alpha\beta} =& \frac{\pi M^2}{24}(4+2) = \frac{\pi M^2}{4}. \end{aligned} \tag{B.22}$$

Therefore, we have

$$B^{\rho\rho'} = (ie)^2\left[\pi M^2 g^{\rho\rho'} - 8\frac{\pi M^2}{24}\left(g^{\rho\rho'} + 2\frac{P^\rho P^{\rho'}}{M^2}\right)\right] = (ie)^2\frac{2\pi}{3}M^2\underbrace{\left[g^{\rho\rho'} - \frac{P^\rho P^{\rho'}}{M^2}\right]}_{\Delta^{\rho\rho'}}. \tag{B.23}$$

Now that all quantities in Eq. (4.20) are determined, we can put everything together, which gives[3]:

$$\begin{aligned} \int \left|\bar{\mathcal{M}}\right|^2 d_2(PS) =& \frac{1}{3}\Delta_{\mu\mu'}\frac{-1}{M^4}\left(\frac{eN\Lambda^4}{4\pi^2}\right)^2\left((ie)^2\frac{2\pi}{3}M^2\right)\times \\ & \times [g^{\mu\nu}((M^2+4m^2)B + 2A)]g_{\nu\rho}\Delta^{\rho\rho'}g_{\rho'\nu'}[g^{\nu'\mu'}((M^2+4m^2)B + 2A)] \\ =& \frac{e^4N^2\Lambda^8}{18\pi M^2}(M^2+4m^2)B + 2A)^2\Delta_{\mu\mu'}\Delta^{\mu\mu'} = \frac{e^4N^2\Lambda^8}{6\pi M^2}((M^2+4m^2)B + 2A)^2 \end{aligned} \tag{B.24}$$

[2] $\lambda = \lambda(1, a^2/M^2, b^2/M^2) = \lambda(1, m_\ell^2/M^2, m_\ell^2/M^2) = 1 - 2m_\ell^2/M^2 \simeq 1$.

[3] Recall the projector property of $\Delta_{\mu\nu}$: $\Delta_{\mu\nu}P^\mu = \Delta_{\mu\nu}P^\nu = 0$.

Eq. (4.19) then gives the width and provide with a relation between Λ and the masses.

Combining this relation with the normalisation condition, it is therefore possible to fully determine the vertex-function parameters. The result obtained by Costa *et al.* [91] are given in Tab. (4.2).

List of Figures

List of Tables

Bibliography

[1] J. J. Aubert *et al.* [E598 Collaboration], Phys. Rev. Lett. **33** (1974) 1404.

[2] J. E. Augustin *et al.* [SLAC-SP-017 Collaboration], Phys. Rev. Lett. **33** (1974) 1406.

[3] H. L. Lynch *et al.*, SLAC-PUB-1536 *Invited talk presented at 2nd Orbis Scientiae, Coral Gables, Florida, Jan 20-25, 1975*

[4] F. Close, CERN Courier, **44**, no. 10, (2004) 25.

[5] C. Bacci and et al., Phys. Rev. Lett. **33** (1974) 1408 [Erratum-ibid. **33** (1974) 1649].

[6] W. Braunschweig and et al. [DASP Collaboration], Phys. Lett. B **57** (1975) 407.

[7] B. Richter, SLAC-PUB-1478 *Plenary Session Report at XVII International Conference on High Energy Physics, London, Eng., Jul 1-10, 1974*

[8] J. D. Bjorken and S. L. Glashow, Phys. Lett. **11** (1964) 255.

[9] S. L. Glashow, J. Iliopoulos and L. Maiani, Phys. Rev. D **2**, (1970) 1285.

[10] T. Appelquist, A. De Rujula, H. D. Politzer and S. L. Glashow, Phys. Rev. Lett. **34** (1975) 365.

[11] G. Goldhaber *et al.*, Phys. Rev. Lett. **37** (1976) 255.

[12] J. Wiss *et al.*, Phys. Rev. Lett. **37** (1976) 1531.

[13] B. Knapp *et al.*, Phys. Rev. Lett. **37**, (1976) 882.

[14] M. L. Perl *et al.*, Phys. Rev. Lett. **35** (1975) 1489.

[15] D. C. Hom *et al.*, Phys. Rev. Lett. **36** (1976) 1236.

[16] S. W. Herb *et al.*, Phys. Rev. Lett. **39** (1977) 252.

[17] W. R. Innes *et al.*, Phys. Rev. Lett. **39** (1977) 1240 [Erratum-ibid. **39** (1977) 1640].

[18] K. Ueno *et al.*, Phys. Rev. Lett. **42** (1979) 486.

[19] C. Bebek *et al.*, Phys. Rev. Lett. **46** (1981) 84.

[20] M. Basile *et al.*, Lett. Nuovo Cim. **31** (1981) 97.

[21] F. Abe *et al.* [CDF Collaboration], Phys. Rev. D **50** (1994) 2966.

[22] L.D. Landau, Dokl.Akad.Nauk Ser.Fiz. 60 (1948) 207; C. N. Yang, Phys. Rev. **77** (1950) 242.

[23] J. C. Collins, D. E. Soper and G. Sterman, Adv. Ser. Direct. High Energy Phys. **5** (1988) 1 [arXiv:hep-ph/0409313];
G. T. Bodwin, Phys. Rev. D **31** (1985) 2616 [Erratum-ibid. D **34** (1986) 3932];
J. w. Qiu and G. Sterman, Nucl. Phys. B **353** (1991) 105. J. w. Qiu and G. Sterman, Nucl. Phys. B **353** (1991) 137.

[24] C-H. Chang, Nucl. Phys. B **172** (1980) 425;
R. Baier and R. Rückl, Phys. Lett. B **102** (1981) 364;
R. Baier and R. Rückl, Z. Phys. C **19** (1983) 251.

[25] E. L. Berger and D. L. Jones, Phys. Rev. D **23** (1981) 1521.

[26] F. Halzen, F. Herzog, E. W. N. Glover and A. D. Martin, Phys. Rev. D **30** (1984) 700.

[27] E. W. N. Glover, A. D. Martin and W. J. Stirling, Z. Phys. C **38** (1988) 473 [Erratum-ibid. C **49** (1991) 526].

[28] C. Albajar *et al.* [UA1 Collaboration], Phys. Lett. B **256** (1991) 112.

[29] H. Fritzsch, Phys. Lett. B **67** (1977) 217.

[30] F. Halzen, Phys. Lett. B **69** (1977) 105.

[31] J.F Amundson, O.J.P. Éboli, E.M. Gregores, F. Halzen, Phys. Lett. B **372** (1996) 127; J.F Amundson *et al.*, Phys. Lett. B **390** (1997) 323.

[32] W. Buchmuller and A. Hebecker, Phys. Lett. B **355** (1995) 573 [arXiv:hep-ph/9504374].

[33] A. Edin, G. Ingelman and J. Rathsman, Phys. Rev. D **56** (1997) 7317 [arXiv:hep-ph/9705311].

[34] N. Brambilla *et al.*, "Heavy quarkonium physics,", to appear as a CERN Yellow Report, [arXiv:hep-ph/0412158].

[35] F. Abe *et al.* [CDF Collaboration], Phys. Rev. Lett. **79** (1997) 572.

[36] E. Braaten and T. C. Yuan, Phys. Rev. Lett. **71** (1993) 1673 [arXiv:hep-ph/9303205].

[37] E. Braaten, K. m. Cheung and T. C. Yuan, Phys. Rev. D **48** (1993) 4230 [arXiv:hep-ph/9302307].

[38] E. Braaten and T. C. Yuan, Phys. Rev. D **50** (1994) 3176 [arXiv:hep-ph/9403401].

[39] M. Cacciari and M. Greco, Phys. Rev. Lett. **73** (1994) 1586 [arXiv:hep-ph/9405241].

[40] E. Braaten, M. A. Doncheski, S. Fleming and M. L. Mangano, Phys. Lett. B **333** (1994) 548 [arXiv:hep-ph/9405407].

[41] G. Curci, W. Furmanski and R. Petronzio, Nucl. Phys. B **175** (1980) 27.

[42] J. C. Collins and D. E. Soper, Nucl. Phys. B **194** (1982) 445.

[43] F. Abe *et al.* [CDF Collaboration], Phys. Rev. Lett. **79** (1997) 578.

[44] M. Kramer, Prog. Part. Nucl. Phys. **47** (2001) 141 [arXiv:hep-ph/0106120].

[45] R. Barbieri, R. Gatto and E. Remiddi, Phys. Lett. B **61** (1976) 465;
R. Barbieri, M. Caffo and E. Remiddi, Nucl. Phys. B **162** (1980) 220;
R. Barbieri, M. Caffo, R. Gatto and E. Remiddi, Phys. Lett. B **95** (1980) 93;
R. Barbieri, M. Caffo, R. Gatto and E. Remiddi, Nucl. Phys. B **192** (1981) 61.

[46] W. E. Caswell and G. P. Lepage, Phys. Lett. B **167** (1986) 437.

[47] G. T. Bodwin, E. Braaten and G. P. Lepage, Phys. Rev. D **51** (1995) 1125 [Erratum-ibid. D **55** (1997) 5853] [arXiv:hep-ph/9407339].

[48] E. Braaten and S. Fleming, Phys. Rev. Lett. **74** (1995) 3327 [arXiv:hep-ph/9411365].

[49] P. L. Cho and M. B. Wise, Phys. Lett. B **346** (1995) 129 [arXiv:hep-ph/9411303].

[50] P. L. Cho and A. K. Leibovich, Phys. Rev. D **53** (1996) 150 [arXiv:hep-ph/9505329].

[51] P. L. Cho and A. K. Leibovich, Phys. Rev. D **53** (1996) 6203 [arXiv:hep-ph/9511315].

[52] T. Affolder *et al.* [CDF Collaboration], Phys. Rev. Lett. **85** (2000) 2886 [arXiv:hep-ex/0004027].

[53] M. Kramer, Nucl. Phys. B **459** (1996) 3 [arXiv:hep-ph/9508409].

[54] S. Abachi *et al.* [D0 Collaboration], Phys. Lett. B **370** (1996) 239.

[55] S. S. Adler *et al.* [PHENIX Collaboration], Phys. Rev. Lett. **92** (2004) 051802 [arXiv:hep-ex/0307019].

[56] R.Balest *et al.*, CLEO Collab., Inclusive Decays of B Mesons to Charmonium, CLNS 94/1315

[57] S. Eidelman *et al.* [Particle Data Group Collaboration], Phys. Lett. B **592** (2004) 1.

[58] F. Abe *et al.* [CDF Collaboration], Phys. Rev. Lett. **71** (1993) 3421.

[59] F. Abe *et al.* [CDF Collaboration], Phys. Rev. Lett. **75** (1995) 4358.

[60] D. Acosta *et al.* [CDF Collaboration], Phys. Rev. Lett. **88** (2002) 161802.

[61] T. Affolder *et al.* [CDF Collaboration], Phys. Rev. Lett. **84** (2000) 2094 [arXiv:hep-ex/9910025].

[62] R. J. Cropp, FERMILAB-THESIS-2000-03

[63] M. Beneke and M. Kramer, Phys. Rev. D **55** (1997) 5269 [arXiv:hep-ph/9611218].

[64] E. Braaten, B. A. Kniehl and J. Lee, Phys. Rev. D **62** (2000) 094005 [arXiv:hep-ph/9911436].

[65] E. Braaten and J. Lee, Phys. Rev. D **63** (2001) 071501 [arXiv:hep-ph/0012244].

[66] H. Sato, Mem. Fac. Sci. Kyoto (Ser. A Phys. Astrophys. Geophys. Chem.) **44** (2003) 89 [arXiv:hep-ph/0305239].

[67] G. C. Nayak, M. X. Liu and F. Cooper, Phys. Rev. D **68** (2003) 034003 [arXiv:hep-ph/0302095].

[68] J.P. Lansberg, *Heavy quarkonium production in hadronic collisions*, Talk at 'JJC2001' (La Hume, France, December 2001) (hep-ph/0201111).

[69] H.Plothow-Besch, *PDFLIB, Users's Manual – Version 8.04, W5051 PDFLIB*, 2000.04.17,CERN-PPE and references therein.

[70] E. E. Salpeter and H. A. Bethe, Phys. Rev. **84** (1951) 1232.

[71] P. Maris and C. D. Roberts, Int. J. Mod. Phys. E **12** (2003) 297 [arXiv:nucl-th/0301049].

[72] C. J. Burden, L. Qian, C. D. Roberts, P. C. Tandy and M. J. Thomson, Phys. Rev. C **55** (1997) 2649 [arXiv:nucl-th/9605027].

[73] M. A. Ivanov, Y. L. Kalinovsky and C. D. Roberts, Phys. Rev. D **60** (1999) 034018 [arXiv:nucl-th/9812063].

[74] M. A. Ivanov, J. G. Korner and P. Santorelli, Phys. Rev. D **63** (2001) 074010 [arXiv:hep-ph/0007169].

[75] M. A. Ivanov, J. G. Korner and P. Santorelli, Phys. Rev. D **70** (2004) 014005 [arXiv:hep-ph/0311300].

[76] T. Appelquist and H. D. Politzer, Phys. Rev. D **12** (1975) 1404.

[77] D. J. Gross and F. Wilczek, Phys. Rev. Lett. **30** (1973) 1343.

[78] H. D. Politzer, Phys. Rev. Lett. **30** (1973) 1346.

[79] D. J. Gross and F. Wilczek, Phys. Rev. D **8** (1973) 3633.

[80] H. D. Politzer, Phys. Rept. **14** (1974) 129.

[81] W. Buchmuller, (ed.), *Quarkonia, Current physics-sources and comments, 9*, North-Holland, Amsterdam, Netherlands, 1992.

[82] E. Eichten, K. Gottfried, T. Kinoshita, J. B. Kogut, K. D. Lane and T. M. Yan, Phys. Rev. Lett. **34**, 369 (1975) [Erratum-ibid. **36**, 1276 (1976)].

[83] B. Z. Kopeliovich and J. Raufeisen, Lect. Notes Phys. **647** (2004) 305 [arXiv:hep-ph/0305094].

[84] E. Eichten, K. Gottfried, T. Kinoshita, K. D. Lane and T. M. Yan, Phys. Rev. D **17** (1978) 3090 [Erratum-ibid. D **21** (1980) 313];
E. Eichten, K. Gottfried, T. Kinoshita, K. D. Lane and T. M. Yan, Phys. Rev. D **21** (1980) 203.

[85] W. Buchmuller and S. H. H. Tye, Phys. Rev. D **24** (1981) 132.

[86] C. Quigg and J. L. Rosner, Phys. Lett. B **71**, 153 (1977).

[87] A. Martin, Phys. Lett. B **93** (1980) 338.

[88] B. Z. Kopeliovich and B. G. Zakharov, Phys. Rev. D **44** (1991) 3466.

[89] J. H. Kuhn, J. Kaplan and E. G. O. Safiani, Nucl. Phys. B **157** (1979) 125.

[90] V.D. Barger and R.J.N. Philips, *Collider Physics*, Addison-Wesley, Menlo Park, 1987.

[91] P. Costa (private communication).

[92] F. Gross, *Relativistic Quantum Mechanics and Field Theory*, Wiley, New-York, 1993.

[93] F. Gross and D. O. Riska, Phys. Rev. C **36** (1987) 1928.

[94] S. D. Drell and T. D. Lee, Phys. Rev. D **5** (1972) 1738.

[95] F. Bissey, J. R. Cudell, J. Cugnon, M. Jaminon, J. P. Lansberg and P. Stassart, Phys. Lett. B **547** (2002) 210 [arXiv:hep-ph/0207107]; J. P. Lansberg, F. Bissey, J. R. Cudell, J. Cugnon, M. Jaminon and P. Stassart, AIP Conf. Proc. **660** (2003) 339 [arXiv:hep-ph/0211450].

[96] F. Bissey, J. R. Cudell, J. Cugnon, J. P. Lansberg and P. Stassart, Phys. Lett. B **587** (2004) 189 [arXiv:hep-ph/0310184].

[97] J. A. M. Vermaseren, arXiv:math-ph/0010025.

[98] J. Pumplin, D. R. Stump, J. Huston, H. L. Lai, P. Nadolsky and W. K. Tung, JHEP **0207** (2002) 012 [arXiv:hep-ph/0201195].

[99] A. D. Martin, R. G. Roberts, W. J. Stirling and R. S. Thorne, Phys. Lett. B **531** (2002) 216 [arXiv:hep-ph/0201127].

[100] P. Hoyer and S. Peigne, Phys. Rev. D **59** (1999) 034011 [arXiv:hep-ph/9806424].

[101] N. Marchal, S. Peigne and P. Hoyer, Phys. Rev. D **62** (2000) 114001 [arXiv:hep-ph/0004234].

[102] Michael E. Peskin, D.V. Schroeder, *An Introduction to Quantum Field Theory*, Addison-Wesley, Reading, 1995.

Index